

The Role of Ligands in the Chemical Synthesis and Applications of Inorganic Nanoparticles

Amelie Heuer-Jungemann,^{†,◇} Neus Feliu,^{‡,⊥} Ioanna Bakaimi,[■] Majd Hamaly,[§] Alaaldin Alkilany,^{||,⊥} Indranath Chakraborty,[⊥] Atif Masood,⁺ Maria F. Casula,^{#,^} Athanasia Kostopoulou,[▽] Eunkeu Oh,^{○,◆} Kimihiro Susumu,^{○,◆} Michael H. Stewart,[◆] Igor L. Medintz,[¶] Emmanuel Stratakis,[¶] Wolfgang J. Parak,[⊥] and Antonios G. Kanaras^{*,†,⊥}

[†]School of Physics and Astronomy, Faculty of Engineering and Physical Sciences, University of Southampton, Southampton SO17 1BJ, U.K.

[‡]Department of Laboratory Medicine (LABMED), Karolinska Institutet, Stockholm 171 77, Sweden

[§]King Hussein Cancer Center, P. O. Box 1269, Al-Jubeiha, Amman 11941, Jordan

^{||}Department of Pharmaceutics & Pharmaceutical Technology, School of Pharmacy, The University of Jordan, Amman 11942, Jordan

[⊥]Fachbereich Physik, CHyN, Universität Hamburg, 22607 Hamburg, Germany

[#]INSTM and Department of Chemical and Geological Sciences, University of Cagliari, 09042 Monserrato, Cagliari, Italy

[▽]Institute of Electronic Structure and Laser, Foundation for Research and Technology—Hellas, Heraklion, 71110 Crete, Greece

[○]KeyW Corporation, Hanover, Maryland 21076, United States

[◆]Optical Sciences Division, Code 5600, U.S. Naval Research Laboratory, Washington, D.C. 20375, United States

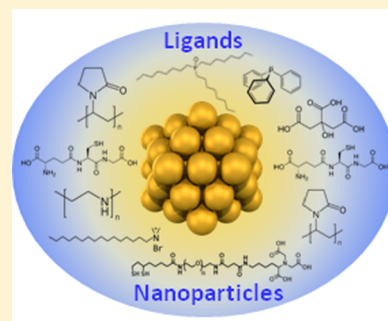
[¶]Center for Bio/Molecular Science and Engineering, Code 6900, U.S. Naval Research Laboratory, Washington, D.C. 20375, United States

⁺Fachbereich Physik, Philipps Universität Marburg, 30357 Marburg, Germany

[■]School of Chemistry, Faculty of Engineering and Physical Sciences, University of Southampton, Southampton SO171BJ, U.K.

[^]Department of Mechanical, Chemical and Materials Engineering, University of Cagliari, Via Marengo 2, 09123 Cagliari, Italy

ABSTRACT: The design of nanoparticles is critical for their efficient use in many applications ranging from biomedicine to sensing and energy. While shape and size are responsible for the properties of the inorganic nanoparticle core, the choice of ligands is of utmost importance for the colloidal stability and function of the nanoparticles. Moreover, the selection of ligands employed in nanoparticle synthesis can determine their final size and shape. Ligands added after nanoparticle synthesis infer both new properties as well as provide enhanced colloidal stability. In this article, we provide a comprehensive review on the role of the ligands with respect to the nanoparticle morphology, stability, and function. We analyze the interaction of nanoparticle surface and ligands with different chemical groups, the types of bonding, the final dispersibility of ligand-coated nanoparticles in complex media, their reactivity, and their performance in biomedicine, photodetectors, photovoltaic devices, light-emitting devices, sensors, memory devices, thermoelectric applications, and catalysis.



CONTENTS

1. Introduction	B
2. Surface Stabilization of Colloidal Nanoparticles	D
2.1. Ligand Coating on Inorganic Nanoparticles Synthesized in Aqueous Media	D
2.1.1. Plasmonic Nanoparticles	D
2.1.2. Magnetic Nanoparticles	J
2.1.3. Luminescent Nanoparticles	K
2.2. Ligand Coating on Nanoparticles Synthesized in Organic Media	N
2.2.1. Plasmonic Nanoparticles	N

2.2.2. Magnetic Nanoparticles	O
2.2.3. Luminescent Nanoparticles	P
2.2.4. Other Nanoparticles	T
3. Ligand Modification for Well-Dispersed and Functional Nanoparticles in Complex Media	U
3.1. Ligand Coating of Nanoparticles for Biomedical Applications	V
3.1.1. Ethylene Glycol Containing Ligands	V

Received: December 3, 2018

3.1.2. Silanes	X
3.1.3. Oligonucleotides	AA
3.1.4. Small Peptides	AC
3.1.5. Proteins	AD
3.1.6. Carbohydrates	AE
3.2. Ligand Coating of Nanoparticles for Other Applications	AF
3.2.1. Photodetectors	AG
3.2.2. Photovoltaic Devices	AH
3.2.3. Light-Emitting Devices	AJ
3.2.4. Sensors	AK
3.2.5. Memory Devices	AL
3.2.6. Thermoelectric Applications	AM
3.2.7. Catalysis	AO
4. Conclusions and Future Perspectives	AP
4.1. Stability of NPs	AQ
4.2. Density and Steric Configuration of Surface Ligands	AQ
Author Information	AQ
Corresponding Author	AQ
ORCID	AQ
Present Address	AQ
Notes	AQ
Biographies	AQ
Acknowledgments	AS
Abbreviations Used	AS
References	AT

1. INTRODUCTION

Nanoparticles (NPs) have attracted great research interest due to their unique properties, which derive from a combination of their intrinsic characteristics such as chemical composition, size, shape, and the type of molecules employed to coat their surface. Owing to the inorganic core composition, metallic NPs (especially gold and silver) can exhibit strong optical absorption and scattering,^{1–4} while semiconductor quantum dots (e.g., cadmium selenide (CdSe) or cadmium telluride (CdTe), lead sulfide (PbS), and perovskite NPs (e.g., methylammonium or cesium lead halides) can be highly fluorescent as a result of their electronic band structure.^{5–7} On the other hand, NPs synthesized from magnetic materials (e.g., iron oxide or cobalt) can exhibit unique magnetic phenomena such as superparamagnetism, which are not encountered in the corresponding bulk counterparts.^{8,9} These properties have rendered NPs highly interesting candidates for a vast variety of applications.^{6,10–13} One of the key parameters to synthesize robust and well crystalline NPs of defined morphologies and function is the choice of surface ligands. Ligands play multiple roles ranging from the regulation of the solubility and availability of active components during NP synthesis to the post synthetic minimization of surface energy of NPs (required for their colloidal stability) as well as the encoding of NP functionality.¹⁴ The type of ligands employed to fulfill these roles include small organic compounds with redox properties or ability to complexate with active components (e.g., trisodium citrate, oleic acid, etc.), large polymers (e.g., polyethylene glycols) with tunable polarity to preferentially bind crystallographic domains on the NP surface, or other functional biomolecules (such as peptides, proteins, and oligonucleotides), which enrich NPs with additional properties. An additional feature of surface ligands is the option to offer multiple functionalities, which can act in a synergistic

manner. For example, NPs can be equipped with targeting and cargo delivery abilities, engineered to be biocompatible or designed to assemble in an ordered manner.^{15–23} The ability to attach a large number of various types of ligands to the surface of a single NP offers additional benefits such as higher reactivity at the local microenvironment around the NP core and multitasking performance. Therefore, the appropriate choice of ligands plays a critical role in the structure, colloidal stability, and function of NPs. Appropriate protocols to coat the NP surface with ligands or perform secondary conjugation ligand reactions define the quality of NPs. To choose suitable ligands for either direct synthesis of NPs or postsynthetic modification of a NP surface, there are many important parameters to consider which will directly affect intended application. These include: (1) *The chemical composition of the NP surface*: The nature and strength of bonding between the ligand and NP surface is strongly correlated to the individual characteristics of each NP type. For example, carboxyl and hydroxyl groups have a strong binding affinity for iron oxide NPs, whereas thiols have high affinity to gold surfaces.²⁴ The strength of ligand binding is critical to the long-term colloidal stability of NPs, and when they are coated with weak affinity ligands they must be stored either as powders or in an excess amount of free ligand in solution to retain sufficient ligand coverage. The use of multidentate anchoring groups on ligands can additionally aid in increasing binding strength and hence colloidal particle stability. Table 1 shows an overview of some

Table 1. Different NPs and Common Anchoring Groups Used for Ligand Conjugation

NP composition	common anchoring group for ligand conjugation
noble metal	thiol (–SH) amine (–NH ₂) carboxyl (–COOH) phosphine (–PR ₃)
semiconducting quantum dot	phosphine oxide (O = PR ₃) thiol (–SH) phosphonyl (–PO(OR) ₂) carboxyl (–COOH)
transition metal oxide	carboxyl (–COOH) hydroxyl (–OH) phosphonyl (–PO(OH) ₂) amine (–NH ₂)

of the NPs discussed in this review as well as common anchoring groups for ligand attachment. Figure 1 shows an example of the variety of different ligands and anchoring groups available for NP functionalization, illustrated here for the case of colloidal quantum dots (QDs). This figure epitomizes the diversity of NP ligand chemistry using the example of QDs and surface ligand strategies applied for biological applications. First it highlights how different strategies can be utilized to attach a ligand to the QD surface by direct coordination or hydrophilic interdigitating of ligands to the native moiety present on the as-synthesized QD. A variety of different mechanisms can be utilized to stabilize QDs such as charge or the hydrophilicity of ethylene glycol repeats. The different sizes of ligands, impact the overall hydrodynamic radius of the nanoparticles, and any downstream utility

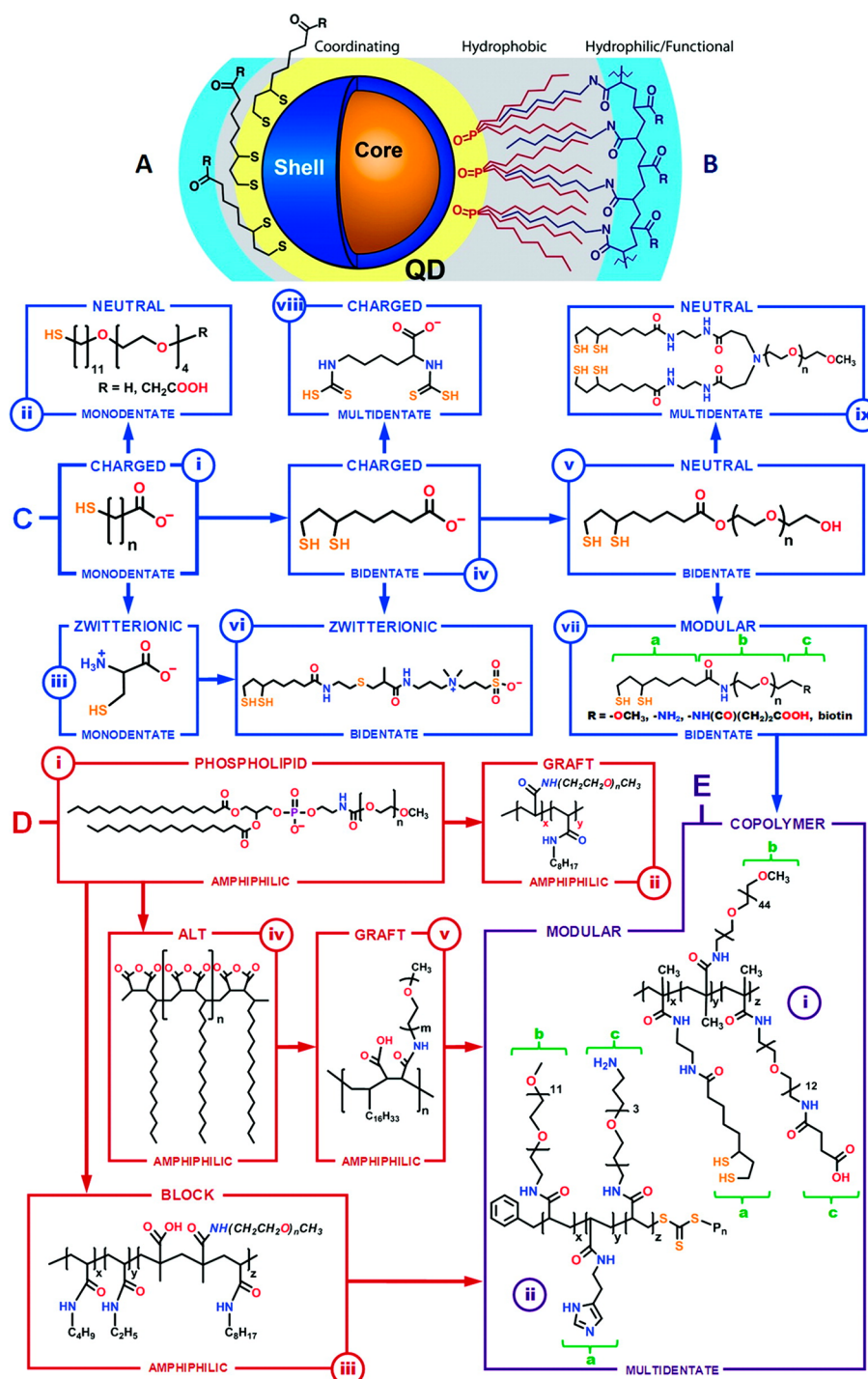


Figure 1. (A) Ligand binding at the QD surface. (B) Association of an amphiphilic (blue) with the native QD ligands (red). (C) Ligand chemistries (i) thioalkyl acids, (ii) PEGylated ligands, (iii) zwitterionic ligands, (iv) dihydrolipoic acid ligands and (v) PEGylated, (vi) zwitterionic and (vii) modular derivatives thereof, (viii) multidentate charged, and (ix) multidentate PEGylated ligands. (D) Amphiphilic coatings (i) phospholipid micelles, (ii) hydrophilic polymer backbones grafted with alkyl chains, (iii) triblock copolymers, and (iv) alternating copolymers that hydrolyze to acids or (v) are grafted with PEG chains. (E) Copolymers with pendant PEG oligomers and (i) dithiol or (ii) imidazole groups. Discrete moieties for (a) QD binding, (b) solubility, and (c) bioconjugation are identified where applicable (green). The arrows illustrate a conceptual progression and not synthetic pathways or chronological development. Reprinted with permission from ref 27. Copyright 2011 American Chemical Society.

especially in a biological context. The end groups displayed on the ligands are also important for bioconjugation of functional molecules to the QD. (2) *The environment the particles are designed for:* The appropriate selection of a ligand to coat NPs is directly correlated to the actual environment that the particles will be utilized in. NPs may need to be dispersed in a

range of different pH values, buffers, and biological or organic media. For example, intracellular applications will limit the choice of ligands to the ones that are biocompatible and can ideally protect the particles from nonspecific binding of biomolecules (e.g., proteins) and will also require ligands that bind strongly to the NPs surface and remain bound in

complex biological media and buffers. (3) *The desired NP morphology*: Ligands will have different binding energies, diffusion rates, and packing characteristics near the NP surface, which, in turn, influences the final morphology imparted to the NPs during synthesis. For example, the presence of thiols during the reduction of gold salts to form gold NPs (Au NPs) usually favors the growth of smaller size particles ranging from 1 to 10 nm.²⁵ On the other hand, the use of weakly interacting ligands (such as citrate ions, which bind electrostatically to Au NPs) allows the growth of colloidal particles ranging from 2 nm up to 100 nm and beyond.²⁶ Other types of ligands, such as the amphiphilic cetyltrimethylammonium bromide (CTAB), act as a stabilizing agent and shape directing agent due to its differential adsorption to gold facets and thus driving the growth not only of spherical but also anisotropic nanomaterials such as gold nanorods (Au NRs), cubes, and stars. (4) *The need for secondary chemical modification of the ligand shell*: For secondary modification of NPs with biomolecules or other desired polymers, specific functional groups are needed to provide a chemical handles for subsequent coupling chemistry. In many cases, these groups are placed at a ligand's termini or periphery. However, these functional groups can limit the choice of a ligand due to potential additional unwanted interactions with the NP surface. The number and availability of these groups are important factors in any subsequent chemistry as is their propensity for cross-linking. In other cases, biomolecules can be attached directly to a NP surface but this may be at the cost of displacing some of the stabilizing ligands or even losing biological activity of the biomolecules due to their interactions with the NP surface. Clearly, the experimental protocols for ligand conjugation to NPs must be customized to the various types of ligands available in conjunction with what is desired in the final application. Fortunately, the depth and diversity of this field continues to grow at an astounding rate and this serves to provide a strong literature resource from which to draw. This review will focus on the role of the ligands in determining the formation, functionalities, and applications of NPs. Various postsynthetic strategies to functionalize and stabilize NPs of different chemical composition (metal, metal oxide, semiconductor, organic) and morphologies dispersed in aqueous or organic media are discussed. As extensive research in the field of NPs' design has demonstrated that the use of ligands during synthesis has a dramatic effect on the resulting size, shape, crystal structure, dispersion, and colloidal stability, the ligands employed to assist NPs synthesis in aqueous or organic media will also be reviewed. Furthermore, commonly chosen ligands to coat various types of NPs for specific biomedical or energy applications will be discussed. Representative examples of ligands and their utility from the literature are employed to accentuate this discussion and highlight key approaches along with many of the remaining issues. Clearly, the vastness of this field precludes us from doing a comprehensive review of every example and our apologies are extended for any and all omissions.

2. SURFACE STABILIZATION OF COLLOIDAL NANOPARTICLES

2.1. Ligand Coating on Inorganic Nanoparticles Synthesized in Aqueous Media

Ligands enable the colloidal stability of NPs via electrostatic and/or steric interactions. NPs stabilized with highly charged

ligands retain their colloidal stability via repulsion forces, while ligands that occupy significant space stabilize the NPs via steric effects.²⁸ The surface stabilizing ligands can be present during the nucleation and growth of the NPs (surface passivation during synthesis), or they can be added post synthetically to exchange ligands to the NPs' surface. In the following section, we focus on the synthesis of NPs in the presence of the surface stabilizing ligands. This route represents the most straightforward approach to introduce surface functionalization on the NP surface and provides a significant example on the multifaceted and powerful role of ligands.

2.1.1. Plasmonic Nanoparticles. Surface Passivation during Synthesis. One of the first chemical syntheses of gold NPs (Au NPs) was reported by Michael Faraday in 1857.²⁹ Gold hydrosols were prepared by the reduction of an aqueous solution of chloraurate and phosphorus (or hydrogen) dissolved in carbon disulfide.²⁹ Later, Turkevich published an alternative chemical method³⁰ to synthesize spherical gold NPs, which involved the thermal reduction of gold ions in an aqueous trisodium citrate solution. When the trisodium citrate was added to the boiling aqueous solution of gold salt under vigorous stirring, a color change from purple to ruby-red could be observed, indicating the formation of spherical Au NPs. The method was further developed by G. Frens to enable control over the Au NP size by varying the ratio of gold salt to sodium citrate.³¹ Since then, numerous modifications and detailed kinetic studies of the Turkevich process have been reported.^{32–37} It was also found that sodium citrate plays multiple roles during the reaction.³³ Besides reducing the gold salt and stabilizing the NP surface via electrostatic repulsion, citrate also plays a crucial role in determining the reaction pH, which in turn is correlated with the final size and dispersity of the resulting NPs.³⁸ Citrate adsorbs onto the gold surface through its carboxyl groups with different possible binding modes.³⁹ It was shown that changes in pH drastically alter its affinity to gold. While at neutral pH, only the central carboxylate group is adsorbed on the surface, at pH ≥ 11 all of the carboxyl and hydroxyl groups are adsorbed.⁴⁰ The negative charge of citrate provides colloidal stability through electrostatic repulsion and electrostatically coated colloids are well-dispersed in water. However, a disadvantage of the electrostatic stabilization is the inherent susceptibility of the NPs to irreversible aggregation induced by high salt concentrations and pH changes. On the other hand, the weak binding of citrate can also be of benefit when a postsynthetic ligand exchange is required.⁴¹ Post ligand exchange is highly feasible for citrate protected Au NPs by considering the weak binding of citrate to the Au NPs (6.7 kJ/mol).⁴² Ligand exchange with numerous other ligands of different anchoring groups such as thiolates^{42–45} and amines^{43,46,47} have been reported, which also enhance their colloidal stabilities and biocompatibilities.^{44,48,49} Among these, thiol exchange has been found more effective and extensively used because thiol interacts strongly with the gold surface (126–167 kJ/mol).^{50,51} Although citrate is often utilized as a capping agent for Au NPs, other types of metal NPs made from Ag, Pt, Pd, or Cu have also been synthesized using sodium citrate. For example, it was shown that triangular core–shell gold–silver nanoprisms with a citrate coating could be grown from citrate Au NPs used as seeds, by irradiating at the plasmon frequency.⁵² In a systematic study, Zhang et al. similarly described how to obtain different sizes/shapes of Ag

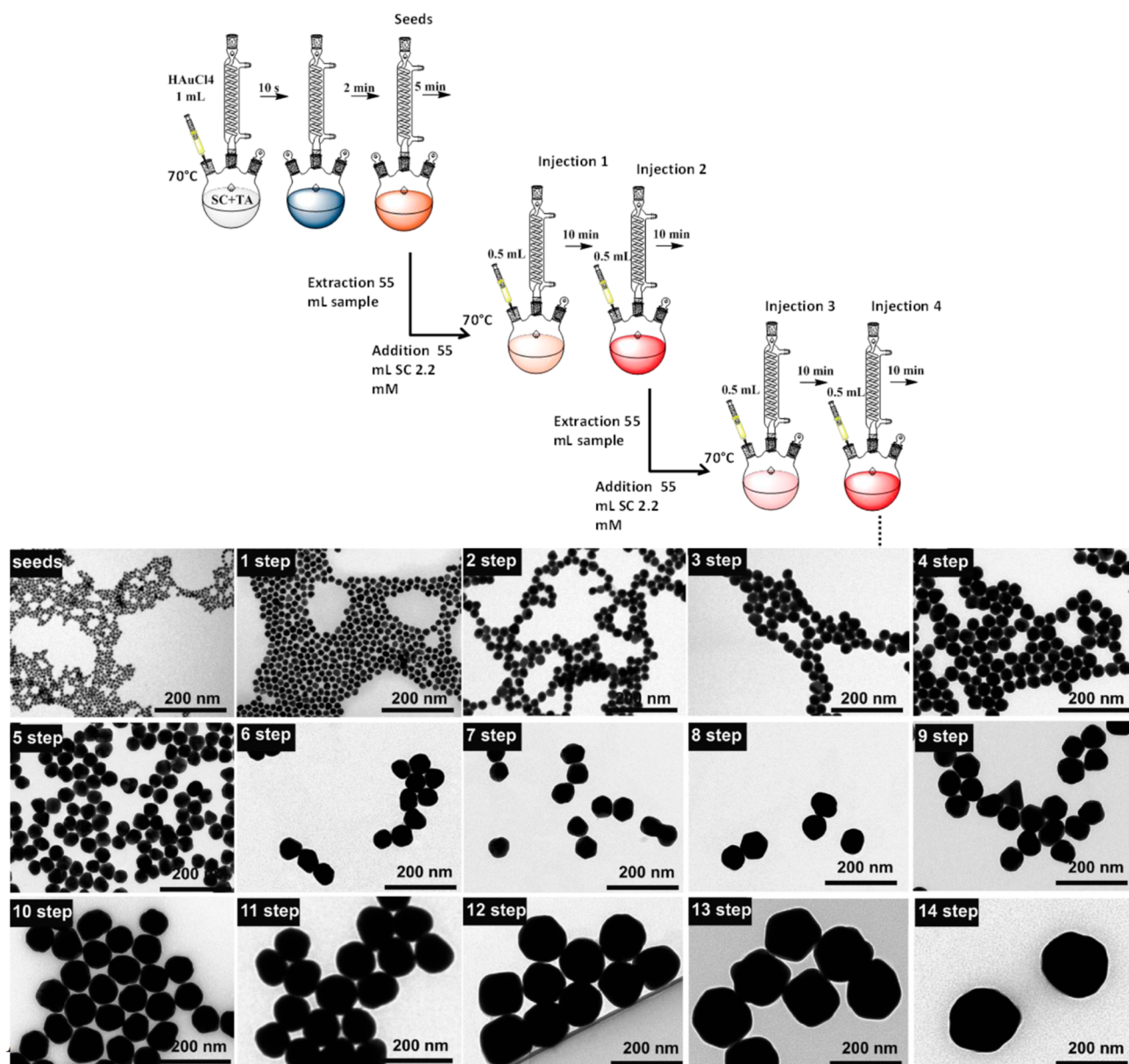


Figure 2. Synthetic scheme and corresponding TEM images of Au@citrate NP synthesis of tunable size. In the first step, NP seeds of 3.6 nm are formed. Subsequent injection steps yield larger NPs with excellent size monodispersity. Reprinted with permission from ref 55. Copyright 2016 American Chemical Society.

nanoplates by using a combination of citrate, PVP, polyol (EG, PEG, TEG, DEG), and hydrogen peroxide.⁵³

Sodium citrate has also been used in conjunction with tannic acid to produce highly monodisperse Au NPs with sizes ranging from 3.6 to 200 nm.^{54,55} The method included a multistep seed-mediated growth reaction as shown in Figure 2.⁵⁵ In another report, sodium citrate has also been used in conjunction with hydroquinone to prepare monodispersed Au NPs at room temperature.⁵⁶

A similar synthetic route employing sodium citrate and tannic acid was also reported for the formation of highly monodisperse silver NPs (Ag NPs) with sizes ranging from 14 to 200 nm.⁵⁷ Following on the early work of Henglein et al., the uniformity, final size, and crystallinity of Ag NPs could be changed as a function of the concentration of citrate because these NPs coalesce at lower citrate concentrations.⁵⁸

Although often used in conjunction with sodium citrate, tannic acid has also been employed on its own for the synthesis of Ag NPs with sizes ranging from 3.3 to 22.1 nm.⁵⁹ Besides citrate and tannic acid, sodium acrylate has also been reported for the synthesis of highly monodisperse Au NPs (2% polydispersity index) with sizes ranging from 10 to 100 nm. Here, repetitive additions of the Au–ligand complex were used to control the resulting particle size.⁶⁰ Both tannic acid and sodium acrylate follow similar mechanisms for NP formation as in the case of citrate, acting both as reducing agents and stabilizing the NPs through carboxylate groups.

Surfactants as Capping Agents. Cetyltrimethylammonium bromide (CTAB) has been widely utilized in the synthesis of both spherical and anisotropic NPs such as gold nanorods (Au NRs). Murphy and co-workers as well as other groups carried out comprehensive studies to prepare high quality Au nanorods (Au NRs) employing a seed-mediated wet chemistry

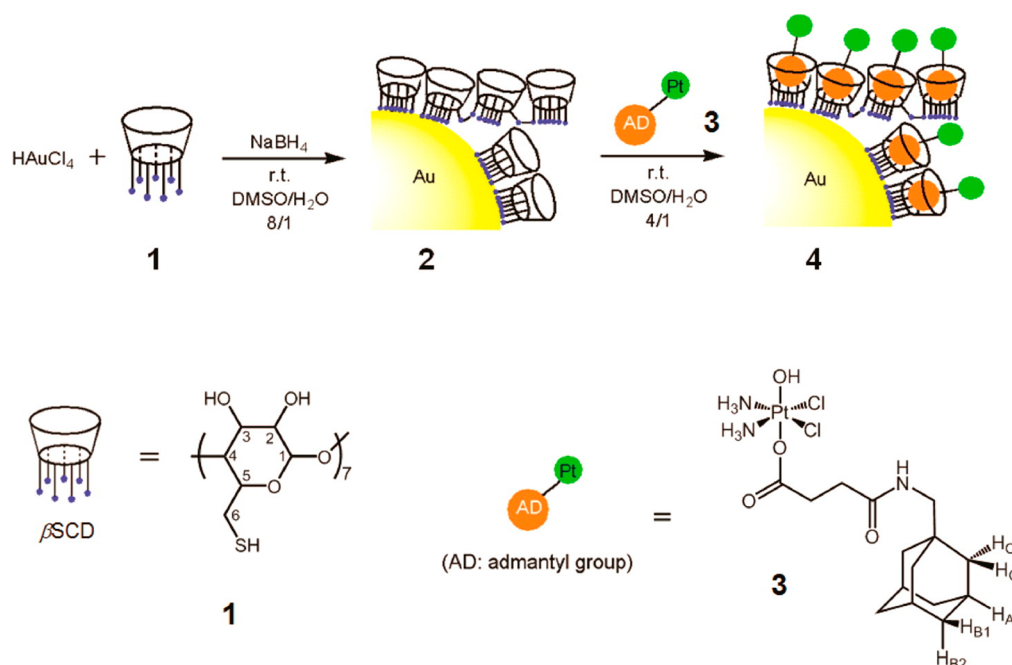


Figure 3. Schematic illustration of the synthesis of a β -cyclodextrin-functionalized Au NP, which can be loaded via a host–guest interaction with an adamantane–Pt(IV) complex. Reprinted with permission from ref 87. Copyright 2013 American Chemical Society.

protocol, in which CTAB was used as a stabilizing and shape directing ligand (promoting the formation of rod shaped particles).^{61–64} Although the exact mechanism for the formation of Au NRs still remains somewhat unclear, it is evident that CTAB binds preferentially to the (100) crystal plane on the side of the NR promoting an anisotropic crystal growth (unidirectionally) on the (111) facets at the tips.⁶⁵ On another example, branched Au NPs with different degrees of branching were prepared in the presence of CTAB, ascorbic acid, and silver. The degree of NP branching and size were also tuned by regulating the amounts of the reducing agent ascorbic acid and inducing preferential binding of CTAB and silver.⁶⁶ The use of surfactant mixture such as sodium oleate combined with CTAB was shown to be a successful strategy to obtain Au NRs with superior quality (percentage of rod-shape particles), dimensional tunability and even stability under oxidizing conditions.⁶⁷ Furthermore, the inclusion of aromatic additives during CTAB-mediated Au NR growth can narrow the size distribution of the resulting NRs. The aromatic additives intercalate in the CTAB micelle altering its micelle behavior. The micellar packing can be tuned according to the type of additive used to derive monodisperse micelles.⁶⁸ The use of other additional cosurfactants such as cetyltrimethylammonium chloride (CTAC) and decyltrimethylammonium bromide (DTAB) was shown to result in shorter aspect ratio rods but with a poorer yield of Au NRs. These observations were attributed to the direct influence of chlorine counterions and DTAB to the CTAB micelles.⁶⁹ CTAC has further been used in the synthesis of triangular Au nanoplatelets in combination with iodine ions. The gold nanoplatelets' growth is promoted by the preferential binding of I^- ions to the Au (111) facet as well as through oxidative etching, removing less stable nuclei.⁷⁰ Tetradecyltrimethylammonium bromide (TTAB) is another micelle-forming ligand, which has been employed to synthesize cubic and cuboctahedra shape of platinum NPs (Pt NPs) during a borohydride reduction.⁷¹

Unlike citrate, alkyl ammonium halide ligands provide the NP with a net positive charge. Similar to citrate, alkyl ammonium halides bind weakly to the NP surface, allowing for facile ligand exchange reactions with stronger binding ligands (e.g., thiol containing compounds), which can render the NPs appropriate for biomedical applications.⁷²

Thiol Containing Ligands on NPs. Because of the strong Au–thiol interaction (bond strength of 40–50 kcal mol^{−1}), the synthesis of Au NPs with thiolated ligands results in NPs which typically have excellent colloidal stability.⁷³ The most commonly accepted model for thiol–Au interaction is the binding of the deprotonated sulfhydryl group (forming a thiyl radical) to Au. In its protonated form, SH is only able to bind to gold through the lone pair electrons on the sulfur, forming coordination-type bonds.⁷⁴ For example, it was shown that the small thiol-containing biomolecule glutathione (GSH), a common antioxidant, could be used to produce ultrasmall Au NPs (0.9 nm) in a methanol–water mixture (2:3).⁷⁵ Some other examples of thiols used to produce ultrasmall Au NPs can be found in ref 76. On the other hand, slightly larger Au NPs with diameters ranging from 2.3 to 10 nm could be prepared by mixing an aqueous solution of gold salt with mercaptopropionate and citrate under reflux.⁷⁷ Dithiol containing compounds such dihydrolipoic acid (DHLLA) have also shown great promise for the synthesis of Au NPs. While the thiol–gold bond provides strong ligand binding, the terminal carboxylate moiety provides the particles with electrostatic stabilization and further offers a site for additional postsynthetic modification. In addition, it was found that the displacement of the DHLLA ligands was more difficult compared to other thiol-containing ligands, which was attributed to the dithiol binding versus monothiol binding.⁷⁸ Another very popular coating for NPs are (thiolated) ethylene glycols and their derivatives.^{79,80} Alkyl-thiol containing ligands such as thioalkylated tetraethylene glycol (TTG) have also been used to stabilize Au NPs.⁸¹ This ligand was superior as opposed to traditional PEG coatings due to its dual functional

properties. While its hydrophobic part could firmly assemble and pack to a monolayer around the hydrophobic Au core, the hydrophilic part (ethylene glycol) rendered the particles very stable in water and challenging biological environments. A one-pot synthesis of Au NPs by using bidentate thiolated PEG (M_w : 550–750 Da), via room temperature Au reduction with sodium borohydride (for 1–16 nm Au NPs), and a seeded growth method in boiling water (for 10–130 nm) was also reported by Oh et al. The thiolated PEG ligands allowed for the functionalization of Au NPs with various biomolecules through amide bond formation (amine-PEG-Au NPs, carboxyl-PEG-Au NPs) and click chemistry (azide-PEG-Au NPs).^{82–84} Furthermore, the thiolated PEG ligands provided enhanced colloidal stability to Au NPs under a wide range of conditions with respect to their monothiolated counterparts.⁸⁵ Thio-sulfates (Bunte salts) have also been used as ligand precursors to synthesize Au NPs (1.5–20 nm) stabilized with mercaptoethoxyethoxyethanol, 9-mercaptononanoic acid, and mercaptopentyl(trimethylammonium) chloride.⁸⁶

Beyond these types of thiols, cage-like molecules such as β -cyclodextrin have also been used as ligands for Au NPs. Si et al. reported a *per*-6-thio- β -cyclodextrin protected Au NP of size 4.7 ± 1.1 nm (Figure 3), which can be used as a cargo for the delivery of a cisplatin prodrug (oxoplatin–adamantane conjugate).⁸⁷ This binding is due to the well-known strong host–guest interaction between adamantane and β -cyclodextrin.

Phosphines as Ligands. Triphenyl phosphine (TPP) and its derivatives have been widely used as ligands to synthesize or coat Au NPs. While TPP is soluble in organic solvents, many of its derivatives, such as bis(*p*-sulfonatophenyl)phenyl phosphine dehydrate (BSPP), are soluble in aqueous solvent. Zhong et al. synthesized monodisperse Au NPs using BSPP as the ligand (figure 2.3⁸⁸). The particle size could be adjusted by controlling the pH of the solution. Synthesis at higher pH (using NaOH, pH \sim 12) yielded ultrasmall sized nanoclusters (NCs), whereas synthesis at neutral pH yielded 4 nm Au NPs as presented in Figure 4.

BSPP and other related derivatives introduced by Schmid et al., have been used extensively for the stabilization of Au nanospheres among other materials.^{89,90} Unlike thiols, phosphines bind to Au via the phosphorus' lone electron pair. This type of bond is stronger than the electrostatic interactions between citrate or alkyl halides and Au, but still not as strong as the sulfur–Au bond, thus allowing for facile ligand exchange. The mechanism by which NPs are stabilized by phosphines is believed to arise from both charge and steric interactions owing to the bulky aromatic rings on TPP derivatives. Additionally, an advantage of using charged phosphines such as BSPP as a capping agent is the ability to redisperse aggregated NPs previously precipitated by the addition of salt. This allows for the concentration of AuNP solutions by centrifugation, which is an important preparatory step for many subsequent applications. On the other hand, citrate capped particles can display irreversible aggregation behavior due to the weak binding to the Au surface.

Polymers and Plasmonic NPs. Polymers can sterically and electrostatically stabilize NPs by physisorption or chemisorption to the NP surface. During NP synthesis, polymers can bind preferentially to specific crystallographic planes of the NP surface and promote preferential anisotropic crystal growth or act as a matrix for nanocrystal growth. For example, the shape of colloidal platinum NPs (Pt NPs) could be controlled in the

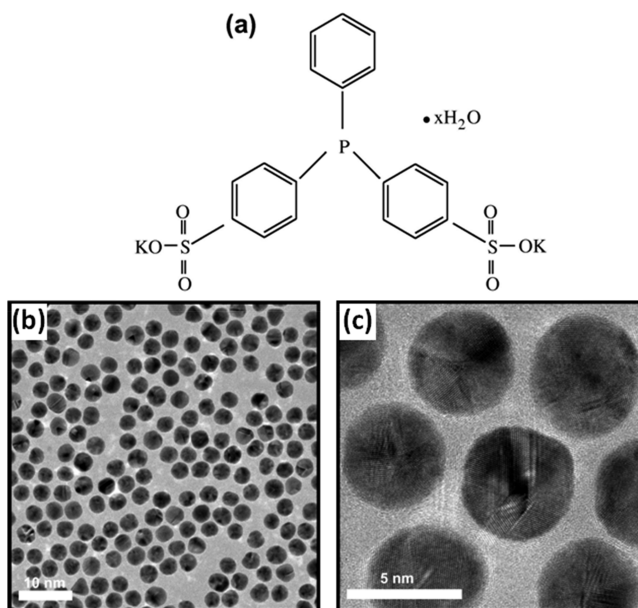


Figure 4. Structure of the BSPP ligand (a). TEM image (b) and HRTEM image (c) of BSPP-stabilized Au NPs prepared in aqueous solvent at room temperature. Adapted with permission from ref 88. Copyright 2011 Elsevier.

presence of sodium polyacrylate, where the concentration ratio of polyacrylate to Pt determined whether cubic, tetrahedral, icosahedral, cuboctahedral, or irregular-prismatic NPs were formed.^{91–93} Another interesting study revealed that poly(vinyl pyrrolidone) (PVP)-stabilized Au NPs showed changes in their optical properties due to energy transfer between the PVP and Au NP core.⁹⁴ In hot water, dispersed PVP molecules served not only as a surface ligand but also governed clustering and growth of polygonal Au NPs (25–50 nm in diameter) using small polymer templates. PVP was also used to synthesize 4–8 nm cuboctahedral Pd NPs by a polyol reduction method using ethylene glycol.⁹⁵ A good summary of the roles of PVP in the synthesis of colloidal NPs can be found in this perspective article.⁹⁶ Similar to PVP, poly(vinyl alcohol) (PVA) has also been shown as a suitable ligand for NP synthesis. Copper NPs (Cu NPs) could be formed by reduction with citrate in the presence of sodium formaldehyde sulfoxylate (SFS) and PVA.⁹⁷ PEG was also tested for stabilizing the Cu NPs during reduction with borohydride/ascorbic acid, and the size (4–28 nm) was controlled by changing the amount of PEG with concomitant plasmon band shifts observed near 560–570 nm.⁹⁸ Near-monodisperse 1.4–4 nm Au NPs were synthesized in an aqueous solution of alkyl thioether end-functionalized poly(methacrylic acid), where the desired product size again depended on the ratio of polymer to Au.⁹⁹ Various sizes of polyelectrolyte-protected Au NPs have been obtained directly by heating AuCl_4^- in an aqueous solution of amine-containing polyelectrolytes such as poly(ethylenimine)¹⁰⁰ and poly(allylamine hydrochloride).¹⁰¹ Wang et al. reported a one-step aqueous preparation of highly monodisperse Au NPs with diameters below 5 nm using thioether- and thiol-functionalized polymer ligands: dodecanethiol (DDT)-poly(acrylic acid), DDT-poly(methacrylic acid), DDT-poly(vinylsulfonic acid), DDT-poly(vinylpyrrolidone), DDT-poly(hydroxyethyl acrylate), and DDT-poly(ethyleneglycol methacrylate).¹⁰² Here particle uniformity and colloidal stability as a function of changes in ionic strength and pH were strongly dependent on

Table 2. Metal NPs Synthesized in Aqueous Media^a

material	reducing agent	ligand/surfactant	size (nm)	shape	other comments
Au ³⁰	sodium citrate	sodium citrate	20	sphere (sp)	thermal single phase Au reduction
Au ³¹	sodium citrate	sodium citrate	16–149	sp	thermal single phase Au reduction
Au ^b	sodium citrate	sodium citrate	20–100	sp	RT seed-growth
Ag ⁵⁸	sodium citrate	sodium citrate	5–30	sp	RT reduction/coalescence
Ag ⁵⁷	sodium citrate	sodium citrate, tannic acid	14–200	sp	thermal seed-growth
Au ³⁴	citrate, ascorbic acid	sodium citrate	9–120	sp	thermal/UV reduction
Au ³⁸	pottasium citrate	sodium citrate	18–100	sp/polygon	thermal single phase Au reduction with pH variation
Au/Ag ^{c,59}	tannic acid	tannic acid	2–10/3.3–21.1	sp	pH adjusted RT
Au:Ag ^d	sodium citrate	sodium citrate	32–172	sp	thermal seed-growth
Ag ⁵³	borohydride	sodium citrate/PVP, EG, TEG, PEG	~50	nanoplate, wire	H ₂ O ₂
Au ²⁹	phosphorus	carbon sulfide		sp	
Au ²⁹	H ₂	carbon sulfide		Rod	
Au ³⁰	hydroxylamine hydrochloride	hydroxylamine	20–119	sp	RT seed-growth
Au ^b	hydroxylamine	hydroxylamine	12.7 × 11.7–116 × 112, 13.7 × 11.2–233.6 × 74.2	sp/rod	iterative RT seed-growth
Au ⁸⁶	borohydride	alkyl thiosulfates	1.5–20	sp	RT reduction
Au ¹¹⁰	ascorbic acid	arabic gum	90–4600	sp	RT reduction
Au ^e	sodium citrate, ascorbic acid, hydrazine, NaBH ₄	SDS	5–30	sp	RT seed-growth, AgNO ₃
Au ^f		SDS	1–5	sp	laser ablation
Ag ⁶⁴		SDS	10	sp	laser ablation
Cu ⁹⁷	sodium citrate, hydrazine hydrate,	sodium formaldehyde sulfoxylate, PVA	30	sp	thermal reduction
Pt ^{92,93}	polyacrylate	polyacrylate	4–18	cube, polygon	Ar gas in RT
Au ⁶¹	ascorbic acid	CTAB	37/200 × 17	sp/rod	iterative RT seed-growth
Au ^g	borohydride, ascorbic acid	CTAB	20–100 (AR: 2–4)	rod	RT seed-growth
Au ⁶⁹	ascorbic acid	DTAB, CTAB	22–25 (W), 25–170 (L)	rod	RT reduction
Au ^h	borohydride	HTAB, CTAB	20–80 (W), 200–800 (L)	elongated rod	40 °C thermal seed-growth
Pt ⁷¹	borohydride	TTAB	12–14	cube, cuboctahedron	H ₂ gas pressure
Au ⁱ	borohydride	ditri-tetra-EG	<5	sp	RT reduction
Au ¹¹³	lemon grass	lemon grass	0.05–1.8 μm	Triangle	bioreduction
Au ¹⁰⁰		PEI	25–100	sp	thermal reduction
Au ^j	BPEI	BPEI	9.4	sp	thermal reduction
Cu ^k	hydrazine	poly(allylamine)	40–50	sp, rod	thermal reduction
Au ⁹⁹	borohydride	poly(methacrylic acid)	1.4–4	sp	RT reduction
Au ^l	borohydride	PEO	3.2–7.4	sp	RT reduction
Au ^m	PVP	PVP	83–95	star	steric effects
Au ⁹⁴		PVP	25–50	polygon	thermal reduction
Pd ⁹⁵	ethylene glycol	PVP	4–8	cubooctahedron	thermal reduction
Pd ⁿ	ascorbic acid	PVP	~9	truncated octahedron	thermal reduction
Pd–Pt ⁿ	ascorbic acid	PVP	~24	nanodentrites	thermal reduction
Au ^o	PDMA	PMPC/PDMA	~10	sp	diblock copolymers
Au ¹⁰²	borohydride	PAA, PMEA, PHA, PVA, PEG-MA	<5	sp	RT reduction
Au ^p		PEG200/8000	15–60	sp	thermal reduction
Cu ⁹⁸	borohydride/ascorbic acid	PEG6000	4–28	sp	multistep
Au ⁸²	borohydride	PEG-thiol	1–16	sp	RT reduction
Au ⁸⁴	borohydride, sodium citrate	PEG-thiol	15–130	sp	thermal seed-growth
Au:D ^q	borohydride	PEG-thiol	1.0–2.5	sp	luminescent, D = Ag, Pt, Zn, Cu, Cd
Ag ^r	borohydride, citrate	PEG-thiol, PVP, citrate	10–12	sp	
Au ^s		polyaniline nanofibers	1–10000	sp-microsheet	thermal reduction, memory devices
Pd ¹⁰³		Pluronic copolymers (PEO/PPO)	5–27	sp	pH adjusted RT
Au@Pd@Pt ¹⁰⁴	ascorbic acid	Pluronic copolymers (PEO/PPO/PEO)	20–55	core/shell NP	nanoporous

Table 2. continued

material	reducing agent	ligand/surfactant	size (nm)	shape	other comments
Au ^f	chitosan	chitosan/TPP	5–300	sp, polygon	cationic polysaccharide
Au ⁷⁵	borohydride	GSH	0.9	sp	RT reduction
Au ¹⁰⁸	borohydride	GSH/NTA-lysine	2–6	sp	RT reduction
Au ^u	borohydride	lysine	6.5	sp	RT reduction
Au ¹⁰⁹		lysine	32–95	Star	37 °C thermal seed-growth
Au ^v	borohydride	protein, antibody, lysine	5 → μ m	sp → rod assembly	freezing, –20 °C
Ag ¹¹⁷	sorghum bran	sorghum bran	50	sp	RT reduction
Ag ¹¹⁵	ammonia	glucose, galatose, maltose, lactose	25–450	sp	antimicrobial/bactericidal
Ag ¹¹¹	ascorbic acid	BSA, lysozyme	50–60	triangle	RT reduction
GO/Ag ¹¹⁶	luminol	luminol	22	sp	GSH sensing

^asp, spherical; rt, room temperature; PVP, poly(vinylpyrrolidone); EG, ethylene glycol; TEG, tetraethylene glycol; PEG, poly(ethylene glycol); SDS, sodium dodecyl sulfate; DTAB, decyltrimethylammonium bromide; PEI, polyethylenimine; BPEI, branched polyethylenimine; PEO, poly(ethylene oxide); PMPC, poly(2-methacryloyloxyethyl phosphorylcholine); PDMA, polydimethylsiloxane; PAA, peroxyacetic acid; PMEA, *para*-methoxyethylamphetamine; PHA, polyhydroxyalkanoate; PEG-MA, poly(ethylene glycol) methacrylate; TPP, triphenyl phosphine, GSH, glutathione; NTA, nitrilotriacetic acid; GO, graphene oxide. ^bReference 120. ^cReference 121. ^dReference 122. ^eReference 123. ^fReference 124. ^gReference 125. ^hReference 126. ⁱReference 127. ^jReference 128. ^kReference 129. ^lReference 130. ^mReference 131. ⁿReference 132. ^oReference 133. ^pReference 134. ^qReference 135. ^rReference 136. ^sReference 137. ^tReference 138. ^uReference 139. ^vReference 140.

the hydrophobicity of the ligand end group. Another group of polymers that was successfully employed for NP synthesis are the block copolymers. Piao et al. reported the synthesis of palladium NPs (Pd NPs) by simply mixing aqueous solutions of palladium salts and triblock Pluronic copolymers, (poly(ethylene oxide)–poly(propylene oxide)–poly(ethylene oxide)) in which the particle size (5–27 nm) and shape was controlled by varying the pH of the reaction mixtures.¹⁰⁵ Later, similar pluronic copolymers were used to synthesize triple-layered Au@Pd@Pt core–shell NPs (25–55 nm), which contained nanopores inside of a multilayered NP.¹⁰⁴ Additionally, polymers have also been used in NP surface patterning.^{105–107} While the creation of surface-patterned or “patchy” microparticles has been efficiently achieved, this is not the case for small inorganic NPs. Choueiri et al. proposed to coat NPs with a uniformly thick polymer brush, which upon reduction in solvent quality breaks into smaller micelles forming the patches.¹⁰⁵ The driving forces behind this process are on the one hand attractive polymer–polymer interactions, and on the other hand, the competition between the polymer grafting constraints and interfacial free energy reduction. This allows for NP surface patterning by segregation of the polymer ligands. The authors validate this approach using a variety of different NPs and polymers (e.g., Au NPs and thiolated polystyrene including block-copolymers). Such “patchy” particles were furthermore able to assemble into controlled structures such as dimers, trimers, or chains and thus demonstrated the programmability derived from the precise placement of the polymer patches.¹⁰⁵ Chen and co-workers similarly employed polymer segregation to create versatile synthetic handles on nanorods, bypyramids, and triangular prisms.¹⁰⁶ They showed that by selecting the right kind of polymer, which protected particles from aggregation, but also possessed fluidity and adjustability, site selectivity in multistep NP synthesis was possible. The utilization of a polymer, which retains its fluidity while being highly stable yet modifiable presents the most critical step in this approach. The authors showed that polystyrene-*block*-poly(acrylic acid) ligands on Au NRs could be selectively transformed through heating into desired patches coating only parts of the Au NRs and even forming helical patterns. On the other hand, Weizmann and

co-workers employed the diblock copolymer (polystyrene-*b*-poly(acrylic acid)) to create patchy NPs, which could further be regioselectively functionalized with thiolated oligonucleotides.¹⁰⁷ This strategy opens up new possibilities in the control of NP assembly and presents an excellent example on the importance of choosing the appropriate ligand for NP coating.

Overall, the use of polymers as ligands for in situ or post synthetic NP coating purposes is quite broad and only a representative cross-section is provided here. Clearly, choosing an existing or new polymer type for a given NP synthesis requires consideration of prior art in the field along with what material exactly is desired.

Biomolecules and Other Ligands for Plasmonic NPs. Although not as common as previously discussed ligands, biomolecules have been reported in the synthesis of plasmonic NPs. Often it is their functional end group (e.g., amine, phosphine, carboxylate, or thiol) that has been used to bind to the NP surface. For example, the thiol containing biomolecule GSH can be used to stabilize Au NPs. As such, Brinas et al. developed a size-controllable synthesis of Au NPs (2–6 nm) capped with GSH by varying the pH (5.5–8.0). Then they prepared nitriloacetate (NTA) functionalized Au NPs by adding a mixed solution of lysine-NTA-SH and GSH to a solution of hydrogen tetrachloroaurate (HAuCl₄).¹⁰⁸ On the other hand, some biomolecules can also be used to stabilize Au NPs electrostatically. For example, lysine (Lys) could electrostatically stabilize anisotropic star-shaped Au NPs ranging from 30 to 100 nm during their growth from 17 nm citrate-seed Au NPs.¹⁰⁹ Arabic gum-stabilized Au NPs ranging from 90 nm to 4.6 μ m in diameter could be produced by controlling the solution pH, while using ascorbic acid as the reducing agent.¹¹⁰ By using proteins as ligand, even the shape of Ag NPs could be tuned.¹¹¹ Besides these, other biomolecules, have been studied in conjunction with Au NP synthesis. Another increasingly popular route for creating Au NPs is through green chemistry methods.¹¹² For example, the addition of boiled broth of lemongrass leaf (*Cymbopogon flexuosus*) to a HAuCl₄ solution was used to induce the reduction of AuCl₄[–] and to yield a high percentage of thin, flat, single-crystalline Au nanotriangles.¹¹³ Also, β -D-glucose was used to synthesize 5.3 nm Ag NPs in the aqueous phase under moderate thermal reduction (40 °C)

with the glucose hydroxyl groups acting to passivate and stabilize the NPs.¹¹⁴ Similarly, other types of saccharides (glucose, galactose, maltose, and lactose) have been used for synthesizing antimicrobial/bacterial Ag NPs in the range of 25–450 nm in water.¹¹⁵

For the preparation of hybrid materials, He et al. developed a one-pot synthetic method for graphene oxide/silver NP (GO/Ag NPs) using luminol (5-amino-2,3-dihydrophthalazine-1,4-dione) in an aqueous/ethanol mixture at room temperature. Apart from acting as a reducing agent, excess luminol stabilizes the Ag NPs via the formation of a Ag–N covalent bonding during synthesis.¹¹⁶ The resulting Ag NPs demonstrated an average size of 22 nm with a relatively uniform size on the surface of GO. This hybrid system was used for GSH sensing, where the GSH enhanced the chemiluminescence intensity between the GO/Ag nanocomposites and hydrogen peroxide. Another example used sorghum bran extract as both the reducing and capping agent at room temperature to produce highly crystalline Ag NPs of ~10 nm.¹¹⁷

There is also a lot of current interest in the synthesis of ultrasmall metal NCs using biomolecules including nucleic acids and proteins; these are discussed separately in the fluorescent NP section (vide infra). For more detailed information on the topic of plasmonic NPs, we refer readers to dedicated relevant reviews.^{118,119}

Table 2 presents a representative overview of the most popular chemical methods and ligands to synthesize a variety of functionalized metal NPs in aqueous media.

2.1.2. Magnetic Nanoparticles. A common synthetic method for preparing iron oxide NPs in the form of magnetite or maghemite (Fe_3O_4 or $\gamma\text{-Fe}_2\text{O}_3$, respectively) is a coprecipitation by aging a stoichiometric mixture of ferrous and ferric salts in an aqueous medium.¹⁴¹ The surface iron atoms of the iron oxide NPs act as Lewis acids and coordinate with molecules that donate lone pairs of electrons. Therefore, in aqueous solutions, the Fe atoms coordinate with water, which dissociates readily to leave the iron oxide surface hydroxyl functionalized. Dependent upon the pH of the solution, the amphoteric surface hydroxyl group of the magnetite will present a positive or negative charge. The actual size, shape, and composition of such magnetic NPs depend upon the type of salts used (e.g., chlorides, sulfates, nitrates). Other functional groups, including carboxylates, hydroxy, phosphates, and sulfates are known to bind to the surface of magnetites in the aqueous phase. Hydrophilic polymers and micelles can also stabilize magnetic NPs as well.^{8,9} For example, Lee et al. prepared ultrafine Fe_3O_4 particles (4–7 nm) by precipitation in an aqueous poly(vinyl alcohol) (PVA) solution.¹⁴² However, when using PVA containing 0.1 mol % carboxyl groups as the stabilizing agent, the magnetite NPs precipitated in the form of chainlike clusters.

Various other types of carboxylated ligands have also been used for stabilizing magnetic NPs, such as citric acid, gluconic acid, dimercaptosuccinic acid, and phosphorylcholine.⁸ For example, 2–8 nm maghemite NPs could be prepared by the thermal oxidation of iron(III) nitrate in an alkaline medium in the presence of trisodium citrate.¹⁴³ Later, it was reported that the surface of magnetite NPs can also be stabilized by the adsorption of citric acid during coprecipitation of iron oxide, leading to a stable aqueous dispersion. The 5–20 nm citric acid-stabilized NPs were further conjugated with rhodamine

110 dye via carbodiimide-assisted covalent bonding and used for cellular imaging.¹⁴⁴ VSOP C184 is a 4 nm citrate-capped iron oxide NP system synthesized via an optimized coprecipitation process in the presence of excess citric acid and is currently being utilized in a clinical investigation as a potent MRI contrast agent.¹⁴⁵ Beyond just iron oxide NPs, Lu et al. used citric acid to synthesize Au/Fe NPs comprising an Au shell with a magnetite/maghemite inclusion.¹⁴⁶

Recently, citric acid was also used to develop a low energy hydrothermal-reduction route to synthesize aqueous ferrofluids of negatively charged ~10 nm $\text{Zn}_x\text{Fe}_{3-x}\text{O}_4$ and ~80 nm Fe_3O_4 for magnetic hyperthermia studies.^{147,148} Similarly, PEGylated iron oxide NPs have been prepared (Figure 5) for MR/optical lymph node imaging.¹⁴⁹ In this method, biocompatible PEG served as a solvent, capping agent, and reducing agent.

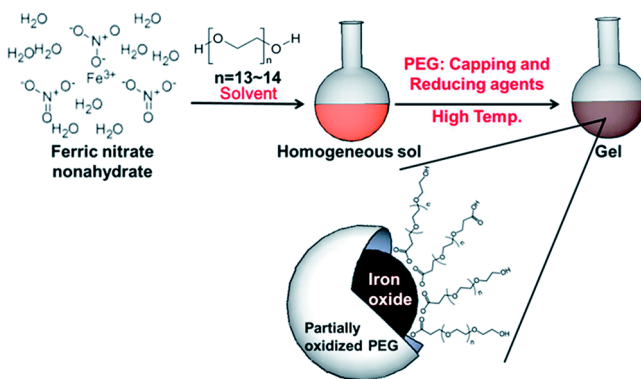


Figure 5. Schematic illustration of the synthesis of PEGylated iron oxide NPs. Reprinted with permission from ref 149. Copyright 2014 Royal Society of Chemistry.

Mixed ferrites can also be prepared by modified coprecipitation routes in aqueous media.¹⁵⁰ However, microemulsion methods have been used more commonly and have been extended for the synthesis of water-soluble magnetic NPs using a water-in-oil phase approach. The synthesis of 4.2 nm Ni NPs by the reduction of nickel chloride with hydrazine in a cationic water-in-oil microemulsions of water/CTAB/*n*-hexanol at 73 °C has also been studied.¹⁵¹ Similarly, a water-in-oil microemulsion system (aqueous FeCl_2 /CTAB/*n*-octane) was used to prepare positively charged $\gamma\text{-Fe}_2\text{O}_3$ or magnetite NPs ranging in diameter from 3.5 to 9.7 nm.¹⁵²

Sun et al. reported the size-controlled synthesis of Fe_3O_4 NPs coated with glucose and gluconic acid by using a sucrose bifunctional hydrothermal method.¹⁵³ Sucrose was used as the chemical reducing agent of Fe(III), as well as a capping agent to prepare colloidal iron oxide NPs ranging from 4 to 16 nm in size. Driven by the growing desire for greener synthesis of NPs, a rapid synthesis of 17–25 nm Fe_3O_4 using brown seaweed (*Sargassum muticum*) extract solution has been demonstrated. This approach relied on the sulfated polysaccharide from seaweed to act as a reducing agent as well as surface stabilizing template of the NPs.¹⁵⁴ In a similar vein, ethylene glycol was used to synthesize 9.2 nm Ni NPs using a hydrazine reduction in the aqueous phase.¹⁵⁵ In a different approach water-soluble magnetite NPs were produced by thermal decomposition of $\text{Fe}(\text{acac})_3$ in 2-pyrrolidone. The experimental results here revealed that 2-pyrrolidone not only serves as a media for high-temperature reaction but also involves surface coordination,

which imparts colloidal stability to the water-soluble magnetite NPs.¹⁵⁶

2.1.3. Luminescent Nanoparticles. Semiconductors. Henglein et al. pioneered the aqueous colloidal synthesis of semiconductor quantum dots (QDs), as well as other NPs, by using $\text{Cd}(\text{ClO}_4)_2$ and Na_2S in Ludox HS30 silicon sol (colloidal silica, SiO_2) and studied their catalysis of free radical reactions in 1982.^{157,158} In the past few years, aqueous syntheses have been intensely studied and now yields stable binary II–VI and IV–VI NPs such as CdS , CdTe , CdSe , ZnSe , HgTe , PbS , and other alloyed particles of good quality, free from defect emission and large polydispersity in size.¹⁵⁹ In general, the synthesis process involves the formation of metal–thiol complexes in water by adjusting the pH, and the injection of a chalcogenide source into the deaerated reaction solution. This results in the formation of metal–chalcogenide precursors. Then, heating of the solution induces the nucleation and NP growth process.

Common ligands for the stabilization of QDs in aqueous syntheses have been short alkyl chain thiols and phosphates.¹⁵⁹ For example, CdTe and ZnTe NPs could be obtained directly in water in the presence of hexametaphosphate.¹⁶⁰ Similarly a mixture of hexametaphosphate and mercapto propanediol,¹⁶¹ as well as mercaptoethanol and thiolglycerol have been used successfully.¹⁶² Rogach and co-workers optimized the process to obtain strongly photoluminescent CdTe NPs with thioglycolic acid (18% quantum yield),¹⁶³ and they revealed a state-of-the-art preparation of visible to NIR (500–800 nm) emitting CdTe NPs with high quantum yields (QY \sim 40–60%), coated with thioglycolic acid.¹⁶⁴

Similar to metallic NPs, GSH could also be utilized in the synthesis of CdTe QDs resulting in GSH-capped QDs with QYs as high as 45%, without any postsynthetic treatment. It was further shown that peptides could be conjugated to them for subsequent use in cells.¹⁶⁵ Recently Zhou et al. published a simple method to synthesize CdTe QDs, in which QDs were synthesized by stepwise addition of water, CdCl_2 , thiol, Na_2TeO_3 , NaBH_4 , and hydrazine.¹⁶⁶ This method allowed the easy functionalization of the QDs with short thiol ligands such as thioglycolic acid, mercaptopropionic acid, thiolglycerol, mercaptoethylamine, GSH, and L-cysteine, as well as mercaptobenzoic acid, *per*-6-thio- α -cyclodextrin, and *per*-7-thio- β -cyclodextrin.

Among different polymers, thiolated PEG has also been employed in the synthesis of CdTe QDs in both water and organic solvents (see Figure 6).¹⁶⁷ Furthermore, Ning et al. reported the fabrication of water-dispersible NP–amphiphilic copolymer composite microspheres, in which the mercaptopropionic acid-stabilized CdTe QDs were encapsulated by dimethyl dioctadecyl ammonium bromide in chloroform and then transferred back into water by making a QD–polymer composite with poly(ethylene glycol) diglycidyl-grafted poly(maleic anhydride-*alt*-octadecene).¹⁶⁸ Hybrid SiO_2 – CdTe NPs have also been obtained where thioglycolic acid-stabilized 2.6 nm green-emissive CdTe QDs were refluxed in the presence of Cd^{2+} , thioglycolic acid, tetraethyl orthosilicate, and NH_3 .¹⁶⁹ The as-prepared hybrid SiO_2 – CdTe NPs showed a red-shift in photoluminescence and changes in QY from 20 to 55%.

Zn-based QDs have attracted scientific interest due to concerns about Cd toxicity and the amount of heavy metal pollutants released into the environment. A successful aqueous synthesis of strong UV-blue emissive 2–3 nm ZnSe NPs was

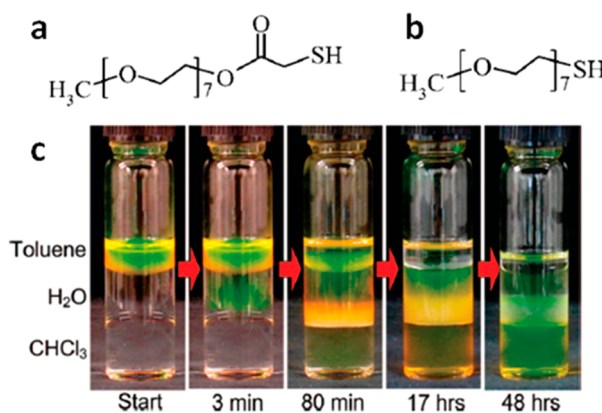


Figure 6. (a,b) mPEG-TGA and mPEG-SH molecules used for the synthesis of CdTe nanoparticles. (c) Photographs of vials showing the time-dependent triphase transfer of CdTe /mPEG-SH nanoparticles from toluene to water to chloroform under daylight. Reprinted with permission from ref 167. Copyright 2009 American Chemical Society.

developed by Shavel et al., who used thioglycerol, thioglycolic acid, or 3-mercaptopropionic acid as stabilizers with a postpreparative treatment (irradiation with white light) leading to the formation of alloyed $\text{ZnSe}(\text{S})$ NPs with improved QYs up to 30%.¹⁷⁰ GSH-capped ZnSe and $\text{Zn}_{1-x}\text{Cd}_x\text{Se}$ alloyed 3–4 nm QDs with tunable fluorescence between 360 and 500 nm, narrow bandwidths (19–32 nm), and QYs up to 50% have also been reported.¹⁷¹ Unfortunately, conditions for such aqueous synthesis do not permit size tuning of ZnSe NP materials over a wide range, thereby limiting their luminescence to a very narrow path, typically 350–400 nm, which conversely drives the demand for alloyed ZnSe QDs. Incorporation of Cd into GSH-stabilized ZnSe QDs helps to shift the photoluminescence to longer wavelengths from 360 to 500 nm.¹⁷¹ Overall, the employment of a variety of ligands for the synthesis of high quality QDs in water has certainly matured as is evident from their robust QYs, which now rival those obtained for QDs synthesized in organic solvents.

Metal Nanoclusters. Many different types of ligands such as dendrimers, thiols, peptides, etc., have been used so far to create fluorescent metal NCs.⁷⁶ Zheng et al. described the formation of size-tunable Au nanoclusters (Au NCs) that are readily synthesized through the slow reduction of AuCl_4^- or AuBr_3 within aqueous polyamidoamine (PAMAM) dendrimer solutions; the latter were used because they can be obtained with well-defined sizes and serve to encapsulate the nascent NC.¹⁷² Both the Au:PAMAM ratio as well as the dendrimer generation of PAMAM allowed for optimization and tuning of the NC emission color. It was found that these NCs showed orders of magnitude higher QYs compared to other NCs, which implied that amines play an important role in Au NC formation. Later, water-soluble platinum nanoclusters (Pt NCs) were also grown by using PAMAM (G4-OH). These Pt NCs showed decreased cytotoxicity and emitted more intensely at 470 nm in comparison to Au NCs.¹⁷³

In a different protocol, 1.1–1.7 nm diameter Au NPs with size dependent fluorescent switching and quantum yields (QY) of \sim 3% were prepared by using aqueous pentaerythritol tetrakis(3-mercaptopropionate)-terminated polymethacrylic acid.¹⁷⁴ NIR fluorescent dihydrolipoic acid (DHLA) stabilized Au NPs were recently prepared using a one-pot synthesis (Figure 7a).^{175,176} Although the particles were highly soluble in

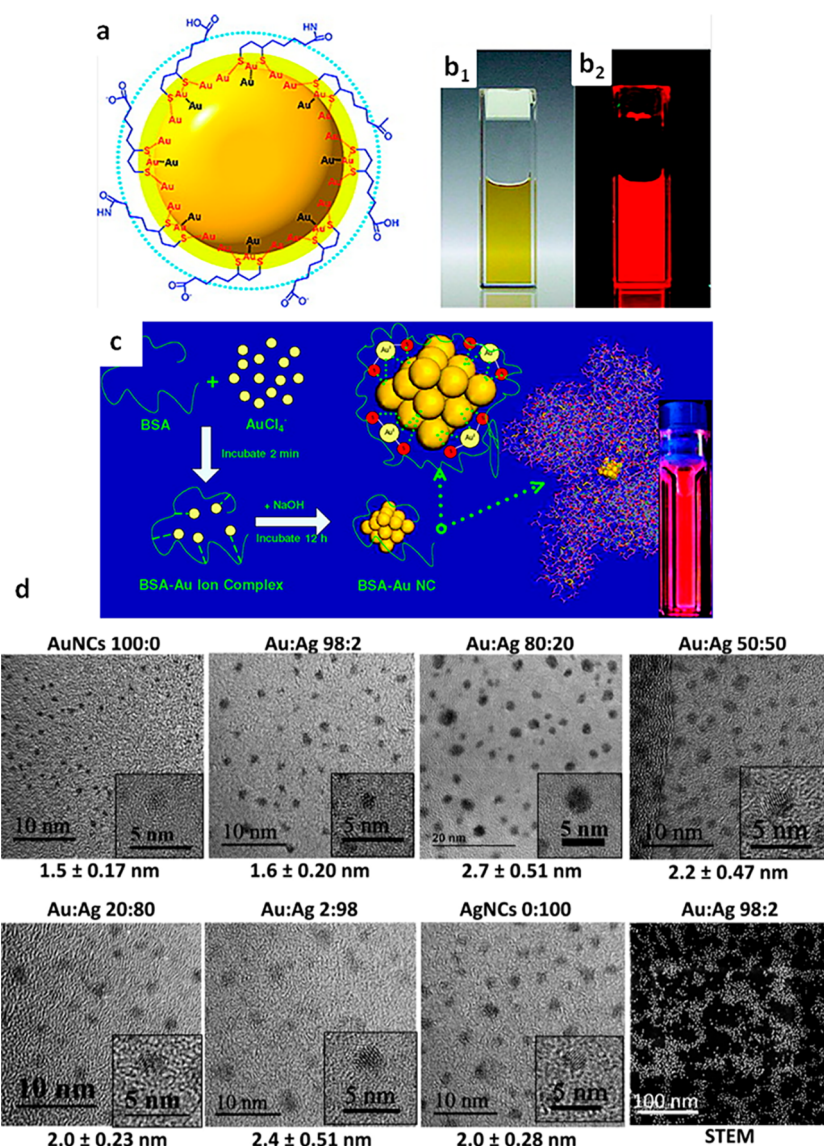


Figure 7. (a) Representative cartoon structure of Au@DHLA nanoparticles. Right side: b_1 and b_2 show the corresponding photographs of the cluster under visible and UV light, respectively. Reprinted with permission from ref 176. Copyright 2009 American Chemical Society. (c) Scheme of the highly fluorescent Au@BSA NC synthesis. Inset shows the photograph of corresponding nanocluster under UV light. Reprinted with permission from ref 179. Copyright 2009 American Chemical Society. (d) TEM images of metal-doped Au NCs with TA-PEG ligand. Reprinted with permission from ref 135. Copyright 2016 American Chemical Society.

water, they had relatively low QYs of 0.6–1.8%. Similar approaches have been used to also synthesize Ag nanoclusters (Ag NCs).¹⁷⁷ Oh et al. synthesized near-infrared emissive Au NPs with bidentate TA-PEG (TA: thioctic acid, lipoic acid) ligands in water that had higher QYs of 4–8%, and a variety of terminal functional groups (amine, carboxyl, azide, and methoxy) available for further conjugation to biomolecules. They demonstrated that these NCs were suitable for biological applications including cell-penetrating peptide-driven cellular uptake along with one- and two-photon cellular imaging.¹⁷⁸ They also synthesized metal-doped luminescent Au NCs and modulated their emission from 670 to 820 nm by changing the ratio of dopant (varied ratio (1–98%) with Ag and 2% of Pt, Cu, Zn, and Cd) added (Figure 7c).¹³⁵

Biomolecules have also been used for the fabrication of metal NCs. For example, GSH-protected Au NCs were synthesized in a water and methanol mixture by Link et al. However, these NCs were polydispersed and displayed a low

QY (0.04–0.3%).¹⁸⁰ GSH has also been used in the synthesis of highly fluorescent Pt NCs by using an etching approach. These NCs began in the Pt(I) oxidation state (90%) exhibiting an intense fluorescence in the yellow region (QY ~ 17%, emission maximum at 570 nm), and etching with GSH led to the formation of blue-emitting species over long periods of time.¹⁸¹ Other biomolecules such as nucleic acids and proteins have also been used in the synthesis of NCs. For example Patel et al. synthesized water-soluble 2.3 nm Ag NCs exhibiting strong two-photon-induced fluorescence ranging from 660–710 nm by using 12-mer nucleic acids,¹⁸² while Sharma et al. reported the synthesis and photophysical properties of Ag NCs templated on DNA, with fluorescence excitation and emission at distinct wavelengths that are tuned to common laser excitation wavelengths.¹⁸³ The use of proteins for stabilizing metal NCs was also demonstrated in the form of bovine serum albumin (BSA) stabilized Au NCs (Figure 7b), which showed relative high QYs of ~6% in water with a red emission centered

Table 3. Plasmonic NPs Synthesized in Organic Media^a

material	precursors and reagents	ligand/surfactant	size (nm)	shape	solvent	other comments
Au ²⁵	AuCl ₄ [−] /NaBH ₄	dodecanethiol	1–3	sp	biphase (water/toluene)	
Au ¹⁸⁷	AuCl ₄ [−] /NaBH ₄	dodecylamine, oleylamine	2.5–7	sp	biphase (water/toluene)	
Au, Pt, Ag ¹⁸⁶	AuCl ₄ [−] /THPC (NaBH ₄ for Ag, Pt)	dodecanethiol	1–10	sp	biphase (hydrosol/toluene)	THPC = tetrakis(hydroxymethyl)phosphonium chloride
Au ¹⁸⁸	HAuCl ₄	PVP	30	sp	formamide	octadecylamine yields spherical particles
Au ¹⁸⁹	AuCl ₄ [−] /NaBH ₄	TOPO, octadecylamine	8.6	sp	TOPO (4- <i>tert</i> -butylpyridine)	
Au ¹⁸⁵	Au vapor	dodecanethiol	4.5	sp	acetone and toluene/SMAD	multistep procedure, SMAD = solvated metal atom dispersion technique
Ag ¹⁹⁰	AgNO ₃ /NaBH ₄	TOPO/octadecylamine	bimodal distribution (2–3 nm and 10–15 nm)	sp	4- <i>tert</i> -butylpyridine	TOPO and alkyl phosphines required for controlled growth, amine dominant ligand
Ag ¹⁹⁴	AgNO ₃	PVP		cubic	ethylene glycol/polyol process	conditions control shape and size
Ag, Au, Cu, Pt ¹⁹¹	AuCl ₃ , hydrazine or TBA-borohydride	dodecylamine, decanoic acid	1–15	sp	toluene with surfactants	single phase approach in toluene with ammonium surfactants
Ag ¹⁹³	Ag myristate	myristate	4.4	sp	tertiary alkylamine solvent (NEt ₃)	
Ag ¹⁹⁵	AgNO ₃	PVP		polyhedral	pentanediol/polyol process	controlled synthesis of uniform polyhedral shapes and sizes
Ag ¹⁹²	Ag-phosphine complex	OLA	8–20	sp	<i>o</i> -dichlorobenzene	
Cu ¹⁹⁸	Cu(acac) ₂ , ammonium diethyldithiocarbamate	OA, 1-dodecanethiol	2–6	hexagonal faceted	OA, 1-dodecanethiol	
Cu ₂ -Se ¹⁹⁷	CuCl, Se	OLA	16	cuboctahedral	ODE	phosphine-free synthesis
Cu ₂ In ₃ S ₂ ¹⁹⁶	Cu(acac) ₂ , In(acac) ₃ , TMS ₂ S	hexadecyl-amine	4–5.6	sp	octadecene, TOPO	potential ligands: dodecylphosphonic acid, TOPO
Cu ₂ -S and Cu ₂ -Se ¹⁹⁹	CuCl, S ₈ , Se	OLA, OA	2.8–13.5 (Cu ₂ -S) and 7.2–16.5 (Cu ₂ -Se)	sp	OLA, OA	strong tunable NIR localized surface plasmon resonance

^aacac, acetylacetonate; ODE, octadecene; OA, oleic acid; OLA, oleylamine; PVP, polyvinylpyrrolidone; sp, sphere; TOPO, trioctylphosphine oxide; TMS, trimethylsilyl.

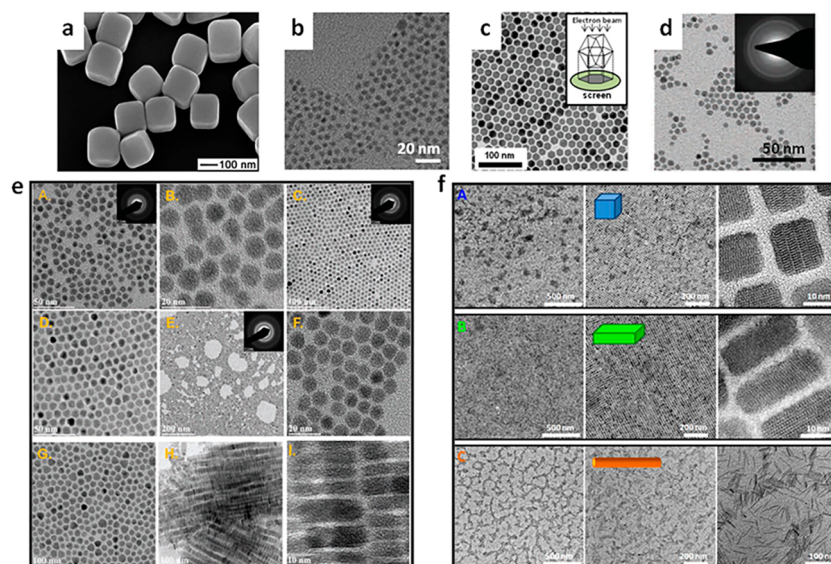


Figure 8. Representative electron microscopy images of (a) truncated Ag nanocubes, (b) $\text{Cu}_x\text{I}_y\text{S}_z$ QDs, (c) Cu_{2-x}Se nanoparticles, (d) Cu_{2-x}S QDs, (e) time-dependent evolution of Cu_{2-x}Se nanoparticles and nanodisks and (f) CuTe NPs. (a) Reprinted with permission from ref 194. Copyright 2002 Science. (b) Reprinted with permission from ref 196. Copyright 2012 American Chemical Society. (c) Reprinted with permission from ref 197. Copyright 2010 American Chemical Society. (d) Reprinted with permission from ref 198. Copyright 2011 Springer Nature. (e) Reprinted with permission from ref 199. Copyright 2013 Wiley. (f) Reprinted with permission from ref 200. Copyright 2013 American Chemical Society.

at ~ 640 nm.¹⁷⁹ Although the QY of noble metal clusters synthesized in aqueous media is not quite at the same level as that of QDs, NCs remain very promising materials due to their small size and better biocompatibility as well as access to red-shifted emissions within the NIR tissue transparency window. Because it is believed that their emission arises from a complex metal-to-ligand charge transfer process, the ability to improve their quantum yields will be directly correlated to the choice of ligand used during synthesis. Thus, further research toward increasing their QY with different ligand types can be expected in the near future.

2.2. Ligand Coating on Nanoparticles Synthesized in Organic Media

In the organic solvents, it is usually feasible to synthesize NPs of a narrow size distribution and crystal uniformity because of the higher temperatures which can be achieved often involved during synthesis. The ligands are usually introduced prior to the formation of the NPs and in many cases their roles are multiple acting as solvents, forming complexes with metals to generate the active species for NP nucleation and stabilizing the NPs by surface binding. A common characteristic of these ligands is that often they do not decompose at the elevated temperatures necessary for the NP nucleation and growth. Postsynthesis functionalization by ligand exchange is also feasible in organic media, and in most cases it is conducted at elevated temperatures.¹⁸⁴

2.2.1. Plasmonic Nanoparticles. One pioneering general approach to synthesize relatively monodispersed Au NPs in organic solvents known as the Brust–Schiffrin method is based on a two-phase surfactant-mediated approach.²⁵ In this seminal methodology, Brust et al. introduced a procedure to transfer Au ions from the aqueous solution to toluene using the phase-transfer agent tetraoctylammonium bromide (TOAB). Then the gold ions were reduced by NaBH_4 to form NPs that were stabilized by dodecanethiol, yielding organic soluble Au colloids.²⁵ Dodecanethiol has also been used in the syntheses

of Au and other noble metal NPs.^{185,186} A similar two phase method was also developed to synthesize alkylamine-capped Au NPs.¹⁸⁷

Han et al. demonstrated a nonaqueous route to synthesize Au colloids coated with PVP by the chemical reduction of HAuCl_4 in oxygen-free formamide.¹⁸⁸ Here, the solvent acted as the reducing agent in oxygen-free conditions at room temperature, yielding ~ 30 nm diameter NPs. Inspired by the high-temperature colloidal synthesis of semiconductor NPs in tri-*n*-octylphosphine oxide (TOPO), which is detailed in section 2.2.3, a one phase synthesis of Au NPs capped with organic ligands was developed.¹⁸⁹ When the reduction of gold chloride was carried out at 190°C in TOPO, uncontrolled growth of the NPs was observed with a variety of shapes and sizes (10–100 nm) being formed. Addition of octadecylamine yielded spherical Au NPs with a diameter of ~ 8.6 nm, highlighting the importance of ligands in the nucleation and growth of NPs. Infrared spectroscopy showed the presence of both TOPO and octadecylamine on the surface of Au NPs as dispersed in organic solvents. This synthesis was later adapted to prepare plasmonic Ag NPs from silver(I) nitrate.¹⁹⁰ TOPO alone was found to bind weakly to the silver surface and was insufficient at providing stable colloids despite providing controlled growth. On the other hand, octadecylamine was critical in this approach for providing stable colloids due to the strong amine–silver interaction at the NP surface.

Other alkylamines have also been used to stabilize Ag NPs in organic-phase syntheses, including dodecylamine¹⁹¹ and oleylamine.¹⁹² Jana et al. utilized dodecylamine as a stabilizing ligand employing two reducing agents, hydrazine and tetrabutylammonium borohydride, to control the plasmonic particle growth in toluene.¹⁹¹ Oleylamine has also been employed not only as the reductant for a silver–phosphine complex in *ortho*-dichlorobenzene, but also as a ligand to stabilize the resulting Ag NPs.¹⁹² In addition to amines, fatty acids such as decanoic acid¹⁹¹ can act as stabilizers to

synthesize Ag, Au, and other plasmonic NPs in organic media. For example, Yamamoto et al. described a one-pot process to synthesize 4.4 nm Ag NPs via thermal decomposition of a silver myristate-amine (1:2) at 80 °C.¹⁹³ The fatty acid alkyl chain length determined the particle size and provided colloidal stability. The longer carbon chain length, with slower diffusion, stearic acid resulted in the synthesis of smaller particles with a narrower size distribution, while the shorter carbon chain octanoic acid, with faster diffusion, yielded larger particles with broader size distributions. Polyvinylpyrrolidone (PVP) has also been used to stabilize silver NPs synthesized using the polyol process, where silver nitrate is reduced in ethylene glycol in the presence of PVP.¹⁹⁴ Depending on the experimental conditions nanocubes, nanowires, multiply twinned particles, and other irregular shapes could be obtained. This method was further adapted to obtain Ag NPs with polyhedral shapes.¹⁹⁵ Clearly there is a complex interplay of processes at work within these types of syntheses. It is probable that a deep understanding of the underlying chemistry could lead to “plug-and-play” recipes for almost any desired noble metal NP shape.

Currently, there is a rapidly growing field of research on nonmetallic nanomaterials that exhibit localized surface plasmon resonance (LSPR) where the ligands play critical roles both in NP synthesis and colloidal NP robustness. There are several methods to obtain these materials, and we focus on those prepared directly by colloidal synthesis in a one-step approach. Niezgoda et al. described the colloidal synthesis of $\text{Cu}_x\text{In}_y\text{S}$ NPs exhibiting a LSPR in the infrared using TOPO, dodecylphosphonic acid, and hexadecylamine.¹⁹⁶ The ratio of TOPO and hexadecylamine influenced the surface energy of the different crystallographic facets and determined whether spherical or rod-shaped NPs are formed. In another study, a phosphine-free synthesis of Cu_{2-x}Se NPs with a NIR LSPR utilized oleylamine as both the reductant and the stabilizing ligand.¹⁹⁷ However, byproducts were also formed and NP size control was not explored. In contrast, control over Cu_{2-x}S NP size was achieved using 1-dodecanethiol and oleic acid.¹⁹⁸ Liu et al. developed a protocol to make Cu_{2-x}E (E = S, Se) NPs, where the oleylamine and oleic acid ligands influenced the resulting NP size and cation deficiency through a complex interplay of reaction time and ligand preference for crystal phase.¹⁹⁹ Furthermore, they also reported on the synthesis of CuTe NPs with different morphologies by reacting a copper salt with trioctylphosphine telluride in the presence of lithium bis(trimethylsilyl)amide and oleylamine.²⁰⁰

Table 3 concentrates some representative literature for a variety of plasmonic NPs synthesized in organic media and the ligands used in each case to highlight the diversity that is achievable and Figure 8 shows some representative electron microscopy images of these materials.

Overall, the syntheses of organic-dispersible plasmonic NPs is more established than water-based approaches providing for control over the size, shape, composition, and energy of the plasmonic feature. This is mainly due to the elevated temperatures used for NP formation in organic solvents, which allow further manipulation of NP nucleation and growth. However, especially for the case of Au and Ag NPs, aqueous approaches provide a broader scope for the synthesis of a plethora of different shapes and sizes.

2.2.2. Magnetic Nanoparticles. While magnetic NPs with varying compositions have been synthesized in organic media using a wide variety of ligand types, here we focus

primarily on broadly used NPs of cobalt, iron oxides, and iron–platinum as representative examples. Cobalt NPs (ϵ -Co) have been prepared via the reduction of cobalt chloride in dioctylether at 200 °C.²⁰¹ The NP growth was controlled by oleic acid and trialkylphosphines used in the reaction mixture, which also provided colloidal stability to the resulting NPs and limited their oxidation. This procedure produced Co NPs from 2 to 11 nm, where the size was predominantly controlled by the use of trialkylphosphine. The use of the shorter tributylphosphine as a synthetic ligand yielded larger particles, while employment of the longer trioctylphosphine conversely yielded smaller particles. Co NPs were also prepared by thermal decomposition of octacarbonyl dicobalt $[\text{Co}_2(\text{CO})_8]$ in toluene and TOPO.²⁰² The phase of cobalt formed was shown to be dependent on the amount of TOPO present in the reaction mixture. Adding oleic acid to the decomposition of $\text{Co}_2(\text{CO})_8$ in *ortho*-dichlorobenzene and TOPO provided a means to control the size and shape of the Co NPs.²⁰³ In fact, these conditions created Co nanodisks that were later prepared in higher yields by adding alkylamines to the reaction mixture.²⁰⁴ See Figure 9 for some representative materials.

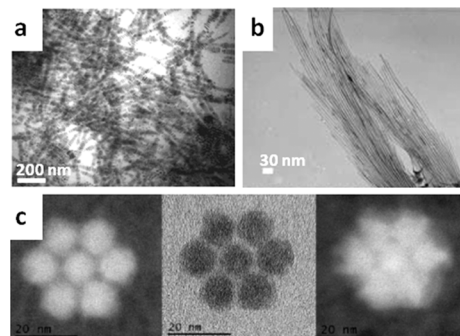


Figure 9. TEM images of (a) Co nanodisks, (b) Co nanowires prepared with oleic acid and oleylamine, and (c) high resolution image of γ - Fe_2O_3 nanocrystals and corresponding energy filtered images showing the distribution of Fe and O. (a) Adapted with permission from ref 204. Copyright 2002 American Chemical Society. (b) Adapted with permission from ref 205. Copyright 2002 Wiley. (c) Reprinted with permission from ref 208. Copyright 2009 American Chemical Society.

Fatty acids (e.g., hexadecylamine and oleic acid) and alkylamines were used to synthesize Co NRs and nanowires from $[\text{Co}(\eta^3\text{-C}_8\text{H}_{13})(\eta^4\text{-C}_8\text{H}_{12})]$ in anisole at 150 °C.^{205,206} These examples serve to highlight the variety of ligands used to stabilize NPs from agglomeration and also how they can impact the resulting NP shape and crystal phase.

Magnetic iron oxide NPs can be made via formation of iron particles that are subsequently oxidized^{207,208} or directly from cationic metal complexes. As such, γ - Fe_2O_3 NPs could be prepared from the thermal decomposition of an iron cupferon complex (FeCup_3) in octylamine/trioctylamine at 300 °C.²⁰⁹ This procedure provided particle sizes from 4 to 10 nm that required postsynthetic size selective processing, yielding materials that were stable for weeks at RT. Using $\text{Fe}(\text{acac})_3$, the synthesis of Fe_3O_4 NPs in the presence of phenyl ether, 1,2-hexadecanediol, oleic acid, and oleylamine at 265 °C without a size-selection procedure was possible.²¹⁰ The larger NPs were prepared using the seed-mediated method with oleic acid and oleylamine as stabilizers in addition to stearyl alcohol. Contrastingly, Fe_3O_4 NPs could be prepared from the pyrolysis

Table 4. Magnetic NPs Synthesized in Organic Media^a

material	precursors and reagents	ligand/surfactant	size (nm)	shape	solvent	other comments
Co ²⁰¹	CoCl ₂ , superhydride	OA, trialkylphosphines	2–11	sp	dioctylether	particle size tuned by phosphine R groups
Fe, Mn, Co oxides ²⁰⁹	M-cupferron	alkylamines	4–10	sp (approx)	trioctylamine	
Co ²⁰²	Co ₂ (CO) ₈	TOPO	20	ap	toluene	phase control with phosphine modified polyol
FePt ²²²	Pt(acac) ₂ and Fe(CO) ₅	OA, OLA	3–10	sp	dioctylether	
Fe ₂ O ₃ ²⁰⁷	Fe(CO) ₅ [trimethylamine oxide]	OA	4–16	sp	octylether	
Co ²⁰⁴	Co ₂ (CO) ₈	alkylamines, TOPO, OA		disk and sp	<i>o</i> -dichlorobenzene, alkylamines, TOPO, OA	amines give higher yields of disks
Fe ₃ O ₄ ²¹⁰	Fe(acac) ₃	OA, OLA	4–20	sp	phenyl ether, hexadecanediol	
Co ²⁰⁶	Co(n-C ₈ H ₁₃)(n-C ₈ H ₁₂)	hexadecylamine, fatty acids		rods	anisole	acids control aspect ratio of rods
FePt ²²⁴	Fe(acac) ₃ , Pt(acac) ₂	OA, OLA	2	sp (approx)	dioctylether	
Fe ₃ O ₄ ²¹²	iron-oleate	OA	5–22	sp	ODE	large scale synthesis

^aacac, acetylacetonate; ODE, octadecene; OA, oleic acid; OLA, oleylamine; sp, sphere; TOPO, trioctylphosphine oxide; TMS, trimethylsilyl.

of metal fatty acid salts (such as lauric, myristic, palmitic, stearic, and oleic acids) in noncoordinating hydrocarbon solvents (such as octadecene, tetracosane, and *n*-eicosane).²¹¹

In addition to reaction time, the concentration and size of the stabilizing fatty acid ligands influenced the resulting NP size and shape. Park et al. developed an experimental protocol for the large scale synthesis of monodisperse iron oxide NPs from inexpensive and nontoxic metal-oleate precursors in octadecene and oleic acid.²¹² Recent work showed that iron oxide NPs could be converted into nanoclusters by replacing the original oleic acid ligand coating with a “stripping ligand” such as diethylene glycol (DEG), which functions to remove all of the oleic acid from the surface.²¹³ Nanoclusters made of iron oxide multiple subunits arranged in a controlled topological fashion have been also formed by utilizing polymers^{214–219} or dendrimers^{220,221} as capping ligands.

Iron alloys are also a large subset of magnetic NPs, including iron–platinum (FePt). In a polyol-based process, FePt NPs could be prepared from the reduction of Pt(acac)₂ with 1,2-hexadecanediol and the thermal decomposition of Fe(CO)₅ in dioctylether using oleic acid and oleylamine as stabilizing ligands.²²² This synthesis allowed for NP size tuneability from 3 to 10 nm with less than 5% standard deviation. Fe(CO)₅ could be replaced with the less hazardous Fe(acac)₂²²³ or Fe(acac)₃²²⁴ to provide FePt NPs using a similar procedures. The inorganic reducing agent superhydride (LiBEt₃H) has also been employed to prepare FePt NPs from FeCl₂ and Pt(acac)₂ in phenyl ether.²²⁵ Oleic acid and oleylamine were utilized to stabilize the resulting 4 nm FePt NPs through preferential binding of the amine with platinum and the carboxylate groups with iron. Costanzo et al. also synthesized Co NPs with various diameters and uniform surfactant capping by regulating the solvation of the ligands.²²⁶

Table 4 compiles examples of ligands used in the synthesis of various types of magnetic NPs, and Figure 9 shows some representative TEM images of magnetic NPs. The controlled growth of magnetic NPs (and others) of different sizes requires a balance between surfactants that will allow the NPs to grow and surfactants that bind strongly to the surface for providing colloidal stability. This becomes more complicated when synthesizing bimetallic or metal oxide NPs such as FePt, Fe₂O₃, and Fe₃O₄ because two different atoms are present on the NP surface versus, for example, single component Co NPs.

Moreover, NPs of different sizes will likely have different ratios and densities of surfactants on their surfaces. It is also worth noting that one repeated theme across many, but not all, ligand types is that the ligand size tends to correlate inversely with the NP size obtained.

2.2.3. Luminescent Nanoparticles. As for other types of NPs, the size and morphology of colloidal QDs, and therefore their properties (in this case optoelectronic properties), depend on the ligands employed for NP synthesis, which influence nucleation, growth, and colloidal stabilization of the QDs. These ligands usually include an alkyl chain to provide solubility in organic solvents, and an anchoring headgroup, which controls the binding strength and adsorption/desorption kinetics on the QD surface. On the basis of the binding fashion, the common surface ligands can be generally categorized as either X-type or L-type ligands.^{227–229} X-type ligands donate one electron to the metal–ligand bond, L-type ligands donate two electrons to metal and Z-type ligands accept two electrons from the metal. Alkyl phosphonates, phosphinates, carboxylates, and thiolates are considered X-Type ligands while the most common L-type ligands often used in QD synthesis are TOPO, trioctylphosphine (TOP), and alkylamine.^{230–232}

Bawendi et al. first developed the synthesis of colloidal semiconductor QDs in organic solvents by reporting a hot injection method to synthesize a series of cadmium chalcogenide QDs (CdS, CdSe, and CdTe).²³³ Cadmium and chalcogenide precursors dissolved in TOP were swiftly injected to TOPO at high temperature (~300 °C). TOP and TOPO were used as high boiling point coordinating solvents, ensuring colloidal stability and controlling the core growth kinetics. This work set the foundations for a broader use of TOP/TOPO as solvents to synthesize various types of QDs, although there are still questions related to role of impurities within these ligands.²³⁴

Peng et al. demonstrated that the toxic and pyrophoric precursor Cd(CH₃)₂ could be stabilized by alkylphosphonic acid, which is one of the major impurities in technical grade TOPO.^{235,236} The air stable Cd–alkylphosphonic acid complexes successfully replaced Cd(CH₃)₂ to synthesize high quality CdSe QDs. Since then, the capability to synthesize high-quality QDs with a variety of reagents and conditions has expanded tremendously.²³⁷ In depth analytical studies of the

ligands present on the QD surface after synthesis have helped to provide key insight into their roles. ^{31}P nuclear magnetic resonance (NMR) studies of CdSe QDs synthesized using technical grade TOPO revealed that the major ligands on the CdSe QDs' surface were *n*-octylphosphonic acid (OPA) and *P,P'*-(di-*n*-octyl)dihydrogen pyrophosphonic acid (PPA), which was formed via dehydrative condensation of OPA during the QD synthesis.²³⁸ Interestingly, the ligand displacement experiment also suggested that TOPO was completely excluded from binding to the CdSe QD surface. A series of NMR studies of CdSe QDs synthesized in the presence of octadecylphosphonic acid (ODPA), TOP, and TOPO were carried out and the results indicated that the QD ligand shell consisted of 55% of ODPA and 45% of octadecylphosphonic anhydride.²³⁹ NMR studies of CdTe QDs synthesized in the presence of tetradecylphosphonic acid and oleylamine revealed that the QD surface is covered by 90% of tetradecylphosphonic anhydride and 10% of oleylamine.²⁴⁰

Dialkylphosphonic acid is also one of the impurities in technical grade TOPO²³⁴ and has been used to prepare the metal precursors and control the NP core growth kinetics. A series of fatty acids were also used as the surface ligands of Cd chalcogenide QDs. Fatty acids were introduced as the ligands coordinated to the metal precursors and controlled the core growth kinetics during the NP synthesis.^{241,242} In parallel, NP synthesis in noncoordinating solvents has also been developed such as the use of fatty acids including oleic acid and stearic acid. The benefit of using noncoordinating solvents for NP synthesis is that the precursor reactivity can be simply tuned by the type of coordinating ligand and the ligand concentration. 1-Octadecene (ODE) has been commonly used as a non-coordinating solvent, primarily due to its low melting point ($\sim 15^\circ\text{C}$) and high boiling point ($\sim 315^\circ\text{C}$). In a representative example of its versatility, Mulvaney et al. used a binary ligand system (bis(2,2,4-trimethylpentyl)phosphonic acid and oleic acid) in ODE to tune the nucleation and growth of CdSe QDs, and successfully synthesized QDs with different size range.²⁴³

While we primarily focus on cadmium chalcogenide QDs, due to their popularity and the better understanding of their properties, surface ligands on some other common QDs need to be briefly addressed. High quality ZnSe QDs are typically synthesized by conventional hot injection methods^{244–246} such as the decomposition of pyrophoric ZnEt_2 and TOP:Se in alkyl amine²⁴⁵ or the decomposition of air stable zinc stearate and TOP:Se in octadecane.²⁴⁶ These reaction conditions indicate that either the alkyl amine or alkyl carboxylate coordinates the ZnSe QD surface and maintains colloidal stability. NMR studies of PbS QDs synthesized using PbCl_2 and elemental sulfur in the presence of oleylamine and TOP revealed that the QD surface was solely passivated by oleylamine.²⁴⁷ The oleylamine ligands exhibited fast adsorption/desorption behavior and were easily replaced by oleic acid. PbSe QDs synthesized using $\text{Pb}(\text{OAc})_2$ and TOP:Se in the presence of oleic acid were also studied in a similar fashion.²⁴⁸ Here, it was found that the QD surface is composed of Pb atoms and primarily coated by oleic acid with only 0–5% of TOP. Hens et al. also synthesized CuInS_2 QDs in the presence of amine ligands (1-octadecylamine or oleylamine).²⁴⁹ Their NMR studies revealed that as-synthesized CuInS_2 QDs have charge-neutral QD surfaces, which are stabilized by L-type amine ligands.

Upconversion NPs (UCNPs) are typically lanthanide-doped inorganic NPs, which convert a lower energy excitation light into a higher energy luminescence.^{250–256} Their unique properties including sharp emission band, large Stokes shift, and high photochemical stability have made UCNPs attractive as novel luminescent materials. While a variety of synthetic methods have been demonstrated for preparing UCNPs, one of the most successful approaches for monodispersed high-quality UCNPs coated with hydrophobic ligands is the thermal decomposition method. In particular, NaYF_4 doped with $\text{Yb}^{3+}/\text{Er}^{3+}$ (or $\text{Yb}^{3+}/\text{Tm}^{3+}$) have been recognized as one of the most efficient UCNPs and their synthetic methods through thermal decomposition have been well explored. The NaYF_4 -based UCNPs are typically synthesized with sodium trifluoroacetate and lanthanide trifluoroacetate in a mixture of ODE and oleic acid (and oleylamine) at $\sim 300^\circ\text{C}$ or higher.^{257–261} Under these conditions the surface ligands are most likely oleic acid and/or oleylamine. TOPO (90%) was also used for NaYF_4 -based UCNP synthesis instead of oleic acid and oleylamine.²⁶² The latter NaYF_4 -based UCNPs have smaller size with narrow size distribution and higher upconversion luminescence efficiency compared with the ones prepared with oleic acid and oleylamine. Another facile route to prepare small and monodispersed UCNPs is use of the coprecipitation method, which usually uses oleic acid as a capping ligand in ODE.^{263–265} While metal oleates are used as lanthanide precursors, NaOH and NH_4F in methanol have successfully worked as sodium and fluoride sources, respectively.

Recently, silicon (Si) NPs have attracted much attention as nanoscale emitters because silicon is abundant on earth and regarded as less toxic compared to the other conventional semiconductor materials.^{266–274} Si NPs are typically synthesized by either etching of bulk silicon (top-down approach) or chemical reaction of silicon precursors (bottom-up approach). The as-prepared Si NPs normally have either hydrogen- or halide-terminated surfaces, which have to be further modified to ensure good colloidal stability in organic media. In contrast to conventional metal chalcogenide QDs, surface modification of Si NPs requires the formation of covalent bonds between surface silicon atoms and carbon, nitrogen, or oxygen atoms. The Si–H surface bond can be modified by hydrosilylation with organic molecules functionalized with a carbon–carbon double bond or triple bond end group in order to produce both hydrophobic and hydrophilic surface types. The Si–X (X = Cl or Br) surface bond can be replaced with a Grignard reagent or alkyl lithium to form the alkyl-terminated surfaces. Similar surface modification strategies can be used to prepare hydrophilic surfaces using organic molecules with polar functional groups including hydroxy, amino, and carboxyl groups.

Recently perovskite nanocrystals of the $\text{CH}_3\text{NH}_3\text{PbX}_3$ or CsPbX_3 (X = Cl, Br, I) type have received increased attention due to their sharp emission peaks and narrow band widths, high photoluminescence quantum yields, and emission color tunability.²⁷⁵ As such they have found widespread optoelectronic applications, especially in light emitting devices (LEDs), which will be discussed later.²⁷⁶ The synthesis of organic–inorganic MAPbX_3 perovskite nanoparticles relies on the reaction of a lead halide salt (PbX_2 , X = Cl, Br, I) with methylammonium bromide and long or medium alkyl chain ammonium cations such as octylammonium bromide or octadecylammonium bromide, which serve as the capping ligands.^{277–279} On the other hand, all inorganic perovskite

Table 5. Representative Luminescent NPs Synthesized in Organic Media^a

material	precursors and reagents	ligand/surfactant	size (nm)	shape (sp)	solvent	other comments
ZnSe ²⁴⁵	ZnEt ₂ , TOP:Se	HDA, TOP		sphere (sp)	HDA, TOP	
ZnSe ²⁴⁶	Zn stearate, TOP:Se	stearic acid, TOP		sp	ODE	
ZnSe ²⁴⁴	Zn stearate, TBP:Se	stearic acid, ODA, TOP		sp	tetracosane, ODE	
ZnTe ^b	ZnEt ₂ , TOP:Te	ODA, TOP	4.5	sp	ODA, TOP	
ZnTe ^c	Zn(OAc) ₂ , TOP:Te, superhydride	OA, TOP	~5	sp	benzyl ether	
CdS ²³³	CdMe ₂ , (TMS) ₂ S	TOP, TOPO		sp	TOP, TOPO	
CdS ²⁴¹	CdO, S	OA	2.0–5.3	sp	ODE	
CdSe ²³³	CdMe ₂ , TOP:Se or (TMS) ₂ Se	TOP, TOPO	1.2–11.5	sp	TOP, TOPO	
CdSe ²³⁵	CdO, TBP:Se	TOPO, HPA (or TDPA)			TOPO	
CdSe ^d	Cd(OAc) ₂ , TOP:Se	TOP, TOPO, HDA, TDPA			TOP, TOPO, HDA	
CdSe ^e	Cd(acac) ₂ , TOP:Se	TOP, TOPO, HDA, HDDO		sp	TOP, TOPO, HDA	
CdSe ^f	Cd(acac) ₂ , TOP:Se	TOP, TOPO, HDA, HDDO, HPA		sp	TOP, TOPO, HDA	
CdSe ²⁴³	CdO, TOP:Se	TMPPA, OA	~1.8–5.6	sp	ODE	
CdSe ^g	CdO, Se	myristic acid	~2–4.5	sp	ODE	heat-up method
CdSe ²⁸³	CdO, Se	myristic acid	~2.6–3.1	sp	ODE	heterogeneous ODE-Se precursor was injected.
CdT ^e ²³³	CdMe ₂ , TOP:Te or (BDMS) ₂ Te	TOP/TOPO		sp	TOP, TOPO	
CdT ^e ^h	CdO, TBP:Te	OA (or ODPA, TDPA), TBP	~2–11	sp	ODE	
InP ^f	In(OAc) ₃ , (TMS) ₃ P	myristic acid, 1-octylamine		sp	ODE	
InP ^j	InCl ₃ , Zn undecylenate, (TMS) ₃ P	stearic acid, HDA		sp	ODE	
InP ^k	InCl ₃ , ZnCl ₂ , P(NMe ₂) ₃	OLA		sp	OLA	
InAs ^l	InCl ₃ , (TMS) ₃ As	TOP	2.3–6	sp	TOP	
InAs ^m	In stearate, (TMS) ₃ As	stearic acid, TOP		sp	ODE	
PbS ⁿ	PbO, (TMS) ₂ S	OA		sp	ODE	
PbS ^o	PbCl ₂ , S	OLA		sp	OLA	
PbS ^p	Pb(OAc) ₂ , (TMS) ₂ S	OA, TOP		sp	ODE	
PbS ²⁴⁷	PbCl ₂ , S	OLA, TOP	3–10	sp	OLA	
PbSe ^q	Pb oleate, TOP:Se	OA, TOP	3.5–15	sp	diphenyl ether	
PbSe ^r	PbO, TOP:Se	OA, TOP	3–13	sp	ODE	
CuInS ₂ ^s	CuI, InI ₃ , S	TOP, OLA		sp	ODE	
CuInS ₂ ^t	Cu(acac) ₂ , In(acac) ₃ , S	OLA	6–12	sp	o-dichlorobenzene	
CuInS ₂ ^u	Cu(OAc), In(OAc) ₃ , DDT	DDT	2–5	sp	ODE	
CuInS ₂ ^v	CuI, In(OAc) ₃ , DDT	DDT		sp	ODE	
CuInS ₂ ^w	CuI, In(OAc) ₃ , DDT	OA, DDT	3.5–7.3	pyramidal	ODE	
CuInS ₂ ²⁸⁴	CuI, In(OAc) ₃ , DDT	DDT	~2.2–3.8	tetrahedral	DDT	
Ag ₂ S ^x	Ag(DDTC)	OA, ODA	10.2–40.1	sp	ODE	
Ag ₂ S ^y	Ag(OAc), (TMS) ₂ S, S	myristic acid, 1-octylamine	1.5–4.6	sp	ODE	
Ag ₂ S ^z	AgCl, (NH ₄) ₂ S	OLA, TOP	2.1–2.8	sp	OLA, TOP	photochemical reaction
Ag ₂ S ²⁸⁵	DDT-functionalized AgNPs, TBBT	DDT, TBBT	1.7	sp	toluene	RE: rare earth metal
NaYF ₄ :Yb ³⁺ , Er ³⁺ (or Tm ³⁺) ²⁵⁸	Na(CF ₃ COO), RE(CF ₃ COO) ₃	OA, OLA	(1) ~11–14 (2) hexagonal plate	(1) polyhedra (2) 187 × 71, 100 × 51	ODE	
NaYF ₄ :Yb ³⁺ , Er ³⁺ (or Tm ³⁺) ²⁵⁷	Na(CF ₃ COO), RE(CF ₃ COO) ₃	OA	10–50	sp	ODE	

Table 5. continued

material	precursors and reagents	ligand/surfactant	size (nm)	shape	solvent	other comments
$\text{NaYF}_4\text{:Yb}^{3+}\text{Er}^{3+}$ (or Ho^{3+} , Tm^{3+}) ²⁶²	$\text{Na}(\text{CF}_3\text{COO})$, $\text{RE}(\text{CF}_3\text{COO})_3$	TOPO, OLA, OA	5–20	sp	ODE	
$\text{NaYF}_4\text{:Yb}^{3+}\text{Er}^{3+}$ (or Tm^{3+}) ²⁶³	RECl_3 , NaOH , NH_4F	OA	(1) 21 (2) 17×22 (3) 30×45	(1) sp (2) ellipse (3) plate	ODE	
$\text{NaYF}_4\text{:Yb}^{3+}\text{Er}^{3+}$ (or Tm^{3+}) ²⁵⁵	NaCl , RECl_3 , NH_4F	PEI	~20	sp	ethylene glycol	
$\text{NaYF}_4\text{:Yb}^{3+}$, Er^{3+} ²⁵⁶	$\text{Na}(\text{CF}_3\text{COO})$, $\text{RE}(\text{CF}_3\text{COO})_3$	OA, TOP	18–200	hexagonal prism	ODE	
Si^{270}	(1) Mg_2Si (or KSi , NaSi), SiCl_4 (2) RLi or RMgCl	(1) Cl (2) alkyl group	2–5	sp	glyme	R: alkyl group
Si^{271}	diphenylsilane, octanol	octanol	1.5–4	sp	octanol, hexane	
Si^{272}	(1) SiCl_4 , TOAB , LiAlH_4 (2) H_2PtCl_6 , 1-heptene	(1) hydrogen (2) 1-heptene	1.8	sp	toluene	
Si^{273}	(1) SiH_4 (2) HF/HNO_3 (3) alkene	(2) hydrogen (3) alkyl group		sp (appr)	(2) MeOH (3) alkene	
Si^{286}	SiCl_4 , $\text{SiCl}_3(\text{hexyl})$, LiAlH_4	hexyl group	~3	sp	toluene	
Si^{274}	SiCl_4 , $\text{SiCl}_3(\text{allyl})$, LiAlH_4	allyl group	3.7	sp	toluene	
$\text{CH}_3\text{NH}_3\text{PbBr}_3$ ²⁷⁷	PbBr_2 , $\text{CH}_3\text{NH}_3\text{Br}$, $\text{CH}_3(\text{CH}_2)_7\text{NH}_3\text{Br}$ or $\text{CH}_3(\text{CH}_2)_{17}\text{NH}_3\text{Br}$	octylammonium bromide or octadecylammonium bromide	6	sp	ODE/OA	
$\text{CH}_3\text{NH}_3\text{PbX}_3$ ($\text{X} = \text{Br}$, I) ²⁷⁸	PbX_2 , OLA, OA, CH_3NH_2	OLA, OA	(2) 35 (4) 10	(1) cubic (2) plate (3) wire (4) sp (dot)	ODE	
$\text{CH}_3\text{NH}_3\text{PbX}_3$ ($\text{X} = \text{Cl}$, Br , I) ²⁷⁹	PbX_2 in OA/OLA, NMF	OA, OLA	17–25	bulk, cubic	DCB (for $\text{X} = \text{Cl}$ and Br), CHCl_3 (for $\text{X} = \text{I}$)	size control achieved by varying injection temperature
CsPbX_3 ($\text{X} = \text{Cl}$, Br , I) ²⁸⁰	Cs_2CO_3 , PbX_2 , OLA, OA	OA, OLA	4–15	cubic	ODE	

^a ZnEt_2 , diethylzinc; TOP, trioctylphosphine; HDA, hexadecylamine; ODE, 1-octadecene; TBP, tributylphosphine; ODA, octadecylamine; $\text{Zn}(\text{OAc})_2$, zinc acetate; OA, oleic acid; CdMe_2 , dimethylcadmium; $(\text{TMS})_2\text{S}$, bis(trimethylsilyl) sulfide; TOPO, trioctylphosphine oxide; $(\text{TMS})_2\text{Se}$, bis(trimethylsilyl)selenide; HPA, *n*-hexylphosphonic acid; TDPA, *n*-tetradecylphosphonic acid; $\text{Cd}(\text{OAc})_2$, cadmium acetate; $\text{Cd}(\text{acac})_2$, cadmium acetylacetonate; HDDO, 1,2-hexadecanediol; TMPPA, bis(2,2,4-trimethylpentyl)phosphine acid; MA, myristic acid; $(\text{BDMs})_2\text{Te}$, bis(*tert*-butyldimethylsilyl) telluride; ODPA, *n*-octadecylphosphonic acid; $\text{In}(\text{OAc})_3$, indium acetate; $(\text{TMS})_3\text{P}$, tris(trimethylsilyl)phosphine; SA, stearic acid; $\text{P}(\text{NMe}_2)_3$, tris(dimethylamino)phosphine; OLA, oleylamine; $(\text{TMS})_3\text{As}$, tris(trimethylsilyl)arsine; $\text{Pb}(\text{OAc})_2$, lead acetate; $\text{Cu}(\text{acac})_2$, copper acetylacetonate; $\text{In}(\text{acac})_3$, indium acetylacetonate; $\text{Cu}(\text{OAc})_2$, copper(II) acetate; DDT, 1-dodecanethiol; Ag(DDTC), silver diethyldithiocarbamate; Ag(OAc), silver acetate; TBBT, 4-*tert*-butylbenzenethiol; RE, rare earth metal; PEI, polyethylenimine; RLi, alkyl lithium; RMgCl , alkyl magnesium chloride; TOAB, tetraoctylammonium bromide; NMF, *N*-methylformamide; DCB, dichlorobenzene. ^bReference 287. ^cReference 288. ^dReference 289. ^eReference 290. ^fReference 291. ^gReference 292. ^hReference 293. ⁱReference 294. ^jReference 295. ^kReference 296. ^lReference 297. ^mReference 298. ⁿReference 299. ^oReference 300. ^pReference 301. ^qReference 302. ^rReference 303. ^sReference 304. ^tReference 305. ^uReference 306. ^vReference 307. ^wReference 308. ^xReference 309. ^yReference 310. ^zReference 311.

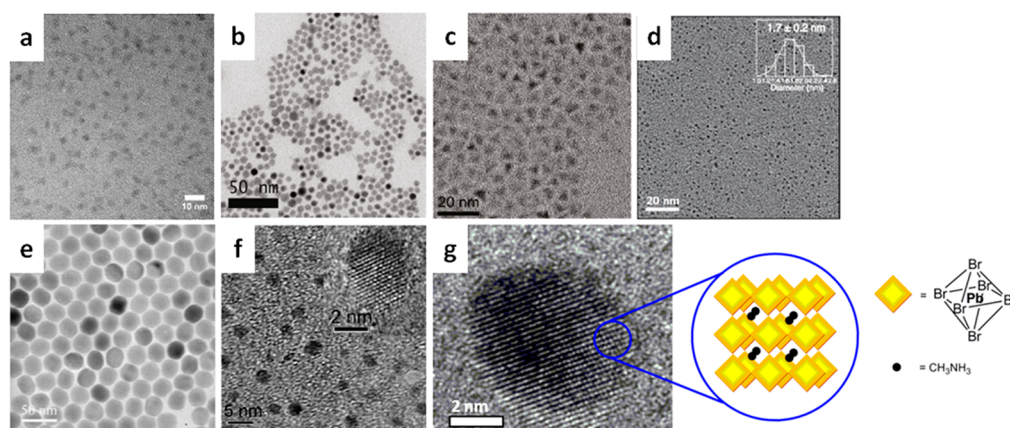


Figure 10. Representative TEM images of (a) ZnSe, (b) PbS, (c) CuInS₂@ZnS, (d) Ag₂S, (e) UCNPs, (f) Si NPs, and (g) MAPbX₃ luminescent nanoparticles. (a) Reproduced with permission from ref 283. Copyright 2013 American Chemical Society. (b) Reproduced with permission from ref 247. Copyright 2011 American Chemical Society. (c) Reproduced with permission from ref 284. Copyright 2011 American Chemical Society. (d) Reprinted with permission from ref 285. Copyright 2016 Wiley. (e) Reprinted with permission from ref 263. Copyright 2008 Wiley. (f) Reprinted with permission from ref 286. Copyright 2011 Royal Society of Chemistry. (g) Reproduced with permission from ref 277. Copyright 2014 American Chemical Society.

nanoparticles are generally produced via a hot-injection method that involves the reaction of cesium-oleate with a lead halide in octadecene at high temperature (140–200 °C). The addition of equimolar amounts of oleic acid and oleylamine stabilizes both the lead precursors as well as the resulting cubic nanocrystals.²⁸⁰ More in depth discussions on the synthesis, properties, and applications of lead halide perovskite nanocrystals can be found in several informative review articles.^{275,281,282}

Table 5 concentrates the literature from a variety of representative fluorescent NPs synthesized in organic media and highlights the relevant ligands employed along with the diversity of materials obtained. Figure 10 shows some representative TEM images of some of these materials.

2.2.4. Other Nanoparticles. Metal oxide NPs are often synthesized by sol–gel processes in which water is usually required as a reactant. The as-prepared particles have hydroxylated polar surfaces. On the other hand, metal oxide NPs dispersible in organic media are synthesized by non-hydrolytic sol–gel methods, aiming for better crystallinity. Among a series of metal oxides, ZnO and TiO₂ have been extensively studied primarily due to their interesting electronic properties and their utility in a variety of electronic devices as well as for catalysis.^{312–314}

ZnO is one of the important wide band gap semiconducting materials and has a broad range of applications in optoelectronics and biomedicine.^{315–317} ZnO NPs can be obtained by a variety of approaches such as using ZnEt₂ in the presence of *n*-octylamine and TOPO³¹⁸ or using dicyclohexylzinc and a series of alkylamine exposed to air at RT.³¹⁹ Furthermore, the thermal decomposition of Zn(OAc)₂ in alkylamines in the presence of *tert*-butylphosphonic acid was demonstrated.³²⁰ The growth of ZnO NPs was governed by the molar ratio of Zn(OAc)₂ and *tert*-butylphosphonic acid, suggesting that the phosphonic acids were the main surface ligands. In contrast to spherical NP materials, ZnO NPs with different shapes could be prepared via nonhydrolytic ester elimination sol–gel reactions with Zn(OAc)₂ and 1,12-dodecanediol.³²¹ The use of TOPO, 1-hexadecylamine, and tetradecylphosphonic acid as the surface ligands in the reaction formed cone-, hexagonal cone-, and rod-shaped NPs,

respectively. Contrastingly, a mixture of Zn(OAc)₂ and oleic acid in ethanol, refluxed in the presence of tetramethylammonium hydroxide could be used to obtain ZnO NPs.³²²

TiO₂ NPs have also found crucial roles in a wide variety of applications including dye-sensitized solar cells, photocatalysis, and batteries.^{323–325} Colvin et al. adopted a hot injection method to synthesize TiO₂ NPs, using titanium halide and titanium alkoxide in the presence of TOPO at 300 °C.³²⁶ While the reactions without TOPO were fast and yielded larger particle sizes (>10 nm), the reaction with TOPO was slower and resulted in smaller NPs (5.5 nm), suggesting that TOPO worked as the surface ligand and played a critical role to control the NP growth.

As opposed to the nearly spherical NPs obtained through the use of TOPO, it was shown that by progressively replacing TOPO by a more facet-selective surfactant such as lauric acid anatase nanocrystals with increased anisotropy and branching are produced.³²⁷

The most influential factor to control the shape of the TiO₂ nanoparticles is by manipulating their growth kinetics. The presence of tertiary amines or quaternary ammonium hydroxides as catalysts is essential to promote fast crystallization under mild conditions³²⁸ and to synthesize TiO₂ NRs with a one-step, low temperature route. When only oleic acid is present, slow hydrolysis reaction takes place and nearly spherical nanoparticles are formed. Anisotropic hyperbranched organic capped TiO₂ topologies have been achieved by sequent exploitation of aminolysis and pyrolysis in a binary surfactant mixture (oleic acid and oleylamine).³²⁹ First-generation branched nanoparticles initially formed upon the aminolysis reaction possess a strained monocrystalline skeleton, while their corresponding second-generation derivatives fed by pyrolysis pathways accommodate additional arms crystallographically mismatched with the lattice underneath. Furthermore, more complex core–antenna structures have been developed by a seed-mediated growth method.³³⁰ According to this, TiO₂ nanoparticle seeds with well-defined shapes followed by the epitaxial growth of nanorod antennas on the seeds along the (110) direction. In a typical synthesis, truncated octahedral bipyramidal nanoparticles are used as seeds, together with oleic acid and a Ti precursor, which are

Table 6. Metal Oxides Synthesized in Organic Media^b

material	precursors and reagents	ligand/surfactant	size (nm)	shape	solvent	other comments
ZnO ³¹⁸	ZnEt ₂	TOPO, octylamine	<4.4	sp	TOPO, octylamine, decane	
ZnO ³¹⁹	ZnCy ₂	HDA, DDA, octylamine		Rod, disk	THF	
ZnO ³²⁰	Zn(OAc) ₂	alkylamine, <i>tert</i> -butylphosphonic acid	3–9	sp, elongated	alkylamine	
ZnO ³²¹	Zn(OAc) ₂ , 1,12-dodecanediol	(1) TOPO, OA (2) HDA (3) TOPO, TDPA	(1) 70 × 170 (2) 40 × 29 (3) 5.5 × 23	(1) cone (2) hexagonal cone (3) rod	(1) dioctyl ether, TOPO (2) HDA (3) dioctyl ether, TOPO	
ZnO ^b	Zn stearate, 1-octadecanol	stearic acid, ODPA		sp	ODE	
ZnO ³²²	Zn(OAc) ₂	OA	5	sp	EtOH	
TiO ₂ ³²⁶	TiX ₄ , Ti(OR) ₄	TOPO			heptadecane	X: halide
TiO ₂ ³³¹	Ti(O- <i>i</i> Pr) ₄	OA	<6		toluene	
TiO ₂ ³³²	Ti(O- <i>i</i> Pr) ₄ , tertiary amine or quaternary ammonium hydroxide	OA	3–4 × <40 (rod)	rod, sp (with ethylene glycol)	OA	
TiO ₂ ³³⁵	TiCl ₄	4- <i>tert</i> -butylcatechol	~5	sp	benzyl alcohol	
TiO ₂ ³³³	Ti(O- <i>i</i> Pr) ₄	OA, OLA	2 × 12–30 (rod) 2.3 (sp)	rod, sp	ODE	
TiO ₂ ³³⁴	Ti(COT) ₂ , DMSO	TBP, TBPO, or TOPO	3–25	sp	<i>o</i> -dichlorobenzene	

^aCy, cyclohexyl; DDA, dodecylamine; ODPA, octadecylphosphonic acid; ZnCy₂, dicyclohexylzinc; TiX₄, titanium halide; Ti(O-*i*Pr)₄, titanium isopropoxide; Ti(COT)₂, bis(cyclooctatetraene)titanium; COT, cyclooctatetraene; TBP, tributylphosphine; TBPO, tributylphosphine oxide
^bReference 338.

heated at high temperature (270 °C). The morphology of the antennas could be controlled by modifying the precursor introduction rate.

Solvothermal synthesis was also applied to synthesize TiO₂ NPs using Ti(*i*PrO)₄ and oleic acid as precursor and surfactant, respectively.³³¹ The reaction with this surfactant led to narrower size distribution than one without surfactant. Weller et al. demonstrated the synthesis of TiO₂ NRs and spherical NPs using Ti(*i*PrO)₄ and oleic acid in the presence of tertiary amines or quaternary ammonium hydroxide as a base.³³² A similar procedure was performed for the synthesis of TiO₂ NRs and spherical NPs via aminolysis using oleylamine.³³³ The low-valent organometallic complex, bis-(cyclooctatetraene)titanium, and DMSO could also be utilized as precursors for TiO₂ NPs, which were formed at temperatures as low as RT.³³⁴ While the reaction without any ligand resulted in precipitation of amorphous TiO₂ powder, the reaction with coordinating ligands such as tributylphosphine, tributylphosphine oxide, and TOPO produced a homogeneous solution with internally crystalline TiO₂ NPs. The reaction between TiCl₄ and benzyl alcohol with 4-*tert*-butylcatechol formed crystalline TiO₂ NPs highly dispersible in organic solvents.³³⁵ ¹H NMR analysis of these NPs revealed the presence of adsorbed 4-*tert*-butylcatechol and benzyl alcohol on the NP surface. Nanofibers of various sizes and layered structures were also fabricated at ambient conditions.³³⁶ This is the first time that phase transitions from the titanate nanostructures to TiO₂ polymorphs take place readily in simple wet-chemical processes at ambient conditions. Hollow nanotubes observed when the obtained nanocrystals react with concentrated basic solution. More complex shapes of TiO₂ nanocrystals such as rhombic, truncated rhombic, spherical, dog-bone, truncated and elongated rhombic, and bar have been synthesized by a simple variation of the oleic acid/oleylamine ratio or the amount of titanium *n*-butoxide or reaction temperature enables a fine control of the growth rate of TiO₂ NPs and, consequently, a control of the shape of these particles.³³⁷ By increasing the molar ratio of OA/OM the

particles transform from rhombic (OA/OM = 4/6) to truncated rhombic (OA/OM = 5/5) and spherical (OA/OM = 6/4).

Table 6 presents some representative examples of ZnO and TiO₂ NPs synthesized in organic media and the ligands used in each case while Figure 11 shows some representative TEM of intermediaries and final examples of the latter.

3. LIGAND MODIFICATION FOR WELL-DISPERSED AND FUNCTIONAL NANOPARTICLES IN COMPLEX MEDIA

This section focuses on the important role of ligands for the colloidal dispersity and function of NPs in complex media such

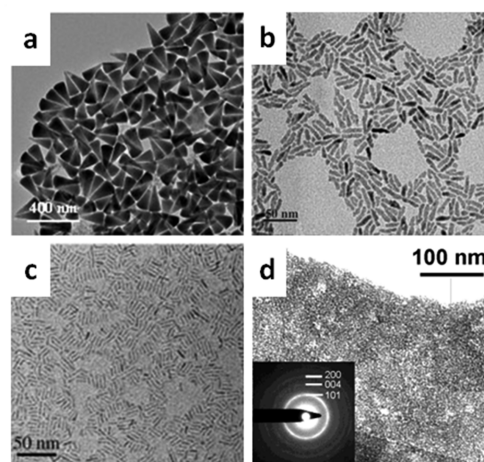


Figure 11. TEM images of (a) OA-stabilized ZnO NPs, (b) ZnO NRs, (c) OA-capped length tunable TiO₂ NRs, and (d) dopamine-stabilized TiO₂ NPs all synthesized in organic media. (a,b) Reprinted with permission from ref 321. Copyright 2005 Wiley. c Reprinted with permission from ref 333. Copyright 2005 Wiley. (d) Reproduced with permission from ref 335. Copyright 2004 American Chemical Society.

as the ones often met in biomedicine, energy harvesting devices, and catalytic systems. Different ligand modification strategies will be discussed for both biological and non-biological applications, including the direct functionalization during the synthesis of NPs or the postsynthetic modification of a NP surface. Particular emphasis will be given to the design of ligand coatings for NPs to be used as therapeutical and diagnostic tools in biomedicine due to the combined relevance and challenging requirements associated with this field.

3.1. Ligand Coating of Nanoparticles for Biomedical Applications

It is well accepted that the NP ligand shell plays a significant role in the design of nanotherapeutic probes regulating their pharmacokinetics, efficacy, and toxicity. Ligands that coat the surface of NPs should exert adequate colloidal stabilization and NP sealing from other molecules in challenging biological environments while functional ligands should increase NP targetability and perform distinct biological roles. Especially for in vivo applications it is critical to minimize NP aggregation by choice of appropriate ligands. The in vivo fate of NPs critically depends on their size. For example, for tumor targeting applications, NP size and characteristics have to be finely tuned in accordance with the tumor state to achieve maximal tumor penetration.³³⁹ Increases in overall NP size, e.g., due to aggregation could inhibit tumor targeting. Additionally, very small NPs might leak into blood vessels, while very large NPs or aggregates of NPs might become subject to macrophage clearance without being able to fulfill their therapeutic role.³⁴⁰ Therefore, it is of utmost importance to choose the right ligand coating for the desired biomedical application. It is also worth mentioning that for biomedical applications, ligand selection should also consider the biocompatibility and biodegradability/excretion of the ligand as a general requirement for clinical use.

Various ligands such as carbohydrates, oligonucleotides, polymers, peptides, and proteins have been utilized in biomedical applications, and in the following sections, we discuss the ones most commonly employed.^{341–343} Figure 12

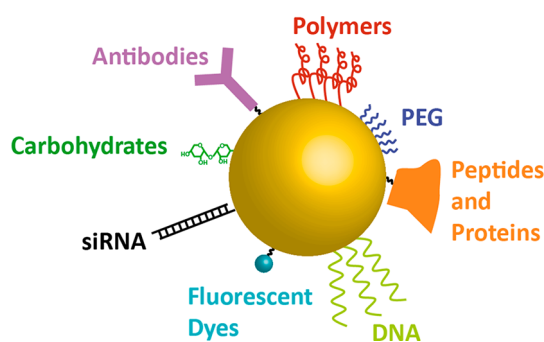


Figure 12. Different ligands commonly used in NPs designed for biomedical applications including antibodies, oligonucleotides, carbohydrates, proteins, polymers, and dyes.

shows some examples of ligands used for biomedical applications while Table 7 summarizes selected examples of nanotherapeutics that are commercially available or under advanced clinical evaluation with various surface ligands.

3.1.1. Ethylene Glycol Containing Ligands. Polyethylene glycol (PEG) is a unique category of various molecular weights polymers, which possess fascinating properties such as biocompatibility, high solubility in water and in a

wide range of organic solvents, as well as exceptional capability to stabilize NPs against aggregation. One of the first examples of the importance of these polymers in NP functionalization was demonstrated during the development of Doxil, the first FDA liposomal nanoformulation of doxorubicin.³⁴⁴ Initially, most of the liposomes loaded with the anticancer drug doxorubicin were accumulated in the spleen and liver rather than the targeting tumor site. The solution came by the functionalization of these liposomes with PEG brushes covering their surface, preventing the nonspecific adsorption of plasma proteins and thus resulting in effective minimization of liposome accumulation into the liver and spleen.³⁴⁴ After these findings, the use of PEG became a common practice in designing nanotherapeutics at both the research and commercial levels in order to stabilize NPs against aggregation, prevent uptake by nontarget organs, increase their circulation time in blood, and enhance accumulation into targeted organs.³⁴⁵ PEGylation of NPs can be achieved via various routes. The simplest way is the addition of PEG molecules during NP synthesis. This approach is commonly employed to coat polymeric NPs, and it has also been demonstrated for the functionalization of inorganic NPs such as Au, Ag, and iron oxide. It was shown that PEG can play multiple roles simultaneously, acting as a solvent/cosolvent, a reducing agent as well as a capping agent.^{79,346–349} Despite the simplicity of the experimental protocols, the PEG molecules are only weakly bound to the NPs, and thus they can easily detach from the NP surface during various processing steps (e.g., dilution/dialysis, centrifugation, heating, drying, aging, mixing with other compounds, etc.). A strategy to make a stable coating of PEGs on NPs has been recently demonstrated as illustrated in Figure 13.³⁵⁰ An amphiphilic polymer grafted with both alkyl chains and PEG molecules is self-assembled into micelles and coats the surface of NPs. The coating stabilizes the NPs as a result of the large conformation entropy repelling any foreign materials.^{80,350} Other strategies involve the functionalization of PEG molecules, with NP binding head groups such as thiols, amines, carboxylic acids, or silanes.^{351–353}

PEG-modified nanomaterials tend to reduce immunological reactions, which can be attributed to the repelling nature of PEG to proteins, as it tends to reduce total serum protein adsorption (opsonization) as a function of grafting density and molecular weight of the polymer.^{354–356} However, some studies also suggest that PEG coating might facilitate the binding of other proteins (albumin for instance)³⁵⁷ and thereby blocking the way for immunoglobulins in a process known as “dysopsonization”.^{354–356,358} While the stability of NPs grafted with PEG-containing ligands in vivo is still unclear, many in vitro experiments have been carried out to shed more light on this family of ligands. For example, Au NPs functionalized with mPEG-thiol (5 or 10 kDa) were found to be prone to ligand displacement by cysteine resulting in increased adsorption of serum proteins. Interestingly, introduction of alkyl moieties as hydrophobic spacers between the thiol and the PEG prevented this displacement.³⁵⁹

While PEG generally display little net-charge, adding functional end groups such as carboxyl or amine can infer a net negative or positive charge, respectively, altering the properties of the PEG ligand and interactions with biomolecules.³⁵¹ Additional functional groups can be employed for the further conjugation of PEG to biomolecules such as homing peptides or antibodies as well as fluorophores.

Table 7. Nanotherapeutic Agents in Clinical Trials and/or FDA Approved

brand name	indication	modality	surface ligand	approval status
Doxil	anticancer	liposome	PEG	FDA approved
AuroLase	anticancer	silica core with gold shell NP	PEG	pilot study
ThermoDox	anticancer	liposome	thermoreponsive polymeric shell	phase III
NanoTherm	anticancer	iron oxide NP	aminosilane	FDA approved
Ferinject	iron deficient anemia	iron oxide NP	carboxymaltose	FDA approved
Feraheme	iron deficient anemia in chronic kidney disease (CKD)	iron oxide NP (SPION)	polyglucose sorbitol carboxymethyl ether	FDA approved
Ferdex/Endorem	imaging agent	iron oxide NP (SPION)	dextran	FDA approved
GastroMARK	imaging agent	iron oxide NP (SPION)	silicone	FDA approved
NBTXR3	radiotherapy	HfO ₂ NP	not explicitly stated, but designed to have antifouling activity	phase II/III

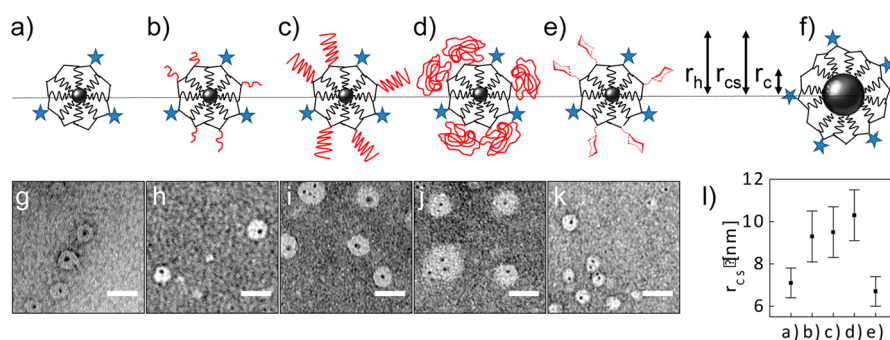


Figure 13. Schematic illustration of NPs containing an inorganic core, coated with the amphiphilic polymer poly(maleic anhydride-*alt*-dodecene) (PMA) and fluorophore DY-636 (light blue). PEG chains of different MW or glucose (red) were attached to the NP surfaces. The resulting NPs are (a) FePt-PMA, (b) FePt-PMA-PEG750, (c) FePt-PMA-PEG5k, (d) FePt-PMA-PEG10k, (e) FePt-PMA-glucose, and (f) Fe₃O₄-PMA respectively. TEM images of (g) FePt-PMA, (h) FePt-PMA-PEG750, (i) FePt-PMA-PEG5k, (j) FePt-PMA-PEG10k, and (k) FePt-PMA-glucose NPs (scale bar: 25 nm). (l) Mean core-shell radius r_{cs} of the FePt NPs. Reprinted with permission from ref 350. Copyright 2015 American Chemical Society.

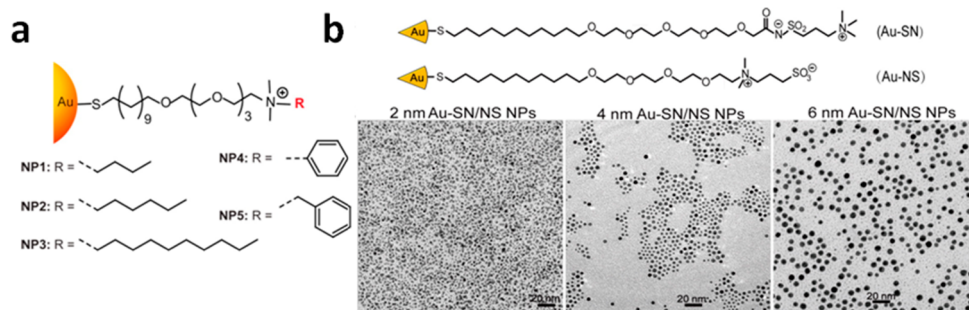


Figure 14. (a) Chemical structures of cationic OEG ligands on Au NPs. (b) Chemical structure of zwitterionic OEG ligands used for Au NP synthesis and corresponding TEM images of zwitterionic Au NPs (2, 4, and 6 nm). (a) Reprinted from ref 367. Copyright 2014 American Chemical Society. (b) Reprinted with permission from ref 366. Copyright 2016 American Chemical Society.

Bifunctional PEG molecules can also serve as cross-linkers/spacers, facilitating further grafting to biomolecules or other groups, while maintaining the stability of the system under different conditions.^{360–363} However, when using homo bifunctional PEG (i.e., two identical end groups), care needs to be taken in order to avoid NP aggregation through cross-linking reactions, which can have detrimental effects on NP function as discussed in section 3.1. Cross-linking and therefore NP aggregation can generally be avoided by using a large excess of such homo bifunctional linkers as has been

shown for iron oxide NPs functionalized with the homo bifunctional linker gallic acid, for example.³⁶⁴

Just like their larger counterparts, the smaller oligo-ethylene glycols (OEGs) have been used as ligand coatings for NPs (e.g., see section 2.1.1).³⁵² For example, carboxy-terminated OEG modified with a hydrophobic alkyl unit including a diacetylene group, which can be photo-cross-linked upon UV irradiation and a terminal thiol for anchoring to the surface of Au NPs have been shown to result in Au NPs with excellent stability toward changes in pH, ionic strength, or ligand

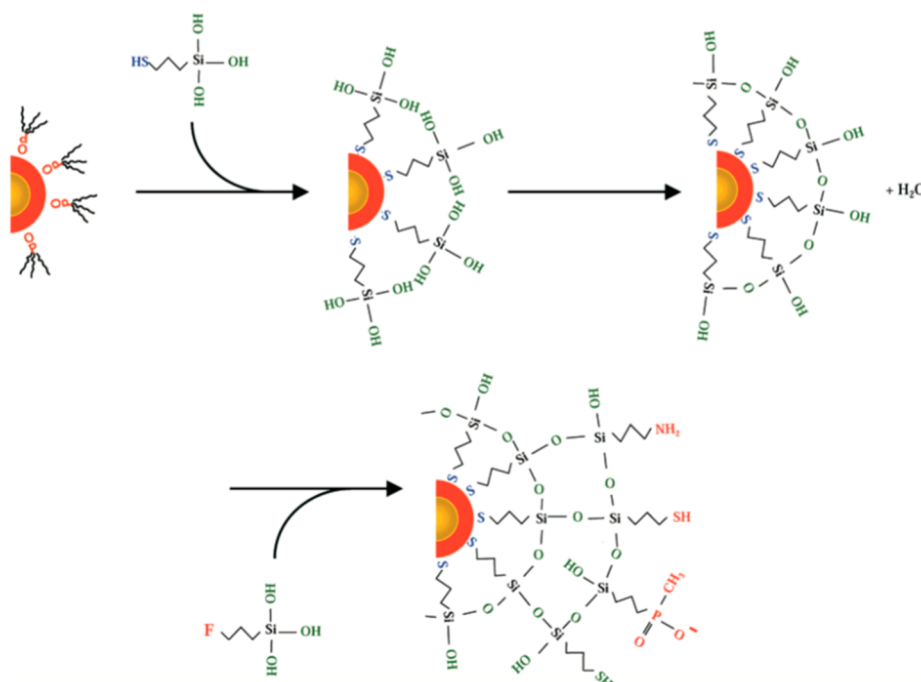
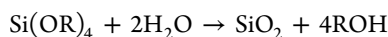


Figure 15. Schematic illustration of the silanization strategy on TOPO-capped CdSe/ZnS core/shell particles. Briefly, the methoxysilane groups (Si-OCH_3) hydrolyze into silanol groups (Si-OH) and produce a primary polymerization layer. Condensation leads to the formation of siloxane bonds and water molecules are released. Next, silane precursors are added into the shell to provide further functionality and finally, to block the shell growth by converting the remaining hydroxyl groups into methyl groups. Reprinted with permission from ref 371. Copyright 2001 American Chemical Society.

displacement and could be selectively polymerized into chains and networks of Au NPs by tuning the density of ligands on the nanoparticle surface.^{353,365} Furthermore, both cationic and zwitterionic OEGs have been shown to provide Au NPs with antimicrobial properties.^{366,367} As discussed for other OEGs, these contained a thiol anchoring group as well as sulfonate and/or quaternary amine groups, which provide negative and positive charges respectively, thus providing electrostatic stabilization (see Figure 14).

3.1.2. Silanes. Among the inorganic coatings used in the design of functional NPs for biomedical applications, silicon-containing ligands are the most widely used due to the combination of its hydrophilic features with chemical and physical stability. These kinds of ligands have been applied to a wide variety of functional NPs (metallic, magnetic, semiconductor) with the purpose of enabling or improving their dispersibility in aqueous media as well as their biocompatibility. In particular, the formation of a cross-linked shell of silicon-containing ligands is a means to reduce particle aggregation in those cases where relevant chemical or physical interactions take place. In the case of metal NPs and QDs, silica shields the functional core from the environment, protecting the NPs toward oxidation and reducing their toxicity.^{368–370}

Several strategies have been devised for the fabrication of NP@SiO₂ core@shell, often relying on the sol–gel synthesis of silica from an alkoxysilane, according to the following chemical reaction:



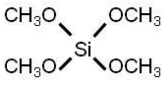
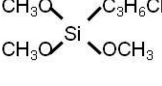
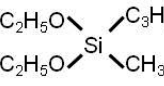
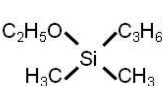
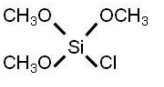
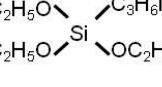
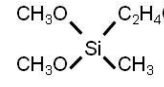
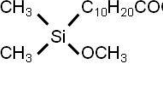
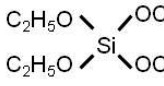
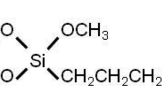
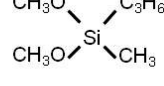
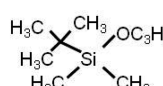
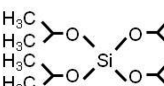
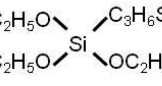
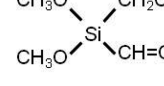
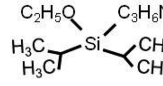
The reaction, which requires the use of acid or basic catalysis, occurs through a multistep equilibrium associated with the hydrolysis of all the alkoxy groups, followed by

condensation of the silanols, which finally leads to the formation of the siloxane bonds. A typical feature of the relevant sol–gel method is that usually condensation does not go to completion under relatively mild reaction conditions, so that a silanol-terminated surface is exhibited. This feature is exploited, both to ensure colloidal stability through repulsion among negatively charged surface core@shells and to enable bioconjugation (Figure 15).³⁷¹ The process of cross-linking of silicon-containing ligands offers the advantage of a well-established sol–gel chemistry, which enables surface functionalization either by reaction with common coupling agents, or by surface condensation of functional alkylsilanes ($\text{R}'\text{Si(OR)}_3$, $\text{R}'\text{R}''\text{Si(OR)}_2$, $\text{R}'\text{R}''\text{R}'''\text{SiOR}$) bearing a nonhydrolyzable functional group R (Table 8).

Most silica-coating protocols have been adapted from the Stöber process for the synthesis of SiO₂ spheres, which relies on controlled hydrolysis and condensation of tetraethylorthosilicate (TEOS, $\text{Si(OC}_2\text{H}_5)_4$) under basic (ammonia) catalysis in ethanolic or hydroalcoholic media.³⁷² The basic idea behind the design of NP@SiO₂ is that the Stöber process is carried out in the occurrence of a NP suspension and that the synthesis parameters are adjusted in such a way that heterogeneous nucleation of silanization on top of the NPs is highly favored as compared to homogeneous nucleation.

This approach was shown to be relatively straightforward in the case of oxide or oxyhydroxide NPs dispersible in ethanol or water. A relevant example was reported by Xia and co-workers, who discussed that deposition of silica from TEOS onto a water-based commercial ferrofluid under ammonia catalysis results in iron oxide@silica with up to 70% of the core@shells containing a single core. By adjusting the TEOS amount, the shell thickness was varied from 2 to 100 nm, and further functionalization with aminopropyl trimethoxysilane (APTS)

Table 8. List of Some Commercially Available Silane Precursors for NP Coating and Functionalization

Si(OR)_4	R'Si(OR)_3	R'R''Si(OR)_2	$\text{R'R''R'''}\text{SiOR}$
Tetramethoxy silane 	3-Chloropropyltrimethoxy silane 	3-aminopropyldiethoxymethyl silane 	3-aminopropylethoxydimethyl silane 
Chloro(trimethoxy) silane 	3-aminopropyltriethoxy silane 	2-Chloro ethyl methyl dimethoxy silane 	10-(Carbomethoxy) Decyldimethoxy silane 
Tetraethoxy silane 	3-glycidoxypopyltrimethoxy silane 	3-mercaptopropylmethyl dimethoxy silane 	(3-Bromopropoxy)-tert-butyl dimethyl silane 
Tetraisopropoxy silane 	3-mercaptopropyltriethoxy silane 	Vinyl(chloromethyl)dimethoxy silane 	3-Aminopropyl siisopropylethoxy silane 

enabled coupling with isothiocyanaterhodamine, producing multifunctional core@shells for magnetic and optical detection.³⁷³ On the other hand, in the case of metal and QD cores, the generation of a silica shell is less trivial, as the use of a primer, with which the initial silica is bound to the NP surface, is needed. The primer needs to have strong affinity for the core surface. Most often vitreophilic groups (typically mercaptopropyltrimethoxysilane or aminopropyltrimethoxysilane) are used for initiating silica shell deposition. By this approach, silanization of several NPs, including Au, Ag, and CdS, has been achieved, provided that the original NPs did not possess covalently bound ligands on their surface.^{369,374}

Improvements of the Stöber approach to core@shell NP design have focused on defining more general protocols, which could include particles not stable in hydroalcoholic media or with limited affinity toward silica. In particular, methoxypoly(ethylene glycol)-thiol (mPEG-SH) was found to be effective in promoting transfer into ethanol of gold spheres and rods without aggregation, enabling subsequent SiO₂ shell growth by Stöber routes.³⁷⁵ A more general procedure relatively independent of the nature of the core includes the use of an amphiphilic nonionic polymer, e.g., PVP, which is adsorbed on the NP surface, enabling the direct transfer of the NPs into an ammonia/ethanol mixture where silica coatings are grown by addition of TEOS. The method was found to be effective for the silanization of Au, Ag, boehmite rods, and gibbsite platelets.³⁷⁶

Another more general modification of core@shell production based on Stöber-like silica shell formation relies on the use of micelles, which are regarded as a nanometer-sized confined environment for controlled nucleation and growth of the silica shell. While early studies focused on the in situ formation of both the core and the silica shell within a micelle template (see for example CdS@SiO₂ in ref 377), nowadays the general approach is to make use of micelle-mediated silica shell deposition on preformed NPs. This is due to a number of reasons, including limited reproducibility associated with the extremely high number of involved synthetic variables, the relatively detrimental effect of micelle synthesis on the physicochemical properties of the inorganic core as compared to high temperature synthetic routes and to the understanding that the vision of micelles as static templates is unrealistic. Recent strategies based on micelle-assisted synthesis take into account the complexity of the synthetic medium, including the possibility of interdroplet exchange due to, e.g., Brownian motions, as well as the effect of the compositional variation in the system with particular reference to ethanol and water, which are directly involved in the sol–gel silica reactions, on the surfactants assemblies.^{378,379} However, the mechanism of NP@SiO₂ formation in microemulsion is not fully elucidated to date. Nevertheless, Koole et al. provided insights in the formation of core@shell NPs obtained by direct TEOS deposition in water-in-oil microemulsion on hydrophobic QDs (CdSe, CdTe, PbSe), which was reported also for the case of CdSe@ZnS dots.³⁸⁰ It is demonstrated that hydrolyzed

TEOS replaces the capping agent originally present on the hydrophobic NP, enabling therefore transfer of the NP into the water phase of the microemulsion, where silica growth takes place. This mechanism is supported by the features of the final core@shell NPs. Silica coating works well when hydrophobic QDs are initially coated with capping agents, which can be easily exchanged by TEOS, leading to NPs with the core exactly in the center of the silica shell. On the other hand, capping agents with a high affinity result in morphologies with off-center core (see Figure 16 a,b).³⁸¹

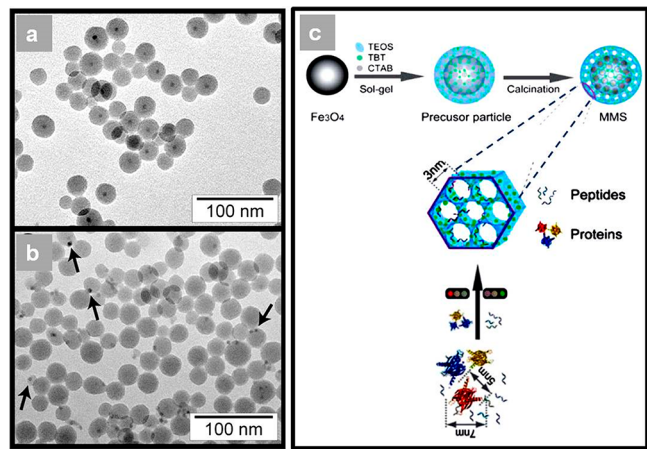


Figure 16. Coating of NPs by dense (a,b) and mesoporous SiO_2 . (c). Silica coating of hydrophobic NPs is affected by the affinity of the original ligands for the NP surface: TEM image of silica coating of NPs coated by ligands with (a) moderate and (b) high surface affinity. Silica with extended mesoporosity (c) may be required to exploit NPs as affinity probes by providing high surface area and pores for size exclusion of undesired analytes. (a,b) Reprinted with permission from ref 381. Copyright 2008 American Chemical Society. (c) Reprinted with permission from ref 382. Copyright 2014 The Royal Society of Chemistry.

Typical microemulsions are based on ternary systems containing water, hexane, or cyclohexane as oil phase, and a commercially available ionic or nonionic surfactant such as Igepal, Triton X-100, AOT, Synperonic NP-5, or CTAB, to name a few. To achieve controlled core@shell morphologies many parameters need to be adjusted, which are relatively independent from the composition of the core.^{383–387}

Recently, it was shown that direct silanization from TMOS can be achieved in one pot during the synthesis of metal halide perovskites QDs. The formation of the core–shell particles is postulated to be affected by the occurrence of oleylamine used as NP capping agent promoting the sol–gel silica shell formation by amine functionalities.³⁸⁸

An alternative approach for core@shell NP/silica production relies on the use of silicic acid as the precursor for the silica shell. Likewise, in the so-called water glass process, silicic acid has to be prepared in situ, usually by passing sodium silicate through cation exchange columns. After addition of silicic acid to the NP suspension, the pH is raised to a suitable value to promote controlled silica condensation on the NP surface. Although a water-based dispersion of the NPs is needed, this approach offers the distinct advantage of enabling the deposition of extremely thin and homogeneous silica shells, whose thickness can be finely modulated by repeated layer deposition. In particular, the occurrence of very thin silica

coatings (1–2 nm) was shown to be highly advantageous in those applications requiring efficient interaction between the core and the biological environment, such as the case of iron oxide@silica NP contrast agents for magnetic resonance imaging (MRI).^{389–392}

Silica coating has been demonstrated to be highly effective in improving the applicability of functional NPs in biomedicine because the pioneering work by Alivisatos and co-workers on the use of silanized QDs as tools for fluorescence imaging and probing of biological systems.^{393,394} State-of-the-art design of silica-based core@shell NPs for biomedical use is focused on exploiting silica shells to achieve multiple functionality such as dual imaging or combined imaging and therapeutic ability (see Figure 17).

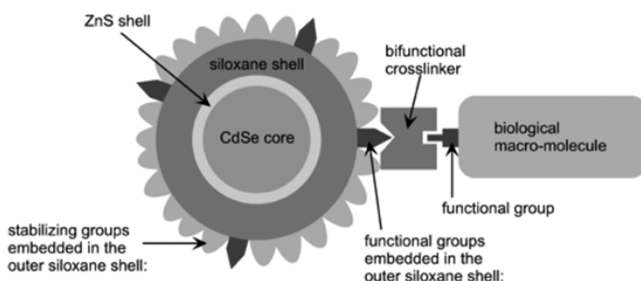


Figure 17. Schematic illustration of a biomolecule–NP conjugate. The core/shell CdSe/ZnS NPs are surrounded by a siloxane shell. To obtain water solubility, stabilizing groups are embedded in the outer siloxane shell, examples of stabilizing groups include phosphonate, PEG, or ammonium. In addition, amines, thiols, or carboxyl groups are incorporated in the siloxane shell as functional groups. Reprinted with permission from ref 394. Copyright 2002 American Chemical Society.

Within the framework of multifunctional NP@ SiO_2 , the synthesis of porous silica shells has been achieved, with particular reference to ordered mesoporous silica shells through Stöber-like approaches mediated by a templating agent such as CTAB. The mesoporosity of the silica shells has been exploited to develop magnetically recoverable core@shell NPs for nucleic acid detection with a high, specific surface area, and to design iron oxide@silica NPs for dual imaging applications by hosting fluorescent dyes and NPs in the porous texture of the mesoporous silica shell.^{395–397} The key role of the porous shell was recently demonstrated with the fabrication of iron oxide NPs coated with mesoporous silica loaded with TiO_2 NPs as a novel affinity probe for proteins. Taking advantage of the strong interaction of TiO_2 to the carboxyl groups of the peptides, of the size-exclusion effect of the ordered mesopores, and of the high available surface area, selective enrichment of endogenous peptides was successfully achieved (see Figure 16c).³⁸²

Although the occurrence of a mesoporous shell may be highly beneficial for the end-use of core@shell NPs in biomedicine, the main limitation of the available synthetic strategies relies on the removal of the templating agent, which generates the porous network. While calcination is the most effective way to promote complete removal of the template and formation of the mesoporous ordered structure, it may alter the functionalities or compromise the dispersibility of the NPs. As an alternative, solvent extraction of the template can be carried out under mild conditions, which however, is usually incomplete. A recent study on the deposition of SiO_2 from

TEOS on CTAB-stabilized AuNRs suggests that CTAB as expected promotes the formation of a mesoporous silica coating and can then be removed by extensive rinsing with ethanol taking advantage of dissolution through the porous silica shell.³⁹⁸ Besides limiting accessible porosity, residual templating agent within the outer silica shell may lead to nonreproducible or undesired interactions between the core@shell NPs and the biological environment.

3.1.3. Oligonucleotides. Their inherent properties of accurate addressability and programmability, high target specificity, as well as ease of synthesis and functionalization have made oligonucleotides attractive ligands for NP functionalization.³⁹⁹ The various types of oligonucleotides do not only play essential roles within living organisms but also have found widespread applications in different research areas ranging from antisense therapy and siRNA delivery to hierarchical self-assembly for the creation of new materials.⁴⁰⁰

On the other hand, chemically modified oligonucleotides, such as locked nucleic acids (LNA) or peptide nucleic acids (PNA), have been developed to increase target binding affinity through increased base-stacking and to be enriched with high stability toward nuclease digestion, respectively. Taking into account the versatility of oligonucleotides, it is unsurprising, that oligonucleotides as ligands to coat NPs play an important role in the function of nanoparticulate systems. Over the last two decades DNA-coated NPs have become increasingly important for applications in biosensing,^{23,401–403} nanomedicine,^{404–414} and metamaterials.^{17,19,415–418} The DNA ligand shell stabilizes the NP core both through sterical and electrostatic interactions resulting in NPs that are highly stable in a variety of complex media. Different conjugation strategies based on direct oligonucleotide chemisorption, physisorption, or involving coupling chemistry have been developed.

Oligonucleotide Conjugation to NPs by Direct Chemisorption. Pioneering work by research groups led by Alivisatos⁴¹⁹ and Mirkin⁴²⁰ in 1996 showed for first time that it was feasible to attach thiol-modified oligonucleotides to Au NPs. While Mirkin and co-workers demonstrated that Au NPs can be modified with a dense DNA corona,^{420,421} Alivisatos and co-workers showed that it was equally possible to produce Au NPs conjugated to a discrete number of oligonucleotides.^{89,419,422,423} To obtain stable DNA-coated NPs for biomedical applications, the covalent conjugation of a dense shell of DNA strands to NPs is often desirable. To achieve high DNA loading on the NP surface, electrostatic repulsion between neighboring DNA strands, as well as between DNA and the anionic Au NP surface must be minimized. This can be achieved by the gradual increase of salts (e.g., by addition of NaCl), or adjustment of the pH, thus utilizing either Na⁺ or H⁺ ions to minimize electrostatic repulsion.^{421,424,425} On the other hand ethylene glycol containing molecules such as OEG can be included as spacers between the DNA and the Au surface, allowing high DNA loading without the need for additional charge screening by ions.⁴²⁶ Recently, a “freeze-and-thaw” conjugation method was reported by Liu and co-workers where Au NPs and thiolated DNA strands were simply frozen and thawed, resulting in very dense DNA loading on NPs.⁴²⁷ The authors hypothesized that during water crystallization, DNA, Au NPs, and salt are repelled out of the growing ice crystals, thus resulting in high local concentrations and facilitating DNA attachment kinetics. The resulting conjugates showed not only increased DNA loading but also increased stability in high salt buffers

compared to conjugates prepared via the “salt-aging” method. Another important factor influencing the stability of DNA-Au NP conjugates is the choice of the anchoring group. As such, it has been shown that di- and trithiol linkages as well as bifunctional linkers such as thiol plus amine provide higher stability conjugates compared to monothiol.⁴²⁸

In certain environments, such as in cell culture media or in other challenging buffers, it is highly important to employ DNA-NPs that are colloidally stable.^{429–431} For example, Funk and co-workers showed that Au NRs coated with a dense shell of DNA could be coupled to DNA origami structures, which generally require high MgCl₂ buffer concentrations to maintain their structural integrity, by hybridization to complementary “handle sequences” on the DNA origami.⁴³² These constructs could then be employed for the detection of mRNA both in buffer and in human serum. On the other hand many reports have investigated the use of densely functionalized DNA-Au NP conjugates for intracellular sensing or drug delivery.^{404,412,433} Mirkin and co-workers showed that the DNA-shell on Au NPs facilitated the cellular uptake through scavenger receptors and resulted in a high number of internalized particles compared to bare Au NPs.^{434–437} The number of uptaken particles was highly dependent on the density of the oligonucleotide loading, with higher loading resulting in higher uptake. Additionally a dense DNA loading greatly increased the stability of conjugates with respect to degradation by nucleases.⁴³⁸ Similarly, the stability of siRNA was enhanced in siRNA-Au NP conjugates and showed great potential in *in vitro* gene silencing.⁴³⁹

Ag NPs can also be functionalized with thiol-terminated DNA, although density functional theory (DFT) and *ab initio* studies have shown that the nature of the Ag–S bond is much weaker than that of the Au–S bond, with the bond being less than 35% covalent and more than 65% electrostatic in nature, therefore resulting in less stable DNA-Ag NP conjugates compared to Au NPs.²⁴ Similar to Au NPs, for creating a dense DNA ligand shell, charge screening must be taken into account. Both the use of triple cyclic disulfides,⁴⁴⁰ as well as monothiolated DNA have been shown to quickly conjugate to Ag NPs.^{441,442} Furthermore, phosphorothioate (pt)-oligonucleotides can be employed. Here a Sulfur atom replaces an oxygen atom in the phosphate backbone of DNA, which does not only render these oligonucleotides stable toward degradation by nucleases but also allows for functionalization of NPs through metal–S interactions. Because many phosphate groups can be replaced by phosphorothioate within a DNA strand, multivalent interactions with a single NP can be achieved, resulting in high stability. As such it was shown that Ag NPs functionalized with 3, 6, or 9 pt-containing DNA strands displayed increasing stability with respect to strand displacement by dithiothreitol (DTT) with increasing numbers of phosphorothioate groups present.⁴⁴³

Oligonucleotide Conjugation of NPs by Physisorption. Although covalent conjugation strategies are among the most popular, some other strategies have been reported in the past decade to coat NPs of various chemical compositions with DNA, where covalent conjugation may not be directly possible.^{444,445} For example pt-DNA, similarly to the case of Au and Ag NPs, has also been employed to functionalize CdS QDs, which showed different binding affinities for pt-DNA depending on their surface properties. For example, Cd²⁺-rich QDs displayed a higher binding affinity toward pt-DNA compared to neutral or S²⁻-rich CdS QDs. The conjugation

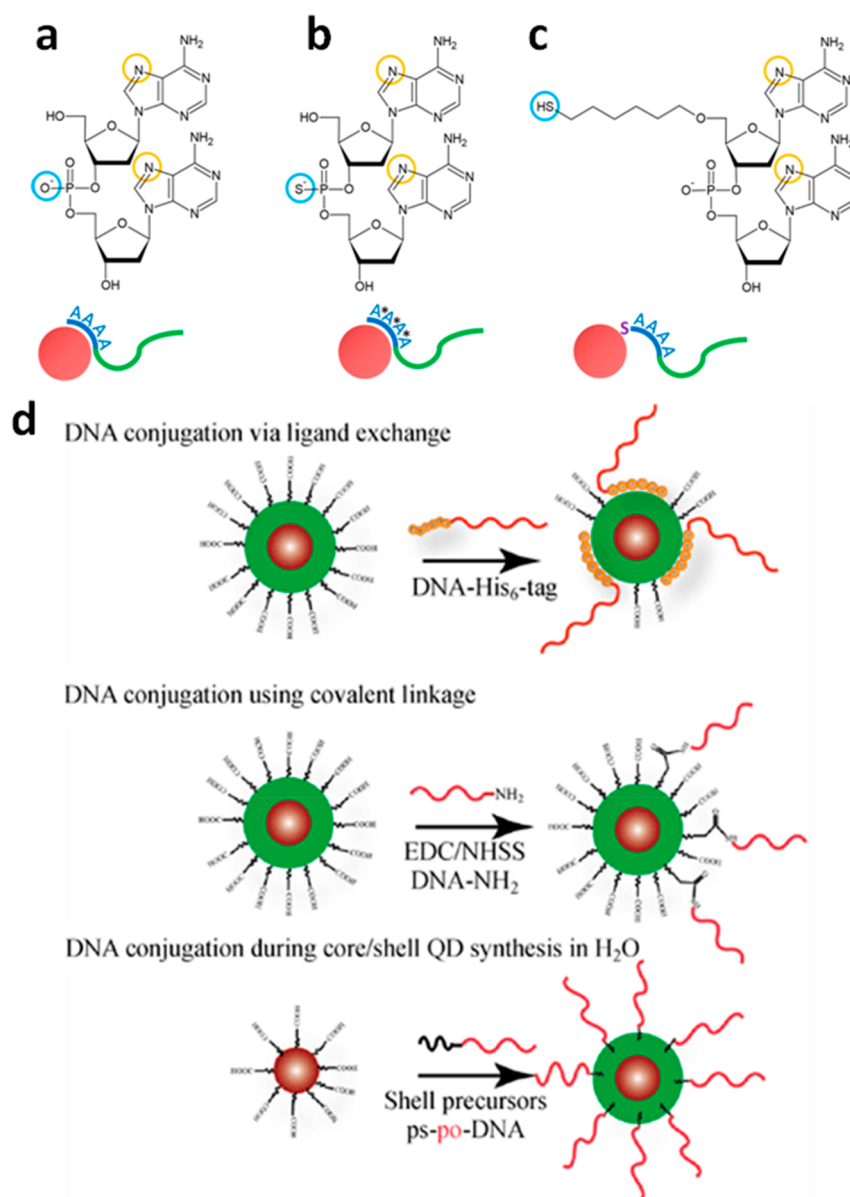


Figure 18. Different methods of functionalizing Au NPs with DNA. (a) physisorption through Adenine bases. (b) Conjugation via pt-DNA. (c) Conjugation via thiol-Au bond. (d) Different strategies to conjugate DNA to colloidal QDs. (a–c) Reprinted with permission from ref 450. Copyright 2014 American Chemical Society. (d) Reprinted with permission from ref 448. Copyright 2013 Springer Nature.

mechanism is most likely electrostatic in nature, although it was shown that CdS QDs displayed greater binding affinities for pt-DNA compared to unmodified DNA.⁴⁴⁶ On the other hand, His-tagged as well as thiolated DNA can be employed for QD conjugation due to affinities for different metal ions on the QD surface.^{447,448} While QD-thiolated DNA conjugates displayed excellent stability at high concentrations, they were highly sensitive to changes in pH, photo-oxidation, and dilutions. His-tag DNA-QD conjugates suffer from limitations in their preparation, being highly pH sensitive. Furthermore, achieving high DNA-loading with this method is difficult as the His-linkers limit the adsorption of other incoming DNA strands due to steric hindrance.⁴⁴⁸

A proposed model for DNA physisorption on citrate-capped Au NPs is that initially the polyanionic DNA adsorbs on the Au surface and thereby displaces citrate anions. This can be facilitated by the addition of cations. To maximize surface contacts, DNA may undergo structural conformation changes.

The adsorbed DNAs also form an “exclusion zone” toward other incoming DNA strands, thus limiting further adsorption.⁴⁴⁹ DNA physisorption is highly specific to the DNA sequence used with the following ranking in adsorption affinity: A > C > G > T. It was shown that the DNA bases can interact with the metal surface through its nitrogen atoms, specifically through N-7 (circled in yellow in Figure 18) and N-9.⁴⁵⁰ Especially, oligonucleotides containing a poly adenine (poly A) tail, have shown superior adsorption properties.⁴⁵¹ The stability of these DNA-Au NP conjugates was found to be highly dependent on the length of the poly-A tail, with a longer tail resulting in decreased desorption upon temperature, pH, or salt concentration due to increased binding interactions, i.e., more DNA bases anchoring to the NP surface.⁴⁵² However, a longer polyA tail also resulted in a decreased number of DNA strands anchored to the Au NPs, which in turn allowed for more precise control of DNA loading. Interestingly, it was shown that Au NPs functionalized with an A30-tail were stable

with only 15% of DNA desorption after being heated to 95 °C for 30 min.⁴⁵² However, the overall stability of these conjugates was still found to be less than those formed with thiol or pt-DNA.⁴⁵⁰ Liu and co-workers proposed the combination of pt-DNA into polyA DNA to harness both the high stability as well as precise conjugation properties.⁴⁵⁰

Oligonucleotide Conjugation to NPs by Coupling Chemistries. Other types of NPs often cannot be directly functionalized with DNA, as they are stabilized by additional ligands such as polymers^{453,454} containing variable functional end-groups such as hydroxyl, carboxyl, amine, alkyne, azide, or aldehydes for further modifications. These functional groups allow for conjugation to oligonucleotides via various different methods. For example azide-functionalized superparamagnetic iron oxide NPs (SPIONs) as well as NPs bearing azido-amphiphilic polymers could be modified with a dense layer of alkyne functionalized oligonucleotides using alkyne-azide click chemistry.^{19,455} On the other hand, the EDC coupling method can be employed to conjugate amine-modified oligonucleotides to any NP functionalized with carboxyl terminated ligands.⁴⁵⁶ For example, UCNPs were functionalized with DNA using the EDC coupling strategy and then used in conjunction with graphene oxide (GO) for the successful detection of zeptomoles of target oligonucleotides in solution. This study was further exploited for the detection of mRNAs in cell lysate and blood plasma.^{402,403}

Figure 18 summarizes the basic strategies for conjugation of NPs with oligonucleotides.

3.1.4. Small Peptides. Small peptides are built up from few amino acids linked by amide bonds and represent another important class of biomolecules that have been widely employed for NP stabilization and biofunctionalization for a variety of applications in biomedical sciences.^{457–459} Peptides have gained attention due their potential role as therapeutic agents in diverse areas such as oncology and infectious disease, as well as metal ion or molecular detection systems such as in colorimetric assays for detection of a wide range of biomolecular targets.^{460,461} The conjugation of peptides to NPs can not only result in increased reactivity due to a high local concentration but also enables multiplexing, thus harnessing the properties of different peptides at the same time, and ref 462, figure 3.7, illustrates some of the roles peptides play in determining NP functionality and stability (Figure 19).

Similar to the case of oligonucleotides, the grafting density of peptides on the surface of the NP has to be carefully controlled, as it will dictate the overall stability, activity, and properties of the resulting peptide–NP conjugate. It also has to be noted that while a dense coating might provide greater NP stability, it may also have a negative impact on the activity of the peptides.⁴⁶² Commonly used peptides for NP conjugation include cell-penetrating peptides (CPPs), which can enhance uptake and delivery of drugs across membranes and improve the efficiency of cell uptake of nanoparticulate systems, as well as homing peptides, which are designed to target cells, tumors, and tumor-associated microenvironments.⁴⁶² One prominent example of a CPP is the HIV-derived Tat peptide, which facilitates the cellular internalization of Au NPs in HeLa cells.⁴⁶³ Various strategies have been reported for the functionalization of NPs with peptides, tailored to the NP's chemical composition. In general, the peptide can be incorporated either by direct chemisorption or by various coupling chemistries.

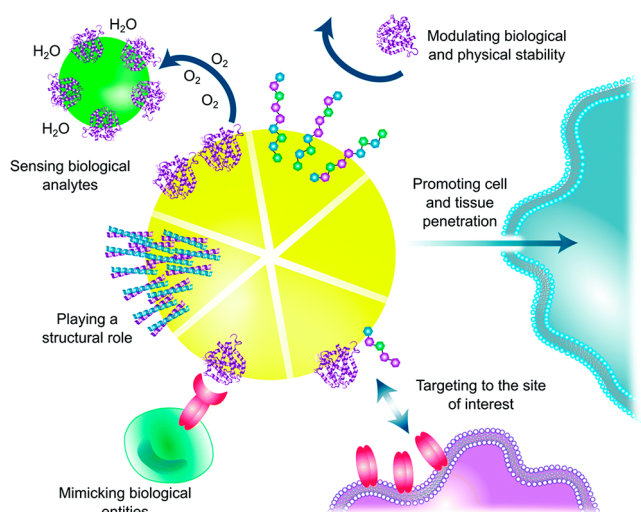


Figure 19. Roles of (poly-)peptides in determining the fate and properties of NPs. Reprinted with permission from ref 462. Copyright 2018 The Royal Society of Chemistry.

Peptide Conjugation to NPs by Chemisorption. Peptides offer various functional moieties such as Cys (–SH) or His (–imidazole), which could be used for conjugation to the NP surface.^{418,464–466} In the case of Au or Ag NPs peptides can be directly conjugated to the NP surface via free thiol-containing cysteine side chains. An example of this strategy was demonstrated by Levy and co-workers. They utilized the (Cys-Ala-Leu-Asn-Asn) CALNN peptide and showed that it presented an excellent ligand for the stabilization of Au NPs.⁴⁶⁵ The major characteristic for the success of this peptide was its amphiphilic character having two hydrophobic amino acids (alanine and leucine) near the binding site and two hydrophilic amino acids (asparagine) further from the binding site. The amino acid cysteine is able to bind to the AuNPs whereas alanine and leucine (hydrophobic) induce peptide self-assembly. This configuration facilitated a firm and stable coating of the peptides around the NPs, ensuring their solubility in water and providing a good stability at distinct pH values and in different buffer ionic strengths. Recently, Kanaras and co-workers showed that Au NPs coated with a mixed monolayer of CALNN and the skin penetrating peptide CALNNR7 (or CALNNTAT) were able to penetrate through human skin,³⁵¹ highlighting the important role of NP functionality and its direct correlation to NPs properties. Furthermore it was demonstrated that Au NPs functionalized with DNA binding peptides could be directed to assemble on DNA templates in a specific manner to form ordered NP assemblies.⁴⁶⁷ The formation and or destruction of such assemblies can be triggered by protease action or metal-ion complexation methods.^{468–470} Poly histidine (HIS)-tags have been utilized by Mattoussi and co-workers to conjugate peptides to DHLA-coated QDs.⁴⁷¹ Another recent study showed that QDs could be modified with a virus-derived lytic peptide fused to a maltose-binding protein containing a hexa HIS-tag resulting in stable QDs, able to perforate the cell membrane.⁴⁷²

Peptide Conjugation to NPs by Coupling Chemistries. Besides direct conjugation, peptides can also be indirectly attached to ligands already covering a NP surface. For example, Bartzak et al. reported a “one-pot” EDC/sulfo-NHS coupling strategy to functionalized OEG-capped NPs with peptides

(Figure 20).⁴⁷³ Then, the same group demonstrated that peptide-capped Au NPs could be successfully employed to

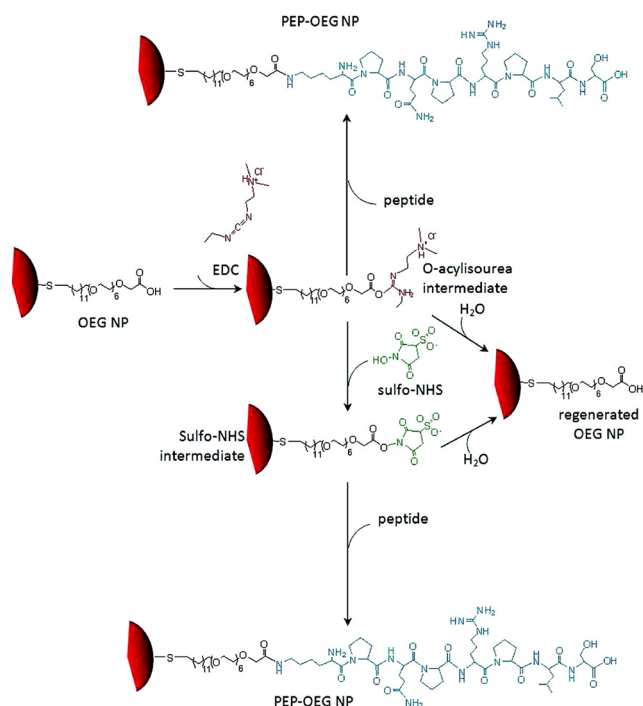


Figure 20. Schematic overview of amide bond formation among the KPQPRLS Peptide (blue) and OEG NPs (red shape) using EDC (red) and sulfo-NHS (green) strategies. Reprinted with permission from ref 473. Copyright 2011 American Chemical Society.

study interactions of Au NPs with endothelial cells as well as manipulate angiogenesis both in vitro and in vivo.^{464,473–479} Peptide-coated CdSe/ZnS QDs have also been shown to be able to target the lung, blood, and/or lymphatic vessels.⁴⁸⁰

3.1.5. Proteins. Proteins, generally defined as polypeptides consisting of more than 50 amino acids, play one of the most diverse roles within a living organism, ranging from receptor or membrane channel formation to molecular transport and catalysis of biochemical reactions.⁴⁸¹ Therefore, it is not surprising that many diseases are the result of protein malfunction due to mutations or misfolding. However, this also presents an opportunity to use proteins as therapeutic agents, an area that has become increasingly popular since the report of the first protein therapeutic, insulin.^{481–483} On the other hand, the use of protein–ligand interactions plays an important role and can be harnessed for nanoscale protein self-assembly.

Similar to their smaller peptide counterparts, the conjugation of proteins to NPs can be advantageous for various reasons, such as increase in overall protein activity resulting from the high local concentration at the microenvironment, increased stability or self-assembly. Hence protein–NP conjugates have emerged as effective and promising tools for a wide range of applications, including diagnosis and therapeutics. In terms of biomedical applications, the protein coating can be designed to modulate the stability of the NPs, determine the clearance of NPs in vivo or to target specific biological sites.⁴⁶² Thus, there has been an increased interest to design NP–protein conjugates for biomedical applications. In general, functionalization of NPs with proteins such as

antibodies can be achieved by direct chemical covalent conjugation or electrostatic interactions.⁴⁸⁴ As discussed previously, noncovalent methods are based on hydrophobic and/or ionic interactions. Although this method of functionalization is generally straightforward and does not involve complex chemistry, it suffers from some disadvantages compared to covalent strategies. For example, in the case of antibodies, nonspecific binding to NPs can result in the loss of antibody activity as well as the destabilization of colloidal NPs. On the other hand, covalent methods use specific sites on the protein for NP conjugation. These are usually present in the form of chemical linkers or employ common protein binding interactions (e.g., streptavidin and biotin).^{484,485} The choice of conjugation method and site should be carefully considered as proteins could be impaired, unfold, and/or lose their properties if an inappropriate method and/or conjugation site was chosen.⁴⁸⁶ Therefore, several efforts have been developed to optimize and control the orientation, density, activity, and accessibility of the protein after functionalization, as will be discussed in the following sections:

Protein Conjugation to NPs by Chemisorption. The covalent conjugation of proteins to NPs can allow for greater control of protein activity but also to control aggregation behavior.²⁶³ Among the most commonly employed proteins for NP modification is avidin (found in egg white). The interaction of avidin/streptavidin with biotin (vitamin H) is one of the strongest noncovalent interactions in biology, and it has been heavily employed in targeting applications and assay methods.^{487,488} While most conjugation strategies rely on physisorption, a covalent functionalization method was reported, which employed cysteamine and glutaraldehyde to link streptavidin to Au-magnetic NPs. Covalently conjugated streptavidin coated NPs showed an increase in stability in PBS containing SDS compared to NPs with a physisorbed streptavidin coating. However, it was found that when compared to conjugation by physisorption, streptavidin loading was lower.⁴⁸⁹ Simonian and co-workers demonstrated that small Au NPs (1.4 nm) displaying a sulfo-NHS or maleimide reactive group could be conjugated with the enzyme organophosphate hydrolase (OPH) through primary amines from lysine residues or sulfhydryl groups from cysteine residues. The resulting conjugates were then used for the detection of the neurotoxin paraoxon.⁴⁹⁰

Protein Conjugation to NPs by Physisorption. Physisorption represents the simplest way to functionalize NPs with proteins. Resulting conjugates have the advantage that conjugation is usually reversible, which can facilitate delivery and sensing applications.²⁶³ As discussed previously, the functionalization of NPs with streptavidin is generally straightforward and mainly relies on electrostatic interactions. For example, it was shown that avidin strongly adsorbs onto DHLA-coated QDs due to charge interactions.⁴⁹¹ Even particles with a controlled number of avidin (or streptavidin) moieties per particle could be prepared.^{176,492}

An interesting work by Murphy and co-workers demonstrated the successful assembly of Au NRs using biotin and streptavidin linkers. Interestingly, linkage was mostly observed in an end to end fashion. The group attributed this observation to the higher reactivity of Au NRs' edges due to their lower coverage with CTAB.⁴⁹³ On the other hand, the functionalization of spherical Au NPs with lipases via a PEG-biotin streptavidin–biotin linker was demonstrated. These protein functionalized particles were able to digest cubosomes

following a different mechanism in comparison to free lipase. The variation of the digestion mechanism was attributed to the overall size of the nanoparticulate system, which restricted access to the inner parts of the cubosomes.⁴⁹⁴

Streptavidin–biotin interactions were also used for signal amplification particularly coupled to electrochemical sensing of microRNA. MicroRNAs are noncoding RNAs that can serve as tumor markers and therapeutic targets for some cancers. Biotinylated nucleotides were used to incorporate biotin into the hybridized microRNA complex. Afterward, Au NPs loaded with large amounts of streptavidin were used to amplify the signal. Signal amplification was based on the ability of the Au–streptavidin scaffold to capture both biotinylated nucleotides and biotinylated alkaline phosphatase. The enzyme catalyzed the conversion of the electrochemically inactive molecule 1-naphthyl phosphate present in the buffering solution into the active naphthol, thereby amplifying the resulting signal. The specificity of the methods allowed for a single nucleotide discrimination between microRNA family members.⁴⁹⁵

Another important protein broadly exploited in literature is bovine serum albumin (BSA). Albumin is biodegradable, nontoxic, and easy to handle, rendering it a good candidate for intravenous applications.⁴⁹⁶ Albumin, being a blood protein was exploited for its ability to minimize recognition and internalization of NPs and thereby prolonging their circulation half-life. Luminescent porous Si NPs are nanomaterials with great potentials for imaging and photothermal therapy. Nevertheless, these particles are susceptible to fast biodegradation, resulting in fluorescence quenching compromising their use in long-term tumor imaging. To overcome this limitation, alkyl-thiol terminated NPs were encapsulated with BSA via hydrophobic interactions, generating stealth products with improved water dispersibility and long-term fluorescence under physiological conditions.⁴⁹⁷

BSA has also been used during NPs synthesis.^{111,498–503} It was shown that when reducing AgNO_3 with NaBH_4 in the presence of BSA, BSA-coated Ag NPs could be produced. Importantly, the secondary structure of BSA was not affected by the conjugation to Ag.⁵⁰⁴ Moreover, albumin can serve as a great platform for the delivery of therapeutic agents. Qi et al. prepared human serum albumin (HSA) NPs functionalized with glycyrrhetic acid and loaded with the anticancer drug doxorubicin for liver cancer targeting. Doxorubicin was encapsulated into the NPs with an efficacy up to 75% and demonstrated superior cytotoxicity compared to untargeted particles.⁵⁰⁵

A universal method to prepare protein-capped QDs has been described by Clapp et al., who demonstrated that both HIS-tags as well as leucine zipper units could be employed to conjugate proteins such as avidin, the maltose binding protein (MBP) or the immunoglobulin-G-binding $\beta 2$ domain of streptococcal protein G (PG).⁵⁰⁶

Furthermore, it should be mentioned that when NPs are in contact with biological fluids, biomacromolecules, including proteins may naturally adsorb to the surface of colloidal particles, often impairing the behavior and properties of NPs and influencing their behavior both in vitro and in vivo,^{507,508} this effect is commonly referred to as protein corona formation.^{508–510} In particular HSA, which is abundant in blood, tends to form a dense corona on NPs.⁵¹¹ For detailed discussions on protein coronae, the reader is referred to detailed reviews on the topic.^{512–514}

Protein Conjugation to NPs by Coupling Chemistries. It is important to mention that bioconjugation of NP surfaces achieved by alternative approaches, such as biotechnological strategies, may have benefits when designing NPs for biomedicine. For instance, Ma et al. developed a systematic method to bioconjugate recombinant proteins to NPs without the need for modification for each specific protein–NPs conjugate. A glutathione S-transferase–SpyCatcher fusion protein conjugated to Au NPs allowed for assembling of additional proteins through the Spy–Catcher/SpyTag system, resulting in a two-step synthesis. First, the Au NPs were modified by glutathione S-transferase (GTS) through Au–S bonds, and second, a covalent link between a SpyCatcher and the SpyTag peptide was formed (by spontaneous formation of an isopeptide bond). Importantly, in this second step, a variety of recombinant proteins could be employed in a reproducible manner, resulting in stable NP–protein conjugates. The authors provided a universal platform to immobilize proteins on the surface of Au NPs, suitable for a wide range of applications.⁵¹⁵ Figure 21 summarizes electrostatic and covalent strategies for protein conjugation to NPs.

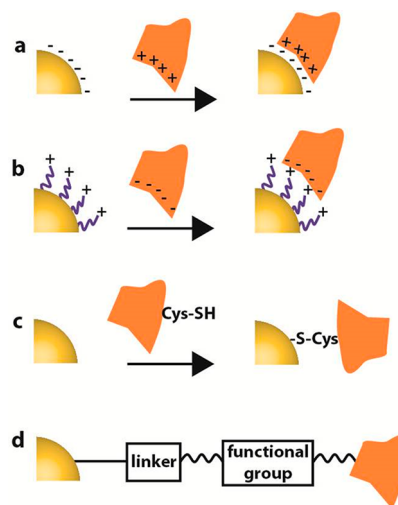


Figure 21. Schematic illustration of different strategies for the formation of NP–protein conjugates. (a) Electrostatic interactions via direct adsorption onto the NP surface. (b) Electrostatic interactions of protein with ligand/monolayer on the NP. (c) Covalent conjugation through active groups (e.g., Cys-SH or Lys-NH₂). (d) Covalent conjugation through a bifunctional linker.

3.1.6. Carbohydrates. Carbohydrates and carbohydrate-conjugated molecules such as glycoproteins are integral to multiple biological processes. For example, carbohydrates present on the cell surface are central to cellular recognition processes. Inflammatory processes and immunological responses are also mediated by carbohydrates expressed on the outer surface of the cells. On the other hand, carbohydrates can serve as an excellent indicator for different diseases. For instance, carbohydrates present on the protein surface are important for proper protein folding, and thereby, abnormal protein glycosylation can be highly suggestive for different diseases including cancer, hepatic, and immune diseases.⁵¹⁶ Carbohydrates are stable, hydrophilic, and exhibit good biocompatibility and biodegradability in vivo. Furthermore, their derivable reactive groups such as amino, carboxyl, and hydroxyl groups allow for successful conjugation to NPs.

Therefore, carbohydrate–protein interactions have been utilized to generate controlled nanoparticulate drug delivery systems. For the synthesis of those conjugates, several methods have been proposed including: (i) the formation of polyelectrolyte complexes of opposite charge, (ii) the formulation of amphiphilic polysaccharides that can self-assemble into NPs, and (iii) the use of cross-linkers which facilitate the formation of stable carbohydrate–NP conjugates. However, the type of carbohydrate, valency, ligand, and density could influence the carbohydrate–NP conjugate, requiring optimized conjugation methods.⁵¹⁷ For instance, Wu et al. reported on mesoporous silica NPs, coated with mannose, as nanocontainers for various cargos, which were encapsulated into the pores by the construction of Concavillin A nanogates. The release of the cargo could be triggered by either a decrease in pH (e.g., in tumor vasculature) or an increased level of glucose (e.g., in diabetes).⁵¹⁸

Different types of carbohydrate-coated NPs interact differently with cells. This was demonstrated by functionalizing different NPs, including iron oxide and QDs with three different sugars: glucose, galactose, and dextrans of varying molecular weights. Functionalization was carried out by applying cyanoborohydride-based conjugation chemistry. Amine-terminated NPs were reacted with the reactive end on the carbohydrate via cyanoborohydride-based reductive amination. Enhanced selectivity of carbohydrate-modified NPs for glycoproteins was reported, as well as reduced nonspecific cellular interactions of dextran-coated NPs when incubated with HeLa cells. These nonspecific cell interactions became more prominent when a higher molecular weight dextran was used as the surface ligand. On the other hand, galactose functionalized NPs showed increased cellular internalization compared to bare NPs (Figure 22).⁵¹⁹

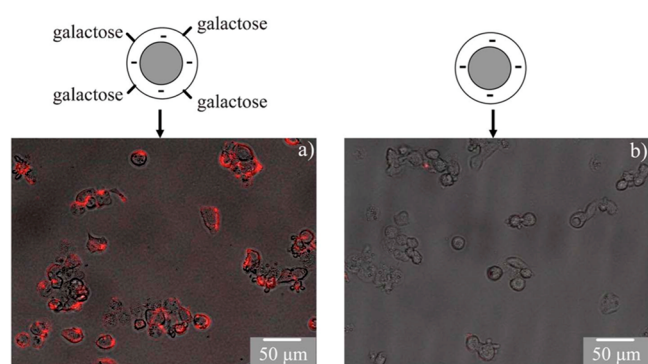


Figure 22. Uptake of galactose QDs exposed to the human liver cancer cell line (HepG2). Higher internalization is observed when functionalized QD–galactose is exposed to HepG2 cells (a) as compared with bare QDs (b). Reprinted with permission from ref 519. Copyright 2012 The Royal Society of Chemistry.

In another study, iron oxide NPs were functionalized with glucose (α and β forms) and mannose via click coupling chemistry. Carbohydrate functionalization aimed to target sugar binding proteins (e.g., lectin) present on particular cell types. Conjugation with lectin, although weak, was amplified by the multivalency of the interaction through the presence of multiple sugar molecules. Mannose-specific binding was demonstrated by the increased cellular uptake of conjugated NPs. Such system could be exploited for MRI as a detection

technique for various biomolecules including influenza antibody, DNA, and apoferritin.⁵²⁰

Carbohydrate-functionalized NPs were also investigated as potential photothermal agents for cancer ablation. Although antibody functionalization can achieve selective targeting of NPs to cancerous tissue, it is faced with several obstacles, including the stability of the antibody itself and the increased cost upon large scaling. Cancer cells express more glycolytic enzymes and glucose transporters than normal tissues, owing to their increased need of glucose in a phenomenon called the Warburg effect. Taking into account this effect, iron oxide magnetic NPs were functionalized with glucose-6-phosphate and then incubated with cancerous cells from different cell lines. Cells were then irradiated with near infrared (NIR laser light). Superior cellular uptake was demonstrated for functionalized particles as compared to the plain ones.⁵²¹

On the other hand, carbohydrate-functionalized NPs were also exploited for targeting resistant bacterial species. *Mycobacterium smegmatis* was used as model bacteria for *Mycobacterium tuberculosis*, a Gram-positive bacterial causing the serious infectious disease tuberculosis. *Mycobacterium tuberculosis* possesses a thick lipid wall, rendering resistance toward many drugs. Nevertheless, small hydrophilic molecules may penetrate the pores known as porins. As such, trehalose was selected for the targeting of such bacteria due to the presence of the high affinity trehalose transporter system. Trehalose was coupled to NPs via photocoupling chemistry. These functional particles demonstrated superior interactions with cells compared to glucose- or dextran-coated particles. TEM imaging revealed the presence of particles in the cell wall and the cytoplasm, opening the door for the management of Gram-positive bacteria and especially *Mycobacterium tuberculosis*.⁵²²

3.2. Ligand Coating of Nanoparticles for Other Applications

Inorganic NPs feature optoelectronic properties that are strongly dependent on the size and shape of the particles. For instance, size-dependent discrete energy levels and Coulomb-blocked charge transport effects have been observed in metallic NPs while semiconductor QDs can be charged like molecules. The unique size-related structures, together with their transport and thermal properties, render NPs efficient nanoscale functional components for different applications in photodetectors,^{231,523} solar cells,^{524,525} sensors,⁵²⁶ and catalysis.²²¹ Moreover, colloidal dispersions of NPs are ideal candidates for inexpensive device fabrication via solution-based techniques including spin-casting, dip-coating, and inkjet printing, which can be further scalable through roll-to-roll processing.

Toward the design and development of NP-based devices, it is well understood that the organic ligands and/or surface termination of colloidal NPs strongly affect their application performance, particularly in technological applications where charge carrier transfer/transport and chemical reactivity/affinity play an important role. For instance, NPs' ligands may significantly affect the position of the energy levels in semiconductor NPs. Furthermore, when considering NPs for electronic and optoelectronic applications, one should keep in mind that the actual device active element may not be individual NPs but rather macroscopic assemblies or NP superstructures. In this case, the nature of the ligand coating plays a crucial role for the electronic/optical communication

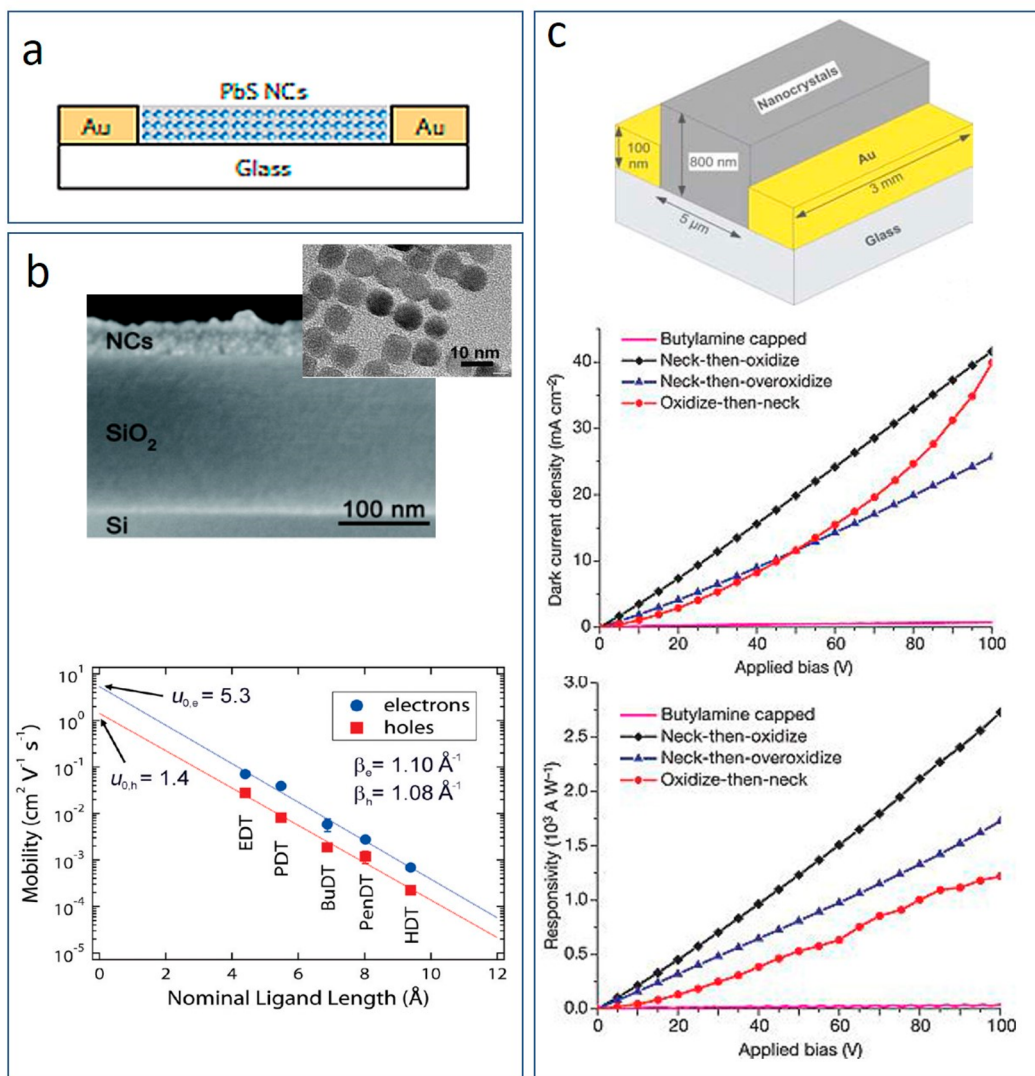


Figure 23. (a) Schematic representation of a NP-based photodetector. (b) Effect of the CdSe NPs surface treatment on the carrier mobility. (c) Photodetectors performance using NP film with different surface treatment (dark current-responsivity measurements). Reprinted by permission from ref 539. Copyright 2006 Macmillan Publishers Ltd., Nature 2006. (a) Reprinted with permission from ref 530. Copyright 2016 Macmillan Publishers Ltd.: Nature Photonics. (b) Reprinted from ref 531. Copyright 2010 American Chemical Society. (c) Reprinted with permission from ref 539. Copyright 2006 Macmillan Publishers Ltd., Nature.

and the macroscopic physical behavior of the final assembly. The interparticle distance, the colloidal dispersion and the packing density, as well as the mutual NPs' orientation in the colloidal medium, are parameters that can be strongly influenced by the ligand nature/coverage and must be taken into account in the development of the respective devices.

3.2.1. Photodetectors. Single phase inorganic semiconductor NPs have been utilized for photon detection due to their narrower band gaps compared to that of conductive polymers and small molecules, which limited their absorption to the visible spectral range. For example, inorganic NPs of PbS, PbSe, PbTe, HgTe, InAs, and InSb have been employed as ideal candidates for application requiring light absorption in the near-IR region; the band gap of such NPs can be precisely tuned from the visible up to 35 μm . Various types of photodetectors using such NPs have been developed, including photoconductors,⁵²⁷ photodiodes,⁵²⁸ and phototransistors.⁵²⁹ The intraparticle characteristics (chemical phase, morphology, size, or dispersity of individual NPs), but also the surface

environment, the type of the capping layer, the NP surface passivation, and the interparticle distances due to the ligand length in the close-packed film determine the electrical conductivity in photodetectors and consequently the device's efficiency. NPs' termination molecules significantly affect the position of the energy levels in semiconductor NPs but also play roles in the charge carrier mobility. The ligand chain length, density of the ligands, and degree of inductive effects have a strong impact on the electron trap density, the carrier multiplication efficiency, and the multiexciton lifetime and have to be optimized to achieve an improved detectivity and detector response time.

Photoconductive Detectors. A NP-based photoconductor comprises a thin homogeneous film of semiconductor NPs deposited onto a prepatterned electrode structure (Figure 23a).⁵³⁰ The electrical conductivity in such devices can be altered under illumination due to the generation of additional charge carriers. The photoconductivity in a close-packed NP structure is dependent on intraparticle characteristics such as

the morphology, size, or dispersity but also on the surface environment such as NP surface passivation, capping layer, and interparticle distances.⁵³¹ For instance, photoconductivity studies in CdSe NPs capped with TOPO-TOP organic ligands revealed that free carriers originate from photogenerated electron–hole pairs within the NPs.⁵³² The charge separation in these nanoparticulate systems is much slower compared to the interband relaxation, while the charge transport is dominated by tunneling of carriers through the interparticle medium. Moreover, the ionization rate is dependent on intraparticle characteristics such as size and surface passivation.

Different density of surface passivation of CdSe QDs with amines have been studied in order to evaluate the effect on their photocurrent.^{533,534} The changes in the photocurrent in conjunction to NP surface alterations were attributed to an increase of the exciton ionization efficiency due to variations in the interparticle distances. This is regardless of whether the molecules used for treatment were conjugated or cross-linked to the QDs.⁵³³ Possible treatment with a base may remove the capping molecules and shorten the interparticle distances, increasing the electron transport between the neighboring particles through an interparticle hopping process.⁵³⁴ Electron and hole mobilities increase exponentially with decreasing the ligand length, demonstrating the inverse relationship between coupling energy and interparticle distance (Figure 23b).⁵³¹ The energy barrier width through which carriers need to tunnel to reach an adjacent NP can be tuned by the spatial separation of the neighboring NPs. The spatial separation and consequently their macroscopic optoelectronic properties can be modified by exchange or functionalization with a new ligand or “chemical cap”.¹⁸⁴ Thus, ligand chain length, density of ligands, and degree of inductive effects are some parameters, which can be optimized to achieve the desired carrier transport properties.^{535–538} Upon careful design of the capping agent properties, carrier multiplication efficiency, multiexciton lifetime, and charge injection through the device can be improved, leading to enhanced detection efficiency.

Moreover, a way to control the chemistry of the surface states which act as electron traps affecting the detector's response time was found. This was realized by treating NP layers with different molecules (i.e., butylamine, formic acid, small thiols, etc.).⁵³⁹ The optimum characteristics were obtained after treating the films with methanol in an inert atmosphere, followed by controllable surface oxidation (Figure 23c). The high gain measured for the fabricated devices was attributed to the presence of long-living electron traps generated by chemical treatment of the NPs' surface.

Hybrid Photodetectors. This type of NP-based photodetector is based on mixing narrow gap NPs, which act as excellent sensitizers, and organic semiconductor materials. The performance of photodetectors is dependent on the synergy of light harvesting and charge transport processes. Higher responsivity and spectral response extension to the infrared spectral region have been recorded for small molecules or π -conjugated polymers. A 3 orders of magnitude enhancement of photocurrent was achieved by sensitizing crystalline arrays of C₆₀ with CdSe NPs.⁵⁴⁰ This enhancement was attributed to the efficient light absorption of CdSe NPs, fast electron transfer from NPs to the C₆₀ and high carrier mobility within the array of C₆₀ molecules.

The influence of the capping ligand layer on the UV detection was studied by comparing two kinds of ultraviolet photodetectors based on TiO₂ NPs, bare or capped with oleic

acid and poly(9,9-dihexylfluorene) (PFH) polymer hybrids.⁵⁴¹ It was observed that even though the ligand coating improved the miscibility of the NPs and PFH, the charge-transfer barrier suppressed the charge transport and lowered the photo-sensitivity of the device.

3.2.2. Photovoltaic Devices. Semiconductor NPs exhibit a completely different behavior from their bulk materials of the same stoichiometry due to quantum confinement size effects. As a consequence, the bandgap of the NPs can be simply tuned by varying the NPs' size.^{542,543} This property enables the use of a single material with different bandgaps to harvest a broad spectral range of the solar radiation. Their fascinating properties together with their colloidal form, which is compatible with solution-processing technologies, including the low-cost roll-to-roll device fabrication, make these materials ideal candidates for photovoltaic applications. Using such technologies, NPs can be easily incorporated into the different layers comprising the solar cell architecture. As a result, different functionalities have been exploited, leading to enhanced light harvesting, solar energy conversion efficiency, and device stability. Semiconductor NPs have been incorporated in (a) hybrid organic/inorganic bulk heterojunction (BHJ), (b) Schottky-based, (c) depleted heterojunction (DHJ), and (d) NP-sensitized solar cells, with the DHJ to be the most efficient NPs-based photovoltaic technology to date (Figure 24).

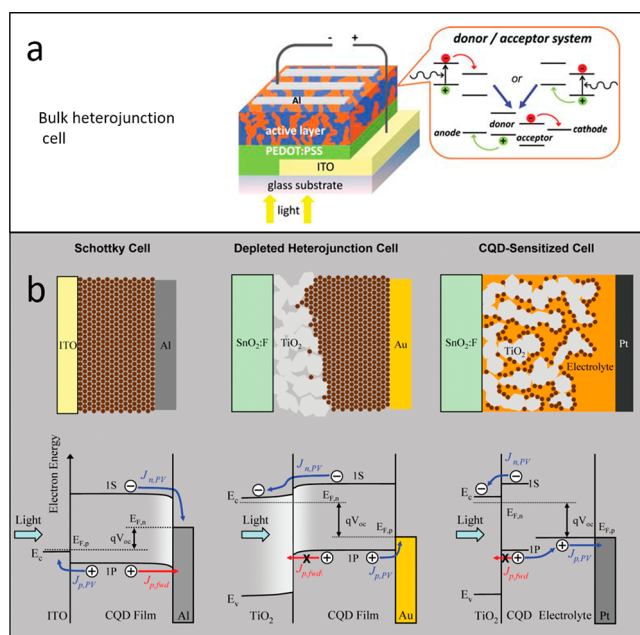


Figure 24. (a) Typical structure and (b) working principle of NP-based solar cells. (a) Reprinted with permission from ref 544. Copyright 2010 The Royal Society of Chemistry. (b) Reproduced with permission from ref 545. Copyright 2010 American Chemical Society.

Despite the rapid improvement of the solar cell efficiency, NP-based photovoltaics still have to overcome many obstacles in order to meet the requirement of large-scale commercialization and long-term usage. While much progress has been made in terms of the device architecture optimization, several material design aspects remain largely unexplored. The role of the interfaces among the randomly distributed crystalline NPs in the charge transport is crucial. Such interfaces include large

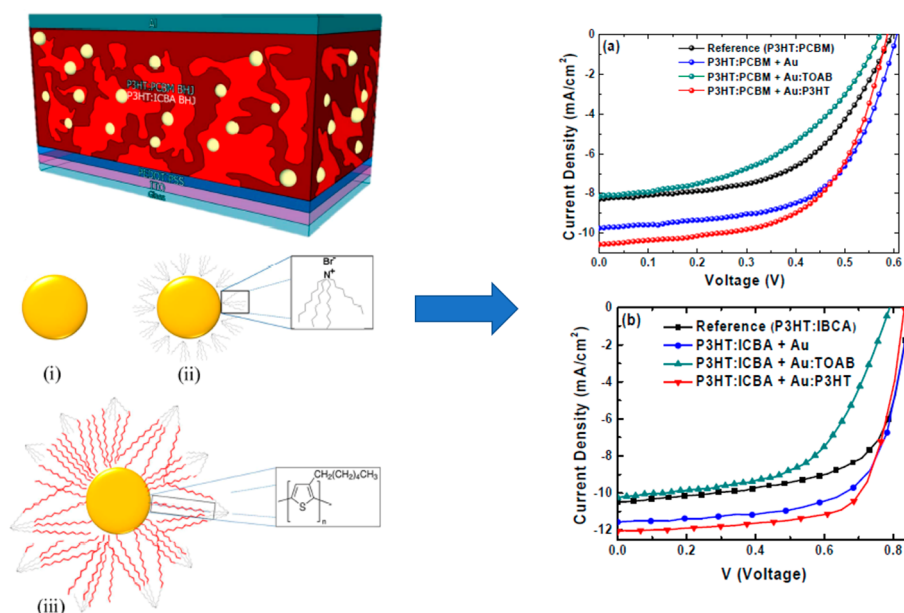


Figure 25. Schematic representation of the BHJ OPV cell with three types of NPs embedded into the active layer, (i) bare, (ii) TOAB-terminated, and (iii) P3HT-terminated J - V curves of the devices with configurations (a) ITO/PEDOT:PSS/P3HT:PCBM/Al and (b) ITO/PEDOT:PSS/P3HT:ICBA/Ca/Al respectively. Reprinted with permission from ref 524. Copyright 2015 American Chemical Society.

surface area junctions between photoelectron donors and acceptors, the intralayer grain boundaries within the absorber, and the interfaces between photoactive layers and the top and bottom contacts.⁵⁴⁶ Controlling the charge collection and minimizing the trapping of charge carriers at these boundaries can lead to further improvement of the solar cell efficiency. Therefore, a deep understanding of the electronic coupling between the NP and its surface ligands and the physical mechanisms responsible for the charge transport among the neighboring particles is required to achieve higher solar cell efficiencies.⁵⁴⁷ Consequently, a robust NP surface passivation and a controllable compact packing of the randomly oriented NPs are required.⁵⁴⁶ Much attention has therefore been devoted to the development of new ligand strategies that minimize the interparticle spacing to promote carrier transport and lower the defect density to reduce the recombination losses.

Electron and hole mobility is dependent on the intrinsic characteristics of the material, the size/morphology of the NPs and the disorder at the surface. Additionally it was recently found that it is also dependent on the ligand length.⁵³¹ Shallow traps originate from the surface disorder and reconstructions, whereas deep traps are due to low coordinated atoms on the NPs surface.^{546,548} Carrier mobilities in semiconducting alkanedithiol-treated PbSe were found to decrease exponentially with increasing ligand length.⁵³¹ While complete removal of the organic insulating ligands led to marked improvements in transport performance.⁵²⁴ For this reason, only the shortest organic ligands were retained for surface passivation, allowing sufficient interconnection between the NPs.⁵⁴⁹ Moreover, the exchange of trioctylphosphine oxide and dodecylamine with 1,2-ethanedithiol or 1,2-ethanediamine was found to significantly improve the exciton dissociation yield and/or charge carrier mobility⁵⁴⁷ while a ligand exchange with 3-mercaptopropionic acid quenched the band edge emission and enhanced deep trap emission.⁵³¹

The conductivity of the linker molecule itself may be important in enhancing carrier transport among the particles. Solar cells utilizing PbSe NPs capped with benzenedithiol have demonstrated a power conversion efficiency of 3.6% along with enhanced stability.⁵⁵⁰ Indeed, the ligand exchange of oleate molecules with a molecular conducting ligand such as benzenedithiol resulted in a more effective pathway for electron transfer. As a consequence, both electron and hole mobilities were increased by more than 1 order of magnitude and an efficiency of 7% was reached for the respective DHJ device.⁵⁴³ Additionally, the cross-linking with the benzenedithiol appears to offer a longer-lived NP-metal interface than amine ligands. In particular, halide anions introduced during solid-state film treatments led to a marked reduction in the density of trap states deep within the bandgap of the colloidal NP solid. The mechanism proposed for such behavior was that the as-exchanged NPs were dominated by a large density of nonpassivated surface states, which were filled in with the atomic halide ligands.

Toward efficient inorganic NP-based photovoltaics, a different ligand strategy utilizing monovalent inorganic ligand (halide anions) passivation was proposed.⁵⁵¹ It was shown that such an approach enabled good passivation of surface defects, high carrier mobility, and good device stability, while using inexpensive chemicals readily processed at ambient conditions. Both time-resolved infrared spectroscopy and transient device characterization indicated that the scheme led to a shallower trap state distribution than the best organic ligands. This atomic passivation strategy resulted in enhancement of the mobility-lifetime product in comparison to ethanedithiol passivation by a factor of 20, indicating superior charge carrier diffusion in the atomic-ligand-passivated films. The respective photovoltaic devices exhibited a solar power conversion efficiency of 6%.

The ligand shell of the metallic NPs also plays an important role in the performance of plasmonic BHJ organic photovoltaic devices (Figure 25). It is argued that the plasmonic effect

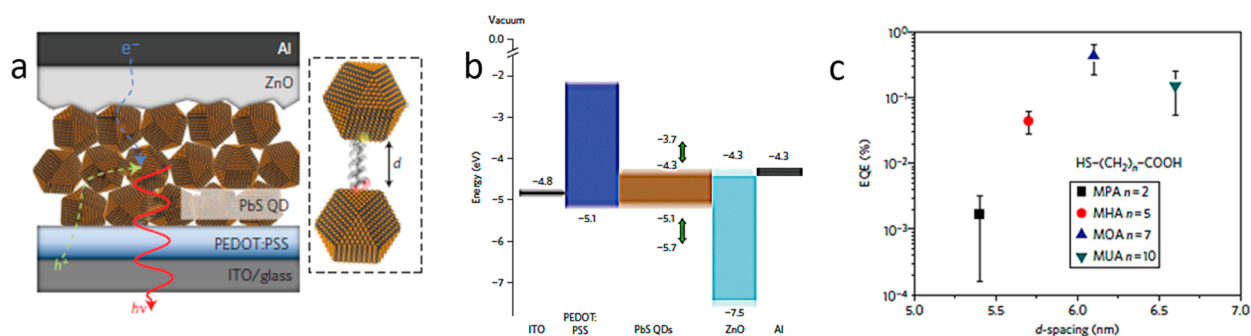


Figure 26. (a) Schematic representation of the NP-based LED, (b) electronic energy levels of each material in the device, and (c) EQE dependence of the LED device on interparticle distance. Reprinted with permission from ref 555. Copyright 2012 Macmillan Publishers Ltd..

accountable for the performance enhancement takes place only if the NPs core is in direct contact with the active layer polymer donor.⁵²⁴ This can be achieved with the utilization of either ligand-free NPs or NPs terminated with the same polymer donor as the active layer. Using this concept an enhanced efficiency of 7.16% in OPV devices incorporating the poly(3-hexylthiophene-2,5-diyl) (P3HT):Indene- C_{60} bisadduct (ICBA) active layer was achieved. On the contrary, devices with ligand-terminated Au NPs showed lower performances, even compared to the reference (NP free) device due to the deteriorated active layer morphology attained.

According to the above literature, the role of the interfaces including the large surface area junctions between photoelectron donors and acceptors, the intralayer grain boundaries within the absorber (interfaces among the NPs), and the interfaces between photoactive layers and the top and bottom contacts are the main factors affecting the efficiency of the photovoltaic devices. NPs free of ligands or terminated with the same polymer donor as the active layer could lead to enhanced efficiency of BHJ organic photovoltaic devices. Controlling the charge collection and minimizing the trapping of charge carriers at these boundaries by including short-length or conductive capping ligands can also lead to an improvement in efficiency. Atomic passivation methods such as monovalent inorganic ligand (halide anions) passivation are important to eliminate surface defects and reduce carrier diffusion leading to improved device stability.

3.2.3. Light-Emitting Devices. Colloidal semiconductor NPs have been explored as the principal emitters for thin film LEDs. These NPs are a unique class of light emitters with size-tunable emission wavelengths, saturated emission colors, near-unity luminance efficiency, inherent photo and thermal stability, and excellent solution processability. The high color purity together with the color-tunable emission make NP-based LEDs promising candidates for next-generation displays and solid-state lighting applications.⁵⁵² A schematic representation of a modern NP-based LED device is illustrated in Figure 26a,b.

The electrical characteristics of the NPs can vary depending on the surface modulation, which can change the luminance and emission efficiency. In view of this, understanding surface ligand effects is essential for improving the performance of such devices.⁵⁵³ Evaluation of the LED properties as a dependence of the ligand length has been performed by the exchange of the 1.1 nm long TOPO ligand with the 1.7 nm long oleic acid ligand.⁵⁵⁴ With all other conditions being identical, the luminance and efficiency of the LEDs with an

oleic acid ligand were approximately 1000 cd/m^2 greater and 1.5 times higher, respectively, than those of the LEDs with the TOPO ligand. These results showed that if the physical length of the surface ligand is relatively long, decreasing the surface area would result in increased injection of electrons and holes into the NPs, increasing the luminance and efficiency. In addition, an order of magnitude improvement in device efficiency was obtained by changing the long-chain oleate ligand on the QDs surface with thiol and carboxylic acid units (Figure 26a,b).⁵⁵⁵ At the same time, when the interparticle spacing increased from 5.4 to 6.1 nm, the external quantum efficiency (EQE) increased by a factor of ~ 150 (Figure 26c). Efficient ligand exchange of the core-shell particles replacing the oleate ligand with octanethiol has also been reported and resulted in a double increased electron mobility and greater balanced carrier injection, leading to the highest EQE of 12.2%.⁵³⁴ Alternatively, the use of 1-dodecanethiol as exchange ligand was reported. The device developed showed the highest EQE up to 20.5% and a long operational lifetime of more than 100000 h at 100 cd/m^2 , representing one of the best-performing solution-processed red NP-based LEDs to date.⁵⁵⁶

Recently, several examples of LEDs utilizing perovskite NPs have been demonstrated.^{557–560} While perovskite NPs are very efficient light emitters, their main disadvantage is that they degrade rather quickly. To tackle this problem, recent studies have focused on the encapsulation of perovskite NPs in polymers.^{561,562} However, in all these cases the particles are encapsulated as a bulk, losing their colloidal dispersity, which may be important when fine films of NPs are required. A new approach to tackle this issue by introducing the low molecular weight polymer poly(maleic anhydride-*alt*-1-octadecene) (PMA) during the synthesis of the perovskite NPs was recently demonstrated.²⁷⁶ The PMA results in stabilization of the NPs by tightening the ligand binding and thus decreasing interactions of the surface with the surrounding medium. The polymer capped perovskite NPs retained their colloidal dispersity and were utilized to produce both monochromatic green and white LEDs.

For NPs of different and more stable chemical compositions in comparison to perovskite NPs, such as CdSe, several other ligands have been employed to improve their blending and function in NP-based optoelectronic devices. Specifically: (i) Branched ligands, namely entropic ligands for NPs, were developed, leading to better charge transport and higher EQE,^{563,564} (ii) multifunctional dendrimer ligands that serve as the charge injection controlling layer as well as the adhesive layer at the interfaces between the NPs and the electron

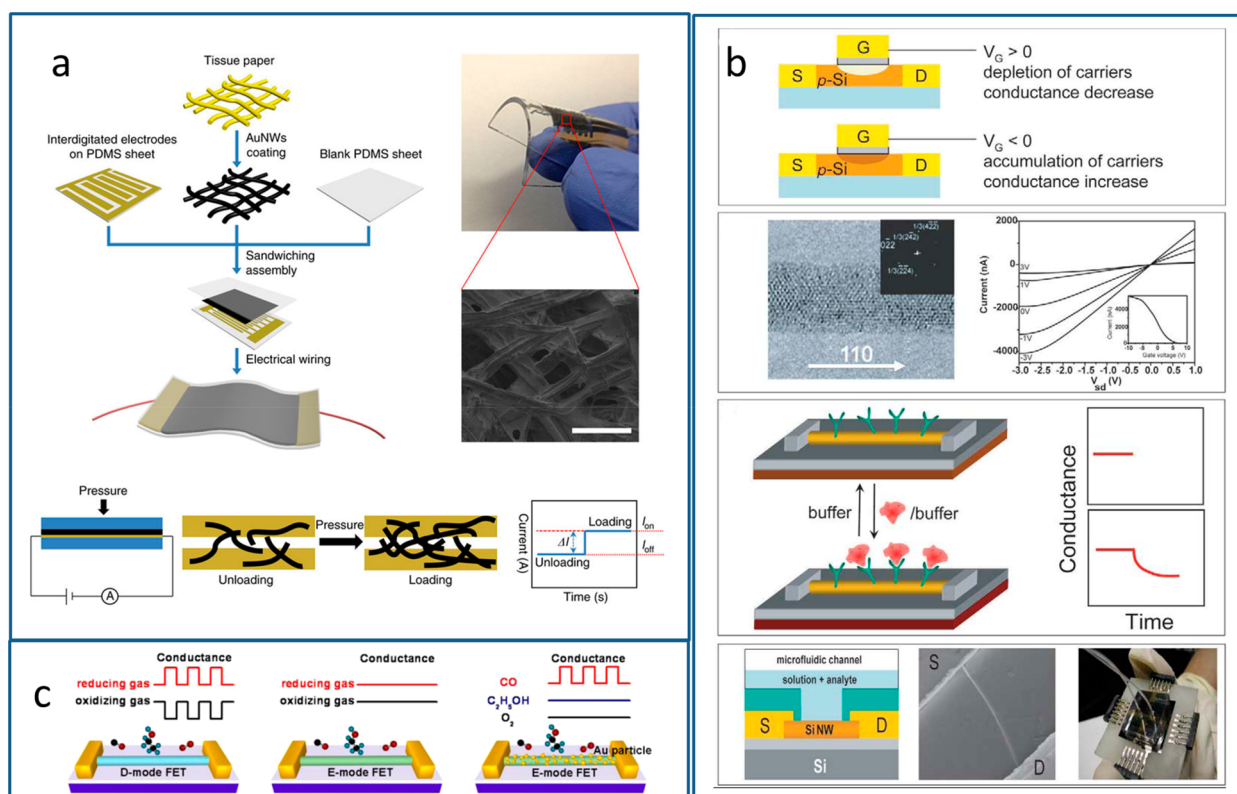


Figure 27. (a) Au-nanowire flexible pressure sensor, (b) FET sensor, and (c) FET gas sensor. (a) Reprinted with permission from ref 572. Copyright 2014 Macmillan Publishers Ltd., Nature. (b) Reproduced with permission from ref 573. Copyright (2005) Elsevier. (c) Reproduced with permission from ref 574. Copyright 2013 American Chemical Society.

transport layer (ETL), which gave promising results,⁵⁶⁵ and (iii) conjugated organic polymers such as block copolymer ligands directly linked on the surface of the NPs.⁵⁶⁶ The copolymers consisted of both semiconductor and reactive functional blocks that contained multidentate thiol-based anchor groups. The key to the success of this architecture was that by being bound to the semiconductor NP surface, the semiconductor ligands improved hole injection into the NPs and resulted in improved device performance (increased electroluminescence intensity and quantum efficiency) compared with a similar device containing unmodified NPs.

The efficiency of LED devices is affected mainly by the luminescence quality and the emission efficiency of the nanoparticulate light emitters. If the ligand length is relatively long, the luminescence and the device efficiency is increased. The efficiency is 1.5 higher by using oleic acid capped NPs instead of utilizing TOPO-capped ones, or is increased from 12.2 to 20.5% when octanethiol is replaced by 1-dodecanethiol. Furthermore, the type of the capping ligand is important in the hole-injection into the NPs but also the stability of the semiconductor NPs, especially in the case of perovskite NPs. To obtain colloidal stability, which is important for the formation of very thin films, polymeric capping ligands of low-molecular weight are introduced. Particular attention should be paid to the retention of the luminance quality.

3.2.4. Sensors. A sensor is an analytical device that detects physical or chemical changes (e.g., in temperature, pressure, light, concentration, etc.) and converts them into measurable signals. In recent years, the interest of researchers and engineers to gas- and liquid-sensitive materials has grown substantially due to the progress in nanotechnology (Figure

27). Among the different NPs-based sensors developed to date, nanowire-based field effect transistors (FETs) have been widely used for detection of a variety of biological and chemical species, of pH value, of metal ions, viruses, proteins, etc. In most of these applications, the mechanism of sensing is based on the functionalization of a homogeneous semiconductor nanowire, such as silicon and In_2O_3 . The extreme sensitivity of nanowire and nanotube field-effect sensors originates from their one-dimensional structure that enables efficient charge transfer between the surface-anchored molecules and the nanostructures.

To use nanomaterials as sensors, the understanding of the peculiarities of both the synthesis and interaction mechanism during the sensing procedure is required. A sensor can ideally satisfy some important requirements: (i) specificity for the target species, (ii) sensitivity to changes in target-species concentrations, (iii) fast response time, (iv) extended lifetime, and (v) reduced size (miniaturization) together with low-cost manufacture. Noble metals,⁵²⁶ metal oxides, or rare-earth doped NPs^{567,568} have been extensively utilized in such applications. NP ligands should play an important role in absorption/adsorption of organic volatile molecules and gases taking place during the sensing process. Furthermore, during the fabrication of sensors, NP film formation is driven by electrostatic interactions and van der Waals dispersion interparticle forces. Such interactions are determined by the NPs' surface ligand coverage.⁵⁶⁹

Indeed, it has been widely reported that careful selection and design of ligands strongly influence the sensitivity and selectivity of a NP-based sensor. For example, Au NPs functionalized with 1,10-phenanthroline have been utilized

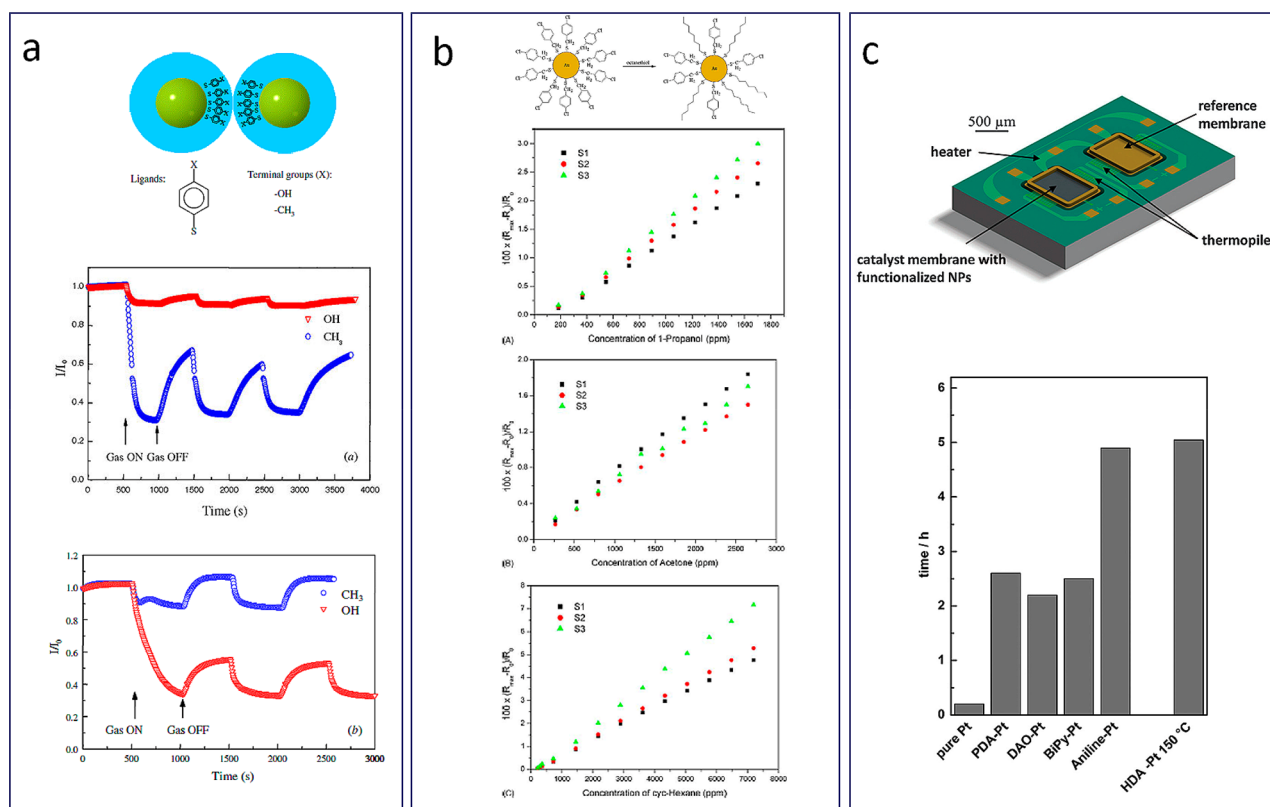


Figure 28. Effect of the ligand on the signal of the vapor and catalytic sensors. (a) Electrical responses of 4-mercaptophenol functionalized (referred to as “OH” NPs) and 4-methylbenzenethiol functionalized gold NPs (referred to as “CH₃” NPs) to the nonpolar solvent dichloromethane (DCM) and to methanol. (b) Maximum relative resistance vs concentration of the analyte vapors of 1-propanol, acetone, and cyclohexane for mixed-ligand NPs (S1, Au NPs with 50% chlorobenzenemethanethiol (CBMT):50% *n*-octanethiol (OT) mixed ligand; S2, Au NPs with 33.3% CBMT:66.7% OT mixed ligand; S3, Au NPs with 16.7% CBMT:83.4% OT mixed ligand). (c) Activation period for the Pt NPs-based catalytic gas sensor for hydrogen sensing. The NPs are covered with different molecules such as phenylenediamine (PDA), 1,8-diaminooctane (DAO), bipyridine (BiPy), aniline, and hexadecylamine (HDA). (a) Reprinted with permission from ref 571. Copyright 2002 IOP Publishing. (b) Reprinted with permission from ref 575. Copyright 2005 Elsevier. (c) Reprinted with permission from ref 576. Copyright 2014 Royal Society of Chemistry.

for the detection of Li ions.⁵⁷⁰ This type of ligand binds selectively to the Li⁺ by forming a 2:1 ligand–metal complex, causing Au NPs to aggregate. Such aggregation causes a shift in the extinction spectrum accompanied by a concomitant color change, providing a useful optical method of detecting Li⁺ in aqueous solution. Furthermore, the electrical response to chemical vapors adsorbed on Au NPs films has been found to vary markedly by the surface functional groups.⁵⁷¹ In particular, two types of ligands namely, 4-mercaptophenol (referred to as “OH” ligand) and 4-methylbenzenethiol (referred to as “CH₃” ligand) have been utilized to functionalize Au NPs. It was found that the conductivity of the respective CH₃–NP film dropped by ~70% from the initial value, while that of the OH–NP film showed a decrease by only ~10% (Figure 28a). Two physical effects were reported to explain such conductivity changes. Under high partial pressure, the change in NP core–core separation was the main contribution to the conductivity change and generally deteriorated the conductivity. However, for relatively low partial pressures the adsorption of vapor molecules lead to permittivity changes that tend to enhance the conductivity.

A different sensing approach is the use of mixed-ligand Au NPs for vapor sensing.⁵⁷⁵ In particular, Au NPs with a mixture of ligands (chlorobenzenemethanethiol (CBMT) and *n*-octanethiol) have been synthesized in order to study the different chemical selectivity due to the modification of the

surface properties (Figure 28b). The respective sensors experienced repeated cycles of analyte vapors (1-propanol, acetone, and cyclohexane) and blank air gas, while the analyte concentrations were varied. It was observed that the variations in compositions of the ligand molecules resulted in remarkable differences in signal amplitudes.

Finally, it should be mentioned that the stability of NP-based sensors is also affected by the ligand coating. For instance, a series of amine ligands (mono- and bifunctional alkyl- and aryl amines) have been used to stabilize Pt NPs as catalytic materials for H₂ gas sensing (Figure 28c).⁵⁷⁶ Depending on the ligand coating used, remarkable differences in the sensor performance, both in terms of the catalytic performance, the activation period as well as stability have been observed.

Careful selection of the NP ligand coating is essential, as ligands strongly influence the sensitivity, the stability and the selectivity of the NP-based sensors. Specific type of ligands can selectively bind to metal-anions and produce changes in color or conductivity alterations. Different types of ligands attached to NPs in the same device can be used for different chemical selectivity. Remarkable differences in the signal amplitude can be originated from variations in compositions of the ligand molecules.

3.2.5. Memory Devices. Memory elements are the integral parts of computers, identity document (ID) cards,

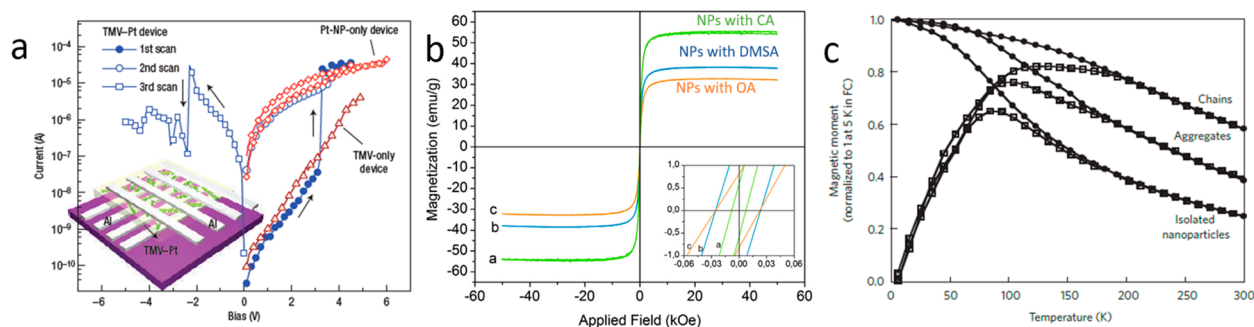


Figure 29. (a) Digital memory device utilizing Pt NPs. (b) Hysteresis loops for NPs functionalized with different capping agents. (c) Magnetization curves for individual γ -Fe₂O₃ NPs and for their ensembles (aggregates and chains). (a) Reprinted with permission from ref 583. Copyright 2006 Macmillan Publishers Ltd., Nature. (b) Reprinted with permission from ref 585. Copyright 2015 Elsevier. (c) Reprinted with permission from ref 590. Copyright 2008 Wiley.

and various consumer electronics. Memory devices utilizing NPs have been extensively explored during the past decade as possible solutions to overcome the scaling issues and improve endurance of nonvolatile memories and hard-disk drives. NPs provide an opportunity to precisely control electronic and magnetic properties of materials by tuning their size and shape. The possibility of device fabrication using colloidal solutions allows significant cost reduction, which is very important for products such as wireless identification tags and smart cards where the prime criterion is cost and miniaturization rather than outstanding performance.⁵⁷⁷

Ferromagnetic NPs are promising candidates for a density increase of magnetic storage devices toward 100 Gbit/inch² up to a few Tbit/inch².⁵⁷⁸ Until recently, increasing the recording density simply meant down-scaling all of the components in a recording system, but what has become clear over the past decade is that the design of magnetic media and the continued increase in density storage is fast encroaching upon the fundamental physical limits imposed by the nature of magnetism on the nanoscale. To be applicable for magnetic storage media, the magnetization direction in a material should be very stable and not reverse due to thermal fluctuations. From a simple geometry viewpoint, the smaller the ferromagnetic NPs, the higher the recording areal density is. But considering the superparamagnetic limit of the ferromagnetic NPs, there should be a balance between NP size and thermal stability of the NP-based recording media. For commercially viable recording media, the energy barrier required to reverse the magnetization from one direction to another should be at least 60 times higher than the thermal energy ($KV/k_B T \geq 60$).⁵⁷⁹ NPs of FePt,⁵⁸⁰ CoPt⁵⁸¹ and SmCo₅ (characterized by a high anisotropy energy)⁵⁸² are among promising candidates for high-density magnetic recording.

A data storage device derived from self-assembled Pt NPs is illustrated in Figure 29a.⁵⁸³ The device showed basic memory operations, such as operating voltages, data retention, and cycle ability. The current–voltage characteristics of the device showed bistable states with an ON/OFF ratio larger than 3 orders of magnitude.

The magnetic behavior of an assembly of magnetic NPs with a randomly oriented easy axis represents a complex and challenging problem. This complexity arises from the coexistence of finite size and surface effects as well as the presence of interparticle interactions.⁵⁸⁴ Below a critical size, magnetic NPs can exhibit unique phenomena such as

superparamagnetism. Their magnetization can be affected strongly by the surface capping ligand (Figure 29b).^{215,585,586} In addition, magnetic NPs can be present in the form of powders, dispersions, or embedded in a matrix, which gives rise to a variation in the interparticle spacing and therefore in the interparticle interactions.^{584,587–589} Ensembles of NPs show properties that may be quite different from those of individual ones (Figure 29c).⁵⁹⁰ The dipolar interactions between magnetic NPs determine their collective state, which shows the features of the magnetic glassy behavior.^{591,592} Therefore, ensembles of magnetic NPs show an increase in the blocking temperature, T_B , compared to that of individual particles (Figure 29c).⁵⁹⁰ Chains of γ -Fe₂O₃ NPs showed a 40K increase in T_B and a faster approach to saturation of magnetization on variation of magnetic field in comparison with individual γ -Fe₂O₃ NPs and their aggregates.

Because of the small size of the NPs, a large fraction of the atoms in the NP is surface atoms. Because the ratio of surface atoms to the bulk atoms is large, surface contribution to magnetization becomes significant. The surface atoms experience a different environment compared to the atoms of the core. Various defects from atomic vacancies to dangling bonds and lattice disorders exist on the NP surface and determine the macroscopic magnetic behavior. The type of the capping ligand is a crucial parameter for the fabrication of ultrasmall NPs of narrow size distribution, but it is also responsible for the disordered spin structure on the surface. Furthermore, the capping ligand length determines the distance between the particles in an assembly and consequently the dipolar interactions between magnetic NPs. Numerous approaches have been proposed correlating the dipole–dipole and exchange interactions to the nature of the assemblies' cooperative magnetic behavior.

3.2.6. Thermoelectric Applications. Thermoelectric materials can be utilized for conversion of heat to electricity, through the Seebeck effect or for cooling or refrigeration through the converse Peltier effect. The basic architecture of a thermoelectric device consists of an element placed between a heat source, e.g., corresponding to waste heat generation and the ambient (heat sink).⁵⁹³ The transfer of heat from the source to the sink is either through the motion of the carriers (electrons/holes) or through the lattice (through collective lattice vibration modes/phonons). The carrier transport results in the development of a potential difference, the Seebeck voltage (ΔV). The thermopower/Seebeck coefficient S is then the ratio of ΔV to the temperature difference (ΔT).⁵⁹³

Thermal to electrical energy conversion, through thermoelectric and thermionic materials, has been proven to be much more efficient in materials at the nanoscale and can provide large values of the figure of merit, ZT , which is defined as $ZT = S^2\sigma T/k$, where T is the average temperature of the hot and cold sides, and σ and k are the electrical and thermal conductivity of the material; k is the direct sum of the contributions from both the carriers (k_c) and the lattice (k_L).^{594,595} Quantum wells, nanowires, and semiconductor NPs are some of the low-dimensional morphologies, which have been used in such applications. The thermoelectric figure of merit can be improved by maximizing the power factor ($P = S\sigma$) and/or minimizing the thermal conductivity. The power factor can be maximized by the development of new low-dimensional materials or optimization of the existing ones by doping processes while the thermal conductivity can be minimized through nanostructuring and use of materials with intrinsically low thermal conductivity.⁵⁹⁴ Specifically, in the nanostructured materials, the thermoelectric performance is mainly attributed to strong decrease of the lattice thermal conductivity (k_L), probably by effectively scattering phonons that otherwise would have relatively long mean free paths, rather than an increase in the electrical power factor.⁵⁹⁶

Surface engineering of the NPs for thermoelectric applications is necessary to control NP growth, drive their assembly, and modulate their functional properties.⁵⁹⁶ This requires additional understanding not only of the surface influence on properties related to such applications but on the effect of each surface treatment on the final surface composition. In thin-film and nanowire thermoelectrics, the free surface in contact with vacuum or the atmosphere may also be an important interface.⁵⁹⁷ The role of the interfaces in the thermoelectric performance is beneficial as they contribute to the reduction of the thermal conductivity, k , and under certain conditions, to the enhancement of the Seebeck coefficient, S . However, interfaces also usually increase the electrical resistivity, ρ , due to the insulating capping layer. Improvement of the ZT requires that the proportional reduction in electronic carrier mobility resulting from increased interfacial scattering is less than the corresponding reduction in thermal conductivity. Thus, balancing the electronic and thermal properties of the interfaces is critical to tailor a material for optimal thermoelectric performance. Interfaces are effective in scattering long mean-free-path electrons and phonons but have minor effects when the mean-free-paths are smaller than the spacing between interfaces. If the interface is a barrier to electronic transport due to the insulating layer and not just a single scattering site, it may have a significant effect on the transport and the ZT .⁵⁹⁸ The thermoelectric performance can be improved by surface engineering through (i) increasing the grain boundary population, (ii) selection of a conducting ligand, (iii) removal/modification of the surface ligands, and (iv) ligand modification for optimum self-assembly.

Ideally, improved thermoelectric performance can be obtained by increasing the grain boundary population toward specific interfaces without decreasing the electronic transport. This can be done with approaches of introducing high densities of relatively well-ordered interfaces such as twin and domain boundaries. Such techniques to increase the twin-boundary density through repeated strain–anneal cycles have been studied widely in metals and could be transferred to thermoelectric materials such as Bi_2Te_3 and related alloys.^{596,597} Annealing results in nanomaterials with enhanced

transport properties, but partial sintering of NPs can modify the distribution and even the chemical phase as it leaves a residual carbon layer that may limit thermoelectric performance. To minimize the effect of the annealing process and the amount of residual carbon, the original surface ligands can be replaced in a previous step with shorter and weakly coordinating molecules such as pyridine, hydrazine, ammonia, and *n*-butylamine. Once the original bulky ligands have been fully replaced, a mild thermal treatment, generally with the NPs already assembled/aggregated, can be applied.⁵⁹⁶ The impact of surface-bound small molecules on the thermoelectric properties of the final-formed film was also demonstrated in the case of self-assembled silver telluride (Ag_2Te) NP thin films which were fabricated by a layer-by-layer (LBL) dip-coating process.⁵⁹⁹ Investigations on the electrical conductivity and Seebeck coefficient on the Ag_2Te NC thin films containing hydrazine, 1,2-ethanedithiol, and ethylenediamine between 300 and 400 K indicated that these molecules could serve as beneficial components to build NC-based thermoelectric devices operating at low temperature. The power factor could also be improved by 2 orders of magnitude by tuning ligand-coupling symmetry (tuning the functionality of the polar headgroup and the coupling symmetry of the organic linkers) through layer-by-layer assembly methods in the case of Cu_{2x}Se NC thin films. These resulted in the highest power factor measured for QD-based thermoelectric inorganic organic composite materials of $\sim 30 \mu\text{W}/\text{m}^3 \text{K}^2$.⁶⁰⁰

Both the ligand type and ligand removal influence the properties of NP. The suitability of the strategy used for ligand removal/replacement is dependent on the type of bonding to the NP surface. Modifications of the NP surface chemistry have been evaluated to improve transport properties of NPs through introduction of inorganic surface ligands with relatively high charge carrier mobilities. The charge carrier concentration can also be adjusted by balancing the ratio of surface cations and anions in polar compounds through the use of proper surface ligands. Surface ligands can also act themselves as donating or accepting dopants.⁶⁰¹ A stripping method using a strong inorganic acid (HCl) was recently demonstrated for removal of the carboxylic acids from the NP surface capped with oleic acid in solution. Chlorine (Cl^-) ions, initially located on the NP surface diffuse, upon a consolidation step, inside the crystal structure to act as a donor, providing the nanomaterial with *n*-type electrical conductivity and a tunable charge carrier concentration.⁶⁰² The procedure takes advantage of a ligand displacement step to incorporate controlled concentrations of halide ions while removing carboxylic acids from the NP surface. Halide passivation and metal cations on the surface have been proven to control the net NP surface charge while at the same time preventing the formation of deep electronic traps by avoiding oxygen absorption.⁶⁰³ In a different approach, metal salts were used to eliminate the organic surface ligands without introducing extrinsic impurities in the final nanomaterial.⁶⁰⁴ A 6-fold increase of the thermoelectric figure of merit of Ag_2Te was obtained when organic ligands were displaced by AgNO_3 .

Finally, the choice of a proper ligand can affect the synthesis of well-dispersed and monodispersed NPs as well the well-ordered self-assembly process.⁶⁰⁵ Self-assembly/superlattice procedures depend both on interactions between NP building blocks and on the process kinetics.⁵⁹⁶ The interactions between NPs can be van der Waals, dipole–dipole, magnetic, or electrostatic. Thus, assembly is usually triggered by

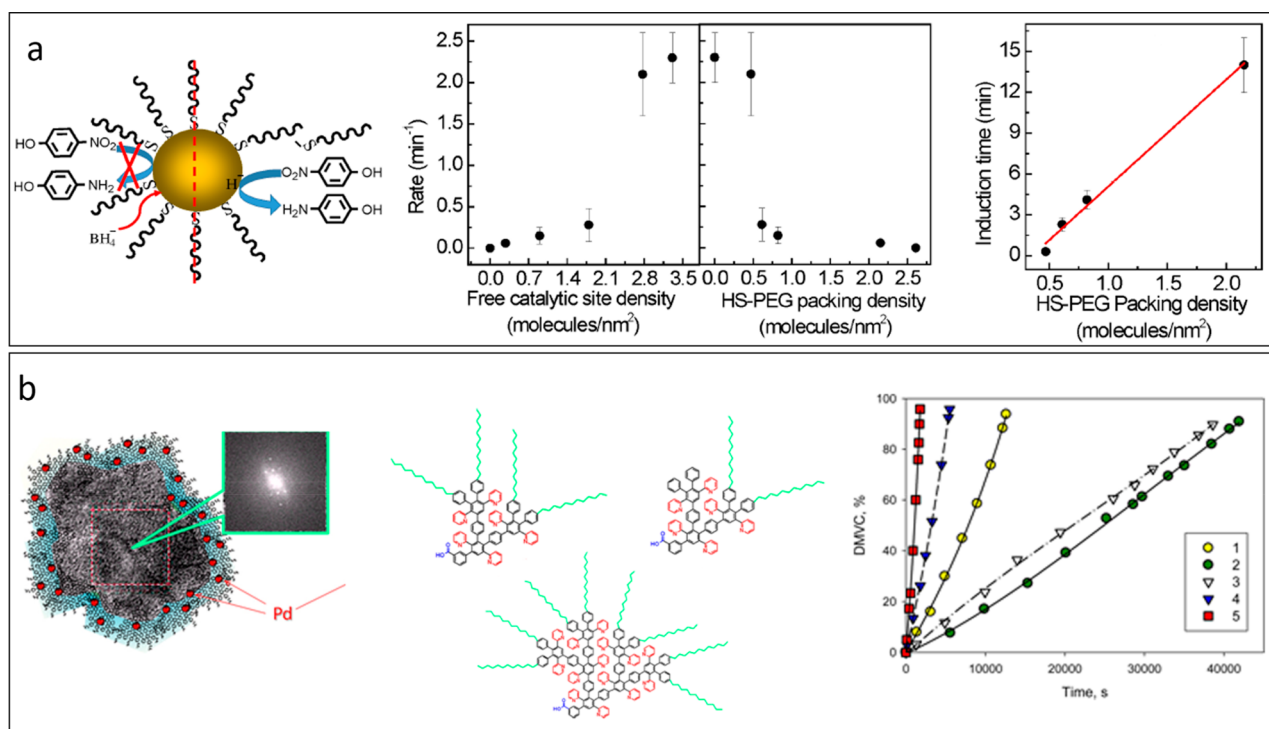


Figure 30. Effect of NP capping agent on the catalytic activity. (a) Rate and induction time of 4-aminophenol reduction of functionalized Au NPs with citrate and PEG-SH. The correlation between the reduction rate and the free catalytic site density on Au NPs is shown as well. (b) Iron oxide nanoparticles covered with polyphenylene-pyridyl dendrons of the second and third generations with dodecyl periphery and the effect of the different coverage on the catalytic performance in the selective hydrogenation of dimethylethynylcarbinol (DMEC) to dimethylvinylcarbinol (DMVC). (a) Reproduced with permission from ref 621. Copyright 2016 American Chemical Society. (b) Reprinted with permission from ref 622. Copyright 2014 American Chemical Society.

adjusting the surface/ligand-related interactions. The most commonly used strategy to produce organized superlattices is to force a slow NP assembly in solution by increasing the concentration through solvent evaporation.⁶⁰⁶ This procedure requires NPs with a very high colloidal stability and narrow-size distribution, which are both affected by the type of surface ligand.

3.2.7. Catalysis. Nanocatalysis, which involves the utilization of NPs to catalyze reactions, has attracted considerable attention during the past decade, both for homogeneous and heterogeneous catalysis applications. Because NPs exhibit a large surface-to-volume ratio compared to bulk materials, they are promising candidates for use as catalysts. NPs of different chemical phases, e.g., metals, semiconductors, oxides, and other compounds, have been widely used for such applications. The chemical reaction is performed on the surface of a catalyst particle at a high temperature while the catalyst particle is in a gaseous environment or in a liquid. In many cases, the chemistry and structure of a catalyst particle during a catalytic reaction could be different from those before catalysis. The challenging issue of nanocatalysis research is to produce catalysts with high selectivity, high activity, low energy consumption, and long lifetime. This can be achieved by a material design process by precisely controlling the size, shape, spatial distribution, surface composition, electronic structure, and thermal/chemical stability of the individual nanocomponents. Catalytic chemical reactions mainly include oxidation reactions, reduction reactions, coupling reactions, and electrochemical reactions.⁶⁰⁷

Ferrite NPs have also been applied in catalytic reactions mainly in processes of synthesis and destruction of organic

compounds. These magnetic particles can be of a single phase⁶⁰⁸ or core-shell double-phase structures.⁶⁰⁹ The separation of the nanocatalysts is an important process and is time and energy consuming, often with environmental implications.⁶¹⁰ Magnetically recoverable catalysts have attracted considerable attention due to their potential to combine catalytic properties and efficient materials' recovery using an external magnetic field, thus minimizing the total cost and helping to preserve the environment.^{611–618} Generally, these catalysts consist of a magnetic part and a noble metal. In bulk noble metal catalysts, the metal particles tend to aggregate during the reaction process, leading to the reduction of the catalytic activity. However, multifunctional, Fe₃O₄-noble metal hybrid nanoparticles present ideal nanomaterials to overcome this limitation.⁶¹⁹

The most important issue to consider when designing a nanocatalyst for use in a solution is to prevent the NPs from aggregating as this limits the specific sites at the surface for catalytic reactions.⁶²⁰ The careful choice of the capping agent can eliminate aggregation, allowing the nanomaterials in the colloidal solution to be used for recyclable catalysts. The role of the ligand and the packing density on the catalytic reduction of 4-nitrophenol has been studied by utilizing PEG-thiol-functionalized Au NPs (Figure 30a).⁶²¹ A direct relationship between the chain length and packing density of the PEG and the Au NP catalytic activity was found. High surface coverage of low molecular weight PEG (1 kDa) completely inhibited the catalytic activity of Au NPs. Increasing the molecular weight and decreasing surface coverage was found to correlate directly with increasing rate constants and decreasing induction time. Instead, the selective blocking of more active sites by adsorbed

thiol functionality was attributed to the induction period and reduced catalytic activity.

A different system proving the important role of the capping agent on the final catalytic activity is a magnetically recoverable catalyst, obtained via encapsulation of Pd NPs in dendron/dendrimer shells of ferrimagnetic magnetite nanoparticles.²²¹ High densities of well-separated metallic NPs could be formed and supported at specific sites on the porous surface of the nanoparticles. This system was subsequently tested for its functionality in the selective hydrogenation of dimethylethynylcarbinol to dimethylvinylcarbinol (Figure 30b). The catalytic activity in these systems is dependent on the dendrimer generation, which determined the specific sites for the growth of the Pd NPs as well as their size. The highest turnover frequency in the hydrogenation was found for an optimum Pd NP size around ~1.5 nm. The catalytic activity was also examined for larger (~3 nm) and smaller (~0.9 nm) Pd NPs, but the catalytic performance was proved weaker. Importantly, the stability of this system was demonstrated by its repeated use in up to three catalytic cycles. These hybrid nanostructures could then exhibit high catalytic performance and fast recovery in the presence of an external magnetic field.

Various research groups have studied the photocatalytic properties of semiconductor nanocrystals capped with different organic molecules. The photocatalytic activity was found to be higher in the case of the oleic acid-capped TiO₂ nanocrystals than both their tri-*n*-phosphine oxide-capped counterparts and commercial TiO₂ P25 Degussa.⁶²³ It is proposed that efficient catalysis strictly depend on microscopic mechanisms that occur at the catalyst surface, basically involving specific dye adsorption and local density of terminal OH moieties. Furthermore, Vorontsov et al. investigated the photocatalytic behavior of different TiO₂ samples with different surface area.⁶²⁴ They found that the size and surface does not have a direct influence on photocatalytic activity but it is rather surface properties such as surface acidity and hydroxyl groups. The nanosized TiO₂ photocatalysts prepared by employing long chain acids, octanoic and palmitic acid, showed better photocatalytic activity than the commercial Degussa P25.⁶²⁵ Apart from acid ligands, another ligand, which increases the photocatalytic activity of the TiO₂ nanostructures, is the low-cost sensitizer PVP. This ligand improves the photocatalytic activity of the NPs through a ligand-to-metal charge transfer mechanism.⁶²⁶

Careful choice of the ligand type and density can improve the catalytic activity, the selectivity, and the lifetime of nanocatalysts. The capping ligand prevents the NPs from aggregating which would have a detrimental effect on the catalytic activity. They also determine the specific sites for growth of well separated metallic NPs in hybrid magnetic-metallic systems.

4. CONCLUSIONS AND FUTURE PERSPECTIVES

The accurate synthesis and functionalization of inorganic NPs is critical for their colloidal stability and their performance in challenging environments. From applications in biology to applications in physical sciences, the choice of NP surface chemistry defines the NP activity and dispersibility and the observations can be very different between particles with adequately designed surface chemistry in comparison to poorly designed surface chemistry. NP toxicity, targeting ability, drug delivery efficiency, circulation in the body, and interaction with proteins, cells, or more complex biological systems depend on

the appropriate selection of ligands, including their hydrophobic/hydrophilic nature as well as their density and packing on the NP surface, which is directly correlated to their reactivity. Equally, the use of NPs in a vast range of optoelectronic applications requires them to be able to easily transfer carriers across their ligand shells and to adequately disperse in media, such as polymers. The NP ligand choice in these cases is critical and directly correlated with the topology of the active blends, which in turn influences the performance characteristics of devices.

Although the field of NP design has seen an unprecedented growth in the last two decades, we still have to gain further experimental knowledge, which correlates the physicochemical characteristics of NPs to their desired function. This is also important in order to better inform the NP design to the suitable choice of ligands. The appropriate selection of ligands to grow NPs in large scales with narrow size distribution and adequate manipulation of their morphology as well as the control of ligand density and hydrophilicity on the NP surface are essential goals to achieve. An important question that needs more elucidation is the exact interactions between ligands and NP. While for some ligands the type of bonding interactions are well-understood, this is by far not the case for other ligand types. For example, the bond between gold and thiols is often discussed to be a covalent one. However, all that is known is that the bond is very strong. As discussed in section 2, the most commonly accepted model for thiol–Au interaction is the binding of the deprotonated sulfhydryl group (forming a thiyl radical) to Au with coordination-type bonds.⁷⁴ Proper understanding of the details of the internal structure and stability of an organic thiolate ligand shell around a metal NP is crucial for adequately controlling important ligand-exchange reactions and requires more in depth research. With respect to semiconductor NPs, many ligands are classified as L, X, or Z type depending on the number of electrons donated or accepted when interacting with a metal center. This notation could be equally useful for the classification of ligands on metallic NPs. However, in many cases, the exact ligand–metal interactions remain not fully understood and thus this presents an important area of research needing to be addressed.

Additionally, the nature of the surface ligands will determine the final application of the NPs. For example, in biomedicine, a popular type of Au NPs commonly employed in phototherapy and drug delivery are those with a rod- or branched- shape. However, in most cases, these particles are synthesized using toxic cationic surfactants such as CTAB and CTAC. Although several ligand exchange steps can be performed to remove these ligands prior to their use in biomedical applications, this is not cost- and time- effective. New methods to produce these NPs directly with nontoxic ligands or biomolecules of interest would be highly beneficial for their broader application. On the other hand, one of the bottlenecks hindering industrial applications of NPs is the difficulty of scaling up their synthesis. While many published protocols are ideal for producing certain types of NPs at the milligram scale, they are not appropriate for larger scale production, so cheap approaches to larger scale production is one of the challenges in the field to be answered. In applications such as photovoltaics, photodetectors and sensors, the performance of the final devices is determined primarily by the morphological and structural features of the NPs but also by the alignment of the NPs during their assembly. Upon assembly, the ligands block the active surface sites and/or

prevent the formation of smooth films that are free of cracks. Different methods have been proposed for such an assembly, but there are many parameters during these processes which are still unexplored or incomprehensible. The removal of the capping ligands in such applications is a necessity in order to fabricate devices with high efficiency. Methods used to remove these ligands typically result in release of NPs from the surface or cause undesired growth of the NP core. This poses an issue for the stability of the devices. The development of new strategies or improvement of the existing methods for the effective removal of the capping ligands without affecting their morphology and structure is a necessity.

4.1. Stability of NPs

The use of dispersible NPs in complex media is very important and directly linked to the function of NPs as already discussed earlier. A vital element for the successful design of well-dispersible and functional NPs is a thorough analytical characterization during their synthesis, something that is missing in various published studies. Understanding the way that ligands pack on the NP surface, the strength of ligand–NP surface interaction, the net charge on the microenvironment around the NP, and how these characteristics change when NP size and morphology is varied are critical parameters to control the stability and function of NPs. Gaining deeper insight and control over these parameters are important goals to be focused on.

Furthermore, in some cases, for example when NPs are used for in vivo applications, it is required that after the NPs complete their role they can be cleared from the organism for example by degradation and extraction through the kidneys. Thus, further work toward the direction NP ligand coatings that facilitate NP degradation is desirable and will significantly benefit the elimination of their toxicity.

4.2. Density and Steric Configuration of Surface Ligands

The reactivity and multifunctional ability of the NPs strongly depends on the presentation and number/type of ligands on the NP surface. Although there are methods to quantify the number of ligands for certain types of NPs such as gold, for most of the cases of various other types of NPs, this is still a great challenge. Also in most cases it remains quite difficult to measure the reactivity of individual functional molecules such as antibodies anchored on the NP surface. Therefore, future developments in these directions will strongly benefit the better understanding of NP design and their most suitable applicability. Additionally, the development of new imaging methods to accurately visualize the conformation of ligands on the NP surface could significantly inform a better NP design and improve functionality. Especially with a view on using biomolecules such as peptides, proteins, or oligonucleotides as ligands, it would be extremely beneficial to be able to directly visualize their conformation on the NP surface as this directly influences their biological activity.

To conclude, this review article focused on highlighting the importance of ligands on (a) NP synthesis, (b) dispersibility of NPs in complex media, and (c) the effectiveness in applications ranging from biology to physics as well as giving an outlook to challenges, which yet remain to be fully addressed and give opportunities for exciting future research. We believe that it will be a valuable addition in setting the scene for future developments to come in the field.

AUTHOR INFORMATION

Corresponding Author

*Phone: (0)23 8059 2466. E-mail: a.kanaras@soton.ac.uk.

ORCID

Neus Feliu: 0000-0002-7886-1711

Indranath Chakraborty: 0000-0003-4195-9384

Eunkeu Oh: 0000-0003-1641-522X

Kimihiro Susumu: 0000-0003-4389-2574

Igor L. Medintz: 0000-0002-8902-4687

Emmanuel Stratakis: 0000-0002-1908-8618

Wolfgang J. Parak: 0000-0003-1672-6650

Antonios G. Kanaras: 0000-0002-9847-6706

Present Address

◇A.H.-J.: Ludwig-Maximilians-Universität München, 80539 Munich, Germany.

Notes

The authors declare no competing financial interest.

Biographies

Amelie Heuer-Jungemann obtained her degree in Chemistry with Biochemistry from Heriot-Watt University, Edinburgh (2011), and a Ph.D. in Physics from the University of Southampton (2015), working on biomolecule–nanoparticle conjugates for biomedical applications in the Laboratory for Inorganic Nanoparticles and Applications. She undertook postdoctoral research at the University of Southampton until 2016, and she is currently a postdoctoral fellow at the Ludwig-Maximilians-University, Munich, where her research is focused on applications of DNA origami.

Neus Feliu graduated in Chemistry from the Universitat de Barcelona (UB) in 2007 and obtained her Master of Science degree in Biomedical Materials from the Royal Institute of Technology (KTH) in Stockholm in 2009. She obtained her Ph.D. in Medical Science from Karolinska Institutet (KI), Stockholm, in the field of Engineered Nanomaterials for Biomedical Applications in 2014. Then, she was a postdoctoral researcher at the Department of Clinical Science and Technology (CLINTEC) at KI. Then, she joined the Department of Laboratory Medicine (LABMED), Clinical research Center, KI, Stockholm, as a Vinmer Fellow and Marie Curie Fellow. Currently, she is a Research Associate at the Center for Hybrid Nanostructures (CHyN), Hamburg University (HUU). Her research interest focuses on understanding the interactions between nanoparticles and biological systems and to explore their use in medical field.

Ioanna Bakaimi received her degree in Physics from the Aristotle University of Thessaloniki and a Masters degree in Applied Physics from the University of Silecia. Then she obtained a Ph.D. degree in Physical Sciences from the Department of Physics, University of Crete, and the Institute of Electronic Structure and Laser, FORTH, specializing on the magnetic properties of materials. Currently, she is a Research Fellow at the School of Chemistry, University of Southampton, UK, working on materials synthesis and characterization for applications in Energy.

Majd Hamaly obtained a B.Sc. in Pharmacy and a master degree in Pharmaceutical Sciences from the University of Jordan before joining the King Hussein Cancer Center. Her research focus is the biomedical application of nanotechnology.

Allaldin Alkilany completed a B.Sc. in Pharmacy (Jordan University of Science and Technology), a Ph.D. in Chemistry (the University of Illinois, USA) and postdoctoral training (Georgia Regents University, USA) before joining the academic staff at the University of Jordan. Dr

Alkilany is an Associate Professor of Nanoscience and Pharmaceutical Technology at the School of Pharmacy (University of Jordan) and the Alexander von Humboldt fellow at the University of Hamburg, Germany. Dr. Alkilany's research focuses on nanotechnology and its biomedical applications, understanding the nanobio interface, and engineering novel drug delivery systems.

Indranath Chakraborty received a Ph.D. in chemistry from the Indian Institute of Technology, Madras. He was a research associate at the University of Illinois at Urbana–Champaign, IL, USA. Later, he was an Alexander von Humboldt Postdoctoral Research Fellow at Philipps University of Marburg, Germany. Currently, he is a research associate at Center for Hybrid Nanostructure, University of Hamburg, Germany. His research area is focused on tuning surfaces of plasmonic and fluorescent nanoparticles for biomedical applications. He is a recipient of the J. C. Bose Patent Award and the Malhotra Weikfield Foundation Nanoscience Fellowship Award.

Atif Masood received his M.Sc. in Medical Physics from from PIEAS, Islamabad. In 2018, he received a Ph.D. from the Faculty of Physics, Phillips University Marburg, specializing on the synthesis, surface modification, and bioconjugation of inorganic (QDs, plasmonic, magnetic, catalytic TiO₂) NPs. Since 2018, he is a Senior Medical Scientist at Karachi Institute of Radiotherapy and Nuclear Medicine (KIRAN), Karachi, Pakistan..

Maria Francesca Casula received her Ph.D. in Chemistry from the University of Cagliari, where she currently is Associate Professor of General and Inorganic Chemistry. She has been a visiting researcher at the University of California, Berkeley, as a postdoctoral fellow. Her research area is focused on the design of functional nanomaterials for biomedical, catalytic, and environmental applications. Synthesis–properties relationships of the developed nanomaterials is achieved by a multitechnique textural and structural characterization, and the corresponding results are reported in 115 scientific papers in peer-reviewed journals and two book chapters.

Athanasia Kostopoulou received her B.Sc. degree in Physics (2004) and her M.Sc. degree (2006) on Materials Physics & Technology from the Physics Department at the Aristotle University of Thessaloniki. In 2012, she received her Ph.D. from the Department of Chemistry at the University of Crete, and since then she was a Postdoctoral Fellow in the Institute of Electronic Structure and Laser at FORTH in Heraklion. Since 2016, she is part of the group of the Ultrafast Laser Micro and Nano Processing (ULMNP) Laboratory and she is working on the chemical synthesis and elucidation of the microscopic physical or photoinduced mechanisms involving nanocrystal systems. The last few months she is the coordinator of a project funded from the Hellenic Foundation for Research and Innovation (HFRI) and the General Secretariat for Research and Technology (GSRT) related to perovskite nanomaterials for photovoltaic applications.

Eunkeu Oh received an M.Sc in physics from Pohang University of Science and Technology (POSTECH) and worked for Samsung since 1996. In 2006, she obtained a Ph.D. in biological science from Korean Advanced Institute of Science and Technology (KAIST) on developing biosensors utilizing the property of energy transfer between quantum dots and gold nanoparticles. She subsequently joined the Naval Research Laboratory through a postdoctoral fellowship of Johns Hopkins University. Currently, she focuses on the development of nanoparticle-based optical materials and their biological application.

Kimihiro Susumu is a Research Chemist in the Optical Sciences Division at the Naval Research Laboratory through KeyW Corporation. His research has focused on the development of

biocompatible quantum dots and gold nanoparticles for biosensing and imaging technologies. Specifically, his recent research interest includes (i) synthesis of a series of core/shell quantum dots and (ii) design and synthesis of a series of multifunctional surface coating ligands to enhance the biocompatibility of quantum dots and gold nanoparticles.

Michael H. Stewart received a BSc. in chemistry from Wittenberg University (2002) and a Ph.D. in materials chemistry from the University of Michigan (2007). As an NRC postdoctoral fellow at the U.S. Naval Research Laboratory (NRL), he developed hydrophilic colloidal semiconductor quantum dots as advanced biosensing platforms. He is currently a federal scientist in the Optical Sciences Division at NRL, where his research efforts focus on advancing colloidal nanocrystal-based technologies for biological and photonic applications. He is a recipient of the Sigma Xi Young Investigator Award and Delores M. Etter Top Navy Scientist of the Year Award.

Igor L. Medintz received a Ph.D. in Molecular, Cellular and Developmental Biology from the City University of New York in 1999. This was followed by a National Cancer Institute Fellowship with Prof. Richard Mathies of the College of Chemistry, University of California, Berkeley, and some industrial experience with Vertex Pharmaceuticals. He began at NRL as a National Research Council Fellow in 2002 and as a Research Biologist in 2004. He currently serves as the Senior Scientist for Biosensors and Biomaterials with the Center for Bio/Molecular Science and Engineering. His research interests include how nanoparticles engage in energy transfer and how biological processes are altered at a nanoparticle interface.

Emmanuel Stratakis is a Research Director at the Foundation for Research and Technology—Hellas (FORTH). He received his Ph.D. in Physics from the University of Crete in 2001, and then he joined the University of California, Berkeley, as a visiting researcher. He is currently leading the Ultrafast Laser Micro- and Nano- Processing group of FORTH (<https://www.iesl.forth.gr/ULMNP>). He has over 170 SCI publications and more than 6000 citations, and he has coordinated many National and EU grants. Since 2015, he is the Director of the European Nanoscience Facility of FORTH, part of the NFFA-Europe EU Infrastructure, where he is a member of the General Assembly. He is a National Representative to the High-Level Group of EU on Nanosciences, Nanotechnology and Advanced Materials and a National Expert in the NMBP Program Committee of the Horizon 2020. He is a member of the Scientific Committee of COST, of the Physical Sciences sectoral scientific council of the National Council for Research & Innovation of Greece, and national delegate of the OECD Working Party on Bio-, Nano-, and Converging Tech (BNCT).

Wolfgang Parak studied physics at the Technische Universität München and obtained his Ph.D. in 1999 at the Ludwig Maximilians Universität München. After a postdoctoral stay from 2000–2002 at the Department of Chemistry at the University of California at Berkeley, he started his own group in the framework of an Emmy Noether fellowship at the Ludwig Maximilians Universität München, which is equivalent to Assistant Professor. In 2005, he held there a temporary position as Associate Professor for Physical Chemistry. In 2007, he became Full Professor at the Physics Department at the Philipps Universität Marburg. Since 2013, he is also group leader at CIC Bimagune in San Sebastian, Spain. In 2017 he moved to the Universität Hamburg as a Full Professor in physics. He is also Associate Editor of ACS Nano.

Antonios G. Kanaras obtained his degree in Chemistry from the University of Crete, and a Master's degree in Bioinorganic Chemistry from the University of Ioannina. Then he received a Ph.D. degree

from the Department of Chemistry, University of Liverpool, working on the organization of gold nanoparticles using biomolecular tools. He was a postdoctoral scientist at the Department of Chemistry, University of California, Berkeley, and Lawrence Berkeley Lab, working on the synthesis and energy applications of semiconductor nanoparticles. Currently, he is a Professor/Chair at the School of Physics and Astronomy, University of Southampton, and the Head of the Laboratory for Inorganic Nanoparticles and Applications. Antonios' research is highly multidisciplinary working at the interface of Physics, Chemistry, Biology, and Materials Science. He is Fellow of the Higher Education Academy, Fellow of the Royal Society of Chemistry, Fellow of the Royal Society of Biology, and Fellow of the Institute of Physics.

ACKNOWLEDGMENTS

A.H.-J. was funded by the Leverhulme Trust (ref RPG-2015-005). A.M. was supported by HEC/DAAD with a Ph.D. fellowship. I.C. was funded by an Alexander von Humboldt postdoctoral fellowship. N.F. acknowledges funding from the Swedish Governmental Agency for Innovation Systems (Vinnova). A.F. was funded by DAAD/HEC. W.J.P. acknowledges funding from the German Research Foundation (DFG grant PA 794/28-1). M.F.C. acknowledges funding from University of Cagliari (under FIR 2018). A.G.K. acknowledges funding from BBSRC (BB/N021150/1, BB/P017711/1). A.K. acknowledges funding from the Hellenic Foundation for Research and Innovation (HFRI) and the General Secretariat for Research and Technology (GSRT), under grand agreement no. 1179.

ABBREVIATIONS USED

Acac	acetylacetonate
Ala	alanine
APTS	aminopropyl trimethoxysilane
Asn	asparagine
Au NP	gold nanoparticle
Au NR	gold nanorod
Ag NP	silver nanoparticle
Ag NC	silver nanocluster
Ag ₂ Te	silver telluride
BHJ	bulk heterojunction
BPEI	branched polyethyleneimine
BSA	bovine serum albumin
BSPP	bis(<i>p</i> -sulfonatophenyl)phenyl phosphine dehydrate
CBMT	chlorobenzenemethanethiol
CKD	chronic kidney disease
Co NP	cobalt nanoparticle
CPP	cell-penetrating peptide
CTAB	cetyltrimethylammonium bromide
CTAC	cetyltrimethylammonium chloride
Cu NP	copper nanoparticle
Cys	cysteine
Da	Dalton
DCB	dichlorobenzene
DDA	dodecylamine
DDT	1-dodecane thiol
DEG	diethylene glycol
DFT	density functional theory
DHJ	depleted heterojunction
DHLA	dihydrolipoic acid
DMEC	dimethylethynylcarbinol

DMSO	dimethylsulfoxide
DMVC	dimethylvinylcarbinol
DNA	deoxyribonucleic acid
DTAB	decyltrimethylammonium bromide
DTT	dithiothreitol
EDC	1-ethyl-3-(3-dimethylaminopropyl)carbodiimide
EG	ethylene glycol
EQE	external quantum efficiency
ETL	electron transport layer
FDA	Food and Drug Administration
FET	field-effect transistor
GO	graphene oxide
GSH	glutathione
GTS	glutathione S-transferase
HDA	hexadecylamine
His	histidine
HIV	human immunodeficiency virus
HPA	<i>n</i> -hexylphosphonic acid
HRTEM	high resolution transmission electron microscopy
HSA	human serum albumin
ICBA	indene-C ₆₀ bisadduct
ID	identity document
ITO	indium tin oxide
LBL	layer-by-layer
LED	light emitting diode
Leu	leucine
LNA	locked nucleic acid
LSPR	localized surface plasmon resonance
Lys	lysine
MBP	maltose binding protein
<i>m</i> PEG	methoxy polyethylene glycol
MRI	magnetic resonance imaging
NC	nanocluster
NHS	<i>N</i> -hydroxysuccinimide
NIR	near infrared
NMF	<i>n</i> -methylformamide
NMR	nuclear magnetic resonance
NP	nanoparticle
NTA	nitriloacetate
OA	oleic acid
ODA	octadecylamine
ODE	octadecene
ODPA	octadecylphosphonic acid
OEG	oligoethylene glycol
OLA	oleylamine
OPA	<i>n</i> -octylphosphonic acid
OPH	organophosphate hydrolase
OPV	organic photovoltaic
OT	<i>n</i> -octanethiol
P3HT	poly(3-hexylthiophene-2,5-diyl)
PAA	peroxyacetic acid
PAMAM	polyamidoamine
PBS	phosphate buffered saline
Pd NP	palladium nanoparticle
PDMA	polydimethylsiloxane
PEDOT	poly(3,4-ethylenedioxythiophene)
PEG	polyethylene glycol
PEG-MA	poly(ethylene glycol) methacrylate
PEG-SH	poly(ethylene glycol) thiol
PEI	polyethyleneimine
PEO	poly(ethylene oxide)
PFH	poly(9,9-dihethylfluorene)
PHA	polyhydroxyalkanoate

PMA	poly(maleic anhydride- <i>alt</i> -1-octadecene)
PMEA	<i>para</i> -methoxyethylamphetamine
PMPC	poly(2-methacryloyloxyethyl phosphorylcholine)
PNA	peptide nucleic acid
PPA	<i>P,P</i> -(di- <i>n</i> -octyl)dihydrogen pyrophosphonic acid
pt DNA	phosphorothioate DNA
Pt NP	platinum nanoparticle
PVA	poly(vinyl alcohol)
PVP	poly(vinyl pyrrolidone)
QD	quantum dot
QY	quantum yield
RNA	ribonucleic acid
RT	room temperature
SDS	sodium dodecyl sulfate
SEM	scanning electron microscopy
SFS	sodium formaldehyde sulfoxylate
Si NP	silica nanoparticle
siRNA	small interfering ribonucleic acid
Sp	spherical
SPION	superparamagnetic iron oxide nanoparticle
SMAD	solvated metal atom dispersion
TA	thioctic acid
TBP	tributylphosphine
TDPA	<i>n</i> -tetradecylphosphonic acid
TEG	triethylene glycol
TEM	transmission electron microscopy
TEOS	tetraethylorthosilicate
THPC	tetrakis (hydroxymethyl) phosphonium chloride
TMS	trimethyl silane
TOAB	tetraoctylammonium bromide
TOP	trioctylphosphine
TOPO	trin-octylphosphine oxide
TPP	triphenyl phosphine
TTAB	tetradecyltrimethylammonium bromide
TTG	thioalkylated tetraethylene glycol
UCNP	upconversion nanoparticle
UV	ultraviolet

REFERENCES

- (1) Zhao, J.; Pinchuk, A. O.; McMahon, J. M.; Li, S. Z.; Ausman, L. K.; Atkinson, A. L.; Schatz, G. C. Methods for Describing the Electromagnetic Properties of Silver and Gold Nanoparticles. *Acc. Chem. Res.* **2008**, *41*, 1710–1720.
- (2) Cortie, M. B.; McDonagh, A. M. Synthesis and Optical Properties of Hybrid and Alloy Plasmonic Nanoparticles. *Chem. Rev.* **2011**, *111*, 3713–3735.
- (3) Huang, X. H.; Jain, P. K.; El-Sayed, I. H.; El-Sayed, M. A. Gold Nanoparticles: Interesting Optical Properties and Recent Applications in Cancer Diagnostic and Therapy. *Nanomedicine* **2007**, *2*, 681–693.
- (4) Jain, P. K.; Huang, X.; El-Sayed, I. H.; El-Sayed, M. A. Review of Some Interesting Surface Plasmon Resonance-Enhanced Properties of Noble Metal Nanoparticles and Their Applications to Biosystems. *Plasmonics* **2007**, *2*, 107–118.
- (5) Michalet, X.; Pinaud, F. F.; Bentolila, L. A.; Tsay, J. M.; Doose, S.; Li, J. J.; Sundaresan, G.; Wu, A. M.; Gambhir, S. S.; Weiss, S. Quantum Dots for Live Cells, in Vivo Imaging, and Diagnostics. *Science* **2005**, *307*, 538–544.
- (6) Medintz, I. L.; Uyeda, H. T.; Goldman, E. R.; Mattoussi, H. Quantum Dot Bioconjugates for Imaging, Labelling and Sensing. *Nat. Mater.* **2005**, *4*, 435–446.
- (7) Chan, W. C. W.; Maxwell, D. J.; Gao, X. H.; Bailey, R. E.; Han, M. Y.; Nie, S. M. Luminescent Quantum Dots for Multiplexed Biological Detection and Imaging. *Curr. Opin. Biotechnol.* **2002**, *13*, 40–46.
- (8) Laurent, S.; Forge, D.; Port, M.; Roch, A.; Robic, C.; Vander Elst, L.; Muller, R. N. Magnetic Iron Oxide Nanoparticles: Synthesis, Stabilization, Vectorization, Physicochemical Characterizations, and Biological Applications. *Chem. Rev.* **2008**, *108*, 2064–2110.
- (9) Lu, A. H.; Salabas, E. L.; Schuth, F. Magnetic Nanoparticles: Synthesis, Protection, Functionalization, and Application. *Angew. Chem., Int. Ed.* **2007**, *46*, 1222–1244.
- (10) Murphy, C. J.; Sau, T. K.; Gole, A. M.; Orendorff, C. J.; Gao, J. X.; Gou, L.; Hunyadi, S. E.; Li, T. Anisotropic Metal Nanoparticles: Synthesis, Assembly, and Optical Applications. *J. Phys. Chem. B* **2005**, *109*, 13857–13870.
- (11) Pankhurst, Q. A.; Connolly, J.; Jones, S. K.; Dobson, J. Applications of Magnetic Nanoparticles in Biomedicine. *J. Phys. D: Appl. Phys.* **2003**, *36*, R167–R181.
- (12) Willets, K. A.; Van Duyne, R. P. Localized Surface Plasmon Resonance Spectroscopy and Sensing. *Annu. Rev. Phys. Chem.* **2007**, *58*, 267–297.
- (13) Nozik, A. J.; Beard, M. C.; Luther, J. M.; Law, M.; Ellingson, R. J.; Johnson, J. C. Semiconductor Quantum Dots and Quantum Dot Arrays and Applications of Multiple Exciton Generation to Third-Generation Photovoltaic Solar Cells. *Chem. Rev.* **2010**, *110*, 6873–6890.
- (14) Chakraborty, I.; Jimenez de Aberasturi, D.; Pazos-Perez, N.; Guerrini, L.; Masood, A.; Alvarez-Puebla, R. A.; Feliu, N.; Parak, W. J. Ion-Selective Ligands: How Colloidal Nano- and Micro-Particles Can Introduce New Functionalities. *Z. Phys. Chem.* **2018**, *232*, 1307–1317.
- (15) Baranov, D.; Manna, L.; Kanaras, A. G. Chemically Induced Self-Assembly of Spherical and Anisotropic Inorganic Nanocrystals. *J. Mater. Chem.* **2011**, *21*, 16694–16703.
- (16) Li, H. B.; Kanaras, A. G.; Manna, L. Colloidal Branched Semiconductor Nanocrystals: State of the Art and Perspectives. *Acc. Chem. Res.* **2013**, *46*, 1387–1396.
- (17) Zhang, Y. G.; Pal, S.; Srinivasan, B.; Vo, T.; Kumar, S.; Gang, O. Selective Transformations between Nanoparticle Superlattices Via the Reprogramming of DNA-Mediated Interactions. *Nat. Mater.* **2015**, *14*, 840–847.
- (18) Macfarlane, R. J.; Lee, B.; Jones, M. R.; Harris, N.; Schatz, G. C.; Mirkin, C. A. Nanoparticle Superlattice Engineering with DNA. *Science* **2011**, *334*, 204–208.
- (19) Zhang, C.; Macfarlane, R. J.; Young, K. L.; Choi, C. H. J.; Hao, L.; Auyeung, E.; Liu, G.; Zhou, X.; Mirkin, C. A. A General Approach to DNA-Programmable Atom Equivalents. *Nat. Mater.* **2013**, *12*, 741–746.
- (20) Zhang, Y. G.; Gang, O. Nanocrystal Superlattices the Pathway to Atomic Alignment. *Nat. Mater.* **2016**, *15*, 1225–1226.
- (21) Liu, W. Y.; Halverson, J.; Tian, Y.; Tkachenko, A. V.; Gang, O. Self-Organized Architectures from Assorted DNA-Framed Nanoparticles. *Nat. Chem.* **2016**, *8*, 867–873.
- (22) Liu, W. Y.; Tagawa, M.; Xin, H. L. L.; Wang, T.; Emamy, H.; Li, H. L.; Yager, K. G.; Starr, F. W.; Tkachenko, A. V.; Gang, O. Diamond Family of Nanoparticle Superlattices. *Science* **2016**, *351*, 582–586.
- (23) Kyriazi, M.-E.; Giust, D.; El-Sagheer, A. H.; Lackie, P. M.; Muskens, O. L.; Brown, T.; Kanaras, A. G. Multiplexed mRNA Sensing and Combinatorial-Targeted Drug Delivery Using DNA-Gold Nanoparticle Dimers. *ACS Nano* **2018**, *12*, 3333–3340.
- (24) Pakiari, A. H.; Jamshidi, Z. Nature and Strength of M–S Bonds (M = Au, Ag, and Cu) in Binary Alloy Gold Clusters. *J. Phys. Chem. A* **2010**, *114*, 9212–9221.
- (25) Brust, M.; Walker, M.; Bethell, D.; Schiffrin, D. J.; Whyman, R. Synthesis of Thiol-Derivatized Gold Nanoparticles in a 2-Phase Liquid-Liquid System. *J. Chem. Soc., Chem. Commun.* **1994**, *0*, 801–802.
- (26) Bastus, N. G.; Comenge, J.; Punter, V. Kinetically Controlled Seeded Growth Synthesis of Citrate-Stabilized Gold Nanoparticles of up to 200 nm: Size Focusing Versus Ostwald Ripening. *Langmuir* **2011**, *27*, 11098–11105.

- (27) Algar, W. R.; Susumu, K.; Delehanty, J. B.; Medintz, I. L. Semiconductor Quantum Dots in Bioanalysis: Crossing the Valley of Death. *Anal. Chem.* **2011**, *83*, 8826–8837.
- (28) Pellegrino, T.; Kudera, S.; Liedl, T.; Muñoz Javier, A. M.; Manna, L.; Parak, W. J. On the Development of Colloidal Nanoparticles Towards Multifunctional Structures and Their Possible Use for Biological Applications. *Small* **2005**, *1*, 48–63.
- (29) Faraday, M. The Bakerian Lecture: W. Experimental Relations of Gold (and Other Metals) to Light. *Philos. Trans. R. Soc. London* **1857**, *147*, 145–181.
- (30) Turkevich, J.; Stevenson, P. C.; Hillier, J. A Study of the Nucleation and Growth Processes in the Synthesis of Colloidal Gold. *Discuss. Faraday Soc.* **1951**, *11*, 55–75.
- (31) Frens, G. Controlled Nucleation for Regulation of Particle-Size in Monodisperse Gold Suspensions. *Nature, Phys. Sci.* **1973**, *241*, 20–22.
- (32) Chow, M. K.; Zukoski, C. F. Gold Sol Formation Mechanisms - Role of Colloidal Stability. *J. Colloid Interface Sci.* **1994**, *165*, 97–109.
- (33) Ji, X. H.; Song, X. N.; Li, J.; Bai, Y. B.; Yang, W. S.; Peng, X. G. Size Control of Gold Nanocrystals in Citrate Reduction: The Third Role of Citrate. *J. Am. Chem. Soc.* **2007**, *129*, 13939–13948.
- (34) Kimling, J.; Maier, M.; Okenve, B.; Kotaidis, V.; Ballot, H.; Plech, A. Turkevich Method for Gold Nanoparticle Synthesis Revisited. *J. Phys. Chem. B* **2006**, *110*, 15700–15707.
- (35) Schulz, F.; Homolka, T.; Bastús, N. G.; Puentes, V.; Weller, H.; Vossmeier, T. Little Adjustments Significantly Improve the Turkevich Synthesis of Gold Nanoparticles. *Langmuir* **2014**, *30*, 10779–10784.
- (36) Polte, J.; Ahner, T. T.; Delissen, F.; Sokolov, S.; Emmerling, F.; Thunemann, A. F.; Kraehnert, R. Mechanism of Gold Nanoparticle Formation in the Classical Citrate Synthesis Method Derived from Coupled in Situ Xanes and SAXS Evaluation. *J. Am. Chem. Soc.* **2010**, *132*, 1296–1301.
- (37) Pong, B. K.; Elim, H. I.; Chong, J. X.; Ji, W.; Trout, B. L.; Lee, J. Y. New Insights on the Nanoparticle Growth Mechanism in the Citrate Reduction of Gold(III) Salt: Formation of the Au Nanowire Intermediate and Its Nonlinear Optical Properties. *J. Phys. Chem. C* **2007**, *111*, 6281–6287.
- (38) Patungwasa, W.; Hodak, J. H. Ph Tunable Morphology of the Gold Nanoparticles Produced by Citrate Reduction. *Mater. Chem. Phys.* **2008**, *108*, 45–54.
- (39) Al-Johani, H.; Abou-Hamad, E.; Jedidi, A.; Widdifield, C. M.; Viger-Gravel, J.; Sangaru, S. S.; Gajan, D.; Anjum, D. H.; Ould-Chikh, S.; et al. The Structure and Binding Mode of Citrate in the Stabilization of Gold Nanoparticles. *Nat. Chem.* **2017**, *9*, 890.
- (40) Park, J. W.; Shumaker-Parry, J. S. Structural Study of Citrate Layers on Gold Nanoparticles: Role of Intermolecular Interactions in Stabilizing Nanoparticles. *J. Am. Chem. Soc.* **2014**, *136*, 1907–1921.
- (41) Hermanson, G. T. *Bioconjugate Techniques*, 3rd ed.; Elsevier/AP: London, Waltham, MA, 2013.
- (42) Dinkel, R.; Braunschweig, B.; Peukert, W. Fast and Slow Ligand Exchange at the Surface of Colloidal Gold Nanoparticles. *J. Phys. Chem. C* **2016**, *120*, 1673–1682.
- (43) Feng, Y.; Xing, S.; Xu, J.; Wang, H.; Lim, J. W.; Chen, H. Probing the Kinetics of Ligand Exchange on Colloidal Gold Nanoparticles by Surface-Enhanced Raman Scattering. *Dalton Trans* **2010**, *39*, 349–351.
- (44) Dreaden, E. C.; Alkilany, A. M.; Huang, X.; Murphy, C. J.; El-Sayed, M. A. The Golden Age: Gold Nanoparticles for Biomedicine. *Chem. Soc. Rev.* **2012**, *41*, 2740–2779.
- (45) Zhu, T.; Vasilev, K.; Kreiter, M.; Mittler, S.; Knoll, W. Surface Modification of Citrate-Reduced Colloidal Gold Nanoparticles with 2-Mercaptosuccinic Acid. *Langmuir* **2003**, *19*, 9518–9525.
- (46) Chi, H.; Liu, B.; Guan, G.; Zhang, Z.; Han, M.-Y. A Simple, Reliable and Sensitive Colorimetric Visualization of Melamine in Milk by Unmodified Gold Nanoparticles. *Analyst* **2010**, *135*, 1070–1075.
- (47) Larson, I.; Chan, D. Y. C.; Drummond, C. J.; Grieser, F. Use of Atomic Force Microscopy Force Measurements to Monitor Citrate Displacement by Amines on Gold in Aqueous Solution. *Langmuir* **1997**, *13*, 2429–2431.
- (48) Chakraborty, I.; Parak, W. J. Protein-Induced Shape Control of Noble Metal Nanoparticles. *Adv. Mater. Interfaces* **2019**, *6*, 1801407.
- (49) Hühn, J.; Carrillo-Carrion, C.; Soliman, M. G.; Pfeiffer, C.; Valdeperez, D.; Masood, A.; Chakraborty, I.; Zhu, L.; Gallego, M.; et al. Selected Standard Protocols for the Synthesis, Phase Transfer, and Characterization of Inorganic Colloidal Nanoparticles. *Chem. Mater.* **2017**, *29*, 399–461.
- (50) Nuzzo, R. G.; Dubois, L. H.; Allara, D. L. Fundamental Studies of Microscopic Wetting on Organic Surfaces. 1. Formation and Structural Characterization of a Self-Consistent Series of Polyfunctional Organic Monolayers. *J. Am. Chem. Soc.* **1990**, *112*, 558–569.
- (51) Nuzzo, R. G.; Fusco, F. A.; Allara, D. L. Spontaneously Organized Molecular Assemblies. 3. Preparation and Properties of Solution Adsorbed Monolayers of Organic Disulfides on Gold Surfaces. *J. Am. Chem. Soc.* **1987**, *109*, 2358–2368.
- (52) Xue, C.; Millstone, J. E.; Li, S.; Mirkin, C. A. Plasmon-Driven Synthesis of Triangular Core–Shell Nanoprisms from Gold Seeds. *Angew. Chem., Int. Ed.* **2007**, *46*, 8436–8439.
- (53) Zhang, Q.; Li, N.; Goebel, J.; Lu, Z.; Yin, Y. A Systematic Study of the Synthesis of Silver Nanoplates: Is Citrate a “Magic” Reagent? *J. Am. Chem. Soc.* **2011**, *133*, 18931–18939.
- (54) Bastús, N. G.; Comenge, J.; Puentes, V. Kinetically Controlled Seeded Growth Synthesis of Citrate-Stabilized Gold Nanoparticles of up to 200 nm: Size Focusing Versus Ostwald Ripening. *Langmuir* **2011**, *27*, 11098–11105.
- (55) Piella, J.; Bastús, N. G.; Puentes, V. Size-Controlled Synthesis of Sub-10-Nanometer Citrate-Stabilized Gold Nanoparticles and Related Optical Properties. *Chem. Mater.* **2016**, *28*, 1066–1075.
- (56) Perrault, S. D.; Chan, W. C. W. Synthesis and Surface Modification of Highly Monodispersed, Spherical Gold Nanoparticles of 50–200 nm. *J. Am. Chem. Soc.* **2009**, *131*, 17042–17043.
- (57) Bastús, N. G.; Merkoçi, F.; Piella, J.; Puentes, V. Synthesis of Highly Monodisperse Citrate-Stabilized Silver Nanoparticles of up to 200 nm: Kinetic Control and Catalytic Properties. *Chem. Mater.* **2014**, *26*, 2836–2846.
- (58) Henglein, A.; Giersig, M. Formation of Colloidal Silver Nanoparticles: Capping Action of Citrate. *J. Phys. Chem. B* **1999**, *103*, 9533–9539.
- (59) Sivaraman, S. K.; Elango, I.; Kumar, S.; Santhanam, V. A Green Protocol for Room Temperature Synthesis of Silver Nanoparticles in Seconds. *Curr. Sci. India* **2009**, *97*, 1055–1059.
- (60) Njoki, P. N.; Luo, J.; Kamundi, M. M.; Lim, S.; Zhong, C. J. Aggregative Growth in the Size-Controlled Growth of Monodispersed Gold Nanoparticles. *Langmuir* **2010**, *26*, 13622–13629.
- (61) Jana, N. R.; Gearheart, L.; Murphy, C. J. Seeding Growth for Size Control of 5–40 nm Diameter Gold Nanoparticles. *Langmuir* **2001**, *17*, 6782–6786.
- (62) Sau, T. K.; Murphy, C. J. Room Temperature, High-Yield Synthesis of Multiple Shapes of Gold Nanoparticles in Aqueous Solution. *J. Am. Chem. Soc.* **2004**, *126*, 8648–8649.
- (63) Perez-Juste, J.; Pastoriza-Santos, I.; Liz-Marzan, L. M.; Mulvaney, P. Gold Nanorods: Synthesis, Characterization and Applications. *Coord. Chem. Rev.* **2005**, *249*, 1870–1901.
- (64) Mafuné, F.; Kohno, J.-y.; Takeda, Y.; Kondow, T.; Sawabe, H. Structure and Stability of Silver Nanoparticles in Aqueous Solution Produced by Laser Ablation. *J. Phys. Chem. B* **2000**, *104*, 8333–8337.
- (65) Gao, J. X.; Bender, C. M.; Murphy, C. J. Dependence of the Gold Nanorod Aspect Ratio on the Nature of the Directing Surfactant in Aqueous Solution. *Langmuir* **2003**, *19*, 9065–9070.
- (66) Day, H. A.; Bartczak, D.; Fairbairn, N.; McGuire, E.; Ardakani, M.; Porter, A. E.; Kanaras, A. G. Controlling the Three-Dimensional Morphology of Nanocrystals. *CrystEngComm* **2010**, *12*, 4312–4316.
- (67) Vassalini, I.; Rotunno, E.; Lazzarini, L.; Alessandri, I. “Stainless” Gold Nanorods: Preserving Shape, Optical Properties, and SERS Activity in Oxidative Environment. *ACS Appl. Mater. Interfaces* **2015**, *7*, 18794–18802.
- (68) Ye, X.; Jin, L.; Caglayan, H.; Chen, J.; Xing, G.; Zheng, C.; Doan-Nguyen, V.; Kang, Y.; Engheta, N.; et al. Improved Size-

Tunable Synthesis of Monodisperse Gold Nanorods through the Use of Aromatic Additives. *ACS Nano* **2012**, *6*, 2804–2817.

(69) Perez-Juste, J.; Liz-Marzan, L. M.; Carnie, S.; Chan, D. Y. C.; Mulvaney, P. Electric-Field-Directed Growth of Gold Nanorods in Aqueous Surfactant Solutions. *Adv. Funct. Mater.* **2004**, *14*, 571–579.

(70) Chen, L.; Ji, F.; Xu, Y.; He, L.; Mi, Y.; Bao, F.; Sun, B.; Zhang, X.; Zhang, Q. High-Yield Seedless Synthesis of Triangular Gold Nanoplates through Oxidative Etching. *Nano Lett.* **2014**, *14*, 7201–7206.

(71) Bratlie, K. M.; Lee, H.; Komvopoulos, K.; Yang, P.; Somorjai, G. A. Platinum Nanoparticle Shape Effects on Benzene Hydrogenation Selectivity. *Nano Lett.* **2007**, *7*, 3097–3101.

(72) Niidome, T.; Yamagata, M.; Okamoto, Y.; Akiyama, Y.; Takahashi, H.; Kawano, T.; Katayama, Y.; Niidome, Y. Peg-Modified Gold Nanorods with a Stealth Character for in Vivo Applications. *J. Controlled Release* **2006**, *114*, 343–347.

(73) Pensa, E.; Cortés, E.; Corthey, G.; Carro, P.; Vericat, C.; Fonticelli, M. H.; Benítez, G.; Rubert, A. A.; Salvarezza, R. C. The Chemistry of the Sulfur–Gold Interface: In Search of a Unified Model. *Acc. Chem. Res.* **2012**, *45*, 1183–1192.

(74) Häkkinen, H. The Gold–Sulfur Interface at the Nanoscale. *Nat. Chem.* **2012**, *4*, 443.

(75) Schaaff, T. G.; Knight, G.; Shafigullin, M. N.; Borkman, R. F.; Whetten, R. L. Isolation and Selected Properties of a 10.4 Kda Gold: Glutathione Cluster Compound. *J. Phys. Chem. B* **1998**, *102*, 10643–10646.

(76) Chakraborty, I.; Pradeep, T. Atomically Precise Clusters of Noble Metals: Emerging Link between Atoms and Nanoparticles. *Chem. Rev.* **2017**, *117*, 8208–8271.

(77) Yonezawa, T.; Kunitake, T. Practical Preparation of Anionic Mercapto Ligand-Stabilized Gold Nanoparticles and Their Immobilization. *Colloids Surf., A* **1999**, *149*, 193–199.

(78) Roux, S.; Garcia, B.; Bridot, J.-L.; Salomé, M.; Marquette, C.; Lemelle, L.; Gillet, P.; Blum, L.; Perriat, P.; Tillement, O. Synthesis, Characterization of Dihydrolipoic Acid Capped Gold Nanoparticles, and Functionalization by the Electroluminescent Luminol. *Langmuir* **2005**, *21*, 2526–2536.

(79) Karakoti, A. S.; Das, S.; Thevuthasan, S.; Seal, S. Pegylated Inorganic Nanoparticles. *Angew. Chem., Int. Ed.* **2011**, *50*, 1980–1994.

(80) Otsuka, H.; Nagasaki, Y.; Kataoka, K. Pegylated Nanoparticles for Biological and Pharmaceutical Applications. *Adv. Drug Delivery Rev.* **2003**, *55*, 403–419.

(81) Kanaras, A. G.; Kamounah, F. S.; Schaumburg, K.; Kiely, C. J.; Brust, M. Thioalkylated Tetraethylene Glycol: A New Ligand for Water Soluble Monolayer Protected Gold Clusters. *Chem. Commun.* **2002**, 2294–2295.

(82) Oh, E.; Susumu, K.; Goswami, R.; Mattoussi, H. One-Phase Synthesis of Water-Soluble Gold Nanoparticles with Control over Size and Surface Functionalities. *Langmuir* **2010**, *26*, 7604–7613.

(83) Oh, E.; Delehanty, J. B.; Sapsford, K. E.; Susumu, K.; Goswami, R.; Blanco-Canosa, J. B.; Dawson, P. E.; Granek, J.; Shoff, M.; et al. Cellular Uptake and Fate of Pegylated Gold Nanoparticles Is Dependent on Both Cell-Penetration Peptides and Particle Size. *ACS Nano* **2011**, *5*, 6434–6448.

(84) Oh, E.; Susumu, K.; Jain, V.; Kim, M.; Huston, A. One-Pot Aqueous Phase Growth of Biocompatible 15–130 nm Gold Nanoparticles Stabilized with Bidentate Peg. *J. Colloid Interface Sci.* **2012**, *376*, 107–111.

(85) Oh, E.; Susumu, K.; Makinen, A. J.; Deschamps, J. R.; Huston, A. L.; Medintz, I. L. Colloidal Stability of Gold Nanoparticles Coated with Multithiol-Poly(Ethylene Glycol) Ligands: Importance of Structural Constraints of the Sulfur Anchoring Groups. *J. Phys. Chem. C* **2013**, *117*, 18947–18956.

(86) Lohse, S. E.; Dahl, J. A.; Hutchison, J. E. Direct Synthesis of Large Water-Soluble Functionalized Gold Nanoparticles Using Bunte Salts as Ligand Precursors. *Langmuir* **2010**, *26*, 7504–7511.

(87) Shi, Y.; Goodisman, J.; Dabrowiak, J. C. Cyclodextrin Capped Gold Nanoparticles as a Delivery Vehicle for a Prodrug of Cisplatin. *Inorg. Chem.* **2013**, *52*, 9418–9426.

(88) Zhong, J.; Qu, J.; Ye, F.; Wang, C.; Meng, L.; Yang, J. The Bis(P-Sulfonatophenyl)Phenylphosphine-Assisted Synthesis and Phase Transfer of Ultrafine Gold Nanoclusters. *J. Colloid Interface Sci.* **2011**, *361*, 59–63.

(89) Pellegrino, T.; Sperling, R. A.; Alivisatos, A. P.; Parak, W. J. Gel Electrophoresis of Gold-DNA Nanoconjugates. *J. Biomed. Biotechnol.* **2007**, *2007*, 26796.

(90) Schmid, G.; Lehnert, A. The Complexation of Gold Colloids. *Angew. Chem., Int. Ed. Engl.* **1989**, *28*, 780–781.

(91) Hühner, J.; Carrillo-Carrion, C.; Soliman, M. G.; Pfeiffer, C.; Valdeperez, D.; Masood, A.; Chakraborty, I.; Zhu, L.; Gallego, M.; et al. Selected Standard Protocols for the Synthesis, Phase Transfer, and Characterization of Inorganic Colloidal Nanoparticles. *Chem. Mater.* **2017**, *29*, 399–461.

(92) Ahmadi, T. S.; Wang, Z. L.; Henglein, A.; El-Sayed, M. A. "Cubic" Colloidal Platinum Nanoparticles. *Chem. Mater.* **1996**, *8*, 1161.

(93) Ahmadi, T. S.; Wang, Z. L.; Green, T. C.; Henglein, A.; ElSayed, M. A. Shape-Controlled Synthesis of Colloidal Platinum Nanoparticles. *Science* **1996**, *272*, 1924–1926.

(94) Ram, S.; Fecht, H. J. Modulating up-Energy Transfer and Violet-Blue Light Emission in Gold Nanoparticles with Surface Adsorption of Poly(Vinyl Pyrrolidone) Molecules. *J. Phys. Chem. C* **2011**, *115*, 7817–7828.

(95) Xiong, Y.; Chen, J.; Wiley, B.; Xia, Y.; Aloni, S.; Yin, Y. Understanding the Role of Oxidative Etching in the Polyol Synthesis of Pd Nanoparticles with Uniform Shape and Size. *J. Am. Chem. Soc.* **2005**, *127*, 7332–7333.

(96) Koczur, K. M.; Mourdikoudis, S.; Polavarapu, L.; Skrabalak, S. E. Polyvinylpyrrolidone (PVP) in Nanoparticle Synthesis. *Dalton Trans* **2015**, *44*, 17883–17905.

(97) Khanna, P. K.; Gaikwad, S.; Adhyapak, P. V.; Singh, N.; Marimuthu, R. Synthesis and Characterization of Copper Nanoparticles. *Mater. Lett.* **2007**, *61*, 4711–4714.

(98) Dang, T. M. D.; Le, T. T. T.; Fribourg-Blanc, E.; Dang, M. C. Synthesis and Optical Properties of Copper Nanoparticles Prepared by a Chemical Reduction Method. *Adv. Nat. Sci.: Nanosci. Nanotechnol.* **2011**, *2*, 015009.

(99) Hussain, I.; Graham, S.; Wang, Z. X.; Tan, B.; Sherrington, D. C.; Rannard, S. P.; Cooper, A. I.; Brust, M. Size-Controlled Synthesis of near-Monodisperse Gold Nanoparticles in the 1–4 nm Range Using Polymeric Stabilizers. *J. Am. Chem. Soc.* **2005**, *127*, 16398–16399.

(100) Sun, X. P.; Dong, S. J.; Wang, E. K. One-Step Synthesis and Characterization of Polyelectrolyte-Protected Gold Nanoparticles through a Thermal Process. *Polymer* **2004**, *45*, 2181–2184.

(101) Newman, J. D. S.; Blanchard, G. J. Formation and Encapsulation of Gold Nanoparticles Using a Polymeric Amine Reducing Agent. *J. Nanopart. Res.* **2007**, *9*, 861–868.

(102) Wang, Z. X.; Tan, B. E.; Hussain, I.; Schaeffer, N.; Wyatt, M. F.; Brust, M.; Cooper, A. I. Design of Polymeric Stabilizers for Size-Controlled Synthesis of Monodisperse Gold Nanoparticles in Water. *Langmuir* **2007**, *23*, 885–895.

(103) Piao, Y. Z.; Jang, Y. J.; Shokouhimehr, M.; Lee, I. S.; Hyeon, T. Facile Aqueous-Phase Synthesis of Uniform Palladium Nanoparticles of Various Shapes and Sizes. *Small* **2007**, *3*, 255–260.

(104) Wang, L.; Yamauchi, Y. Autoprogrammed Synthesis of Triple-Layered Au@Pd@Pt Core–Shell Nanoparticles Consisting of a Au@Pd Bimetallic Core and Nanoporous Pt Shell. *J. Am. Chem. Soc.* **2010**, *132*, 13636–13638.

(105) Choueiri, R. M.; Galati, E.; Thérien-Aubin, H.; Klinkova, A.; Larin, E. M.; Querejeta-Fernández, A.; Han, L.; Xin, H. L.; Gang, O.; et al. Surface Patterning of Nanoparticles with Polymer Patches. *Nature* **2016**, *538*, 79.

(106) Wang, Z.; He, B.; Xu, G.; Wang, G.; Wang, J.; Feng, Y.; Su, D.; Chen, B.; Li, H.; Wu, Z.; Zhang, H.; Shao, L.; Chen, H. Transformable Masks for Colloidal Nanosynthesis. *Nat. Commun.* **2018**, *9*, 563.

- (107) Chen, G.; Gibson, K. J.; Liu, D.; Rees, H. C.; Lee, J.-H.; Xia, W.; Lin, R.; Xin, H. L.; Gang, O.; Weizmann, Y. Regioselective Surface Encoding of Nanoparticles for Programmable Self-Assembly. *Nat. Mater.* **2019**, *18*, 169–174.
- (108) Brinas, R. P.; Hu, M. H.; Qian, L. P.; Lyman, E. S.; Hainfeld, J. F. Gold Nanoparticle Size Controlled by Polymeric Au(I) Thiolate Precursor Size. *J. Am. Chem. Soc.* **2008**, *130*, 975–982.
- (109) Plascencia-Villa, G.; Torrente, D.; Marucho, M.; Jose-Yacamán, M. Biodirected Synthesis and Nanostructural Characterization of Anisotropic Gold Nanoparticles. *Langmuir* **2015**, *31*, 3527–3536.
- (110) Goia, D. V.; Matijević, E. Tailoring the Particle Size of Monodispersed Colloidal Gold. *Colloids Surf., A* **1999**, *146*, 139–152.
- (111) Chakraborty, I.; Feliu, N.; Roy, S.; Dawson, K.; Parak, W. J. Protein-Mediated Shape Control of Silver Nanoparticles. *Bioconjugate Chem.* **2018**, *29*, 1261–1265.
- (112) Dahl, J. A.; Maddux, B. L. S.; Hutchison, J. E. Toward Greener Nanosynthesis. *Chem. Rev.* **2007**, *107*, 2228–2269.
- (113) Shankar, S. S.; Rai, A.; Ankamwar, B.; Singh, A.; Ahmad, A.; Sastry, M. Biological Synthesis of Triangular Gold Nanoprisms. *Nat. Mater.* **2004**, *3*, 482–488.
- (114) Raveendran, P.; Fu, J.; Wallen, S. L. Completely “Green” Synthesis and Stabilization of Metal Nanoparticles. *J. Am. Chem. Soc.* **2003**, *125*, 13940–13941.
- (115) Panáček, A.; Kvítek, L.; Prucek, R.; Kolář, M.; Večeřová, R.; Pizúrová, N.; Sharma, V. K.; Nevěčná, T. J.; Zbořil, R. Silver Colloid Nanoparticles: Synthesis, Characterization, and Their Antibacterial Activity. *J. Phys. Chem. B* **2006**, *110*, 16248–16253.
- (116) He, Y.; Cui, H. Synthesis of Highly Chemiluminescent Graphene Oxide/Silver Nanoparticle Nano-Composites and Their Analytical Applications. *J. Mater. Chem.* **2012**, *22*, 9086–9091.
- (117) Njagi, E. C.; Huang, H.; Stafford, L.; Genuino, H.; Galindo, H. M.; Collins, J. B.; Hoag, G. E.; Suib, S. L. Biosynthesis of Iron and Silver Nanoparticles at Room Temperature Using Aqueous Sorghum Bran Extracts. *Langmuir* **2011**, *27*, 264–271.
- (118) Lu, X.; Rycenga, M.; Skrabalak, S. E.; Wiley, B.; Xia, Y. Chemical Synthesis of Novel Plasmonic Nanoparticles. *Annu. Rev. Phys. Chem.* **2009**, *60*, 167–192.
- (119) Daniel, M.-C.; Astruc, D. Gold Nanoparticles: Assembly, Supramolecular Chemistry, Quantum-Size-Related Properties, and Applications toward Biology, Catalysis, and Nanotechnology. *Chem. Rev.* **2004**, *104*, 293–346.
- (120) Brown, K. R.; Natan, M. J. Hydroxylamine Seeding of Colloidal Au Nanoparticles in Solution and on Surfaces. *Langmuir* **1998**, *14*, 726–728.
- (121) Sivaraman, S. K.; Kumar, S.; Santhanam, V. Room-Temperature Synthesis of Gold Nanoparticles—Size-Control by Slow Addition. *Gold Bulletin* **2010**, *43*, 275–286.
- (122) Rioux, D.; Meunier, M. Seeded Growth Synthesis of Composition and Size-Controlled Gold–Silver Alloy Nanoparticles. *J. Phys. Chem. C* **2015**, *119*, 13160–13168.
- (123) Jana, N. R.; Gearheart, L.; Murphy, C. J. Evidence for Seed-Mediated Nucleation in the Chemical Reduction of Gold Salts to Gold Nanoparticles. *Chem. Mater.* **2001**, *13*, 2313–2322.
- (124) Mafuné, F.; Kohno, J.-y.; Takeda, Y.; Kondow, T.; Sawabe, H. Formation of Gold Nanoparticles by Laser Ablation in Aqueous Solution of Surfactant. *J. Phys. Chem. B* **2001**, *105*, S114–S120.
- (125) Sau, T. K.; Murphy, C. J. Seeded High Yield Synthesis of Short Au Nanorods in Aqueous Solution. *Langmuir* **2004**, *20*, 6414–6420.
- (126) Takenaka, Y.; Kitahata, H.; Yamada, N. L.; Seto, H.; Hara, M. Growth of Gold Nanorods in Gelled Surfactant Solutions. *J. Colloid Interface Sci.* **2011**, *356*, 111–117.
- (127) Zheng, M.; Davidson, F.; Huang, X. Y. Ethylene Glycol Monolayer Protected Nanoparticles for Eliminating Nonspecific Binding with Biological Molecules. *J. Am. Chem. Soc.* **2003**, *125*, 7790–7791.
- (128) Kim, R.; Park, H. S.; Yu, T.; Yi, J.; Kim, W.-S. Aqueous Synthesis and Stabilization of Highly Concentrated Gold Nanoparticles Using Sterically Hindered Functional Polymer. *Chem. Phys. Lett.* **2013**, *575*, 71–75.
- (129) Wang, Y.; Asefa, T. Poly(Allylamine)-Stabilized Colloidal Copper Nanoparticles: Synthesis, Morphology, and Their Surface-Enhanced Raman Scattering Properties. *Langmuir* **2010**, *26*, 7469–7474.
- (130) Filali, M.; Meier, M. A.; Schubert, U. S.; Gohy, J.-F. Star-Block Copolymers as Templates for the Preparation of Stable Gold Nanoparticles. *Langmuir* **2005**, *21*, 7995–8000.
- (131) Yamamoto, M.; Kashiwagi, Y.; Sakata, T.; Mori, H.; Nakamoto, M. Synthesis and Morphology of Star-Shaped Gold Nanoplates Protected by Poly (N-Vinyl-2-Pyrrolidone). *Chem. Mater.* **2005**, *17*, 5391–5393.
- (132) Lim, B.; Jiang, M. J.; Camargo, P. H. C.; Cho, E. C.; Tao, J.; Lu, X. M.; Zhu, Y. M.; Xia, Y. N. Pd-Pt Bimetallic Nanodendrites with High Activity for Oxygen Reduction. *Science* **2009**, *324*, 1302–1305.
- (133) Yuan, J.-J.; Schmid, A.; Armes, S. P.; Lewis, A. L. Facile Synthesis of Highly Biocompatible Poly (2-(Methacryloyloxy) Ethyl Phosphorylcholine)-Coated Gold Nanoparticles in Aqueous Solution. *Langmuir* **2006**, *22*, 11022–11027.
- (134) Leopold, N.; Chiş, V.; Mircescu, N. E.; Marişca, O. T.; Buja, O. M.; Leopold, L. F.; Socaci, C.; Braicu, C.; Irimie, A.; Berindan-Neagoe, I. One Step Synthesis of Sers Active Colloidal Gold Nanoparticles by Reduction with Polyethylene Glycol. *Colloids Surf., A* **2013**, *436*, 133–138.
- (135) Oh, E.; Delehanty, J. B.; Field, L. D.; Mäkinen, A. J.; Goswami, R.; Huston, A. L.; Medintz, I. L. Synthesis and Characterization of Pegylated Luminescent Gold Nanoclusters Doped with Silver and Other Metals. *Chem. Mater.* **2016**, *28*, 8676–8688.
- (136) Tejamaya, M.; Römer, I.; Merrifield, R. C.; Lead, J. R. Stability of Citrate, Pvp, and Peg Coated Silver Nanoparticles in Ecotoxicology Media. *Environ. Sci. Technol.* **2012**, *46*, 7011–7017.
- (137) Baker, C. O.; Shedd, B.; Tseng, R. J.; Martinez-Morales, A. A.; Ozkan, C. S.; Ozkan, M.; Yang, Y.; Kaner, R. B. Size Control of Gold Nanoparticles Grown on Polyaniline Nanofibers for Bistable Memory Devices. *ACS Nano* **2011**, *5*, 3469–3474.
- (138) Huang, H.; Yang, X. Synthesis of Chitosan-Stabilized Gold Nanoparticles in the Absence/Presence of Tripolyphosphate. *Biomacromolecules* **2004**, *5*, 2340–2346.
- (139) Selvakkannan, P.; Mandal, S.; Phadtare, S.; Pasricha, R.; Sastry, M. Capping of Gold Nanoparticles by the Amino Acid Lysine Renders Them Water-Dispersible. *Langmuir* **2003**, *19*, 3545–3549.
- (140) Bhattacharya, R.; Patra, C. R.; Wang, S. F.; Lu, L. C.; Yaszemski, M. J.; Mukhopadhyay, D.; Mukherjee, P. Assembly of Gold Nanoparticles in a Rod-Like Fashion Using Proteins as Templates. *Adv. Funct. Mater.* **2006**, *16*, 395–400.
- (141) Jolivet, J. P.; Chaneac, C.; Tronc, E. Iron Oxide Chemistry. From Molecular Clusters to Extended Solid Networks. *Chem. Commun.* **2004**, 481–483.
- (142) Lee, J.; Isobe, T.; Senna, M. Preparation of Ultrafine Fe₃O₄ Particles by Precipitation in the Presence of Pva at High Ph. *J. Colloid Interface Sci.* **1996**, *177*, 490–494.
- (143) Bee, A.; Massart, R.; Neveu, S. Synthesis of Very Fine Maghemite Particles. *J. Magn. Magn. Mater.* **1995**, *149*, 6–9.
- (144) Sahoo, Y.; Goodarzi, A.; Swihart, M. T.; Ohulchanskyy, T. Y.; Kaur, N.; Furlani, E. P.; Prasad, P. N. Aqueous Ferrofluid of Magnetite Nanoparticles: Fluorescence Labeling and Magnetophoretic Control. *J. Phys. Chem. B* **2005**, *109*, 3879–3885.
- (145) Wagner, S.; Schnorr, J.; Pilgrimm, H.; Hamm, B.; Taupitz, M. Monomer-Coated Very Small Superparamagnetic Iron Oxide Particles as Contrast Medium for Magnetic Resonance Imaging - Preclinical in Vivo Characterization. *Invest. Radiol.* **2002**, *37*, 167–177.
- (146) Lu, Q. H.; Yao, K. L.; Xi, D.; Liu, Z. L.; Luo, X. P.; Ning, Q. Synthesis and Characterization of Composite Nanoparticles Comprised of Gold Shell and Magnetic Core/Cores. *J. Magn. Magn. Mater.* **2006**, *301*, 44–49.
- (147) Behdadfar, B.; Kermanpur, A.; Sadeghi-Aliabadi, H.; Morales, M. D.; Mozaffari, M. Synthesis of Aqueous Ferrofluids of Zn_{0.9}Fe_{0.1}O₄ Nanoparticles by Citric Acid Assisted Hydrothermal-Reduction Route

for Magnetic Hyperthermia Applications. *J. Magn. Magn. Mater.* **2012**, *324*, 2211–2217.

(148) Behdadfar, B.; Kermanpur, A.; Sadeghi-Aliabadi, H.; Morales, M. D.; Mozaffari, M. Synthesis of High Intrinsic Loss Power Aqueous Ferrofluids of Iron Oxide Nanoparticles by Citric Acid-Assisted Hydrothermal-Reduction Route. *J. Solid State Chem.* **2012**, *187*, 20–26.

(149) Yang, K. M.; Cho, H.-I.; Choi, H. J.; Piao, Y. Synthesis of Water Well-Dispersed Pegylated Iron Oxide Nanoparticles for Mr/Optical Lymph Node Imaging. *J. Mater. Chem. B* **2014**, *2*, 3355–3364.

(150) Cabuil, V.; Dupuis, V.; Talbot, D.; Neveu, S. Ionic Magnetic Fluid Based on Cobalt Ferrite Nanoparticles: Influence of Hydrothermal Treatment on the Nanoparticle Size. *J. Magn. Magn. Mater.* **2011**, *323*, 1238–1241.

(151) Chen, D. H.; Wu, S. H. Synthesis of Nickel Nanoparticles in Water-in-Oil Microemulsions. *Chem. Mater.* **2000**, *12*, 1354–1360.

(152) Chin, A. B.; Yaacob, I. I. Synthesis and Characterization of Magnetic Iron Oxide Nanoparticles Via W/O Microemulsion and Massart's Procedure. *J. Mater. Process. Technol.* **2007**, *191*, 235–237.

(153) Sun, X. H.; Zheng, C. M.; Zhang, F. X.; Yang, Y. L.; Wu, G. J.; Yu, A. M.; Guan, N. J. Size-Controlled Synthesis of Magnetite (Fe₃O₄) Nanoparticles Coated with Glucose and Gluconic Acid from a Single Fe(III) Precursor by a Sucrose Bifunctional Hydrothermal Method. *J. Phys. Chem. C* **2009**, *113*, 16002–16008.

(154) Mahdavi, M.; Namvar, F.; Bin Ahmad, M.; Mohamad, R. Green Biosynthesis and Characterization of Magnetic Iron Oxide (Fe₃O₄) Nanoparticles Using Seaweed (Sargassum Muticum) Aqueous Extract. *Molecules* **2013**, *18*, 5954–5964.

(155) Wu, S. H.; Chen, D. H. Synthesis and Characterization of Nickel Nanoparticles by Hydrazine Reduction in Ethylene Glycol. *J. Colloid Interface Sci.* **2003**, *259*, 282–286.

(156) Li, Z.; Chen, H.; Bao, H. B.; Gao, M. Y. One-Pot Reaction to Synthesize Water-Soluble Magnetite Nanocrystals. *Chem. Mater.* **2004**, *16*, 1391–1393.

(157) Henglein, A. Photochemistry of Colloidal Cadmium-Sulfide 0.2. Effects of Adsorbed Methyl Viologen and of Colloidal Platinum. *J. Phys. Chem.* **1982**, *86*, 2291–2293.

(158) Henglein, A. Small-Particle Research - Physicochemical Properties of Extremely Small Colloidal Metal and Semiconductor Particles. *Chem. Rev.* **1989**, *89*, 1861–1873.

(159) Lesnyak, V.; Gaponik, N.; Eychmuller, A. Colloidal Semiconductor Nanocrystals: The Aqueous Approach. *Chem. Soc. Rev.* **2013**, *42*, 2905–2929.

(160) Resch, U.; Weller, H.; Henglein, A. Photochemistry and Radiation-Chemistry of Colloidal Semiconductors 0.33. Chemical-Changes and Fluorescence in Cdte and Znte. *Langmuir* **1989**, *5*, 1015–1020.

(161) Rajh, T.; Micic, O. I.; Nozik, A. J. Synthesis and Characterization of Surface-Modified Colloidal Cdte Quantum Dots. *J. Phys. Chem.* **1993**, *97*, 11999–12003.

(162) Rogach, A. L.; Katsikas, L.; Kornowski, A.; Su, D. S.; Eychmuller, A.; Weller, H. Synthesis and Characterization of Thiol-Stabilized Cdte Nanocrystals. *Ber. Bunsen Phys. Chem.* **1996**, *100*, 1772–1778.

(163) Gao, M. Y.; Kirstein, S.; Mohwald, H.; Rogach, A. L.; Kornowski, A.; Eychmuller, A.; Weller, H. Strongly Photoluminescent Cdte Nanocrystals by Proper Surface Modification. *J. Phys. Chem. B* **1998**, *102*, 8360–8363.

(164) Rogach, A. L.; Franzl, T.; Klar, T. A.; Feldmann, J.; Gaponik, N.; Lesnyak, V.; Shavel, A.; Eychmuller, A.; Rakovich, Y. P.; Donegan, J. F. Aqueous Synthesis of Thiol-Capped Cdte Nanocrystals: State-of-the-Art. *J. Phys. Chem. C* **2007**, *111*, 14628.

(165) Zheng, Y. G.; Gao, S. J.; Ying, J. Y. Synthesis and Cell-Imaging Applications of Glutathione-Capped Cdte Quantum Dots. *Adv. Mater.* **2007**, *19*, 376–380.

(166) Zhou, D.; Lin, M.; Chen, Z. L.; Sun, H. Z.; Zhang, H.; Sun, H. C.; Yang, B. Simple Synthesis of Highly Luminescent Water-Soluble Cdte Quantum Dots with Controllable Surface Functionality. *Chem. Mater.* **2011**, *23*, 4857–4862.

(167) Dubavik, A.; Lesnyak, V.; Thiessen, W.; Gaponik, N.; Wolff, T.; Eychmuller, A. Synthesis of Amphiphilic Cdte Nanocrystals. *J. Phys. Chem. C* **2009**, *113*, 4748–4750.

(168) Ning, Y.; Zhang, H.; Han, J. S.; Yang, C. H.; Liu, Y.; Zhou, D.; Yang, B. Versatile Fabrication of Water-Dispersible Nanoparticle-Amphiphilic Copolymer Composite Microspheres with Specific Functionalities. *J. Mater. Chem.* **2011**, *21*, 6837–6843.

(169) Yang, P.; Yuan, Z. M.; Yang, J.; Zhang, A. Y.; Cao, Y. Q.; Jiang, Q. H.; Shi, R. X.; Liu, F. T.; Cheng, X. Science as Art: Self-Assembly of Hybrid SiO₂-Coated Nanocrystals. *CrystEngComm* **2011**, *13*, 1814–1820.

(170) Shavel, A.; Gaponik, N.; Eychmuller, A. Efficient Uv-Blue Photoluminescing Thiol-Stabilized Water-Soluble Alloyed Znse(S) Nanocrystals. *J. Phys. Chem. B* **2004**, *108*, 5905–5908.

(171) Zheng, Y. G.; Yang, Z. C.; Ying, J. Y. Aqueous Synthesis of Glutathione-Capped Znse and Zn1-Xcdxse Alloyed Quantum Dots. *Adv. Mater.* **2007**, *19*, 1475.

(172) Zheng, J.; Zhang, C. W.; Dickson, R. M. Highly Fluorescent, Water-Soluble, Size-Tunable Gold Quantum Dots. *Phys. Rev. Lett.* **2004**, *93*, 077402.

(173) Tanaka, S. I.; Miyazaki, J.; Tiwari, D. K.; Jin, T.; Inouye, Y. Fluorescent Platinum Nanoclusters: Synthesis, Purification, Characterization, and Application to Bioimaging. *Angew. Chem., Int. Ed.* **2011**, *50*, 431–435.

(174) Schaeffer, N.; Tan, B.; Dickinson, C.; Rosseinsky, M. J.; Laromaine, A.; McComb, D. W.; Stevens, M. M.; Wang, Y. Q.; Petit, L.; Barentin, C.; Spiller, D. G.; Cooper, A. I.; Lévy, R. Fluorescent or Not? Size-Dependent Fluorescence Switching for Polymer-Stabilized Gold Clusters in the 1.1–1.7 nm Size Range. *Chem. Commun.* **2008**, 3986–3988.

(175) Shang, L.; Azadfar, N.; Stockmar, F.; Send, W.; Trouillet, V.; Bruns, M.; Gerthsen, D.; Nienhaus, G. U. One-Pot Synthesis of near-Infrared Fluorescent Gold Clusters for Cellular Fluorescence Lifetime Imaging. *Small* **2011**, *7*, 2614–2620.

(176) Lin, C.-A. J.; Yang, T.-Y.; Lee, C.-H.; Huang, S. H.; Sperling, R. A.; Zanella, M.; Li, J. K.; Shen, J.-L.; Wang, H.-H.; et al. Synthesis, Characterization, and Bioconjugation of Fluorescent Gold Nanoclusters toward Biological Labeling Applications. *ACS Nano* **2009**, *3*, 395–401.

(177) Huang, S.; Pfeiffer, C.; Hollmann, J.; Friede, S.; Chen, J. J.-C.; Beyer, A.; Volz, K.; Heimbrodt, W.; Montenegro Martos, J. M.; et al. Synthesis and Characterization of Colloidal Fluorescent Silver Nanoclusters. *Langmuir* **2012**, *28*, 8915–8919.

(178) Oh, E.; Fatemi, F. K.; Currie, M.; Delehanty, J. B.; Pons, T.; Fragola, A.; Leveque-Fort, S.; Goswami, R.; Susumu, K.; et al. Pegylated Luminescent Gold Nanoclusters: Synthesis, Characterization, Bioconjugation, and Application to One- and Two-Photon Cellular Imaging. *Part. Part. Syst. Char.* **2013**, *30*, 453–466.

(179) Xie, J. P.; Zheng, Y. G.; Ying, J. Y. Protein-Directed Synthesis of Highly Fluorescent Gold Nanoclusters. *J. Am. Chem. Soc.* **2009**, *131*, 888.

(180) Link, S.; Beeby, A.; FitzGerald, S.; El-Sayed, M. A.; Schaaff, T. G.; Whetten, R. L. Visible to Infrared Luminescence from a 28-Atom Gold Cluster. *J. Phys. Chem. B* **2002**, *106*, 3410–3415.

(181) Le Guevel, X.; Trouillet, V.; Spies, C.; Jung, G.; Schneider, M. Synthesis of Yellow-Emitting Platinum Nanoclusters by Ligand Etching. *J. Phys. Chem. C* **2012**, *116*, 6047–6051.

(182) Patel, S. A.; Richards, C. I.; Hsiang, J. C.; Dickson, R. M. Water-Soluble Ag Nanoclusters Exhibit Strong Two-Photon-Induced Fluorescence. *J. Am. Chem. Soc.* **2008**, *130*, 11602.

(183) Sharma, J.; Yeh, H. C.; Yoo, H.; Werner, J. H.; Martinez, J. S. A Complementary Palette of Fluorescent Silver Nanoclusters. *Chem. Commun.* **2010**, *46*, 3280–3282.

(184) Yin, Y.; Alivisatos, A. P. Colloidal Nanocrystal Synthesis and the Organic-Inorganic Interface. *Nature* **2005**, *437*, 664–670.

(185) Stoeva, S.; Klabunde, K. J.; Sorensen, C. M.; Dragieva, I. Gram-Scale Synthesis of Monodisperse Gold Colloids by the Solvated Metal Atom Dispersion Method and Digestive Ripening and Their

Organization into Two- and Three-Dimensional Structures. *J. Am. Chem. Soc.* **2002**, *124*, 2305–2311.

(186) Vijaya Sarathy, K.; Kulkarni, G. U.; Rao, C. N. R. A Novel Method of Preparing Thiol-Derivatized Nanoparticles of Gold, Platinum and Silver Forming Superstructures. *Chem. Commun.* **1997**, 537–538.

(187) Leff, D. V.; Brandt, L.; Heath, J. R. Synthesis and Characterization of Hydrophobic, Organically-Soluble Gold Nanocrystals Functionalized with Primary Amines. *Langmuir* **1996**, *12*, 4723–4730.

(188) Han, M. Y.; Quek, C. H.; Huang, W.; Chew, C. H.; Gan, L. M. A Simple and Effective Chemical Route for the Preparation of Uniform Nonaqueous Gold Colloids. *Chem. Mater.* **1999**, *11*, 1144–1147.

(189) Green, M.; O'Brien, P. A Simple One Phase Preparation of Organically Capped Gold Nanocrystals. *Chem. Commun.* **2000**, 183–184.

(190) Green, M.; Allsop, N.; Wakefield, G.; Dobson, P. J.; Hutchison, J. L. Trialkylphosphine Oxide/Amine Stabilised Silver Nanocrystals - the Importance of Steric Factors and Lewis Basicity in Capping Agents. *J. Mater. Chem.* **2002**, *12*, 2671–2674.

(191) Jana, N. R.; Peng, X. G. Single-Phase and Gram-Scale Routes toward Nearly Monodisperse Au and Other Noble Metal Nanocrystals. *J. Am. Chem. Soc.* **2003**, *125*, 14280–14281.

(192) Tang, Y.; Ouyang, M. Tailoring Properties and Functionalities of Metal Nanoparticles through Crystallinity Engineering. *Nat. Mater.* **2007**, *6*, 754–759.

(193) Yamamoto, M.; Nakamoto, M. Novel Preparation of Monodispersed Silver Nanoparticles Via Amine Adducts Derived from Insoluble Silver Myristate in Tertiary Alkylamine. *J. Mater. Chem.* **2003**, *13*, 2064–2065.

(194) Sun, Y. G.; Xia, Y. N. Shape-Controlled Synthesis of Gold and Silver Nanoparticles. *Science* **2002**, *298*, 2176–2179.

(195) Tao, A.; Sinsermsuksakul, P.; Yang, P. D. Polyhedral Silver Nanocrystals with Distinct Scattering Signatures. *Angew. Chem., Int. Ed.* **2006**, *45*, 4597–4601.

(196) Niezgoda, J. S.; Harrison, M. A.; McBride, J. R.; Rosenthal, S. J. Novel Synthesis of Chalcopyrite CuxIn₂S₂ Quantum Dots with Tunable Localized Surface Plasmon Resonances. *Chem. Mater.* **2012**, *24*, 3294–3297.

(197) Deka, S.; Genovese, A.; Zhang, Y.; Misztal, K.; Bertoni, G.; Krahne, R.; Giannini, C.; Manna, L. Phosphine-Free Synthesis of P-Type Copper(I) Selenide Nanocrystals in Hot Coordinating Solvents. *J. Am. Chem. Soc.* **2010**, *132*, 8912.

(198) Luther, J. M.; Jain, P. K.; Ewers, T.; Alivisatos, A. P. Localized Surface Plasmon Resonances Arising from Free Carriers in Doped Quantum Dots. *Nat. Mater.* **2011**, *10*, 361–366.

(199) Liu, X.; Wang, X. L.; Zhou, B.; Law, W. C.; Cartwright, A. N.; Swihart, M. T. Size-Controlled Synthesis of Cu₂Xe (E = S, Se) Nanocrystals with Strong Tunable near-Infrared Localized Surface Plasmon Resonance and High Conductivity in Thin Films. *Adv. Funct. Mater.* **2013**, *23*, 1256–1264.

(200) Li, W. H.; Zamani, R.; Rivera Gil, P.; Pelaz, B.; Ibanez, M.; Cadavid, D.; Shavel, A.; Alvarez-Puebla, R. A.; Parak, W. J.; Arbiol, J.; Cabot, A. Cute Nanocrystals: Shape and Size Control, Plasmonic Properties, and Use as Sensing Probes and Photothermal Agents. *J. Am. Chem. Soc.* **2013**, *135*, 7098–7101.

(201) Sun, S. H.; Murray, C. B. Synthesis of Monodisperse Cobalt Nanocrystals and Their Assembly into Magnetic Superlattices (Invited). *J. Appl. Phys.* **1999**, *85*, 4325–4330.

(202) Dinega, D. P.; Bawendi, M. G. A Solution-Phase Chemical Approach to a New Crystal Structure of Cobalt. *Angew. Chem., Int. Ed.* **1999**, *38*, 1788–1791.

(203) Puentes, V. F.; Krishnan, K. M.; Alivisatos, A. P. Colloidal Nanocrystal Shape and Size Control: The Case of Cobalt. *Science* **2001**, *291*, 2115–2117.

(204) Puentes, V. F.; Zanchet, D.; Erdonmez, C. K.; Alivisatos, A. P. Synthesis of Hcp-Co Nanodisks. *J. Am. Chem. Soc.* **2002**, *124*, 12874–12880.

(205) Dumestre, F.; Chaudret, B.; Amiens, C.; Fromen, M. C.; Casanove, M. J.; Renaud, P.; Zurcher, P. Shape Control of Thermodynamically Stable Cobalt Nanorods through Organometallic Chemistry. *Angew. Chem., Int. Ed.* **2002**, *41*, 4286–4289.

(206) Dumestre, F.; Chaudret, B.; Amiens, C.; Respaud, M.; Fejes, P.; Renaud, P.; Zurcher, P. Unprecedented Crystalline Super-Lattices of Monodisperse Cobalt Nanorods. *Angew. Chem., Int. Ed.* **2003**, *42*, 5213–5216.

(207) Hyeon, T.; Lee, S. S.; Park, J.; Chung, Y.; Na, H. B. Synthesis of Highly Crystalline and Monodisperse Maghemite Nanocrystallites without a Size-Selection Process. *J. Am. Chem. Soc.* **2001**, *123*, 12798–12801.

(208) Corrias, A.; Mountjoy, G.; Loche, D.; Puentes, V.; Falqui, A.; Zanella, M.; Parak, W. J.; Casula, M. F. Identifying Spinel Phases in Nearly Monodisperse Iron Oxide Colloidal Nanocrystal. *J. Phys. Chem. C* **2009**, *113*, 18667–18675.

(209) Rockenberger, J.; Scher, E. C.; Alivisatos, A. P. A New Nonhydrolytic Single-Precursor Approach to Surfactant-Capped Nanocrystals of Transition Metal Oxides. *J. Am. Chem. Soc.* **1999**, *121*, 11595–11596.

(210) Sun, S. H.; Zeng, H. Size-Controlled Synthesis of Magnetite Nanoparticles. *J. Am. Chem. Soc.* **2002**, *124*, 8204–8205.

(211) Jana, N. R.; Chen, Y. F.; Peng, X. G. Size- and Shape-Controlled Magnetic (Cr, Mn, Fe, Co, Ni) Oxide Nanocrystals Via a Simple and General Approach. *Chem. Mater.* **2004**, *16*, 3931–3935.

(212) Park, J.; An, K. J.; Hwang, Y. S.; Park, J. G.; Noh, H. J.; Kim, J. Y.; Park, J. H.; Hwang, N. M.; Hyeon, T. Ultra-Large-Scale Syntheses of Monodisperse Nanocrystals. *Nat. Mater.* **2004**, *3*, 891–895.

(213) Fu, J. X.; He, L.; Xu, W. J.; Zhuang, J. L.; Yang, X. F.; Zhang, X. Z.; Wu, M. M.; Yin, Y. D. Formation of Colloidal Nanocrystal Clusters of Iron Oxide by Controlled Ligand Stripping. *Chem. Commun.* **2016**, *52*, 128–131.

(214) Kostopoulou, A.; Brintakis, K.; Fragogeorgi, E.; Anthousi, A.; Manna, L.; Begin-Colin, S.; Billotey, C.; Ranella, A.; Loudos, G.; Athanassakis, I.; Lappas, A. Iron Oxide Colloidal Nanoclusters as Theranostic Vehicles and Their Interactions at the Cellular Level. *Nanomaterials* **2018**, *8*, 315.

(215) Kostopoulou, A.; Lappas, A. Colloidal Magnetic Nanocrystal Clusters: Variable Length-Scale Interaction Mechanisms, Synergistic Functionalities and Technological Advantages. *Nanotechnol. Rev.* **2015**, *4*, 595–624.

(216) Zoppellaro, G.; Kolokithas-Ntoukas, A.; Polakova, K.; Tucek, J.; Zboril, R.; Loudos, G.; Fragogeorgi, E.; Diwocky, C.; Tomankova, K.; et al. Theranostics of Epitaxially Condensed Colloidal Nanocrystal Clusters, through a Soft Biomineralization Route. *Chem. Mater.* **2014**, *26*, 2062–2074.

(217) Xu, F.; Cheng, C.; Chen, D.-X.; Gu, H. Magnetite Nanocrystal Clusters with Ultra-High Sensitivity in Magnetic Resonance Imaging. *ChemPhysChem* **2012**, *13*, 336–341.

(218) Ge, J.; Hu, Y.; Yin, Y. Highly Tunable Superparamagnetic Colloidal Photonic Crystals. *Angew. Chem., Int. Ed.* **2007**, *46*, 7428–7431.

(219) Lartigue, L.; Hugounenq, P.; Alloyeau, D.; Clarke, S. P.; Lévy, M.; Bacri, J.-C.; Bazzi, R.; Brougham, D. F.; Wilhelm, C.; Gazeau, F. Cooperative Organization in Iron Oxide Multi-Core Nanoparticles Potentiates Their Efficiency as Heating Mediators and MRI Contrast Agents. *ACS Nano* **2012**, *6*, 10935–10949.

(220) Morgan, D. G.; Boris, B. S.; Kuchkina, N. V.; Yuzik-Klimova, E. Y.; Sorokina, S. A.; Stein, B. D.; Svergun, D. I.; Spilotros, A.; Kostopoulou, A.; et al. Multicore Iron Oxide Mesocrystals Stabilized by a Poly(Phenylene-pyridyl) Dendron and Dendrimer: Role of the Dendron/Dendrimer Self-Assembly. *Langmuir* **2014**, *30*, 8543–8550.

(221) Kuchkina, N. V.; Morgan, D. G.; Kostopoulou, A.; Lappas, A.; Brintakis, K.; Boris, B. S.; Yuzik-Klimova, E. Y.; Stein, B. D.; Svergun, D. I.; et al. Hydrophobic Periphery Tails of Polyphenylene-pyridyl Dendrons Control Nanoparticle Formation and Catalytic Properties. *Chem. Mater.* **2014**, *26*, 5654–5663.

- (222) Sun, S. H.; Murray, C. B.; Weller, D.; Folks, L.; Moser, A. Monodisperse Fept Nanoparticles and Ferromagnetic Fept Nanocrystal Superlattices. *Science* **2000**, *287*, 1989–1992.
- (223) Liu, C.; Wu, X. W.; Klemmer, T.; Shukla, N.; Yang, X. M.; Weller, D.; Roy, A. G.; Tanase, M.; Laughlin, D. Polyol Process Synthesis of Monodispersed Fept Nanoparticles. *J. Phys. Chem. B* **2004**, *108*, 6121–6123.
- (224) Elkins, K. E.; Vedantam, T. S.; Liu, J. P.; Zeng, H.; Sun, S. H.; Ding, Y.; Wang, Z. L. Ultrafine Fept Nanoparticles Prepared by the Chemical Reduction Method. *Nano Lett.* **2003**, *3*, 1647–1649.
- (225) Sun, S. H.; Anders, S.; Thomson, T.; Baglin, J. E. E.; Toney, M. F.; Hamann, H. F.; Murray, C. B.; Terris, B. D. Controlled Synthesis and Assembly of Fept Nanoparticles. *J. Phys. Chem. B* **2003**, *107*, 5419–5425.
- (226) Costanzo, S.; Simon, G.; Richardi, J.; Colomban, P.; Lisiecki, I. Solvent Effects on Cobalt Nanocrystal Synthesis—a Facile Strategy to Control the Size of Co Nanocrystals. *J. Phys. Chem. C* **2016**, *120*, 22054–22061.
- (227) Owen, J. S.; Park, J.; Trudeau, P.-E.; Alivisatos, A. P. Reaction Chemistry and Ligand Exchange at Cadmium–Selenide Nanocrystal Surfaces. *J. Am. Chem. Soc.* **2008**, *130*, 12279–12281.
- (228) Morris-Cohen, A. J.; Donakowski, M. D.; Knowles, K. E.; Weiss, E. A. The Effect of a Common Purification Procedure on the Chemical Composition of the Surfaces of Cdse Quantum Dots Synthesized with Trioctylphosphine Oxide. *J. Phys. Chem. C* **2010**, *114*, 897–906.
- (229) Anderson, N. C.; Hendricks, M. P.; Choi, J. J.; Owen, J. S. Ligand Exchange and the Stoichiometry of Metal Chalcogenide Nanocrystals: Spectroscopic Observation of Facile Metal-Carboxylate Displacement and Binding. *J. Am. Chem. Soc.* **2013**, *135*, 18536–18548.
- (230) Kudera, S.; Zanella, M.; Giannini, C.; Rizzo, A.; Li, Y.; Gigli, G.; Cingolani, R.; Ciccarella, G.; Spahl, W.; et al. Sequential Growth of Magic-Size Cdse Nanocrystals. *Adv. Mater.* **2007**, *19*, 548–552.
- (231) Rizzo, A.; Li, Y. Q.; Kudera, S.; Della Sala, F.; Zanella, M.; Parak, W. J.; Cingolani, R.; Manna, L.; Gigli, G. Blue Light Emitting Diodes Based on Fluorescent Cdse/Zns Nanocrystals. *Appl. Phys. Lett.* **2007**, *90*, 051106.
- (232) Owen, J. The Coordination Chemistry of Nanocrystal Surfaces. *Science* **2015**, *347*, 615–616.
- (233) Murray, C. B.; Norris, D. J.; Bawendi, M. G. Synthesis and Characterization of Nearly Monodisperse Cde (E = S, Se, Te) Semiconductor Nanocrystallites. *J. Am. Chem. Soc.* **1993**, *115*, 8706–8715.
- (234) Wang, F.; Tang, R.; Buhro, W. E. The Trouble with Topo; Identification of Adventitious Impurities Beneficial to the Growth of Cadmium Selenide Quantum Dots, Rods, and Wires. *Nano Lett.* **2008**, *8*, 3521–3524.
- (235) Peng, Z. A.; Peng, X. Formation of High-Quality Cdte, Cdse, and Cds Nanocrystals Using Cdo as Precursor. *J. Am. Chem. Soc.* **2001**, *123*, 183–184.
- (236) Peng, X. Green Chemical Approaches toward High-Quality Semiconductor Nanocrystals. *Chem. - Eur. J.* **2002**, *8*, 334–339.
- (237) Carbone, L.; Kudera, S.; Carlino, E.; Parak, W. J.; Giannini, C.; Cingolani, R.; Manna, L. Multiple Wurtzite Twinning in Cdte Nanocrystals Induced by Methylphosphonic Acid. *J. Am. Chem. Soc.* **2006**, *128*, 748–755.
- (238) Kopping, J. T.; Patten, T. E. Identification of Acidic Phosphorus-Containing Ligands Involved in the Surface Chemistry of Cdse Nanoparticles Prepared in Tri-N-Octylphosphine Oxide Solvents. *J. Am. Chem. Soc.* **2008**, *130*, 5689–5698.
- (239) Gomes, R.; Hassinen, A.; Szczygiel, A.; Zhao, Q.; Vantomme, A.; Martins, J. C.; Hens, Z. Binding of Phosphonic Acids to Cdse Quantum Dots: A Solution NMR Study. *J. Phys. Chem. Lett.* **2011**, *2*, 145–152.
- (240) Hassinen, A.; Gomes, R.; De Nolf, K.; Zhao, Q.; Vantomme, A.; Martins, J. C.; Hens, Z. Surface Chemistry of Cdte Quantum Dots Synthesized in Mixtures of Phosphonic Acids and Amines: Formation of a Mixed Ligand Shell. *J. Phys. Chem. C* **2013**, *117*, 13936–13943.
- (241) Yu, W. W.; Peng, X. Formation of High-Quality Cds and Other Ii-Vi Semiconductor Nanocrystals in Noncoordinating Solvents: Tunable Reactivity of Monomers. *Angew. Chem., Int. Ed.* **2002**, *41*, 2368–2371.
- (242) Bullen, C. R.; Mulvaney, P. Nucleation and Growth Kinetics of Cdse Nanocrystals in Octadecene. *Nano Lett.* **2004**, *4*, 2303–2307.
- (243) Van Embden, J.; Mulvaney, P. Nucleation and Growth of Cdse Nanocrystals in a Binary Ligand System. *Langmuir* **2005**, *21*, 10226–10233.
- (244) Li, L. S.; Pradhan, N.; Wang, Y.; Peng, X. High Quality Znse and Zns Nanocrystals Formed by Activating Zinc Carboxylate Precursors. *Nano Lett.* **2004**, *4*, 2261–2264.
- (245) Hines, M. A.; Guyot-Sionnest, P. Bright Uv-Blue Luminescent Colloidal Znse Nanocrystals. *J. Phys. Chem. B* **1998**, *102*, 3655–3657.
- (246) Reiss, P.; Quemard, G.; Carayon, S.; Bleuse, J.; Chandezon, F.; Pron, A. Luminescent Znse Nanocrystals of High Color Purity. *Mater. Chem. Phys.* **2004**, *84*, 10–13.
- (247) Moreels, I.; Justo, Y.; De Geyter, B.; Haustraete, K.; Martins, J. C.; Hens, Z. Size-Tunable, Bright, and Stable Pbs Quantum Dots: A Surface Chemistry Study. *ACS Nano* **2011**, *5*, 2004–2012.
- (248) Moreels, I.; Fritzinger, B.; Martins, J. C.; Hens, Z. Surface Chemistry of Colloidal Pbse Nanocrystals. *J. Am. Chem. Soc.* **2008**, *130*, 15081–15086.
- (249) Dierick, R.; Van den Broeck, F.; De Nolf, K.; Zhao, Q.; Vantomme, A.; Martins, J. C.; Hens, Z. Surface Chemistry of Cuins2 Colloidal Nanocrystals, Tight Binding of L-Type Ligands. *Chem. Mater.* **2014**, *26*, 5950–5957.
- (250) Wang, F.; Liu, X. Recent Advances in the Chemistry of Lanthanide-Doped Upconversion Nanocrystals. *Chem. Soc. Rev.* **2009**, *38*, 976–989.
- (251) Haase, M.; Schäfer, H. Upconverting Nanoparticles. *Angew. Chem., Int. Ed.* **2011**, *50*, 5808–5829.
- (252) Wang, M.; Abbineni, G.; Clevenger, A.; Mao, C.; Xu, S. Upconversion Nanoparticles: Synthesis, Surface Modification and Biological Applications. *Nanomedicine* **2011**, *7*, 710–729.
- (253) Chen, G.; Qiu, H.; Prasad, P. N.; Chen, X. Upconversion Nanoparticles: Design, Nanochemistry, and Applications in Theranostics. *Chem. Rev.* **2014**, *114*, 5161–5214.
- (254) Li, X.; Zhang, F.; Zhao, D. Lab on Upconversion Nanoparticles: Optical Properties and Applications Engineering Via Designed Nanostructure. *Chem. Soc. Rev.* **2015**, *44*, 1346–1378.
- (255) Wang, F.; Liu, X. Upconversion Multicolor Fine-Tuning: Visible to near-Infrared Emission from Lanthanide-Doped Nayf₄ Nanoparticles. *J. Am. Chem. Soc.* **2008**, *130*, 5642–5643.
- (256) Shan, J.; Ju, Y. A Single-Step Synthesis and the Kinetic Mechanism for Monodisperse and Hexagonal-Phase Nayf₄:Yb, Er Upconversion Nanophosphors. *Nanotechnology* **2009**, *20*, 275603.
- (257) Boyer, J.-C.; Vetrone, F.; Cuccia, L. A.; Capobianco, J. A. Synthesis of Colloidal Upconverting Nayf₄ Nanocrystals Doped with Er³⁺, Yb³⁺ and Tm³⁺, Yb³⁺ Via Thermal Decomposition of Lanthanide Trifluoroacetate Precursors. *J. Am. Chem. Soc.* **2006**, *128*, 7444–7445.
- (258) Mai, H.-X.; Zhang, Y.-W.; Si, R.; Yan, Z.-G.; Sun, L.-d.; You, L.-P.; Yan, C.-H. High-Quality Sodium Rare-Earth Fluoride Nanocrystals: Controlled Synthesis and Optical Properties. *J. Am. Chem. Soc.* **2006**, *128*, 6426–6436.
- (259) Boyer, J.-C.; Cuccia, L. A.; Capobianco, J. A. Synthesis of Colloidal Upconverting Nayf₄: Er³⁺/Yb³⁺ and Tm³⁺/Yb³⁺ Monodisperse Nanocrystals. *Nano Lett.* **2007**, *7*, 847–852.
- (260) Mai, H.-X.; Zhang, Y.-W.; Sun, L.-D.; Yan, C.-H. Size- and Phase-Controlled Synthesis of Monodisperse Nayf₄:Yb,Er Nanocrystals from a Unique Delayed Nucleation Pathway Monitored with Upconversion Spectroscopy. *J. Phys. Chem. C* **2007**, *111*, 13730–13739.
- (261) Ye, X.; Collins, J. E.; Kang, Y.; Chen, J.; Chen, D. T. N.; Yodh, A. G.; Murray, C. B. Morphologically Controlled Synthesis of Colloidal Upconversion Nanophosphors and Their Shape-Directed Self-Assembly. *Proc. Natl. Acad. Sci. U. S. A.* **2010**, *107*, 22430–22435.

- (262) Shan, J.; Qin, X.; Yao, N.; Ju, Y. Synthesis of Monodisperse Hexagonal $\text{NaYf}_4\text{:Yb, Ln}$ ($\text{Ln} = \text{Er, Ho and Tm}$) Upconversion Nanocrystals in Topo. *Nanotechnology* **2007**, *18*, 445607.
- (263) Li, Z.; Zhang, Y.; Jiang, S. Multicolor Core/Shell-Structured Upconversion Fluorescent Nanoparticles. *Adv. Mater.* **2008**, *20*, 4765–4769.
- (264) Wang, F.; Wang, J.; Liu, X. Direct Evidence of a Surface Quenching Effect on Size-Dependent Luminescence of Upconversion Nanoparticles. *Angew. Chem., Int. Ed.* **2010**, *49*, 7456–7460.
- (265) Wang, F.; Deng, R. R.; Liu, X. G. Preparation of Core-Shell NaGdF_4 Nanoparticles Doped with Luminescent Lanthanide Ions to Be Used as Upconversion-Based Probes. *Nat. Protoc.* **2014**, *9*, 1634–1644.
- (266) Chinnathambi, S.; Chen, S.; Ganesan, S.; Hanagata, N. Silicon Quantum Dots for Biological Applications. *Adv. Healthcare Mater.* **2014**, *3*, 10–29.
- (267) Dohnalová, K.; Gregorkiewicz, T.; Kůsová, K. Silicon Quantum Dots: Surface Matters. *J. Phys.: Condens. Matter* **2014**, *26*, 173201.
- (268) Cheng, X.; Lowe, S. B.; Reece, P. J.; Gooding, J. J. Colloidal Silicon Quantum Dots: From Preparation to the Modification of Self-Assembled Monolayers (Sams) for Bio-Applications. *Chem. Soc. Rev.* **2014**, *43*, 2680–2700.
- (269) Ghosh, B.; Shirahata, N. Colloidal Silicon Quantum Dots: Synthesis and Luminescence Tuning from the near-Uv to the near-IR Range. *Sci. Technol. Adv. Mater.* **2014**, *15*, 014207.
- (270) Yang, C.-S.; Bley, R. A.; Kaulzarich, S. M.; Lee, H. W. H.; Delgado, G. R. Synthesis of Alkyl-Terminated Silicon Nanoclusters by a Solution Route. *J. Am. Chem. Soc.* **1999**, *121*, 5191–5195.
- (271) Holmes, J. D.; Ziegler, K. J.; Doty, R. C.; Pell, L. E.; Johnston, K. P.; Korgel, B. A. Highly Luminescent Silicon Nanocrystals with Discrete Optical Transitions. *J. Am. Chem. Soc.* **2001**, *123*, 3743–3748.
- (272) Tilley, R. D.; Warner, J. H.; Yamamoto, K.; Matsui, I.; Fujimori, H. Micro-Emulsion Synthesis of Monodisperse Surface Stabilized Silicon Nanocrystals. *Chem. Commun.* **2005**, 1833–1835.
- (273) Hua, F.; Swihart, M. T.; Ruckenstein, E. Efficient Surface Grafting of Luminescent Silicon Quantum Dots by Photoinitiated Hydrosilylation. *Langmuir* **2005**, *21*, 6054–6062.
- (274) Cheng, X.; Gondosiswanto, R.; Ciampi, S.; Reece, P. J.; Gooding, J. J. One-Pot Synthesis of Colloidal Silicon Quantum Dots and Surface Functionalization Via Thiol–Ene Click Chemistry. *Chem. Commun.* **2012**, *48*, 11874–11876.
- (275) Fu, P.; Shan, Q.; Shang, Y.; Song, J.; Zeng, H.; Ning, Z.; Gong, J. Perovskite Nanocrystals: Synthesis, Properties and Applications. *Sci. Bull.* **2017**, *62*, 369–380.
- (276) Meyns, M.; Perálvarez, M.; Heuer-Jungemann, A.; Hertog, W.; Ibáñez, M.; Nafria, R.; Genç, A.; Arbiol, J.; Kovalenko, M. V.; et al. Polymer-Enhanced Stability of Inorganic Perovskite Nanocrystals and Their Application in Color Conversion Leds. *ACS Appl. Mater. Interfaces* **2016**, *8*, 19579–19586.
- (277) Schmidt, L. C.; Pertegás, A.; González-Carrero, S.; Malinkiewicz, O.; Agouram, S.; Mínguez Espallargas, G.; Bolink, H. J.; Galian, R. E.; Pérez-Prieto, J. Nontemplate Synthesis of $\text{CH}_3\text{NH}_3\text{PbBr}_3$ Perovskite Nanoparticles. *J. Am. Chem. Soc.* **2014**, *136*, 850–853.
- (278) Vybornyi, O.; Yakunin, S.; Kovalenko, M. V. Polar-Solvent-Free Colloidal Synthesis of Highly Luminescent Alkylammonium Lead Halide Perovskite Nanocrystals. *Nanoscale* **2016**, *8*, 6278–6283.
- (279) Shamsi, J.; Abdelhady, A. L.; Accornero, S.; Arciniegas, M.; Goldoni, L.; Kandada, A. R. S.; Petrozza, A.; Manna, L. N-Methylformamide as a Source of Methylammonium Ions in the Synthesis of Lead Halide Perovskite Nanocrystals and Bulk Crystals. *ACS Energy Lett.* **2016**, *1*, 1042–1048.
- (280) Protesescu, L.; Yakunin, S.; Bodnarchuk, M. I.; Krieg, F.; Caputo, R.; Hendon, C. H.; Yang, R. X.; Walsh, A.; Kovalenko, M. V. Nanocrystals of Cesium Lead Halide Perovskites (CsPbX_3 , $\text{X} = \text{Cl, Br, and I}$): Novel Optoelectronic Materials Showing Bright Emission with Wide Color Gamut. *Nano Lett.* **2015**, *15*, 3692–3696.
- (281) Luo, B. B.; Naghadeh, S. B.; Zhang, J. Z. Lead Halide Perovskite Nanocrystals: Stability, Surface Passivation, and Structural Control. *Chem. Nano. Mater.* **2017**, *3*, 456–465.
- (282) Huang, H.; Polavarapu, L.; Sichert, J. A.; Sussha, A. S.; Urban, A. S.; Rogach, A. L. Colloidal Lead Halide Perovskite Nanocrystals: Synthesis, Optical Properties and Applications. *NPG Asia Mater.* **2016**, *8*, e328.
- (283) Flamee, S.; Cirillo, M.; Abe, S.; De Nolf, K.; Gomes, R.; Aubert, T.; Hens, Z. Fast, High Yield, and High Solid Loading Synthesis of Metal Selenide Nanocrystals. *Chem. Mater.* **2013**, *25*, 2476–2483.
- (284) Li, L.; Pandey, A.; Werder, D. J.; Khanal, B. P.; Pietryga, J. M.; Klimov, V. I. Efficient Synthesis of Highly Luminescent Copper Indium Sulfide-Based Core/Shell Nanocrystals with Surprisingly Long-Lived Emission. *J. Am. Chem. Soc.* **2011**, *133*, 1176–1179.
- (285) Cao, Y.; Geng, W.; Shi, R.; Shang, L.; Waterhouse, G. I. N.; Liu, L.; Wu, L.-Z.; Tung, C.-H.; Yin, Y.; Zhang, T. Thiolate-Mediated Photoinduced Synthesis of Ultrafine Ag_2S Quantum Dots from Silver Nanoparticles. *Angew. Chem., Int. Ed.* **2016**, *55*, 14952–14957.
- (286) Wang, J.; Sun, S.; Peng, F.; Cao, L.; Sun, L. Efficient One-Pot Synthesis of Highly Photoluminescent Alkyl-Functionalised Silicon Nanocrystals. *Chem. Commun.* **2011**, *47*, 4941–4943.
- (287) Xie, R.; Zhong, X.; Basché, T. Synthesis, Characterization, and Spectroscopy of Type II Core/Shell Semiconductor Nanocrystals with ZnTe Cores. *Adv. Mater.* **2005**, *17*, 2741–2745.
- (288) Mekis, I.; Talapin, D. V.; Kornowski, A.; Haase, M.; Weller, H. One-Pot Synthesis of Highly Luminescent CdSe/Cds Core-Shell Nanocrystals Via Organometallic and “Greener” Chemical Approaches. *J. Phys. Chem. B* **2003**, *107*, 7454–7462.
- (289) Fisher, B. R.; Eisler, H.-J.; Stott, N. E.; Bawendi, M. G. Emission Intensity Dependence and Single-Exponential Behavior in Single Colloidal Quantum Dot Fluorescence Lifetimes. *J. Phys. Chem. B* **2004**, *108*, 143–148.
- (290) Zhang, J.; Sun, K.; Kumbhar, A.; Fang, J. Shape-Control of ZnTe Nanocrystal Growth in Organic Solution. *J. Phys. Chem. C* **2008**, *112*, 5454–5458.
- (291) Snee, P. T.; Chan, Y.; Nocera, D. G.; Bawendi, M. G. Whispering-Gallery-Mode Lasing from a Semiconductor Nanocrystal/Microsphere Resonator Composite. *Adv. Mater.* **2005**, *17*, 1131–1136.
- (292) Yang, Y. A.; Wu, H.; Williams, K. R.; Cao, Y. C. Synthesis of Cdse and Cdte Nanocrystals without Precursor Injection. *Angew. Chem., Int. Ed.* **2005**, *44*, 6712–6715.
- (293) Yu, W. W.; Wang, Y. A.; Peng, X. Formation and Stability of Size-, Shape-, and Structure-Controlled Cdte Nanocrystals: Ligand Effects on Monomers and Nanocrystals. *Chem. Mater.* **2003**, *15*, 4300–4308.
- (294) Xie, R.; Battaglia, D.; Peng, X. Colloidal Inp Nanocrystals as Efficient Emitters Covering Blue to near-Infrared. *J. Am. Chem. Soc.* **2007**, *129*, 15432–15433.
- (295) Xu, S.; Ziegler, J.; Nann, T. Rapid Synthesis of Highly Luminescent Inp and Inp/Zns Nanocrystals. *J. Mater. Chem.* **2008**, *18*, 2653–2656.
- (296) Song, W.-S.; Lee, H.-S.; Lee, J. C.; Jang, D. S.; Choi, Y.; Choi, M.; Yang, H. Amine-Derived Synthetic Approach to Color-Tunable Inp/Zns Quantum Dots with High Fluorescence Qualities. *J. Nanopart. Res.* **2013**, *15*, 1750.
- (297) Peng, X. G.; Wickham, J.; Alivisatos, A. P. Kinetics of II-VI and II-V Colloidal Semiconductor Nanocrystal Growth: “Focusing” of Size Distribution. *J. Am. Chem. Soc.* **1998**, *120*, 5343–5344.
- (298) Xie, R.; Peng, X. Synthetic Scheme for High-Quality Inas Nanocrystals Based on Self-Focusing and One-Pot Synthesis of Inas-Based Core-Shell Nanocrystals. *Angew. Chem., Int. Ed.* **2008**, *47*, 7677–7680.
- (299) Hines, M. A.; Scholes, G. D. Colloidal Pbs Nanocrystals with Size-Tunable near-Infrared Emission: Observation of Post-Synthesis Self-Narrowing of the Particle Size Distribution. *Adv. Mater.* **2003**, *15*, 1844–1849.

- (300) Cademartiri, L.; Bertolotti, J.; Sapienza, R.; Wiersma, D. S.; von Freymann, G.; Ozin, G. A. Multigram Scale, Solventless, and Diffusion-Controlled Route to Highly Monodisperse Pbs Nanocrystals. *J. Phys. Chem. B* **2006**, *110*, 671–673.
- (301) Abel, K. A.; Shan, J.; Boyer, J.-C.; Harris, F.; van Veggel, F. C. J. M. Highly Photoluminescent Pbs Nanocrystals: The Beneficial Effect of Trioctylphosphine. *Chem. Mater.* **2008**, *20*, 3794–3796.
- (302) Murray, C. B.; Sun, S.; Gaschler, W.; Doyle, H.; Betley, T. A.; Kagan, C. R. Colloidal Synthesis of Nanocrystals and Nanocrystal Superlattices. *IBM J. Res. Dev.* **2001**, *45*, 47–56.
- (303) Yu, W. W.; Falkner, J. C.; Shih, B. S.; Colvin, V. L. Preparation and Characterization of Monodisperse Pbse Semiconductor Nanocrystals in a Noncoordinating Solvent. *Chem. Mater.* **2004**, *16*, 3318–3322.
- (304) Nakamura, H.; Kato, W.; Uehara, M.; Nose, K.; Omata, T.; Otsuka-Yao-Matsuo, S.; Miyazaki, M.; Maeda, H. Tunable Photoluminescence Wavelength of Chalcopyrite Cuins₂-Based Semiconductor Nanocrystals Synthesized in a Colloidal System. *Chem. Mater.* **2006**, *18*, 3330–3335.
- (305) Panthani, M. G.; Akhavan, V.; Goodfellow, B.; Schmidtke, J. P.; Dunn, L.; Dodabalapur, A.; Barbara, P. F.; Korgel, B. A. Synthesis of Cuins₂, Cuinse₂, and Cu(In_{0.9}Ga_{0.1})Se₂ (Cigs) Nanocrystal “Inks” for Printable Photovoltaics. *J. Am. Chem. Soc.* **2008**, *130*, 16770–16777.
- (306) Zhong, H.; Zhou, Y.; Ye, M.; He, Y.; Ye, J.; He, C.; Yang, C.; Li, Y. Controlled Synthesis and Optical Properties of Colloidal Ternary Chalcogenide Cuins₂ Nanocrystals. *Chem. Mater.* **2008**, *20*, 6434–6443.
- (307) Li, L.; Daou, T. J.; Texier, I.; Chi, T. T. K.; Liem, N. Q.; Reiss, P. Highly Luminescent Cuins₂/Zns Core/Shell Nanocrystals: Cadmium-Free Quantum Dots for in Vivo Imaging. *Chem. Mater.* **2009**, *21*, 2422–2429.
- (308) Zhong, H.; Lo, S. S.; Mirkovic, T.; Li, Y.; Ding, Y.; Li, Y.; Scholes, G. D. Noninjection Gram-Scale Synthesis of Monodisperse Pyramidal Cuins₂ Nanocrystals and Their Size-Dependent Properties. *ACS Nano* **2010**, *4*, S253–S262.
- (309) Du, Y.; Xu, B.; Fu, T.; Cai, M.; Li, F.; Zhang, Y.; Wang, Q. Near-Infrared Photoluminescent Ag₂s Quantum Dots from a Single Source Precursor. *J. Am. Chem. Soc.* **2010**, *132*, 1470–1471.
- (310) Jiang, P.; Tian, Z.-Q.; Zhu, C.-N.; Zhang, Z.-L.; Pang, D.-W. Emission-Tunable near-Infrared Ag₂s Quantum Dots. *Chem. Mater.* **2012**, *24*, 3–5.
- (311) Zhang, H.; Hyun, B.-R.; Wise, F. W.; Robinson, R. D. A Generic Method for Rational Scalable Synthesis of Monodisperse Metal Sulfide Nanocrystals. *Nano Lett.* **2012**, *12*, S856–S860.
- (312) Joo, J. B.; Dahl, M.; Li, N.; Zaera, F.; Yin, Y. Tailored Synthesis of Mesoporous Tio₂ Hollow Nanostructures for Catalytic Applications. *Energy Environ. Sci.* **2013**, *6*, 2082–2092.
- (313) Dahl, M.; Liu, Y. D.; Yin, Y. D. Composite Titanium Dioxide Nanomaterials. *Chem. Rev.* **2014**, *114*, 9853–9889.
- (314) Jose, R.; Thavasi, V.; Ramakrishna, S. Metal Oxides for Dye-Sensitized Solar Cells. *J. Am. Ceram. Soc.* **2009**, *92*, 289–301.
- (315) Spanhel, L. Colloidal ZnO Nanostructures and Functional Coatings: A Survey. *J. Sol-Gel Sci. Technol.* **2006**, *39*, 7–24.
- (316) Klingshirn, C. ZnO: Material, Physics and Applications. *ChemPhysChem* **2007**, *8*, 782–803.
- (317) Xiong, H.-M. ZnO Nanoparticles Applied to Bioimaging and Drug Delivery. *Adv. Mater.* **2013**, *25*, S329–S335.
- (318) Shim, M.; Guyot-Sionnest, P. Organic-Capped ZnO Nanocrystals: Synthesis and N-Type Character. *J. Am. Chem. Soc.* **2001**, *123*, 11651–11654.
- (319) Monge, M.; Kahn, M. L.; Maisonnat, A.; Chaudret, B. Room-Temperature Organometallic Synthesis of Soluble and Crystalline ZnO Nanoparticles of Controlled Size and Shape. *Angew. Chem., Int. Ed.* **2003**, *42*, S321–S324.
- (320) Cozzoli, P. D.; Curri, M. L.; Agostiano, A.; Leo, G.; Lomascolo, M. ZnO Nanocrystals by a Non-Hydrolytic Route: Synthesis and Characterization. *J. Phys. Chem. B* **2003**, *107*, 4756–4762.
- (321) Joo, J.; Kwon, S. G.; Yu, J. H.; Hyeon, T. Synthesis of ZnO Nanocrystals with Cone, Hexagonal Cone, and Rod Shapes Via Non-Hydrolytic Ester Elimination Sol-Gel Reactions. *Adv. Mater.* **2005**, *17*, 1873–1877.
- (322) Jana, N. R.; Yu, H.-h.; Ali, E. M.; Zheng, Y.; Ying, J. Y. Controlled Photostability of Luminescent Nanocrystalline ZnO Solution for Selective Detection of Aldehydes. *Chem. Commun.* **2007**, 1406–1408.
- (323) Fröschl, T.; Hörmann, U.; Kubiak, P.; Kučerová, G.; Pfanzelt, M.; Weiss, C. K.; Behm, R. J.; Hüsing, N.; Kaiser, U.; et al. High Surface Area Crystalline Titanium Dioxide: Potential and Limits in Electrochemical Energy Storage and Catalysis. *Chem. Soc. Rev.* **2012**, *41*, S313–S360.
- (324) Sang, L.; Zhao, Y.; Burda, C. Tio₂ Nanoparticles as Functional Building Blocks. *Chem. Rev.* **2014**, *114*, 9283–9318.
- (325) Schneider, J.; Matsuoka, M.; Takeuchi, M.; Zhang, J.; Horiuchi, Y.; Anpo, M.; Bahnemann, D. W. Understanding Tio₂ Photocatalysis: Mechanisms and Materials. *Chem. Rev.* **2014**, *114*, 9919–9986.
- (326) Trentler, T. J.; Denler, T. E.; Bertone, J. F.; Agrawal, A.; Colvin, V. L. Synthesis of Tio₂ Nanocrystals by Nonhydrolytic Solution-Based Reactions. *J. Am. Chem. Soc.* **1999**, *121*, 1613–1614.
- (327) Jun, Y.-w.; Casula, M. F.; Sim, J.-H.; Kim, S. Y.; Cheon, J.; Alivisatos, A. P. Surfactant-Assisted Elimination of a High Energy Facet as a Means of Controlling the Shapes of Tio₂ Nanocrystals. *J. Am. Chem. Soc.* **2003**, *125*, 15981–15985.
- (328) Cozzoli, P. D.; Kornowski, A.; Weller, H. Low-Temperature Synthesis of Soluble and Processable Organic-Capped Anatase Tio₂ Nanorods. *J. Am. Chem. Soc.* **2003**, *125*, 14539–14548.
- (329) Buonsanti, R.; Carlino, E.; Giannini, C.; Altamura, D.; De Marco, L.; Giannuzzi, R.; Manca, M.; Gigli, G.; Cozzoli, P. D. Hyperbranched Anatase Tio₂ Nanocrystals: Nonaqueous Synthesis, Growth Mechanism, and Exploitation in Dye-Sensitized Solar Cells. *J. Am. Chem. Soc.* **2011**, *133*, 19216–19239.
- (330) Liu, Y.; Tang, A.; Zhang, Q.; Yin, Y. Seed-Mediated Growth of Anatase Tio₂ Nanocrystals with Core–Antenna Structures for Enhanced Photocatalytic Activity. *J. Am. Chem. Soc.* **2015**, *137*, 11327–11339.
- (331) Kim, C.-S.; Moon, B. K.; Park, J.-H.; Choi, B.-C.; Seo, H.-J. Solvothermal Synthesis of Nanocrystalline Tio₂ in Toluene with Surfactant. *J. Cryst. Growth* **2003**, *257*, 309–315.
- (332) Cozzoli, P. D.; Kornowski, A.; Weller, H. Low-Temperature Synthesis of Soluble and Processable Organic-Capped Anatase Tio₂ Nanorods. *J. Am. Chem. Soc.* **2003**, *125*, 14539–14548.
- (333) Zhang, Z.; Zhong, X.; Liu, S.; Li, D.; Han, M. Aminolysis Route to Monodisperse Titania Nanorods with Tunable Aspect Ratio. *Angew. Chem., Int. Ed.* **2005**, *44*, 3466–3470.
- (334) Tang, J.; Redl, F.; Zhu, Y.; Siegrist, T.; Brus, L. E.; Steigerwald, M. L. An Organometallic Synthesis of Tio₂ Nanoparticles. *Nano Lett.* **2005**, *5*, S43–S48.
- (335) Niederberger, M.; Garnweitner, G.; Krumeich, F.; Nesper, R.; Cölfen, H.; Antonietti, M. Tailoring the Surface and Solubility Properties of Nanocrystalline Titania by a Nonaqueous in Situ Functionalization Process. *Chem. Mater.* **2004**, *16*, 1202–1208.
- (336) Zhu, H. Y.; Lan, Y.; Gao, X. P.; Ringer, S. P.; Zheng, Z. F.; Song, D. Y.; Zhao, J. C. Phase Transition between Nanostructures of Titanate and Titanium Dioxides Via Simple Wet-Chemical Reactions. *J. Am. Chem. Soc.* **2005**, *127*, 6730–6736.
- (337) Dinh, C.-T.; Nguyen, T.-D.; Kleitz, F.; Do, T.-O. Shape-Controlled Synthesis of Highly Crystalline Titania Nanocrystals. *ACS Nano* **2009**, *3*, 3737–3743.
- (338) Chen, Y.; Kim, M.; Lian, G.; Johnson, M. B.; Peng, X. Side Reactions in Controlling the Quality, Yield, and Stability of High Quality Colloidal Nanocrystals. *J. Am. Chem. Soc.* **2005**, *127*, 13331–13337.
- (339) Sykes, E. A.; Dai, Q.; Sarsons, C. D.; Chen, J.; Rocheleau, J. V.; Hwang, D. M.; Zheng, G.; Cramb, D. T.; Rinker, K. D.; Chan, W. C. W. Tailoring Nanoparticle Designs to Target Cancer Based on

- Tumor Pathophysiology. *Proc. Natl. Acad. Sci. U. S. A.* **2016**, *113*, E1142–E1151.
- (340) Rizvi, S. A. A.; Saleh, A. M. Applications of Nanoparticle Systems in Drug Delivery Technology. *Saudi Pharm. J.* **2018**, *26*, 64–70.
- (341) Jain, P. K.; Huang, X.; El-Sayed, I. H.; El-Sayed, M. A. Noble Metals on the Nanoscale: Optical and Photothermal Properties and Some Applications in Imaging, Sensing, Biology, and Medicine. *Acc. Chem. Res.* **2008**, *41*, 1578–1586.
- (342) Krumpfer, J. W.; Schuster, T.; Klapper, M.; Müllen, K. Make It Nano-Keep It Nano. *Nano Today* **2013**, *8*, 417–438.
- (343) Rana, S.; Yeh, Y.-C.; Rotello, V. M. Engineering the Nanoparticle–Protein Interface: Applications and Possibilities. *Curr. Opin. Chem. Biol.* **2010**, *14*, 828–834.
- (344) Barenholz, Y. Doxil — the First Fda-Approved Nano-Drug: Lessons Learned. *J. Controlled Release* **2012**, *160*, 117–134.
- (345) Suk, J. S.; Xu, Q.; Kim, N.; Hanes, J.; Ensign, L. M. Pegylation as a Strategy for Improving Nanoparticle-Based Drug and Gene Delivery. *Adv. Drug Delivery Rev.* **2016**, *99*, 28–51.
- (346) Tai, M. F.; Lai, C. W.; Abdul Hamid, S. B. Facile Synthesis Polyethylene Glycol Coated Magnetite Nanoparticles for High Colloidal Stability. *J. Nanomater.* **2016**, *2016*, 8612505.
- (347) Masoudi, A.; Madaah Hosseini, H. R.; Shokrgozar, M. A.; Ahmadi, R.; Oghabian, M. A. The Effect of Poly (Ethylene Glycol) Coating on Colloidal Stability of Superparamagnetic Iron Oxide Nanoparticles as Potential Mri Contrast Agent. *Int. J. Pharm.* **2012**, *433*, 129–141.
- (348) Luo, C.; Zhang, Y.; Zeng, X.; Zeng, Y.; Wang, Y. The Role of Poly(Ethylene Glycol) in the Formation of Silver Nanoparticles. *J. Colloid Interface Sci.* **2005**, *288*, 444–448.
- (349) Fleitas-Salazar, N.; Silva-Campa, E.; Pedroso-Santana, S.; Tanori, J.; Pedroza-Montero, M. R.; Riera, R. Effect of Temperature on the Synthesis of Silver Nanoparticles with Polyethylene Glycol: New Insights into the Reduction Mechanism. *J. Nanopart. Res.* **2017**, *19*, 113.
- (350) Pelaz, B.; Del Pino, P.; Maffre, P.; Hartmann, R.; Gallego, M.; Rivera-Fernandez, S.; de la Fuente, J. M.; Nienhaus, G. U.; Parak, W. J. Surface Functionalization of Nanoparticles with Polyethylene Glycol: Effects on Protein Adsorption and Cellular Uptake. *ACS Nano* **2015**, *9*, 6996–7008.
- (351) Fernandes, R.; Smyth, N. R.; Muskens, O. L.; Nitti, S.; Heuer-Jungemann, A.; Ardern-Jones, M. R.; Kanaras, A. G. Interactions of Skin with Gold Nanoparticles of Different Surface Charge, Shape, and Functionality. *Small* **2015**, *11*, 713–721.
- (352) Bartzczak, D.; Muskens, O. L.; Nitti, S.; Sanchez-Elsner, T.; Millar, T. M.; Kanaras, A. G. Interactions of Human Endothelial Cells with Gold Nanoparticles of Different Morphologies. *Small* **2012**, *8*, 122–130.
- (353) Bartzczak, D.; Kanaras, A. G. Diacetylene-Containing Ligand as a New Capping Agent for the Preparation of Water-Soluble Colloidal Nanoparticles of Remarkable Stability. *Langmuir* **2010**, *26*, 7072–7077.
- (354) Elbert, D. L.; Hubbell, J. A. Surface Treatments of Polymers for Biocompatibility. *Annu. Rev. Mater. Sci.* **1996**, *26*, 365–394.
- (355) Lee, J. H.; Lee, H. B.; Andrade, J. D. Blood Compatibility of Polyethylene Oxide Surfaces. *Prog. Polym. Sci.* **1995**, *20*, 1043–1079.
- (356) Walkey, C. D.; Olsen, J. B.; Guo, H.; Emili, A.; Chan, W. C. W. Nanoparticle Size and Surface Chemistry Determine Serum Protein Adsorption and Macrophage Uptake. *J. Am. Chem. Soc.* **2012**, *134*, 2139–2147.
- (357) Vert, M.; Domurado, D. Poly (Ethylene Glycol): Protein-Repulsive or Albumin-Compatible? *J. Biomater. Sci., Polym. Ed.* **2000**, *11*, 1307–1317.
- (358) Naahidi, S.; Jafari, M.; Edalat, F.; Raymond, K.; Khademhosseini, A.; Chen, P. Biocompatibility of Engineered Nanoparticles for Drug Delivery. *J. Controlled Release* **2013**, *166*, 182–194.
- (359) Larson, T. A.; Joshi, P. P.; Sokolov, K. Preventing Protein Adsorption and Macrophage Uptake of Gold Nanoparticles Via a Hydrophobic Shield. *ACS Nano* **2012**, *6*, 9182–9190.
- (360) Sperling, R. A.; Parak, W. Surface Modification, Functionalization and Bioconjugation of Colloidal Inorganic Nanoparticles. *Philos. Trans. R. Soc., A* **2010**, *368*, 1333–1383.
- (361) Colombo, M.; Mazzucchelli, S.; Montenegro, J. M.; Galbiati, E.; Corsi, F.; Parak, W. J.; Prosperi, D. Protein Oriented Ligation on Nanoparticles Exploiting O6-Alkylguanine-DNA Transferase (Snap) Genetically Encoded Fusion. *Small* **2012**, *8*, 1492–1497.
- (362) Sun, C.; Du, K.; Fang, C.; Bhattarai, N.; Veis, O.; Kievit, F.; Stephen, Z.; Lee, D.; Ellenbogen, R. G.; et al. Peg-Mediated Synthesis of Highly Dispersive Multifunctional Superparamagnetic Nanoparticles: Their Physicochemical Properties and Function in Vivo. *ACS Nano* **2010**, *4*, 2402–2410.
- (363) Susumu, K.; Uyeda, H. T.; Medintz, I. L.; Pons, T.; Delehanty, J. B.; Mattoussi, H. Enhancing the Stability and Biological Functionalities of Quantum Dots Via Compact Multifunctional Ligands. *J. Am. Chem. Soc.* **2007**, *129*, 13987–13996.
- (364) Huy, T. Q.; Van Chung, P.; Thuy, N. T.; Blanco-Andujar, C.; Thanh, N. T. K. Protein a-Conjugated Iron Oxide Nanoparticles for Separation of Vibrio Cholerae from Water Samples. *Faraday Discuss.* **2014**, *175*, 73–82.
- (365) Fernandes, R.; Li, M.; Dujardin, E.; Mann, S.; Kanaras, A. G. Ligand-Mediated Self-Assembly of Polymer-Enveloped Gold Nanoparticle Chains and Networks. *Chem. Commun.* **2010**, *46*, 7602–7604.
- (366) Huo, S.; Jiang, Y.; Gupta, A.; Jiang, Z.; Landis, R. F.; Hou, S.; Liang, X.-J.; Rotello, V. M. Fully Zwitterionic Nanoparticle Antimicrobial Agents through Tuning of Core Size and Ligand Structure. *ACS Nano* **2016**, *10*, 8732–8737.
- (367) Li, X.; Robinson, S. M.; Gupta, A.; Saha, K.; Jiang, Z.; Moyano, D. F.; Sahar, A.; Riley, M. A.; Rotello, V. M. Functional Gold Nanoparticles as Potent Antimicrobial Agents against Multi-Drug-Resistant Bacteria. *ACS Nano* **2014**, *8*, 10682–10686.
- (368) Correa-Duarte, M. A.; Giersig, M.; Liz-Marzán, L. M. Stabilization of Cds Semiconductor Nanoparticles against Photodegradation by a Silica Coating Procedure. *Chem. Phys. Lett.* **1998**, *286*, 497–501.
- (369) Mulvaney, P.; Liz-Marzán, L. M.; Giersig, M.; Ung, T. Silica Encapsulation of Quantum Dots and Metal Clusters. *J. Mater. Chem.* **2000**, *10*, 1259–1270.
- (370) Kirchner, C.; Liedl, T.; Kudera, S.; Pellegrino, T.; Muñoz Javier, A.; Gaub, H. E.; Stölzle, S.; Fertig, N.; Parak, W. J. Cytotoxicity of Colloidal Cdse and Cdse/Zns Nanoparticles. *Nano Lett.* **2005**, *5*, 331–338.
- (371) Gerion, G.; Pinaud, F.; Williams, S. C.; Parak, W. J.; Zanchet, D.; Weiss, S.; Alivisatos, A. P. Synthesis and Properties of Biocompatible Water-Soluble Silica-Coated Cdse/Zns Semiconductor Quantum Dots. *J. Phys. Chem. B* **2001**, *105*, 8861–8871.
- (372) Stöber, W.; Fink, A.; Bohn, E. Controlled Growth of Monodisperse Silica Spheres in the Micron Size Range. *J. Colloid Interface Sci.* **1968**, *26*, 62–69.
- (373) Lu, Y.; Yin, Y.; Mayers, B. T.; Xia, Y. Modifying the Surface Properties of Superparamagnetic Iron Oxide Nanoparticles through a Sol–Gel Approach. *Nano Lett.* **2002**, *2*, 183–186.
- (374) Liz-Marzán, L. M.; Giersig, M.; Mulvaney, P. Synthesis of Nanosized Gold–Silica Core–Shell Particles. *Langmuir* **1996**, *12*, 4329–4335.
- (375) Fernández-López, C.; Mateo-Mateo, C.; Álvarez-Puebla, R. A.; Pérez-Juste, J.; Pastoriza-Santos, I.; Liz-Marzán, L. M. Highly Controlled Silica Coating of Peg-Capped Metal Nanoparticles and Preparation of Sers-Encoded Particles. *Langmuir* **2009**, *25*, 13894–13899.
- (376) Graf, C.; Vossen, D. L. J.; Imhof, A.; van Blaaderen, A. A General Method to Coat Colloidal Particles with Silica. *Langmuir* **2003**, *19*, 6693–6700.
- (377) Chang, S.-Y.; Liu, L.; Asher, S. A. Preparation and Properties of Tailored Morphology, Monodisperse Colloidal Silica-Cadmium Sulfide Nanocomposites. *J. Am. Chem. Soc.* **1994**, *116*, 6739–6744.

- (378) López-Quintela, M. A. Synthesis of Nanomaterials in Microemulsions: Formation Mechanisms and Growth Control. *Curr. Opin. Colloid Interface Sci.* **2003**, *8*, 137–144.
- (379) Venditti, F.; Angelico, R.; Palazzo, G.; Colafemmina, G.; Ceglie, A.; Lopez, F. Preparation of Nanosize Silica in Reverse Micelles: Ethanol Produced During Teos Hydrolysis Affects the Microemulsion Structure. *Langmuir* **2007**, *23*, 10063–10068.
- (380) Darbandi, M.; Thomann, R.; Nann, T. Single Quantum Dots in Silica Spheres by Microemulsion Synthesis. *Chem. Mater.* **2005**, *17*, 5720–5725.
- (381) Koole, R.; van Schooneveld, M. M.; Hilhorst, J.; de Mello Donega, C.; 't Hart, D. C.; van Blaaderen, A.; Vanmaekelbergh, D.; Meijerink, A. On the Incorporation Mechanism of Hydrophobic Quantum Dots in Silica Spheres by a Reverse Microemulsion Method. *Chem. Mater.* **2008**, *20*, 2503–2512.
- (382) Cheng, G.; Wang, Y.; Wang, Z.-G.; Sui, X.-J.; Zhang, J.-L.; Ni, J.-Z. Magnetic Mesoporous Silica Incorporated with TiO₂ for Selective and Rapid Capture of Peptides. *RSC Adv.* **2014**, *4*, 7694–7702.
- (383) Cushing, B. L.; Kolesnichenko, V. L.; O'Connor, C. J. Recent Advances in the Liquid-Phase Syntheses of Inorganic Nanoparticles. *Chem. Rev.* **2004**, *104*, 3893–3946.
- (384) Okada, T.; Watanabe, N.; Sakai, T.; Haeiwa, T.; Mishima, S. Fabrication of Acid-Tolerant Magnetic Co@SiO₂ Core–Shell Particles with Dense Silica Shell. *Chem. Lett.* **2011**, *40*, 106–107.
- (385) Hong, Y.; Kim, H. J.; Yang, D.; Lee, G.; Nam, K. M.; Jung, M.-H.; Kim, Y.-M.; Choi, S.-I.; Seo, W. S. Facile Synthesis of Fully Ordered L10-FePt Nanoparticles with Controlled Pt-Shell Thicknesses for Electrocatalysis. *Nano Res.* **2017**, *10*, 2866–2880.
- (386) Grasset, F.; Labhsetwar, N.; Li, D.; Park, D. C.; Saito, N.; Haneda, H.; Cador, O.; Roisnel, T.; Mornet, S.; et al. Synthesis and Magnetic Characterization of Zinc Ferrite Nanoparticles with Different Environments: Powder, Colloidal Solution, and Zinc Ferrite–Silica Core–Shell Nanoparticles. *Langmuir* **2002**, *18*, 8209–8216.
- (387) Aslam, M.; Li, S.; Dravid, V. P. Controlled Synthesis and Stability of Co@SiO₂ Aqueous Colloids. *J. Am. Ceram. Soc.* **2007**, *90*, 950–956.
- (388) Zhong, Q.; Cao, M.; Hu, H.; Yang, D.; Chen, M.; Li, P.; Wu, L.; Zhang, Q. One-Pot Synthesis of Highly Stable CsPbBr₃@SiO₂ Core–Shell Nanoparticles. *ACS Nano* **2018**, *12*, 8579–8587.
- (389) Philipse, A. P.; van Bruggen, M. P. B.; Pathmamanoharan, C. Magnetic Silica Dispersions: Preparation and Stability of Surface-Modified Silica Particles with a Magnetic Core. *Langmuir* **1994**, *10*, 92–99.
- (390) Bruce, I. J.; Taylor, J.; Todd, M.; Davies, M. J.; Borioni, E.; Sangregorio, C.; Sen, T. Synthesis, Characterisation and Application of Silica-Magnetite Nanocomposites. *J. Magn. Magn. Mater.* **2004**, *284*, 145–160.
- (391) Casula, M. F.; Corrias, A.; Arosio, P.; Lascialfari, A.; Sen, T.; Floris, P.; Bruce, I. J. Design of Water-Based Ferrofluids as Contrast Agents for Magnetic Resonance Imaging. *J. Colloid Interface Sci.* **2011**, *357*, 50–55.
- (392) Joshi, H. M.; De, M.; Richter, F.; He, J.; Prasad, P. V.; Dravid, V. P. Effect of Silica Shell Thickness of Fe(3)O(4)–SiO(X) Core–Shell Nanostructures on Mri Contrast. *J. Nanopart. Res.* **2013**, *15*, 1448.
- (393) Bruchez, M., Jr.; Moronne, M.; Gin, P.; Weiss, S.; Alivisatos, A. P. Semiconductor Nanocrystals as Fluorescent Biological Labels. *Science* **1998**, *281*, 2013–2016.
- (394) Parak, W. J.; Gerion, D.; Zanchet, D.; Woerz, A. S.; Pellegrino, T.; Micheel, C.; Williams, S. C.; Seitz, M.; Bruehl, R. E.; et al. Conjugation of DNA to Silanized Colloidal Semiconductor Nanocrystalline Quantum Dots. *Chem. Mater.* **2002**, *14*, 2113–2119.
- (395) Sen, T.; Sebastianelli, A.; Bruce, I. J. Mesoporous Silica–Magnetite Nanocomposite: Fabrication and Applications in Magnetic Bioseparations. *J. Am. Chem. Soc.* **2006**, *128*, 7130–7131.
- (396) Kim, J.; Lee, J. E.; Lee, J.; Yu, J. H.; Kim, B. C.; An, K.; Hwang, Y.; Shin, C.-H.; Park, J.-G.; et al. Magnetic Fluorescent Delivery Vehicle Using Uniform Mesoporous Silica Spheres Embedded with Monodisperse Magnetic and Semiconductor Nanocrystals. *J. Am. Chem. Soc.* **2006**, *128*, 688–689.
- (397) Kim, J.; Kim, H. S.; Lee, N.; Kim, T.; Kim, H.; Yu, T.; Song, I. C.; Moon, W. K.; Hyeon, T. Multifunctional Uniform Nanoparticles Composed of a Magnetite Nanocrystal Core and a Mesoporous Silica Shell for Magnetic Resonance and Fluorescence Imaging and for Drug Delivery. *Angew. Chem., Int. Ed.* **2008**, *47*, 8438–8441.
- (398) Rowe, L. R.; Chapman, B. S.; Tracy, J. B. Understanding and Controlling the Morphology of Silica Shells on Gold Nanorods. *Chem. Mater.* **2018**, *30*, 6249–6258.
- (399) Parak, W. J.; Pellegrino, T.; Micheel, C. M.; Gerion, D.; Williams, S. C.; Alivisatos, A. P. Conformation of Oligonucleotides Attached to Gold Nanocrystals Probed by Gel Electrophoresis. *Nano Lett.* **2003**, *3*, 33–36.
- (400) Seeman, N. C.; Sleiman, H. F. DNA Nanotechnology. *Nat. Rev. Mater.* **2017**, *3*, 17068.
- (401) Giust, D.; Lucio, M. I.; El-Sagheer, A. H.; Brown, T.; Williams, L. E.; Muskens, O. L.; Kanaras, A. G. Graphene Oxide–Upconversion Nanoparticle Based Portable Sensors for Assessing Nutritional Deficiencies in Crops. *ACS Nano* **2018**, *12*, 6273–6279.
- (402) Vilela, P.; El-Sagheer, A.; Millar, T. M.; Brown, T.; Muskens, O. L.; Kanaras, A. G. Graphene Oxide–Upconversion Nanoparticle Based Optical Sensors for Targeted Detection of Mrna Biomarkers Present in Alzheimer's Disease and Prostate Cancer. *ACS Sens* **2017**, *2*, 52–56.
- (403) Alonso-Cristobal, P.; Vilela, P.; El-Sagheer, A.; Lopez-Cabarcos, E.; Brown, T.; Muskens, O. L.; Rubio-Retama, J.; Kanaras, A. G. Highly Sensitive DNA Sensor Based on Upconversion Nanoparticles and Graphene Oxide. *ACS Appl. Mater. Interfaces* **2015**, *7*, 12422–12429.
- (404) Heuer-Jungemann, A.; Harimech, P. K.; Brown, T.; Kanaras, A. G. Gold Nanoparticles and Fluorescently-Labelled DNA as a Platform for Biological Sensing. *Nanoscale* **2013**, *5*, 9503–9510.
- (405) Briley, W. E.; Bondy, M. H.; Randeria, P. S.; Dupper, T. J.; Mirkin, C. A. Quantification and Real-Time Tracking of Rna in Live Cells Using Sticky-Flares. *Proc. Natl. Acad. Sci. U. S. A.* **2015**, *112*, 9591–9595.
- (406) Alexander, C. M.; Hamner, K. L.; Maye, M. M.; Dabrowiak, J. C. Multifunctional DNA-Gold Nanoparticles for Targeted Doxorubicin Delivery. *Bioconjugate Chem.* **2014**, *25*, 1261–1271.
- (407) Li, N.; Yang, H.; Pan, W.; Diao, W.; Tang, B. A Tumour Mrna-Trigged Nanocarrier for Multimodal Cancer Cell Imaging and Therapy. *Chem. Commun.* **2014**, *50*, 7473–7476.
- (408) Seferos, D. S.; Giljohann, D. A.; Hill, H. D.; Prigodich, A. E.; Mirkin, C. A. Nano-Flares: Probes for Transfection and Mrna Detection in Living Cells. *J. Am. Chem. Soc.* **2007**, *129*, 15477–15479.
- (409) Prigodich, A. E.; Seferos, D. S.; Massich, M. D.; Giljohann, D. A.; Lane, B. C.; Mirkin, C. A. Nano-Flares for Mrna Regulation and Detection. *ACS Nano* **2009**, *3*, 2147–2152.
- (410) Giljohann, D. A.; Seferos, D. S.; Prigodich, A. E.; Patel, P. C.; Mirkin, C. A. Gene Regulation with Polyvalent Sirna-Nanoparticle Conjugates. *J. Am. Chem. Soc.* **2009**, *131*, 2072.
- (411) Prigodich, A. E.; Randeria, P. S.; Briley, W. E.; Kim, N. J.; Daniel, W. L.; Giljohann, D. A.; Mirkin, C. A. Multiplexed Nanoflakes: Mrna Detection in Live Cells. *Anal. Chem.* **2012**, *84*, 2062–2066.
- (412) Rosi, N. L.; Giljohann, D. A.; Thaxton, C. S.; Lytton-Jean, A. K. R.; Han, M. S.; Mirkin, C. A. Oligonucleotide-Modified Gold Nanoparticles for Intracellular Gene Regulation. *Science* **2006**, *312*, 1027–1030.
- (413) Dhar, S.; Daniel, W. L.; Giljohann, D. A.; Mirkin, C. A.; Lippard, S. J. Polyvalent Oligonucleotide Gold Nanoparticle Conjugates as Delivery Vehicles for Platinum(IV) Warheads. *J. Am. Chem. Soc.* **2009**, *131*, 14652–14653.
- (414) Alexander, C. M.; Maye, M. M.; Dabrowiak, J. C. DNA-Capped Nanoparticles Designed for Doxorubicin Drug Delivery. *Chem. Commun.* **2011**, *47*, 3418–3420.
- (415) Heuer-Jungemann, A.; Kirkwood, R.; El-Sagheer, A. H.; Brown, T.; Kanaras, A. G. Copper-Free Click Chemistry as an

Emerging Tool for the Programmed Ligation of DNA-Functionalised Gold Nanoparticles. *Nanoscale* **2013**, *5*, 7209–7212.

(416) Heuer-Jungemann, A.; Kiessling, L.; Stratakis, E.; Kymakis, E.; El-Sagheer, A. H.; Brown, T.; Kanaras, A. G. Programming the Assembly of Gold Nanoparticles on Graphene Oxide Sheets Using DNA. *J. Mater. Chem. C* **2015**, *3*, 9379–9384.

(417) Harimech, P. K.; Gerrard, S. R.; El-Sagheer, A. H.; Brown, T.; Kanaras, A. G. Reversible Ligation of Programmed DNA-Gold Nanoparticle Assemblies. *J. Am. Chem. Soc.* **2015**, *137*, 9242–9245.

(418) Coomber, D.; Bartczak, D.; Gerrard, S. R.; Tyas, S.; Kanaras, A. G.; Stulz, E. Programmed Assembly of Peptide-Functionalized Gold Nanoparticles on DNA Templates. *Langmuir* **2010**, *26*, 13760–13762.

(419) Alivisatos, A. P.; Johnsson, K. P.; Peng, X. G.; Wilson, T. E.; Loweth, C. J.; Bruchez, M. P.; Schultz, P. G. Organization of 'Nanocrystal Molecules' Using DNA. *Nature* **1996**, *382*, 609–611.

(420) Mirkin, C. A.; Letsinger, R. L.; Mucic, R. C.; Storhoff, J. J. A DNA-Based Method for Rationally Assembling Nanoparticles into Macroscopic Materials. *Nature* **1996**, *382*, 607–609.

(421) Hurst, S. J.; Lytton-Jean, A. K. R.; Mirkin, C. A. Maximizing DNA Loading on a Range of Gold Nanoparticle Sizes. *Anal. Chem.* **2006**, *78*, 8313–8318.

(422) Zanchet, D.; Micheel, C. M.; Parak, W. J.; Gerion, D.; Alivisatos, A. P. Electrophoretic Isolation of Discrete Au Nanocrystal/DNA Conjugates. *Nano Lett.* **2001**, *1*, 32–35.

(423) Claridge, S. A.; Liang, H. W.; Basu, S. R.; Frechet, J. M. J.; Alivisatos, A. P. Isolation of Discrete Nanoparticle - DNA Conjugates for Plasmonic Applications. *Nano Lett.* **2008**, *8*, 1202–1206.

(424) Zhang, X.; Servos, M. R.; Liu, J. Instantaneous and Quantitative Functionalization of Gold Nanoparticles with Thiolated DNA Using a Ph-Assisted and Surfactant-Free Route. *J. Am. Chem. Soc.* **2012**, *134*, 7266–7269.

(425) Kanaras, A. G.; Wang, Z. X.; Bates, A. D.; Cosstick, R.; Brust, M. Towards Multistep Nanostructure Synthesis: Programmed Enzymatic Self-Assembly of DNA/Gold Systems. *Angew. Chem., Int. Ed.* **2003**, *42*, 191.

(426) Xu, Q.; Lou, X.; Wang, L.; Ding, X.; Yu, H.; Xiao, Y. Rapid, Surfactant-Free, and Quantitative Functionalization of Gold Nanoparticles with Thiolated DNA under Physiological pH and Its Application in Molecular Beacon-Based Biosensor. *ACS Appl. Mater. Interfaces* **2016**, *8*, 27298–27304.

(427) Liu, B.; Liu, J. Freezing Directed Construction of Bio/Nano Interfaces: Reagentless Conjugation, Denser Spherical Nucleic Acids, and Better Nanoflakes. *J. Am. Chem. Soc.* **2017**, *139*, 9471–9474.

(428) Carnevale, K. J. F.; Strouse, G. F. Intracellular DNA Cargo Release from a Gold Nanoparticle Modulated by the Nature of the Surface Coupling Functionality. *Bioconjugate Chem.* **2018**, *29*, 3429.

(429) Zhang, T.; Hartl, C.; Frank, K.; Heuer-Jungemann, A.; Fischer, S.; Nickels, P. C.; Nickl, B.; Liedl, T. DNA Nanotechnology: 3d DNA Origami Crystals. *Adv. Mater.* **2018**, *30*, 1870203.

(430) Liu, N.; Liedl, T. DNA-Assembled Advanced Plasmonic Architectures. *Chem. Rev.* **2018**, *118*, 3032–3053.

(431) Hartl, C.; Frank, K.; Amenitsch, H.; Fischer, S.; Liedl, T.; Nickel, B. Position Accuracy of Gold Nanoparticles on DNA Origami Structures Studied with Small-Angle X-Ray Scattering. *Nano Lett.* **2018**, *18*, 2609–2615.

(432) Funck, T.; Nicoli, F.; Kuzyk, A.; Liedl, T. Sensing Picomolar Concentrations of RNA Using Switchable Plasmonic Chirality. *Angew. Chem., Int. Ed.* **2018**, *57*, 13495–13498.

(433) Heuer-Jungemann, A.; El-Sagheer, A. H.; Lackie, P. M.; Brown, T.; Kanaras, A. G. Selective Killing of Cells Triggered by Their mRNA Signature in the Presence of Smart Nanoparticles. *Nanoscale* **2016**, *8*, 16857–16861.

(434) Giljohann, D. A.; Seferos, D. S.; Daniel, W. L.; Massich, M. D.; Patel, P. C.; Mirkin, C. A. Gold Nanoparticles for Biology and Medicine. *Angew. Chem., Int. Ed.* **2010**, *49*, 3280–3294.

(435) Patel, P. C.; Giljohann, D. A.; Daniel, W. L.; Zheng, D.; Prigodich, A. E.; Mirkin, C. A. Scavenger Receptors Mediate Cellular

Uptake of Polyvalent Oligonucleotide-Functionalized Gold Nanoparticles. *Bioconjugate Chem.* **2010**, *21*, 2250–2256.

(436) Cutler, J. I.; Auyeung, E.; Mirkin, C. A. Spherical Nucleic Acids. *J. Am. Chem. Soc.* **2012**, *134*, 1376–1391.

(437) Wu, X. C. A.; Choi, C. H. J.; Zhang, C.; Hao, L. L.; Mirkin, C. A. Intracellular Fate of Spherical Nucleic Acid Nanoparticle Conjugates. *J. Am. Chem. Soc.* **2014**, *136*, 7726–7733.

(438) Ding, Y.; Jiang, Z.; Saha, K.; Kim, C. S.; Kim, S. T.; Landis, R. F.; Rotello, V. M. Gold Nanoparticles for Nucleic Acid Delivery. *Mol. Ther.* **2014**, *22*, 1075–1083.

(439) Melamed, J. R.; Riley, R. S.; Valcourt, D. M.; Billingsley, M. M.; Kreuzberger, N. L.; Day, E. S. Quantification of siRNA Duplexes Bound to Gold Nanoparticle Surfaces. *Methods Mol. Biol.* **2017**, *1570*, 1–15.

(440) Lee, J.-S.; Lytton-Jean, A. K. R.; Hurst, S. J.; Mirkin, C. A. Silver Nanoparticle–Oligonucleotide Conjugates Based on DNA with Triple Cyclic Disulfide Moieties. *Nano Lett.* **2007**, *7*, 2112–2115.

(441) Zhang, X.; Servos, M. R.; Liu, J. Fast Ph-Assisted Functionalization of Silver Nanoparticles with Monothiolated DNA. *Chem. Commun.* **2012**, *48*, 10114–10116.

(442) Zheng, Y.; Li, Y.; Deng, Z. Silver Nanoparticle–DNA Bionanoconjugates Bearing a Discrete Number of DNA Ligands. *Chem. Commun.* **2012**, *48*, 6160–6162.

(443) Weadick, D. S.; Liu, J. Phosphorothioate DNA Stabilized Fluorescent Gold and Silver Nanoclusters. *Nanomaterials* **2015**, *5*, 804–813.

(444) Carnerero, J. M.; Jimenez-Ruiz, A.; Castillo, P. M.; Prado-Gotor, R. Covalent and Non-Covalent DNA–Gold-Nanoparticle Interactions: New Avenues of Research. *ChemPhysChem* **2017**, *18*, 17–33.

(445) Li, L.-L.; Wu, P.; Hwang, K.; Lu, Y. An Exceptionally Simple Strategy for DNA-Functionalized up-Conversion Nanoparticles as Biocompatible Agents for Nanoassembly, DNA Delivery, and Imaging. *J. Am. Chem. Soc.* **2013**, *135*, 2411–2414.

(446) Jiang, L.; Yang, B. Q.; Ma, Y. D.; Liu, Y. C.; Yang, W. S.; Li, T. J.; Sun, C. C. The Binding of Phosphorothioate Oligonucleotides to Cds Nanoparticles. *Chem. Phys. Lett.* **2003**, *380*, 29–33.

(447) Banerjee, A.; Pons, T.; Lequeux, N.; Dubertret, B. Quantum Dots–DNA Bioconjugates: Synthesis to Applications. *Interface Focus* **2016**, *6*, 20160064.

(448) Samanta, A.; Deng, Z.; Liu, Y.; Yan, H. A Perspective on Functionalizing Colloidal Quantum Dots with DNA. *Nano Res.* **2013**, *6*, 853–870.

(449) Zhang, X.; Servos, M. R.; Liu, J. Surface Science of DNA Adsorption onto Citrate-Capped Gold Nanoparticles. *Langmuir* **2012**, *28*, 3896–3902.

(450) Zhou, W.; Wang, F.; Ding, J.; Liu, J. Tandem Phosphorothioate Modifications for DNA Adsorption Strength and Polarity Control on Gold Nanoparticles. *ACS Appl. Mater. Interfaces* **2014**, *6*, 14795–14800.

(451) Zhang, X.; Liu, B.; Servos, M. R.; Liu, J. Polarity Control for Nonthiolated DNA Adsorption onto Gold Nanoparticles. *Langmuir* **2013**, *29*, 6091–6098.

(452) Lu, W.; Wang, L.; Li, J.; Zhao, Y.; Zhou, Z.; Shi, J.; Zuo, X.; Pan, D. Quantitative Investigation of the Poly-Adenine DNA Dissociation from the Surface of Gold Nanoparticles. *Sci. Rep.* **2015**, *5*, 10158.

(453) Lin, C.-A. J.; Sperling, R. A.; Li, J. K.; Yang, T.-Y.; Li, P.-Y.; Zanella, M.; Chang, W. H.; Parak, W. J. Design of an Amphiphilic Polymer for Nanoparticle Coating and Functionalization. *Small* **2008**, *4*, 334–341.

(454) Quarta, A.; Curcio, A.; Kakwere, H.; Pellegrino, T. Polymer Coated Inorganic Nanoparticles: Tailoring the Nanocrystal Surface for Designing Nanoprobes with Biological Implications. *Nanoscale* **2012**, *4*, 3319–3334.

(455) Cutler, J. I.; Zheng, D.; Xu, X.; Giljohann, D. A.; Mirkin, C. A. Polyvalent Oligonucleotide Iron Oxide Nanoparticle “Click” Conjugates. *Nano Lett.* **2010**, *10*, 1477–1480.

- (456) Sun, D. Z.; Gang, O. DNA-Functionalized Quantum Dots: Fabrication, Structural, and Physicochemical Properties. *Langmuir* **2013**, *29*, 7038–7046.
- (457) Pinaud, F.; King, D.; Moore, H.-P.; Weiss, S. Bioactivation and Cell Targeting of Semiconductor CdSe/ZnS Nanocrystals with Phytochelatin-Related Peptides. *J. Am. Chem. Soc.* **2004**, *126*, 6115–6123.
- (458) Clarke, S.; Pinaud, F.; Beutel, O.; You, C. J.; Piehler, J.; Dahan, M. Covalent Monofunctionalization of Peptide-Coated Quantum Dots for Single-Molecule Assays. *Nano Lett.* **2010**, *10*, 2147–2154.
- (459) Pelaz, B.; Alexiou, C.; Alvarez-Puebla, R. A.; Alves, F.; Andrews, A. M.; Ashraf, S.; Balogh, L. P.; Ballerini, L.; Bestetti, A.; et al. Diverse Applications of Nanomedicine. *ACS Nano* **2017**, *11*, 2313–2381.
- (460) Du, A. W.; Stenzel, M. H. Drug Carriers for the Delivery of Therapeutic Peptides. *Biomacromolecules* **2014**, *15*, 1097–1114.
- (461) Si, S.; Kotal, A.; Mandal, T. K. One-Dimensional Assembly of Peptide-Functionalized Gold Nanoparticles: An Approach toward Mercury Ion Sensing. *J. Phys. Chem. C* **2007**, *111*, 1248–1255.
- (462) Spicer, C. D.; Jumeaux, C.; Gupta, B.; Stevens, M. M. Peptide and Protein Nanoparticle Conjugates: Versatile Platforms for Biomedical Applications. *Chem. Soc. Rev.* **2018**, *47*, 3574–3620.
- (463) Lewin, M.; Carlesso, N.; Tung, C. H.; Tang, X. W.; Cory, D.; Scadden, D. T.; Weissleder, R. Tat Peptide-Derivatized Magnetic Nanoparticles Allow in Vivo Tracking and Recovery of Progenitor Cells. *Nat. Biotechnol.* **2000**, *18*, 410–414.
- (464) Bartczak, D.; Muskens, O. L.; Sanchez-Elsner, T.; Kanaras, A. G.; Millar, T. M. Manipulation of in Vitro Angiogenesis Using Peptide-Coated Gold Nanoparticles. *ACS Nano* **2013**, *7*, 5628–5636.
- (465) Levy, R.; Thanh, N. T. K.; Doty, R. C.; Hussain, I.; Nichols, R. J.; Schiffrin, D. J.; Brust, M.; Fernig, D. G. Rational and Combinatorial Design of Peptide Capping Ligands for Gold Nanoparticles. *J. Am. Chem. Soc.* **2004**, *126*, 10076–10084.
- (466) Chowdhury, R.; Ilyas, H.; Ghosh, A.; Ali, H.; Ghorai, A.; Midya, A.; Jana, N. R.; Das, S.; Bhunia, A. Multivalent Gold Nanoparticle–Peptide Conjugates for Targeting Intracellular Bacterial Infections. *Nanoscale* **2017**, *9*, 14074–14093.
- (467) Coomber, D.; Bartczak, D.; Gerrard, S. R.; Tyas, S.; Kanaras, A. G.; Stulz, E. Programmed Assembly of Peptide-Functionalized Gold Nanoparticles on DNA Templates. *Langmuir* **2010**, *26*, 13760–13762.
- (468) Zong, J.; Cobb, S. L.; Cameron, N. R. Peptide-Functionalized Gold Nanoparticles: Versatile Biomaterials for Diagnostic and Therapeutic Applications. *Biomater. Sci.* **2017**, *5*, 872–886.
- (469) Sabela, M.; Balme, S.; Bechelany, M.; Janot, J.-M.; Bisetty, K. A Review of Gold and Silver Nanoparticle-Based Colorimetric Sensing Assays. *Adv. Eng. Mater.* **2017**, *19*, 1700270.
- (470) Laromaine, A.; Koh, L.; Murugesan, M.; Ulijn, R. V.; Stevens, M. M. Protease-Triggered Dispersion of Nanoparticle Assemblies. *J. Am. Chem. Soc.* **2007**, *129*, 4156–4157.
- (471) Medintz, I. L.; Clapp, A. R.; Brunel, F. M.; Tiefenbrunn, T.; Tetsuo Uyeda, H.; Chang, E. L.; Deschamps, J. R.; Dawson, P. E.; Mattoussi, H. Proteolytic Activity Monitored by Fluorescence Resonance Energy Transfer through Quantum-Dot–Peptide Conjugates. *Nat. Mater.* **2006**, *5*, 581–589.
- (472) Safi, M.; Domitrovic, T.; Kapur, A.; Zhan, N.; Aldeek, F.; Johnson, J. E.; Mattoussi, H. Intracellular Delivery of Luminescent Quantum Dots Mediated by a Virus-Derived Lytic Peptide. *Bioconjugate Chem.* **2017**, *28*, 64–74.
- (473) Bartczak, D.; Kanaras, A. G. Preparation of Peptide-Functionalized Gold Nanoparticles Using One Pot EDC/Sulfo-NHS Coupling. *Langmuir* **2011**, *27*, 10119–10123.
- (474) Bartczak, D.; Muskens, O. L.; Millar, T. M.; Sanchez-Elsner, T.; Kanaras, A. G. Laser-Induced Damage and Recovery of Plasmonically Targeted Human Endothelial Cells. *Nano Lett.* **2011**, *11*, 1358–1363.
- (475) Bartczak, D.; Muskens, O. L.; Nitti, S.; Millar, T. M.; Kanaras, A. G. Nanoparticles for Inhibition of in Vitro Tumour Angiogenesis: Synergistic Actions of Ligand Function and Laser Irradiation. *Biomater. Sci.* **2015**, *3*, 733–741.
- (476) Roma-Rodrigues, C.; Heuer-Jungemann, A.; Fernandes, A. R.; Kanaras, A. G.; Baptista, P. V. Peptide-Coated Gold Nanoparticles for Modulation of Angiogenesis in Vivo. *Int. J. Nanomed.* **2016**, *11*, 2633–2639.
- (477) Bartczak, D.; Sanchez-Elsner, T.; Louafi, F.; Millar, T. M.; Kanaras, A. G. Receptor-Mediated Interactions between Colloidal Gold Nanoparticles and Human Umbilical Vein Endothelial Cells. *Small* **2011**, *7*, 388–394.
- (478) Bartczak, D.; Nitti, S.; Millar, T. M.; Kanaras, A. G. Exocytosis of Peptide Functionalized Gold Nanoparticles in Endothelial Cells. *Nanoscale* **2012**, *4*, 4470–4472.
- (479) Pedrosa, P.; Heuer-Jungemann, A.; Kanaras, A. G.; Fernandes, A. R.; Baptista, P. V. Potentiating Angiogenesis Arrest in Vivo Via Laser Irradiation of Peptide Functionalised Gold Nanoparticles. *J. Nanobiotechnol.* **2017**, *15*, 85.
- (480) Akerman, M. E.; Chan, W. C. W.; Laakkonen, P.; Bhatia, S. N.; Ruoslahti, E. Nanocrystal Targeting in Vivo. *Proc. Natl. Acad. Sci. U. S. A.* **2002**, *99*, 12617–12621.
- (481) Leader, B.; Baca, Q. J.; Golan, D. E. Protein Therapeutics: A Summary and Pharmacological Classification. *Nat. Rev. Drug Discovery* **2008**, *7*, 21.
- (482) Sauna, Z. E.; Lagasse, D.; Pedras-Vasconcelos, J.; Golding, B.; Rosenberg, A. S. Evaluating and Mitigating the Immunogenicity of Therapeutic Proteins. *Trends Biotechnol.* **2018**, *36*, 1068–1084.
- (483) Serna, N.; Sanchez-Garcia, L.; Unzueta, U.; Diaz, R.; Vazquez, E.; Mangués, R.; Villaverde, A. Protein-Based Therapeutic Killing for Cancer Therapies. *Trends Biotechnol.* **2018**, *36*, 318–335.
- (484) Aubin-Tam, M. E. Conjugation of Nanoparticles to Proteins. *Methods Mol. Biol.* **2013**, *1025*, 19–27.
- (485) Kumar, S.; Aaron, J.; Sokolov, K. Directional Conjugation of Antibodies to Nanoparticles for Synthesis of Multiplexed Optical Contrast Agents with Both Delivery and Targeting Moieties. *Nat. Protoc.* **2008**, *3*, 314–320.
- (486) Aubin-Tam, M. E.; Hamad-Schifferli, K. Gold Nanoparticle–Cytochrome C Complexes: The Effect of Nanoparticle Ligand Charge on Protein Structure. *Langmuir* **2005**, *21*, 12080–12084.
- (487) Hermanson, G. T. *Bioconjugate Techniques*; Academic Press, 2013.
- (488) Wilchek, M.; Bayer, E. A. Avidin-Biotin Technology. *Methods Enzymol.* **1990**, *184*, 3–746.
- (489) Li, S.; Liu, H. N.; He, N. Y. Covalent Binding of Streptavidin on Gold Magnetic Nanoparticles for Bead Array Fabrication. *J. Nanosci. Nanotechnol.* **2010**, *10*, 4875–4882.
- (490) Simonian, A. L.; Good, T. A.; Wang, S. S.; Wild, J. R. Nanoparticle-Based Optical Biosensors for the Direct Detection of Organophosphate Chemical Warfare Agents and Pesticides. *Anal. Chim. Acta* **2005**, *534*, 69–77.
- (491) Goldman, E. R.; Balighian, E. D.; Mattoussi, H.; Kuno, M. K.; Mauro, J. M.; Tran, P. T.; Anderson, G. P. Avidin: A Natural Bridge for Quantum Dot–Antibody Conjugates. *J. Am. Chem. Soc.* **2002**, *124*, 6378–6382.
- (492) Itano, M. S.; Neumann, A. K.; Liu, P.; Zhang, F.; Gratton, E.; Parak, W. J.; Thompson, N. L.; Jacobson, K. Dc-Sign and Influenza Hemagglutinin Dynamics in Plasma Membrane Microdomains Are Markedly Different. *Biophys. J.* **2011**, *100*, 2662–2670.
- (493) Caswell, K.; Wilson, J. N.; Bunz, U. H.; Murphy, C. J. Preferential End-to-End Assembly of Gold Nanorods by Biotin–Streptavidin Connectors. *J. Am. Chem. Soc.* **2003**, *125*, 13914–13915.
- (494) Brennan, J. L.; Kanaras, A. G.; Nativo, P.; Tshikhudo, T. R.; Rees, C.; Fernandez, L. C.; Dirvianskyte, N.; Razumas, V.; Skjot, M.; et al. Enzymatic Activity of Lipase–Nanoparticle Conjugates and the Digestion of Lipid Liquid Crystalline Assemblies. *Langmuir* **2010**, *26*, 13590–13599.
- (495) Peng, Y.; Jiang, J.; Yu, R. A Sensitive Electrochemical Biosensor for MicroRNA Detection Based on Streptavidin–Gold Nanoparticles and Enzymatic Amplification. *Anal. Methods* **2014**, *6*, 2889–2893.

- (496) Elzoghby, A. O.; Samy, W. M.; Elgindy, N. A. Albumin-Based Nanoparticles as Potential Controlled Release Drug Delivery Systems. *J. Controlled Release* **2012**, *157*, 168–182.
- (497) Xia, B.; Zhang, W.; Shi, J.; Xiao, S.-j. Engineered Stealth Porous Silicon Nanoparticles Via Surface Encapsulation of Bovine Serum Albumin for Prolonging Blood Circulation in Vivo. *ACS Appl. Mater. Interfaces* **2013**, *5*, 11718–11724.
- (498) Gause, K. T.; Yan, Y.; Cui, J.; O'Brien-Simpson, N. M.; Lenzo, J. C.; Reynolds, E. C.; Caruso, F. Physicochemical and Immunological Assessment of Engineered Pure Protein Particles with Different Redox States. *ACS Nano* **2015**, *9*, 2433–2444.
- (499) Brzoska, M.; Langer, K.; Coester, C.; Loitsch, S.; Wagner, T. O.; Mallinckrodt, C. Incorporation of Biodegradable Nanoparticles into Human Airway Epithelium Cells-in Vitro Study of the Suitability as a Vehicle for Drug or Gene Delivery in Pulmonary Diseases. *Biochem. Biophys. Res. Commun.* **2004**, *318*, 562–570.
- (500) Kufleitner, J.; Worek, F.; Kreuter, J. Incorporation of Obidoxime into Human Serum Albumin Nanoparticles: Optimisation of Preparation Parameters for the Development of a Stable Formulation. *J. Microencapsulation* **2010**, *27*, 594–601.
- (501) Kufleitner, J.; Wagner, S.; Worek, F.; von Briesen, H.; Kreuter, J. Adsorption of Obidoxime onto Human Serum Albumin Nanoparticles: Drug Loading, Particle Size and Drug Release. *J. Microencapsulation* **2010**, *27*, 506–513.
- (502) Hawkins, M. J.; Soon-Shiong, P.; Desai, N. Protein Nanoparticles as Drug Carriers in Clinical Medicine. *Adv. Drug Delivery Rev.* **2008**, *60*, 876–885.
- (503) Zeng, Y.; Chang, Y.-H.; Gharib, M.; Parak, W. J.; Chakraborty, I. Understanding the Interaction of Glutamate Salts with Serum Albumin Protected Prism-Shaped Silver Nanoparticles toward Glutamate Sensing. *Part. Part. Syst. Char.* **2019**, *36*, 1800229.
- (504) Bhan, C.; Mandlewala, R.; Gebregeorgis, A.; Raghavan, D. Adsorption-Desorption Study of Bsa Conjugated Silver Nanoparticles (Ag/Bsa Nps) on Collagen Immobilized Substrates. *Langmuir* **2012**, *28*, 17043–17052.
- (505) Qi, W.-W.; Yu, H.-Y.; Guo, H.; Lou, J.; Wang, Z.-M.; Liu, P.; Sapin-Minet, A.; Maincent, P.; Hong, X.-C.; Hu, X.-M.; Xiao, Y.-L. Doxorubicin-Loaded Glycyrrhetic Acid Modified Recombinant Human Serum Albumin Nanoparticles for Targeting Liver Tumor Chemotherapy. *Mol. Pharmaceutics* **2015**, *12*, 675–683.
- (506) Clapp, A. R.; Goldman, E. R.; Mattoussi, H. Capping of Cdse-Zns Quantum Dots with Dhl and Subsequent Conjugation with Proteins. *Nat. Protoc.* **2006**, *1*, 1258–1266.
- (507) Carril, M.; Padro, D.; del Pino, P.; Carrillo-Carrion, C.; Gallego, M.; Parak, W. J. In Situ Detection of the Protein Corona in Complex Environments. *Nat. Commun.* **2017**, *8*, 1542.
- (508) Ke, P. C.; Lin, S.; Parak, W. J.; Davis, T. P.; Caruso, F. A Decade of the Protein Corona. *ACS Nano* **2017**, *11*, 11773–11776.
- (509) Cedervall, T.; Lynch, I.; Lindman, S.; Berggård, T.; Thulin, E.; Nilsson, H.; Dawson, K. A.; Linse, S. Understanding the Nanoparticle-Protein Corona Using Methods to Quantify Exchange Rates and Affinities of Proteins for Nanoparticles. *Proc. Natl. Acad. Sci. U. S. A.* **2007**, *104*, 2050–2055.
- (510) O'Connell, D. J.; Bombelli, F. B.; Pitek, A. S.; Monopoli, M. P.; Cahill, D. J.; Dawson, K. A. Characterization of the Bionano Interface and Mapping Extrinsic Interactions of the Corona of Nanomaterials. *Nanoscale* **2015**, *7*, 15268–15276.
- (511) Röcker, C.; Pötl, M.; Zhang, F.; Parak, W. J.; Nienhaus, G. U. A Quantitative Fluorescence Study of Protein Monolayer Formation on Colloidal Nanoparticles. *Nat. Nanotechnol.* **2009**, *4*, 577–580.
- (512) Pino, P. d.; Pelaz, B.; Zhang, Q.; Maffre, P.; Nienhaus, G. U.; Parak, W. J. Protein Corona Formation around Nanoparticles - from the Past to the Future. *Mater. Horiz.* **2014**, *1*, 301–313.
- (513) Docter, D.; Westmeier, D.; Markiewicz, M.; Stolte, S.; Knauer, S. K.; Stauber, R. H. The Nanoparticle Biomolecule Corona: Lessons Learned - Challenge Accepted? *Chem. Soc. Rev.* **2015**, *44*, 6094–6121.
- (514) Pederzoli, F.; Tosi, G.; Vandelli, M. A.; Belletti, D.; Forni, F.; Ruozi, B. Protein Corona and Nanoparticles: How Can We Investigate On? *Wiley Interdiscip. Rev. Nanomed. Nanobiotechnol.* **2017**, *9*, e1467.
- (515) Ma, W.; Saccardo, A.; Roccatano, D.; Aboagye-Mensah, D.; Alkaseem, M.; Jewkes, M.; Di Nezza, F.; Baron, M.; Soloviev, M.; Ferrari, E. Modular Assembly of Proteins on Nanoparticles. *Nat. Commun.* **2018**, *9*, 1489.
- (516) Fratila, R. M.; Moros, M.; de la Fuente, J. M. Recent Advances in Biosensing Using Magnetic Glyconanoparticles. *Anal. Bioanal. Chem.* **2016**, *408*, 1783–1803.
- (517) Swierczewska, M.; Han, H. S.; Kim, K.; Park, J. H.; Lee, S. Polysaccharide-Based Nanoparticles for Theranostic Nanomedicine. *Adv. Drug Delivery Rev.* **2016**, *99*, 70–84.
- (518) Wu, S.; Huang, X.; Du, X. Glucose-and Ph-Responsive Controlled Release of Cargo from Protein-Gated Carbohydrate-Functionalized Mesoporous Silica Nanocontainers. *Angew. Chem., Int. Ed.* **2013**, *52*, 5580–5584.
- (519) Basiruddin, S.; Ranjan Maity, A.; Jana, N. R. Glucose/Galactose/Dextran-Functionalized Quantum Dots, Iron Oxide and Doped Semiconductor Nanoparticles with < 100 nm Hydrodynamic Diameter. *RSC Adv.* **2012**, *2*, 11915–11921.
- (520) Basuki, J. S.; Esser, L.; Duong, H. T.; Zhang, Q.; Wilson, P.; Whittaker, M. R.; Haddleton, D. M.; Boyer, C.; Davis, T. P. Magnetic Nanoparticles with Diblock Glycopolymers Shells Give Lectin Concentration-Dependent Mri Signals and Selective Cell Uptake. *Chem. Sci.* **2014**, *5*, 715–726.
- (521) Wu, C.-Y.; Lin, C.-H.; Chen, Y.-C. Using Glucose-Bound Fe₃O₄ Magnetic Nanoparticles as Photothermal Agents for Targeted Hyperthermia of Cancer Cells. *J. Nanomed. Nanotechnol.* **2015**, *6*, 264.
- (522) Jayawardana, K. W.; Jayawardana, H. S. N.; Wijesundera, S. A.; De Zoysa, T.; Sundhoro, M.; Yan, M. Selective Targeting of Mycobacterium Smegmatis with Trehalose-Functionalized Nanoparticles. *Chem. Commun.* **2015**, *51*, 12028–12031.
- (523) Kharitonov, A. B.; Shipway, A. N.; Katz, E.; Willner, I. Gold-Nanoparticle/Bis-Bipyridinium Cyclophane-Functionalized Ion-Sensitive Field-Effect Transistors: Novel Assemblies for the Sensing of Neurotransmitters. *Rev. Anal. Chem.* **1999**, *18*, 255–260.
- (524) Kymakis, E.; Spyropoulos, G. D.; Fernandes, R.; Kakavelakis, G.; Kanaras, A. G.; Stratakis, E. Plasmonic Bulk Heterojunction Solar Cells: The Role of Nanoparticle Ligand Coating. *ACS Photonics* **2015**, *2*, 714–723.
- (525) Cahen, D.; Hodes, G.; Grätzel, M.; Guillemoles, J. F.; Riess, I. Nature of Photovoltaic Action in Dye-Sensitized Solar Cells. *J. Phys. Chem. B* **2000**, *104*, 2053–2059.
- (526) Zhang, Y. C.; Chu, W. D.; Foroushani, A. D.; Wang, H. B.; Li, D.; Liu, J. Q.; Barrow, C. J.; Wang, X.; Yang, W. R. New Gold Nanostructures for Sensor Applications: A Review. *Materials* **2014**, *7*, 5169–5201.
- (527) Talapin, D. V.; Lee, J.-S.; Kovalenko, M. V.; Shevchenko, E. V. Prospects of Colloidal Nanocrystals for Electronic and Optoelectronic Applications. *Chem. Rev.* **2010**, *110*, 389–458.
- (528) Clifford, J. P.; Konstantatos, G.; Johnston, K. W.; Hoogland, S.; Levina, L.; Sargent, E. H. Fast, Sensitive and Spectrally Tuneable Colloidal-Quantum-Dot Photodetectors. *Nat. Nanotechnol.* **2009**, *4*, 40–44.
- (529) Konstantatos, G.; Badioli, M.; Gaudreau, L.; Osmond, J.; Bernechea, M.; Garcia de Arquer, F. P.; Gatti, F.; Koppens, F. H. L. Hybrid Graphene-Quantum Dot Phototransistors with Ultrahigh Gain. *Nat. Nanotechnol.* **2012**, *7*, 363–368.
- (530) Saran, R.; Curry, R. J. Lead Sulphide Nanocrystal Photodetector Technologies. *Nat. Photonics* **2016**, *10*, 81–92.
- (531) Liu, Y.; Gibbs, M.; Puthussery, J.; Gaik, S.; Ihly, R.; Hillhouse, H. W.; Law, M. Dependence of Carrier Mobility on Nanocrystal Size and Ligand Length in Pbse Nanocrystal Solids. *Nano Lett.* **2010**, *10*, 1960–1969.
- (532) Leatherdale, C. A.; Kagan, C. R.; Morgan, N. Y.; Empedocles, S. A.; Kastner, M. A.; Bawendi, M. G. Photoconductivity in Cdse Quantum Dot Solids. *Phys. Rev. B: Condens. Matter Mater. Phys.* **2000**, *62*, 2669–2680.

- (533) Jarosz, M. V.; Porter, V. J.; Fisher, B. R.; Kastner, M. A.; Bawendi, M. G. Photoconductivity Studies of Treated CdSe Quantum Dot Films Exhibiting Increased Exciton Ionization Efficiency. *Phys. Rev. B: Condens. Matter Mater. Phys.* **2004**, *70*, 195327.
- (534) Yu, D.; Wehrenberg, B. L.; Jha, P.; Ma, J.; Guyot-Sionnest, P. Electronic Transport of N-Type CdSe Quantum Dot Films: Effect of Film Treatment. *J. Appl. Phys.* **2006**, *99*, 104315.
- (535) Sarasqueta, G.; Choudhury, K. R.; So, F. Effect of Solvent Treatment on Solution-Processed Colloidal PbSe Nanocrystal Infrared Photodetectors. *Chem. Mater.* **2010**, *22*, 3496–3501.
- (536) Schut, D. M.; Williams, G. M.; Arteaga, S.; Allen, T. L.; Novet, T. Nanocrystal Sensitized Photovoltaics and Photodetectors with Performance Enhanced Using Ligand Engineering. *Proc. SPIE* **2011**, 80351B.
- (537) Milliron, D. J.; Alivisatos, A. P.; Pitois, C.; Edder, C.; Frechet, J. M. J. Electroactive Surfactant Designed to Mediate Electron Transfer between CdSe Nanocrystals and Organic Semiconductors. *Adv. Mater.* **2003**, *15*, 58–61.
- (538) Tomczak, N.; Janczewski, D.; Han, M. Y.; Vancso, G. J. Designer Polymer-Quantum Dot Architectures. *Prog. Polym. Sci.* **2009**, *34*, 393–430.
- (539) Konstantatos, G.; Howard, I.; Fischer, A.; Hoogland, S.; Clifford, J.; Klem, E.; Levina, L.; Sargent, E. H. Ultrasensitive Solution-Cast Quantum Dot Photodetectors. *Nature* **2006**, *442*, 180–183.
- (540) Biebersdorf, A.; Diettmüller, R.; Susa, A. S.; Rogach, A. L.; Poznyak, S. K.; Talapin, D. V.; Weller, H.; Klar, T. A.; Feldmann, J. Semiconductor Nanocrystals Photosensitize C-60 Crystals. *Nano Lett.* **2006**, *6*, 1559–1563.
- (541) Han, Y. G.; Wu, L. L. Influence of Surface Ligand on Ultraviolet Photodetection Property of TiO₂ Nanocrystal/Polymer Hybrids. *J. Electron. Mater.* **2011**, *40*, 2147–2151.
- (542) Kramer, I. J.; Sargent, E. H. Colloidal Quantum Dot Photovoltaics: A Path Forward. *ACS Nano* **2011**, *5*, 8506–8514.
- (543) Ip, A. H.; Thon, S. M.; Hoogland, S.; Voznyy, O.; Zhitomirsky, D.; Debnath, R.; Levina, L.; Rollny, L. R.; Carey, G. H.; et al. Hybrid Passivated Colloidal Quantum Dot Solids. *Nat. Nanotechnol.* **2012**, *7*, 577–582.
- (544) Borchert, H. Elementary Processes and Limiting Factors in Hybrid Polymer/Nanoparticle Solar Cells. *Energy Environ. Sci.* **2010**, *3*, 1682–1694.
- (545) Pattantyus-Abraham, A. G.; Kramer, I. J.; Barkhouse, A. R.; Wang, X. H.; Konstantatos, G.; Debnath, R.; Levina, L.; Raabe, I.; Nazeeruddin, M. K.; et al. Depleted-Heterojunction Colloidal Quantum Dot Solar Cells. *ACS Nano* **2010**, *4*, 3374–3380.
- (546) Graetzel, M.; Janssen, R. A. J.; Mitzi, D. B.; Sargent, E. H. Materials Interface Engineering for Solution-Processed Photovoltaics. *Nature* **2012**, *488*, 304–312.
- (547) Talgorn, E.; Moysidou, E.; Abellon, R. D.; Savenije, T. J.; Goossens, A.; Houtepen, A. J.; Siebbeles, L. D. A. Highly Photoconductive CdSe Quantum-Dot Films: Influence of Capping Molecules and Film Preparation Procedure. *J. Phys. Chem. C* **2010**, *114*, 3441–3447.
- (548) Voznyy, O. Mobile Surface Traps in CdSe Nanocrystals with Carboxylic Acid Ligands. *J. Phys. Chem. C* **2011**, *115*, 15927–15932.
- (549) Johnston, K. W.; Pattantyus-Abraham, A. G.; Clifford, J. P.; Myrskog, S. H.; MacNeil, D. D.; Levina, L.; Sargent, E. H. Schottky-Quantum Dot Photovoltaics for Efficient Infrared Power Conversion. *Appl. Phys. Lett.* **2008**, *92*, 151115.
- (550) Koleilat, G. I.; Levina, L.; Shukla, H.; Myrskog, S. H.; Hinds, S.; Pattantyus-Abraham, A. G.; Sargent, E. H. Efficient, Stable Infrared Photovoltaics Based on Solution-Cast Colloidal Quantum Dots. *ACS Nano* **2008**, *2*, 833–840.
- (551) Tang, J.; Kemp, K. W.; Hoogland, S.; Jeong, K. S.; Liu, H.; Levina, L.; Furukawa, M.; Wang, X. H.; Debnath, R.; et al. Colloidal-Quantum-Dot Photovoltaics Using Atomic-Ligand Passivation. *Nat. Mater.* **2011**, *10*, 765–771.
- (552) Dai, X. L.; Deng, Y. Z.; Peng, X. G.; Jin, Y. Z. Quantum-Dot Light-Emitting Diodes for Large-Area Displays: Towards the Dawn of Commercialization. *Adv. Mater.* **2017**, *29*, 1607022.
- (553) McDowell, M.; Wright, A. E.; Hammer, N. I. Semiconductor Nanocrystals Hybridized with Functional Ligands: New Composite Materials with Tunable Properties. *Materials* **2010**, *3*, 614–637.
- (554) Kang, B. H.; Lee, S. W.; Lim, S. W.; Kim, J. S.; Sai-Anand, G.; Lee, S. H.; Kwon, D. H.; Kang, S. W. Enhanced Performance of Light-Emitting Diodes by Surface Ligand Modification on Quantum Dots. *J. Nanosci. Nanotechnol.* **2015**, *15*, 7169–7172.
- (555) Sun, L. F.; Choi, J. J.; Stachnik, D.; Bartnik, A. C.; Hyun, B. R.; Malliaras, G. G.; Hanrath, T.; Wise, F. W. Bright Infrared Quantum-Dot Light-Emitting Diodes through Inter-Dot Spacing Control. *Nat. Nanotechnol.* **2012**, *7*, 369–373.
- (556) Dai, X. L.; Zhang, Z. X.; Jin, Y. Z.; Niu, Y.; Cao, H. J.; Liang, X. Y.; Chen, L. W.; Wang, J. P.; Peng, X. G. Solution-Processed, High-Performance Light-Emitting Diodes Based on Quantum Dots. *Nature* **2014**, *515*, 96–99.
- (557) Zhang, X.; Sun, C.; Zhang, Y.; Wu, H.; Ji, C.; Chuai, Y.; Wang, P.; Wen, S.; Zhang, C.; Yu, W. W. Bright Perovskite Nanocrystal Films for Efficient Light-Emitting Devices. *J. Phys. Chem. Lett.* **2016**, *7*, 4602–4610.
- (558) Li, G.; Rivalora, F. W. R.; Davis, N. J. L. K.; Bai, S.; Jellicoe, T. C.; de la Peña, F.; Hou, S.; Ducati, C.; Gao, F.; et al. Highly Efficient Perovskite Nanocrystal Light-Emitting Diodes Enabled by a Universal Crosslinking Method. *Adv. Mater.* **2016**, *28*, 3528–3534.
- (559) Perumal, A.; Shendre, S.; Li, M. J.; Tay, Y. K. E.; Sharma, V. K.; Chen, S.; Wei, Z. H.; Liu, Q.; Gao, Y.; Buenconsejo, P. J. S.; Tan, S. T.; Gan, C. L.; Xiong, Q.; Sum, T. C.; Demir, H. V. High Brightness Formamidinium Lead Bromide Perovskite Nanocrystal Light Emitting Devices. *Sci. Rep.* **2016**, *6*, 36733.
- (560) Du, X.; Wu, G.; Cheng, J.; Dang, H.; Ma, K.; Zhang, Y.-W.; Tan, P.-F.; Chen, S. High-Quality CsPbBr₃ Perovskite Nanocrystals for Quantum Dot Light-Emitting Diodes. *RSC Adv.* **2017**, *7*, 10391–10396.
- (561) Raja, S. N.; Bekenstein, Y.; Koc, M. A.; Fischer, S.; Zhang, D.; Lin, L.; Ritchie, R. O.; Yang, P.; Alivisatos, A. P. Encapsulation of Perovskite Nanocrystals into Macroscale Polymer Matrices: Enhanced Stability and Polarization. *ACS Appl. Mater. Interfaces* **2016**, *8*, 35523–35533.
- (562) Zhang, H.; Wang, X.; Liao, Q.; Xu, Z.; Li, H.; Zheng, L.; Fu, H. Embedding Perovskite Nanocrystals into a Polymer Matrix for Tunable Luminescence Probes in Cell Imaging. *Adv. Funct. Mater.* **2017**, *27*, 1604382.
- (563) Yang, Y.; Qin, H. Y.; Jiang, M. W.; Lin, L.; Fu, T.; Dai, X. L.; Zhang, Z. X.; Niu, Y.; Cao, H. J.; et al. Entropic Ligands for Nanocrystals: From Unexpected Solution Properties to Outstanding Processability. *Nano Lett.* **2016**, *16*, 2133–2138.
- (564) Yang, Y.; Qin, H. Y.; Peng, X. G. Intramolecular Entropy and Size-Dependent Solution Properties of Nanocrystal-Ligands Complexes. *Nano Lett.* **2016**, *16*, 2127–2132.
- (565) Cho, I.; Jung, H.; Jeong, B. G.; Chang, J. H.; Kim, Y. C.; Char, K.; Lee, D. C.; Lee, C.; Cho, J.; Bae, W. K. Multi-Functional Dendrimer Ligands for High-Efficiency, Solution-Processed Quantum Dot Light-Emitting Diodes. *ACS Nano* **2017**, *11*, 684–692.
- (566) Cho, I.; Jung, H.; Jeong, B. G.; Chang, J. H.; Kim, Y.; Char, K.; Lee, D. C.; Lee, C.; Cho, J.; Bae, W. K. Multifunctional Dendrimer Ligands for High-Efficiency, Solution-Processed Quantum Dot Light-Emitting Diodes. *ACS Nano* **2017**, *11*, 684–692.
- (567) Hao, S. W.; Chen, G. Y.; Yang, C. H. Sensing Using Rare-Earth-Doped Upconversion Nanoparticles. *Theranostics* **2013**, *3*, 331–345.
- (568) Yao, L. M.; Zhou, J.; Liu, J. L.; Feng, W.; Li, F. Y. Iridium-Complex-Modified Upconversion Nanophosphors for Effective LRET Detection of Cyanide Anions in Pure Water. *Adv. Funct. Mater.* **2012**, *22*, 2667–2672.
- (569) Yang, G.; Hallinan, D. T. Gold Nanoparticle Monolayers from Sequential Interfacial Ligand Exchange and Migration in a Three-Phase System. *Sci. Rep.* **2016**, *6*, 35339.

- (570) Obare, S. O.; Hollowell, R. E.; Murphy, C. J. Sensing Strategy for Lithium Ion Based on Gold Nanoparticles. *Langmuir* **2002**, *18*, 10407–10410.
- (571) Zhang, H. L.; Evans, S. D.; Henderson, J. R.; Miles, R. E.; Shen, T. H. Vapour Sensing Using Surface Functionalized Gold Nanoparticles. *Nanotechnology* **2002**, *13*, 439–444.
- (572) Gong, S.; Schwalb, W.; Wang, Y. W.; Chen, Y.; Tang, Y.; Si, J.; Shirinzadeh, B.; Cheng, W. L. A Wearable and Highly Sensitive Pressure Sensor with Ultrathin Gold Nanowires. *Nat. Commun.* **2014**, *5*, 3132.
- (573) Patolsky, F.; Lieber, C. M. Nanowire Nanosensors. *Mater. Today* **2005**, *8*, 20–28.
- (574) Zou, X. M.; Wang, J. L.; Liu, X. Q.; Wang, C. L.; Jiang, Y.; Wang, Y.; Xiao, X. H.; Ho, J. C.; Li, J. C.; et al. Rational Design of Sub-Parts Per Million Specific Gas Sensors Array Based on Metal Nanoparticles Decorated Nanowire Enhancement-Mode Transistors. *Nano Lett.* **2013**, *13*, 3287–3292.
- (575) Kim, Y. J.; Yang, Y. S.; Ha, S. C.; Cho, S. M.; Kim, Y. S.; Kim, H. Y.; Yang, H.; Kim, Y. T. Mixed-Ligand Nanoparticles of Chlorobenzenemethanethiol and N-Octanethiol as Chemical Sensors. *Sens. Actuators, B* **2005**, *106*, 189–198.
- (576) Morsbach, E.; Brauns, E.; Kowalik, T.; Lang, W.; Kunz, S.; Baumer, M. Ligand-Stabilized Pt Nanoparticles (Nps) as Novel Materials for Catalytic Gas Sensing: Influence of the Ligand on Important Catalytic Properties. *Phys. Chem. Chem. Phys.* **2014**, *16*, 21243–21251.
- (577) Talapin, D. V.; Lee, J. S.; Kovalenko, M. V.; Shevchenko, E. V. Prospects of Colloidal Nanocrystals for Electronic and Optoelectronic Applications. *Chem. Rev.* **2010**, *110*, 389–458.
- (578) Moser, A.; Takano, K.; Margulies, D. T.; Albrecht, M.; Sonobe, Y.; Ikeda, Y.; Sun, S. H.; Fullerton, E. E. Magnetic Recording: Advancing into the Future. *J. Phys. D: Appl. Phys.* **2002**, *35*, R157–R167.
- (579) Wu, L. H.; Mendoza-Garcia, A.; Li, Q.; Sun, S. H. Organic Phase Syntheses of Magnetic Nanoparticles and Their Applications. *Chem. Rev.* **2016**, *116*, 10473–10512.
- (580) Huang, T.; Wang, H. W.; Zou, Y. H.; Cheng, W. M.; Xie, C. S. Explorations on Size Limit of Li(0)-FePt Nanoparticles for Practical Magnetic Storage. *APL Adv.* **2016**, *6*, 115302.
- (581) Dong, Q. C.; Qu, W. S.; Liang, W. Q.; Guo, K. P.; Xue, H. B.; Guo, Y. Y.; Meng, Z. G.; Ho, C. L.; Leung, C. W.; Wong, W. Y. Metallopolymer Precursors to Li(0)-Copt Nanoparticles: Synthesis, Characterization, Nanopatterning and Potential Application. *Nanoscale* **2016**, *8*, 7068–7074.
- (582) Hou, Y. L.; Xu, Z. C.; Peng, S.; Rong, C. B.; Liu, J. P.; Sun, S. H. A Facile Synthesis of SmCo₅ Magnets from Core/Shell Co/Sm₂O₃ Nanoparticles. *Adv. Mater.* **2007**, *19*, 3349.
- (583) Tseng, R. J.; Tsai, C.; Ma, L.; Ouyang, J.; Ozkan, C. S.; Yang, Y. Digital Memory Device Based on Tobacco Mosaic Virus Conjugated with Nanoparticles. *Nat. Nanotechnol.* **2006**, *1*, 72–77.
- (584) Kostopoulou, A.; Brintakis, K.; Vasilakaki, M.; Trohidou, K. N.; Douvalis, A. P.; Lascialfari, A.; Manna, L.; Lappas, A. Assembly-Mediated Interplay of Dipolar Interactions and Surface Spin Disorder in Colloidal Maghemite Nanoclusters. *Nanoscale* **2014**, *6*, 3764–3776.
- (585) Palma, S. I. C. J.; Marciello, M.; Carvalho, A.; Veintemillas-Verdaguer, S.; Morales, M. D.; Roque, A. C. A. Effects of Phase Transfer Ligands on Monodisperse Iron Oxide Magnetic Nanoparticles. *J. Colloid Interface Sci.* **2015**, *437*, 147–155.
- (586) Nadeem, K.; Krenn, H.; Traussing, T.; Letofsky-Papst, I. Distinguishing Magnetic Blocking and Surface Spin-Glass Freezing in Nickel Ferrite Nanoparticles. *J. Appl. Phys.* **2011**, *109*, 013912.
- (587) Hiroi, K.; Komatsu, K.; Sato, T. Superspin Glass Originating from Dipolar Interaction with Controlled Interparticle Distance among Gamma-Fe₂O₃ Nanoparticles with Silica Shells. *Phys. Rev. B: Condens. Matter Mater. Phys.* **2011**, *83*, 224423.
- (588) Suzuki, M.; Fullem, S. I.; Suzuki, I. S.; Wang, L. Y.; Zhong, C. J. Observation of Superspin-Glass Behavior in Fe₃O₄ Nanoparticles. *Phys. Rev. B: Condens. Matter Mater. Phys.* **2009**, *79*, 024418.
- (589) Hansen, M. F.; Jönsson, P. E.; Nordblad, P.; Svedlindh, P. Critical Dynamics of an Interacting Magnetic Nanoparticle System. *J. Phys.: Condens. Matter* **2002**, *14*, 4901.
- (590) Nakata, K.; Hu, Y.; Uzun, O.; Bakr, O.; Stellacci, F. Chains of Superparamagnetic Nanoparticles. *Adv. Mater.* **2008**, *20*, 4294–4299.
- (591) Peddis, D.; Rinaldi, D.; Ennas, G.; Scano, A.; Agostinelli, E.; Fiorani, D. Superparamagnetic Blocking and Superspin-Glass Freezing in Ultra Small [Small Delta]-(Fe_{0.67}Mn_{0.33})O_{oh} Particles. *Phys. Chem. Chem. Phys.* **2012**, *14*, 3162–3169.
- (592) Okamoto, J.; Mamiya, K.; Fujimori, S. I.; Okane, T.; Saitoh, Y.; Muramatsu, Y.; Yoshii, K.; Fujimori, A.; Tanaka, A.; Abbate, M.; Koide, T.; Ishiwata, S.; Kawasaki, S.; Takano, M. Antiferromagnetic-to-Ferromagnetic Transition Induced by Diluted Co in SrFe_{1-x}Co_xO₃: Magnetic Circular X-Ray Dichroism Study. *Phys. Rev. B: Condens. Matter Mater. Phys.* **2005**, *71*, 104401.
- (593) Pichanusakorn, P.; Bandaru, P. Nanostructured Thermoelectrics. *Mater. Sci. Eng., R* **2010**, *67*, 19–63.
- (594) Sootsman, J. R.; Chung, D. Y.; Kanatzidis, M. G. New and Old Concepts in Thermoelectric Materials. *Angew. Chem., Int. Ed.* **2009**, *48*, 8616–8639.
- (595) Vineis, C. J.; Shakouri, A.; Majumdar, A.; Kanatzidis, M. G. Nanostructured Thermoelectrics: Big Efficiency Gains from Small Features. *Adv. Mater.* **2010**, *22*, 3970–3980.
- (596) Ortega, S.; Ibanez, M.; Liu, Y.; Zhang, Y.; Kovalenko, M. V.; Cadavid, D.; Cabot, A. Bottom-up Engineering of Thermoelectric Nanomaterials and Devices from Solution-Processed Nanoparticle Building Blocks. *Chem. Soc. Rev.* **2017**, *46*, 3510.
- (597) Medlin, D. L.; Snyder, G. J. Interfaces in Bulk Thermoelectric Materials: A Review for Current Opinion in Colloid and Interface Science. *Curr. Opin. Colloid Interface Sci.* **2009**, *14*, 226–235.
- (598) Sharp, J. W.; Poon, S. J.; Goldsmid, H. J. Boundary Scattering and the Thermoelectric Figure of Merit. *Phys. Status Solidi A* **2001**, *187*, S07–S16.
- (599) Sun, Y. M.; Fang, H. Y.; Pan, L. J.; Han, M.; Xu, S.; Wang, X. W.; Xu, B.; Wu, Y. Impact of Surface-Bound Small Molecules on the Thermoelectric Property of Self-Assembled Ag₂Te Nanocrystal Thin Films. *Nano Lett.* **2015**, *15*, 3748–3756.
- (600) Lynch, J.; Kotiuga, M.; Doan-Nguyen, V. V. T.; Queen, W. L.; Forster, J. D.; Schlitz, R. A.; Murray, C. B.; Neaton, J. B.; Chabiny, M. L.; Urban, J. J. Ligand Coupling Symmetry Correlates with Thermopower Enhancement in Small-Molecule/Nanocrystal Hybrid Materials. *ACS Nano* **2014**, *8*, 10528–10536.
- (601) Stavriniadis, A.; Konstantatos, G. Strategies for the Controlled Electronic Doping of Colloidal Quantum Dot Solids. *ChemPhysChem* **2016**, *17*, 632–644.
- (602) Ibanez, M.; Korkosz, R.; Luo, Z. S.; Riba, P.; Cadavid, D.; Ortega, S.; Cabot, A.; Kanatzidis, M. G. Electron Doping in Bottom-up Engineered Thermoelectric Nanomaterials through Hcd-Mediated Ligand Displacement (Vol 137, Pg 4046, 2015). *J. Am. Chem. Soc.* **2015**, *137*, 11854–11854.
- (603) Voznyy, O.; Zhitomirsky, D.; Stadler, P.; Ning, Z. J.; Hoogland, S.; Sargent, E. H. A Charge-Orbital Balance Picture of Doping in Colloidal Quantum Dot Solids. *ACS Nano* **2012**, *6*, 8448–8455.
- (604) Cadavid, D.; Ibanez, M.; Shavel, A.; Dura, O. J.; López de la Torre, M. A. L.; Cabot, A. Organic Ligand Displacement by Metal Salts to Enhance Nanoparticle Functionality: Thermoelectric Properties of Ag₂Te. *J. Mater. Chem. A* **2013**, *1*, 4864–4870.
- (605) Wang, Z. W.; Schliehe, C.; Bian, K. F.; Dale, D.; Bassett, W. A.; Hanrath, T.; Klinke, C.; Weller, H. Correlating Superlattice Polymorphs to Internanoparticle Distance, Packing Density, and Surface Lattice in Assemblies of Pbs Nanoparticles. *Nano Lett.* **2013**, *13*, 1303–1311.
- (606) Dong, A. G.; Chen, J.; Vora, P. M.; Kikkawa, J. M.; Murray, C. B. Binary Nanocrystal Superlattice Membranes Self-Assembled at the Liquid-Air Interface. *Nature* **2010**, *466*, 474–477.
- (607) Wang, J. Q.; Gu, H. W. Novel Metal Nanomaterials and Their Catalytic Applications. *Molecules* **2015**, *20*, 17070–17092.

- (608) Moghaddam, F. M.; Foroushani, B. K.; Rezvani, H. R. Nickel Ferrite Nanoparticles: An Efficient and Reusable Nanocatalyst for a Neat, One-Pot and Four-Component Synthesis of Pyrroles. *RSC Adv.* **2015**, *5*, 18092–18096.
- (609) Wang, H. W.; Covarrubias, J.; Prock, H.; Wu, X. R.; Wang, D. H.; Bossmann, S. H. Acid-Functionalized Magnetic Nanoparticle as Heterogeneous Catalysts for Biodiesel Synthesis. *J. Phys. Chem. C* **2015**, *119*, 26020–26028.
- (610) Astruc, D.; Boisselier, E.; Ornelas, C. Dendrimers Designed for Functions: From Physical, Photophysical, and Supramolecular Properties to Applications in Sensing, Catalysis, Molecular Electronics, Photonics, and Nanomedicine. *Chem. Rev.* **2010**, *110*, 1857–1959.
- (611) Wang, Z.; Shen, B.; Aihua, Z.; He, N. Synthesis of Pd/Fe₃O₄ Nanoparticle-Based Catalyst for the Cross-Coupling of Acrylic Acid with Iodobenzene. *Chem. Eng. J.* **2005**, *113*, 27–34.
- (612) Yinghuai, Z.; Peng, S. C.; Emi, A.; Zhenshun, S.; Monalisa; Kemp, R. A. Supported Ultra Small Palladium on Magnetic Nanoparticles Used as Catalysts for Suzuki Cross-Coupling and Heck Reactions. *Adv. Synth. Catal.* **2007**, *349*, 1917–1922.
- (613) Polshettiwar, V.; Luque, R.; Fihri, A.; Zhu, H.; Bouhrara, M.; Basset, J. M. Magnetically Recoverable Nanocatalysts. *Chem. Rev.* **2011**, *111*, 3036–3075.
- (614) Rossi, L. M.; Silva, F. P.; Vono, L. L. R.; Kiyohara, P. K.; Duarte, E. L.; Itri, R.; Landers, R.; Machado, G. Superparamagnetic Nanoparticle-Supported Palladium: A Highly Stable Magnetically Recoverable and Reusable Catalyst for Hydrogenation Reactions. *Green Chem.* **2007**, *9*, 379–385.
- (615) Saha, A.; Leazer, J.; Varma, R. S. O-Allylation of Phenols with Allylic Acetates in Aqueous Media Using a Magnetically Separable Catalytic System. *Green Chem.* **2012**, *14*, 67–71.
- (616) Vaddula, B. R.; Saha, A.; Leazer, J.; Varma, R. S. A Simple and Facile Heck-Type Arylation of Alkenes with Diaryliodonium Salts Using Magnetically Recoverable Pd-Catalyst. *Green Chem.* **2012**, *14*, 2133–2136.
- (617) Sun, W.; Li, Q.; Gao, S.; Shang, J. K. Monometallic Pd/Fe₃O₄ Catalyst for Denitrification of Water. *Appl. Catal., B* **2012**, *125*, 1–9.
- (618) Wang, D.; Astruc, D. Fast-Growing Field of Magnetically Recyclable Nanocatalysts. *Chem. Rev.* **2014**, *114*, 6949–6985.
- (619) Yuzik-Klimova, E. Y.; Kuchkina, N. V.; Sorokina, S. A.; Morgan, D. G.; Boris, B.; Nikoshvili, L. Z.; Lyubimova, N. A.; Matveeva, V. G.; Sulman, E. M.; et al. Magnetically Recoverable Catalysts Based on Polyphenylenepyridyl Dendrons and Dendrimers. *RSC Adv.* **2014**, *4*, 23271–23280.
- (620) Dai, B.; Wang, Q.; Yu, F.; Zhu, M. Effect of Au Nano-Particle Aggregation on the Deactivation of the AuCl₃/Ac Catalyst for Acetylene Hydrochlorination. *Sci. Rep.* **2015**, *5*, 10553.
- (621) Ansar, S. M.; Kitchens, C. L. Impact of Gold Nanoparticle Stabilizing Ligands on the Colloidal Catalytic Reduction of 4-Nitrophenol. *ACS Catal.* **2016**, *6*, 5553–5560.
- (622) Kuchkina, N. V.; Morgan, D. G.; Kostopoulou, A.; Lappas, A.; Brintakis, K.; Boris, B. S.; Yuzik-Klimova, E. Y.; Stein, B. D.; Svergun, D. I.; et al. Hydrophobic Periphery Tails of Polyphenylenepyridyl Dendrons Control Nanoparticle Formation and Catalytic Properties. *Chem. Mater.* **2014**, *26*, 5654–5663.
- (623) Comparelli, R.; Fanizza, E.; Curri, M. L.; Cozzoli, P. D.; Mascolo, G.; Passino, R.; Agostiano, A. Photocatalytic Degradation of Azo Dyes by Organic-Capped Anatase TiO₂ Nanocrystals Immobilized onto Substrates. *Appl. Catal., B* **2005**, *55*, 81–91.
- (624) Vorontsov, A. V.; Kabachkov, E. N.; Balikhin, I. L.; Kurkin, E. N.; Troitskii, V. N.; Smirnotis, P. G. Correlation of Surface Area with Photocatalytic Activity of TiO₂. *J. Adv. Ox. Technol.* **2018**, *21*, 127–137.
- (625) Bakre, P. V.; Volvoikar, P. S.; Vernekar, A. A.; Tilve, S. G. Influence of Acid Chain Length on the Properties of TiO₂ Prepared by Sol-Gel Method and Lc-Ms Studies of Methylene Blue Photodegradation. *J. Colloid Interface Sci.* **2016**, *474*, 58–67.
- (626) Zhang, G.; Kim, C.; Choi, W. Poly(4-Vinylphenol) as a New Stable and Metal-Free Sensitizer of Titania for Visible Light

Photocatalysis through Ligand-to-Metal Charge Transfer Process. *Catal. Today* **2017**, *281*, 109–116.